The Role of Anillin and ESCRT Proteins in the Control of Cytokinesis in Eukaryotes

Wandiahyel Gaiuson Yaduma
B. Tech, M. Tech (Hons)

Thesis submitted in fulfilment of the requirements for the Degree of Doctor of Philosophy

July 2023

School of Molecular Biosciences, College of Medical, Veterinary and Life Sciences

University of Glasgow

Abstract

Cytokinesis is the final step of the cell division cycle, and the major events of the process are conserved from fungi to animal cells when cellular constituents are separated to produce two daughter cells. Cytokinesis by the fission yeast *Schizosaccharomyces pombe* is compromised by the loss of anillin/Mid1p and they assemble slowly into an abnormal contractile ring. Phosphorylation by aurora and polo kinase during different cell cycle steps regulates several aspects of Mid1p function. In this thesis, we focussed on understanding the genetic interactions between the *mid1* and *vps4* genes, the physical interactions between Mid1p and Vps4p proteins, and the mechanisms by which they work together to regulate one another during cytokinesis.

In this thesis, we identified genetic interactions between *mid1* phospho-mutants *plo1-ts35*, *ark1-ts11,* and *vps4Δ* genes using tetrad analysis. Synthetic viability and morphological studies identified potentially important Mid1p amino acid residues that are required for successful cytokinesis. We observed defective growth and morphology in cells with mutations in Mid1p at serine positions 332, 523, and 531. This analysis suggested a strong genetic interaction between *mid1* and *vps4* genes. Furthermore, Mid1p is phosphorylated by aurora *ark1* and polo *plo1* kinases, genetic interactions between *mid1*, *ark1,* and *plo1* kinase genes is essential for cell viability, and it is also required for the correct cellular localization of Mid1p protein. Such analysis revealed serine residues S332, S523, and S531 to be required for the Mid1p function and its interaction with *vps4*, *ark1*, and *plo1* genes.

Pull-down assay was used to determine the physical interaction between the N-terminal domain, middle and C-terminal domains of Mid1p with Vps4p. We observed a positive physical interaction between the C-terminal domain and Vps4p, suggesting physical interaction between C-terminal and Vps4p. However, a negative physical interaction between N-terminal and Middle with Vps4p was observed. Bioimage analysis showed septation defects and mislocalization at serine positions S332, 523, and 531 of *mid1* phospho-mutant indicating the importance of phosphorylation of Mid1p in cortical anchorage and nuclear localization during cell division. The mislocalization patterns observed present evidence that Mid1p is implicated in the recruitment of nodes and endosomal

vesicle elements to drive cytokinesis processes. Combined, these data suggest a genetic and biochemical interaction between Mid1p and Vps4p is important for cytokinesis and further implied that phosphorylation of Mid1p by aurora and polo kinases is significant for this processes.

Dedication

I dedicate this research project to my late father Mr Gaiuson Umaru Sule Yaduma (GUSY). His role, sacrifices, and intentional commitment set me up academically and to develop a lifelong love for learning. My father was not only an incredibly loving father, but also a teacher, a kind-hearted and generous man, and a pillar of strength for my family and our community. I hope that this dedication page will live on as a collection of the various ways that he's touched people's lives.

Table of Contents

List of Tables

List of Figures

Acknowledgement

First and foremost, I want to thank God Almighty for blessings and endowing me with sound health, strength, and ability throughout the period of my PhD journey despite all the challenges encountered.

I want to express my heartfelt gratitude to Dr Christopher McInerny for his guidance, support, and encouragement throughout the period of my PhD. I would also like to thank and acknowledge my second supervisor Professor Gwyn Gould for his continued support, valuable comments, and encouragement.

I also want to appreciative the entire members of Lab 241 past and present for their help and moral support. In particular Dr Imane Rezig, Dr Omar Janha, Dr Gonzalo Tejeda, Dr Yazeed Alshuweishi, Woroud Al Shammari, Niniola Olaniyan, Dr Eloise Euston, Jose Alepuz, and Chiamaka Okoli whose advice, friendship, and company has helped during my time in the laboratory.

My profound gratitude and appreciate goes to my beloved wife and kids Tsamari Yaduma, William-Nachamada Yaduma and Adana'a Yaduma for their unconditional love, sacrifices, and support throughout the time of my study, I wish to thank, and appreciate my beloved mother Mrs Philomina Yaduma, my siblings Mr Adaiti Yaduma, Mrs Melody Mamman and Mrs Neftia Johnson for their love, support and encouragements during my study.

My profound gratitude goes to my uncles Mr James Kefas Tagwi, Dr Ishaya Wanonyi, Mr Jocktan Gaius Yaduma, Engr Saidu Mamman, and Prof. Johnson Joseph for their encouragements and support throughout my career right from my undergraduate days.

Finally, I want to thank the immediate past and current chief executives of Adamawa State College of Education Hong ADSCOEH, Professor Johnson H. Pungri and Professor Yusuf Benson Baha, for approving and supporting me before and during my entire period of study. I thank the Yaduma family, the management of ADSCOEH, Tertiary Education Trust Fund TETFUND, and Nigerian Government for the study fellowship and funding.

Author's Declaration

I declare that the work presented in this Thesis has been carried out by me, unless otherwise cited or acknowledged. It is entirely of my own composition and has not, in whole or in part been submitted for any other degree.

Wandiahyel Gaiuson Yaduma,

July 2023

Definitions/Abbreviations

~	Approximately
^{0}C	Degrees Celsius
µ	Micro-prefix
6His	Six histidine residue tag
aa	Amino acid
AAA-ATPase	ATPase associated with diverse cellular activities
ACR	Actin-myosin contractile ring
AHD	Anillin homology domain
ADP	Adenosine diphosphate
Al	Alanine
ALIX	Apoptosis-linked gene 2-interacting protein
Amp	Ampicillin
APC	Anaphase promoting complex
APS	Ammonium persulphate
Ark1p	Aurora-related kinase (fission yeast protein)
ATP	Adenosine 5'-triphosphate
Bp	DNA base pair(s)
BSA	Bovine serum albumin
CAR	Contractile actomyosin ring
C-terminal	Carboxy terminal
Cdc	Cell division cycle
Cdk	Cyclin-dependent kinase
CEP55	Centrosomal protein of 55 kDa
CHMP	Charged multivesicular body protein
$CaCl_2$	Calcium chloride
CR	Contractile ring
CS	Constriction site
D	Aspartic acid
DAPI	4'6-diamidino-2-phenylindole, dihydrochloride
DISPHOS	Disorder-enhanced phosphorylation predictor
dH_2O	Distilled water
DNA	Deoxyribonucleic acid
DTT	Dithiothreitol

EDTA	Ethylenediaminetetraacetic acid
E. coli	*Escherichia coli*
EMM	Edinburgh minimal medium
eMTOCs	equatorial microtubule organizing centers
ESCRT	Endosomal sorting complex required for transport
F-actin	Filamentous actin
g	Gramme
g	Relative centrifugation force
GDP	Guanosine-5'-diphosphate
GFP	Green fluorescent protein
GST	Glutathione S transferase
h	Hour
HCl	Hydrochloric acid
HEPES	2-[4-(2-Hydroxyethyl)-1-piperazine] ethane sulfonic acid
HIV	Human immunodeficiency virus
ICB	Intercellular bridge
ILV	Intraluminal vesicle
IST1	Increased sodium Tolerance-1
IPTG	Isopropyl-ß-D-thiogalactopyranoside
k	Kilo-prefix
kb	Kilobases
kDa	Kilo Daltons
L	Litre
LB	Luria-Bertani (medium)
LSB	Laemmli sample buffer
LiAC	Lithium acetate
m	Milli-prefix
M	Molar
MAP	Mitogen-activated protein
MALDI	Matrix-assisted laser desorption/ionization
MB	Midbody
MBR	Midbody remnant
ME	Malt extract
min	Minutes
ml	Millilitre

MIMs	MIT-domain interaction motifs
MIT	Microtubule interaction and trafficking (MIT)
MS	Mass spectrometry
MVB	Multivesicular body
NES	Nuclear exclusion signal
NETO	New-end takeoff
N-terminal	Amino terminal
Ni-NTA	Nickle-nitrilotriacetic acid
NLC	Nuclear localization
OD	Optical density
PAA	Post-anaphase array
PAGE	Polyacrylamide gel electrophoresis
PBS	Phosphate buffered saline
Plk1	Polo-like kinase (Mammalian protein)
Plo1p	Pol-like kinase (fission yeast protein)
PS	Phosphatidylserine
PTM	Post-translational modification
RNA	Ribonucleic acid
rpm	Rotations per minutes
S. cerevisiae	*Saccharomyces cerevisiae*
SDS	Sodium dodecyl sulphate
SIN	Septation initiation network
SPB	Spindle pole body
S. japonicus	*Schizosaccharomyces japonicus*
S. pombe	*Schizosaccharomyces pombe*
Sr	Serine
STAM	Signal transducing adaptor molecule
TB	Terrific broth
TBS	Tris-buffered saline
TBST	Tris-buffered saline + Tween 20
TEMED	N, N, N', N',- tetramethyl ethylenediamine
TOR	Target of rapamycin
TSG101	Tumour susceptibility gene 101
UIMs	Ubiquitin interacting motifs
Vps	Vacuolar protein sorting

(v/v)	Units volume per unit volume
W-T	Wild-type
(w/v)	Units weight per unit volume
YE	Yeast extract

Chapter 1 Introduction

1.1 The cell cycle in *Schizosaccharomyces pombe*

1.1.1 History of *Schizosaccharomyces pombe*

Over the last half century, the fission yeast *Schizosaccharomyces pombe* (*S. pombe*) has been used increasingly as a model organism for investigating eukaryotic cellular and molecular processes (Hayles and Nurse, 2016). This has been driven primarily by the development of new investigative ideas, methodologies, and the fact that several biological processes conserved in *S. pombe* and other eukaryotic organisms (Vyas *et al.*, 2021). The fission yeast is a model organism first discovered in 1893 that has been used in brewing even though it is not as well recognized for its usage in brewing and baking as *Saccharomyces cerevisiae,* a budding yeast. Pombe, the Swahili word for "beer" is given to a fermented beverage with East African roots. *S. pombe* was initially isolated by Saare and colleagues from contaminated millet beer. It is abundant in a range of natural foods such as fruits, syrups, and "kombucha" which is produced by fermenting tea with yeasts and bacteria (Vyas *et al.*, 2021). The establishment of fission yeast as an experimental laboratory organism came with Urs Leupold who as his PhD project in the 1940s, developed *S. pombe* analysis. The Strains he derived are not from the Lindner strain and are thought to be from strain deposited in the yeast collection in Delft the Netherland in 1924 under the name *S. pombe* var. *liquefaciens*. Osterwalder had isolated this strain from rancid wine at the Experimental Station of Vini-and Horticulture in Wadenswil, Switzerland (Hayles and Nurse, 2016).

Leupold isolated two homothallic strains h^{90} (968) and h^{40} and two heterothallic strains with opposite mating types h^- and h^+ thus allowing the development of classical genetic procedure (Leupold, 1950). From the 1950s until the 1970s, genetic studies were carried out in several laboratories including those of Urs Leupold, Jurg Kohli and Peter Munz in Bern working mainly on genetics and Murdoch Mitchison in Edinburgh studying cell biology particularly cell cycle (Mitchison, 1957; Munz and Leupold, 1970; Kohli *et al.*, 1977). Early in the 1890s, Paul Linder and colleagues advanced the perception of *S. pombe* by giving it the binomial name *S. pombe* to distinguish it from *S. cerevisiae*. The name *Schizosaccharomyces* indicates that the organism is an ascomycete yeast that

belongs to the Fungi kingdom, reproduces through fission, and can ferment sugars (Gomes *et al.*, 2002, Fantes and Hoffman, 2016; Hayles and Nurse, 2016).

In the interest of science, Paul Nurse a pioneer in the field of cell cycle using *S. pombe* as a model organism visited a local brewery in Uganda, near the Virunga volcanoes to taste *pombe* himself and wrote: “The taste was sweet and very alcoholic but definitely drinkable” (Hayles and Nurse, 2016). In Mitchison's laboratory at Edinburgh University, Nurse utilized a genetic technique he had learned in Leupold's laboratory at the University of Bern to isolate fission yeast cell division cycle (*cdc*) mutants (Nurse, 1975). Research on *S. pombe* combines genetics and cell biology. This resulted in the widespread use of this model organism in various biological disciplines, and a global *S. pombe* research community has emerged (Hoffman *et al.*, 2015; Fantes and Hoffman, 2016).

1.1.2 Difference between *S. pombe* and *S. cerevisiae*

S. pombe as a fission yeast is more related to complex eukaryotes than the budding yeast *S. cerevisiae*. This is in addition to the biological differences between the two yeasts. First, despite both being unicellular eukaryotes and ascomycete yeasts, *S. pombe* and *S. cerevisiae* evolved apart from one another between 350 and 400 million years ago (Sipiczki, 2000). *S. pombe* and *S. cerevisiae* are not any closer to one another than humans since the evolutionary distance between these two yeasts are on the same scale as that between yeast and mammals. Second, *S. pombe* represents a more "basal" yeast group than *S. cerevisiae* and preserves more common ancestral traits following the break between fungi and metazoans, according to the protein and DNA sequence data (Hoffman *et al.*, 2015). *S. cerevisiae*, in contrast, has evolved more rapidly than *S. pombe* and lost more than 300 genes as well as a number of biological functions that are shared by both *S. pombe* and complex eukaryotes (Wood, 2006).

Additionally, unlike other eukaryotes like *S. cerevisiae* and *Arabidopsis*, chromosomal sequence research of *S. pombe* has not shown evidence of extensive genome duplications. 3536 of the 5064 protein-coding genes in fission yeast have human homologues, and 1244 of them are disease-related genes

(Wood *et al.*, 2002). Given the great evolutionary gap between *S. pombe* and *S. cerevisiae*, it is likely that mammals, including humans, have homologous genes for every gene or biological activity that is conserved in both yeasts. To compare the two divergent yeasts in an evolutionary context and determine if a gene function or a biological process of interest is conserved in all eukaryotes, including humans.

On the other hand, differences in cellular functions between the two yeasts, such as the various stages of gene expression, enable us to ascertain whether and how alternative mechanisms have evolved to counteract environmental threats. *S. pombe* and *S. cerevisiae* are both eukaryotic models that are suitable for systems biology methods as well as for classical and molecular genetics (Vyas *et al.*, 2021). *S. pombe*, a fission yeast, has gained popularity as a research model because it maintains several conserved cellular processes, including the organization of the cell cycle, the presence of introns, and gene and chromosome structures involving telomeres, centromeres, and origins of replication (Kim *et al.*, 2010; Hayles and Nurse, 2016).

In terms of structure, *S. pombe* chromatin has several features common to mammalian cells that are absent or significantly modified in budding yeast, telomeric DNA is ~300 bp in length and is composed of a double-stranded stretch of repeats with the consensus TTAC(A)GG(G_{1-4}) followed by a 5' single stranded overhang of the G-rich strand (Nandakumar and Cech, 2013). Similarly, centromeres in *S. pombe* are considerably larger and more complex than those of budding yeast, and like centromeres of higher eukaryotes contain numerous repeated sequences (French and Straight, 2013; Hayles and Nurse, 2016). In fission yeast, the origin of replication is larger and more complex than the defined origins of replication found in budding yest. *S. pombe* origins are between 0.5 and 3 kb in length and there is no obvious consensus sequence other than AT richness (~ 75% or greater) and a preferential localization within intergenic regions. Several studies using different approaches have given largely similar result about origin number and efficiency during the cell cycle. Fission yeast is estimated to have between 1000-1200 origins, with only a subset of these firing in any one cell cycle (Daigaku *et al.*, 2015; Kaykov and Nurse, 2015; Hayles and Nurse, 2016).

Chromatin modification in fission yeast shows a high degree of conservation with that found in higher eukaryotes (Cam and Whitehall, 2016). Assembly of heterochromatin occurs by posttranslational modification of histones and common feature of these regions of heterochromatin is the presence of repetitive elements. The RNAi pathway is present in *S. pombe* but not in *S. cerevisiae* and is necessary for the assembly of heterochromatin in specialized regions of the genome, ensuring centromere function, mating type silencing, and silencing of repetitive elements (Zofall and Grewal, 2006).

1.1.3 Life cycle of *S. pombe*

Fission yeast is a rod-shaped unicellular eukaryote that can be cultured on minimal or rich media at a temperature range of 25 ^{0}C to 36 ^{0}C, with a generation time of 2 to 4 hours. *S. pombe* can reproduce in either a diploid or a haploid condition, even though most yeast strains used in laboratories are haploid strains (Forsburg, 2003). *S. pombe* can be induced to enter the meiotic cycle when nutrients are scarce (Egel, 1971). Conjugation must occur between two haploid cells of distinct mating types, h^+ and h^-, that are physically near to one another. The cells enter a brief diploid zygotic stage after being conjugated, the zygote subsequently starts the meiotic process, which results in four haploid nuclei. Within the zygote, each of these nuclei grows an ascus, which is a spore wall. Tetrad ascus has a recognizable bending form (zygotic ascus) (Tang, 2016).

The zygote wall lyses and the homologous chromosomes experience possible recombination events when the conditions are suitable for cell development. Four additional haploid cells are created as a result, and they enter the mitotic cell cycle to begin growing vegetatively (Hayles and Nurse, 2016). The resulting diploid cell can be recovered and kept in the vegetative diploid cycle in laboratory settings, if the two haploid cells are given nutrients immediately after their conjugation. Only when a diploid cell receives a mating-type h^+/h composition does it become meiosis-competent and have the potential to initiate meiosis. This diploid cell similarly proceeds through post-zygotic meiosis to produce an ascus with four haploid offspring. Figure 1-1 represents a schematic of life cycle of fission yeast *S. pombe* in haploid and diploid states through vegetative and sexual reproductive stages.

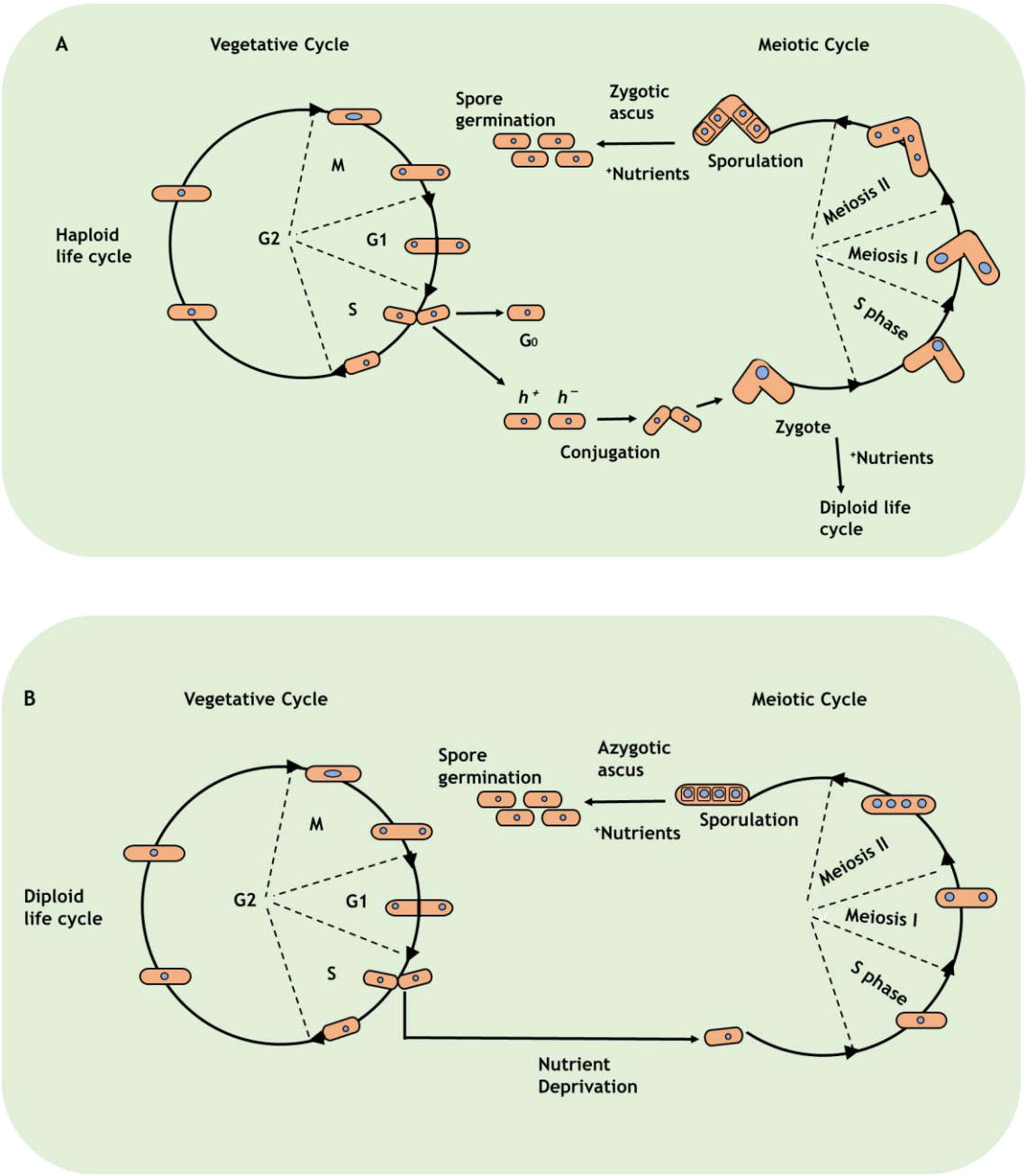

Figure 1-1 Life cycle of fission yeast *S. pombe* in the haploid and diploid state through vegetative and sexual reproduction stages. (**A**) The fission yeast *S. pombe* haploid life cycle. Fission yeast *S. pombe* cells are typically in the haploid life cycle state and can switch between the vegetative and sexual reproductive (meiotic) cycles. Conjugation can be activated between cells of opposite mating types (h^+ and h^-) through stress such as nutrient deprivation, resulting in the brief generation of a zygote that can undergo the meiotic cycle to produce four zygotic spores once nutrient availability improves. Though, if the conditions are regulated, the conjugated zygote is provided with nutrients and can go through and sustain itself as a diplontic cell. (**B**) The fission yeast *S. pombe* diploid life cycle. The diplontic *S. pombe* cell is sustained and propagated under laboratory conditions. The diploid *S. pombe* can be switched between the vegetative and meiotic cycles. When it enters the meiotic cycle, it results in haploid spores that can then re-enter the haplontic life cycle (Adapted and modified from Vyas *et al*., 2021).

1.1.4 Growth and morphology

Fission yeast cells typically attain a length of ~14 μm before undergoing the G_2-M transition, the size at which cells initiates mitosis is modulated by environmental cues such as nutrient level and stress (Fantes and Nurse, 1977). In Inadequate nutrient environments, cells divide at a smaller size than in nutrient-rich media or environment. The size modulation occurs through MAP (mitogen-activated protein) kinase and TOR (target of rapamycin) signalling pathways acting on Cdc25 (Petersen and Russell, 2016). Cell size at mitosis is also affected by Pom1 pathway which acts through Wee1 bringing about Cdc2 Y15 phosphorylation to prevent entry into mitosis (Navarro and Nurse, 2012).

As cells enter mitosis, cell growth ceases as actin is delocalized from the growing ends and becomes localized at the cell center (Hayles and Nurse, 2016). Actin in newly divided daughter cells relocated to the end that was present in the mother cell and growth is initiated. Later in the cell cycle, actin also becomes localized at the new end, formed at septation resulting in initiation of growth at this site, this process is known as new-end takeoff (NETO). During normal cell cycle, NETO is reliant on the attainment of both a certain cell size and DNA replication. (Mitchison and Nurse, 1985). Because *S. pombe* is rod shaped and has this highly polarized growth pattern, it is an excellent model for researching cell morphology. The identification of a range of shape mutants and the development of excellent imaging techniques has been instrumental to our understanding of how cell shape is generated and maintained (Hagan and Badgley, 2016; Mulvihill, 2016; Mclntosh *et al.*, 2016).

Several forms of mutants exhibit defects in microtubules organisation, the positioning and the size of the growth zones (Mishra *et al.*, 2014). The interphase microtubule cytoskeleton consists of three to four bundles of the microtubules orientated with the plus ends toward the cell tips and the minus ends overlapping at the center (Foethke *et al.*, 2009). These microtubule bundles are essential for transporting constituents to the cell end to promote growth along the long axis of the cell, thus maintaining a rod shape (Brunner and Nurse, 2000; Martin, 2009). The defects in the cell wall structure can also lead to cell shape defects suggesting that the cell wall and the cytoskeleton work together to determine the overall shape of the cell (Perez and Ribas, 2016).

Stationary phase in fission yeast has often been compared with the G_0 stage during the cell cycle of multicellular eukaryotes (Hayles and Nurse, 2016). However, there are distinctions between the two cellular states, stationary phase cell (quiescence) has significantly decreased metabolic activity (Su *et al.*, 1996). Whereas G_0 cells are still metabolically active, *S. pombe* cells can enter and exit stationary phase from any phase of the mitotic cell cycle (for example when nitrogen is limited cells arrested in G_1), and if glucose is limited cells arrested in G_2. When the level of nitrogen or glucose is elevated, cells exit the stationary phase and re-enter the cell cycle in G_1 or G_2, respectively (Vyas *et al.*, 2021). Recent metabolomic analysis have admitted that genes required for several processes have been identified that are necessary for both normal proliferation and entry into stationary phase in response to nitrogen starvation (Sajiki *et al.*, 2009).

1.1.5 Mitotic cell cycle in fission yeast

The mitotic cell cycle of fission yeast *S. pombe* comprises sequential G_1, S, G_2, and M phases, which often occur in metazoans (Hagan *et al.*, 2016). In fission yeast, G_2 is typically the longest phase (Hayles and Nurse, 2016). In contrast, budding yeast *S. cerevisiae* cells spend majority of their time in G_1 phase (Alberst *et al.*, 2007). The two yeasts have varied cell cycle characteristics which determine their variant control points in the cell cycle, the G_2/M transition appears as a major visible regulator in the *S. pombe* cell cycle while the G_1/S transition known as *Start,* serves as a notable restriction in the *S. cerevisiae* cell cycle (Vyas e*t al.*, 2021). This describes why most of the cell division cycle (*cdc*) mutants were initially isolated from fission yeast and budding yeast arrest in G_2 and G_1 respectively (Figure 1-1) at the restrictive temperature (Nurse *et al.*, 1976).

The G_1/S regulation can also be uncovered in fission yeast mutants such as *wee1*$^-$ (Figure 1-1). Typically, the G_2/M transition presents the evident and major size control point. Because each cell is of a larger size than that required to pass G_1/S, the control point *Start* is invisible in wild-type cells (Figure 1-1). However, *wee1* mutant cells enter mitosis prematurely and produce new cells smaller than needed for passing through *Start,* which triggers the control at G_1/S transition

and unravels additional restriction points in the *S. pombe* cell cycle (Nurse and Thuriaux, 1980; Hayles and Nurse, 2016). Hence, as in higher eukaryotes, G_1/S transition and G_1/M transition are two control points that regulate the *S. pombe* cycle to guarantee that cells do not initiate DNA replication or enter mitosis, respectively. The cyclin-dependent serine/threonine protein kinase CDK1 (humans) and Cdc2 *(S. pombe)* is needed for the timing and size regulation at which cells progress through both G_1/S and G_2/M transitions in the *S. pombe* (Hayles and Nurse, 2016).

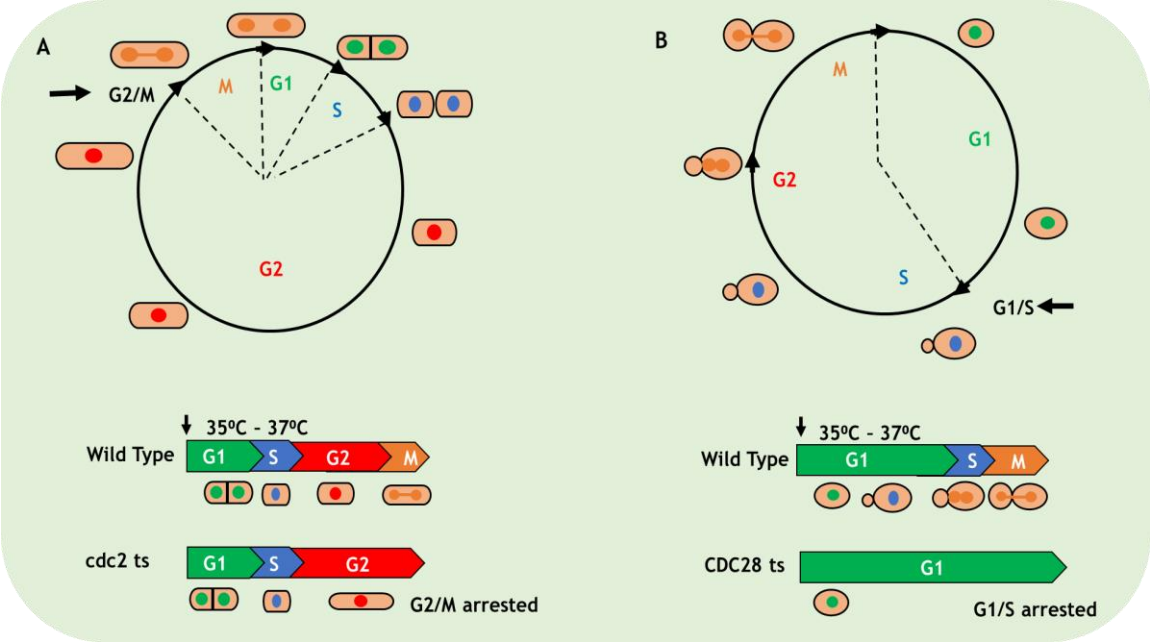

Figure 1-2 Comparison of the mitotic cell cycles between *S. pombe* and *S. cerevisiae*. (**A**) The fission yeast follows the conventional mitotic distinct consecutive G_1, S, G_2, and M phases. A cell typically spends the longest time in the G_2 phase (~70-80%). The daughter nuclei segregate and initiate G_1, however, cytokinesis and the final separation of the new cells do not take place until S-phase. The G_2-M transition is usually the major control point for the cell cycle. Most cell-division cycle (*cdc*) mutants are blocked at G_2 and thus are incapable of entering mitosis displaying a cell elongation phenotype at a restrictive temperature. *Cdc-ts* encodes a master protein kinase that is involved in cell cycle regulation. (**B**) The budding yeast cell cycle features distinct G_1 and S phases, the G_2 and M phases are not clearly defined. The G_1 – S transition is the major control point for the cell cycle. *CDC28-ts* encodes a Cdc2 master protein kinase homolog at the restrictive temperature this mutant cannot progress into S-phase exhibiting a non-budding phenotype (Adapted and modified from Vyas *et al*., 2021).

There are two major controls regulating progress through the cell cycle, the G_1 to S transition and the G_1 to M transition, the highly conserved CDK1 chich form a complex with regulatory cyclin subunit. This is required at both these control points for the timing and size at which cells undergo these transitions (Nurse and Thuriaux, 1980). During the fission cell cycle, the major size control occurs at the G_2-M transition, G_1-S control is cryptic as newly divided cells are of greater cell size than required to undergo the G_1-S transition. However, mutants that enter mitosis and divide at a small cell size to generate newborn cells of smaller than the size requirement for G_1-S transition have a longer G_1 phase before entering S phase (Hayles and Nurse, 2016).

Particularly, as yeast *S. pombe* and *S. cerevisiae* share an analogous process of closed mitosis, in which the nuclear envelope does not break down as it usually does in most multi-cellular animal cells exhibiting a morphology known *as open mitosis* (Vyas *et al.*, 2021). Since fission yeast cells do not complete cytokinesis until the end of G_1 in the following cycle, each cell contains a 2C DNA content through most of the cell cycle stages. Importantly, a key life feature that renders *S. pombe* a powerful model for cell cycle study is it's growth polarity and symmetrical dividing pattern. Unlike *S. cerevisiae,* which divides by medial fission while its cell diameter remains relatively unchanged. Growth polarity allows the cell cycle stages to be followed conveniently and precisely by measuring cell size, specifically cell length thereby permitting detailed analysis of the control in the cell cycle progression. The remarkable contributions of *S. pombe* as a model system for the discovery of fundamental mechanisms governing cell cycle regulation conserved through evolution in eukaryotes will be elaborated further in notable discoveries (Hayles and Nurse, 2016; Vyas *et al.*, 2021).

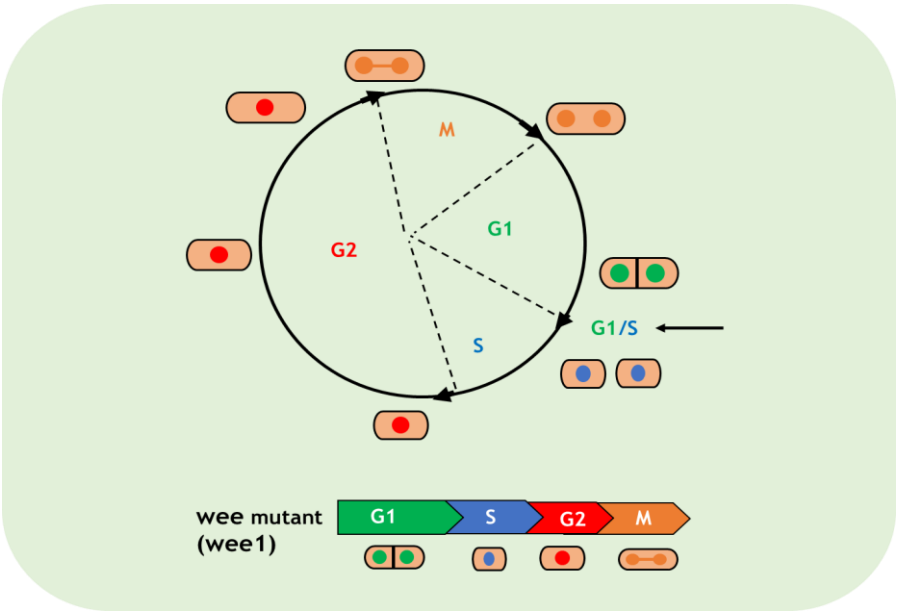

Figure 1-3 A *wee* mutant mitotic cell cycle. Newly dividing *wt* cells are of greater size than that required to enter S phase and thus spend minimal time in G_1. In contrast, *wee* mutant cells enter mitosis at a size that is smaller than that required for undergoing G_1/S. The need to spend more time in G_1 to attain a standard size and then pass through G_1/S. The major control point of cell cycle progression is the G_1/S transition. Therefore, the total cell cycle length is the same for a wild type or a *wee* mutant strain, the difference is the alteration in the length of G_1 and G_2 (Adapted and modified from Vyas *et al.*, 2021).

1.1.6 Mating type locus

The capability of *S. pombe* to switch between haploid and diploid states in response to various conditions provides a powerful tool for research in experimental systems. The mating behaviour of *S. pombe* can be altered and manipulated in the laboratory to modify the organism's ploidy state through minimal changes of its reproduction environment (Vyas *et al.*, 2021). In a haploid strain that harbours a loss-of-function mutation of a gene, the recessive trait can be readily displayed under proper conditions such as restrictive temperature, which would be otherwise masked due to the presence of a dominant wild-type allele in a diploid strain. This technique has proven to be a effective strategy for genetically dissecting a variety of cellular processes, particularly the elements in the regulatory circuits of the cell cycle (Kim *et al.*, 2010).

The birth of *S. pombe* as research model organism came about during Leupold's quest to identify the genetic mating type locus in this species now known as a complex region harbouring expressed and silenced gene. The major factor dictating conjugation is the presence of two different *pombe* is identified by the expression of either the P allele or the M allele from the mating-type locus (Leupold, 1950). The mating-type locus is on Chromosome 2 and consist of three transcriptional loci *mat1, mat2-P and mat3-M*, the *mat2-P* and *mat3-M* alleles act as information donors for the *mat1 locus* (Beach and Klar, 1984).

In homothallic strains, those that can find conjugation partners in the same culture, the *mat1* locus can undergo spontaneous switching with either the *mat2* or the *mat3* locus via replication recombination events (Beach and Klar, 1984). The strain expresses either the P or the M factor as a result of the switching, respectively. The most used homothallic strain is h^{90} strain which may switch its mating type at the *mat1* locus every 3 generations (>90% of cells in a culture at a time). Hence, about half the cells in the culture of h^{90} mating type strain would express the P factor while the other half express the M factor facilitating conjugation. In contrast to the homothallic strains, heterothallic strains are restricted to only expressing either the P or M factor from the *mat2* or *mat3* locus respectively (Egel *et al.*, 1984). The two most used heterothallic strains are 972 h^- and 975 h^+. The h^+ strain only has a transcriptionally active *mat2P* locus while the h^- strain is only transcriptionally active at its *mat3M* locus for the informational switch *mat1*.

Nutritional deprivation or starvation conditions induce the heterothallic mating types h^+ and h^- strains to conjugate with each other and undergo meiotic sporulation. A similar circumstance also initiates the homothallic mating-type strain h^{90} to either mate with itself or with either of the heterothallic strains. However, zygotic diploids are only formed between strains with opposite mating types h^+ and h^- from heterothallic strains or homothallic h^{90} strains. A diploid homozygous for either h^+ or h^- is incompetent for meiosis and sporulation (Hoffman *et al.*, 2015).

1.1.7 Fission yeast as a model organism

S. pombe possesses a typical eukaryotic cell cycle that exhibits a strongly polarized growth pattern and has definite shape features that make it very useful for studying processes such as mitotic and meiotic cell cycle, cell shape and cellular growth (Hayles and Nurse, 2016). It can also be used for the study of developmental switches that occur in response to environmental cues such as those that control the transition between the vegetative and sexual life cycles, *S. pombe genome* consist of only three chromosomes of 5.6, 4.8, and 3.6 Mb respectively. Genome organisation in *S. pombe* shows several features also found in higher eukaryotes (Petrova *et al.*, 2013), the telomeres, centromeres and origins of replication are more similar to complex eukaryotes than is the for budding yeast (Wood *et al.*, 2002).

S. pombe has excellent classical and molecular genetics which has the enabled the isolation of many mutants to study specific cell and molecular biological processes (Ekwall and Thon, 2016). They introduced the basic classical genetic protocols and described how these are used to isolate mutants in processes of interest. Johanne Murray and colleagues described the basic molecular genetic techniques available for research (Murray *et al.*, 2016). *S. pombe* was the fourth eukaryote to be sequenced and it is 14-Mb genome currently has 5059 protein coding genes annotated of which 67% are conserved in humans (Wood *et al.*, 2002). The sequencing and annotation of the *S. pombe* genome paved the way for the development of range of methodologies for genome wide analyses in fission yeast (High Throughput Quantitative Genetic Interaction Mapping in the Fission yeast *Schizosaccharomyces pombe*) (Roguev *et al.*, 2016).

1.2 Cytokinesis in fission yeast

Cell division is an essential and irreversible step in the life cycle to ensure accurate segregation into daughter cells of a specific cell shape and size. The strategies that cell use to regulate the position of the division plane must take into account both the global geometry of the cell as well as the position of the genetic material (Rincon and Paoletti, 2012). The formation and constriction of medially positioned actomyosin ring determines the division plane position in *S. pombe,* which is largely depends on the anillin-like protein Mid1p (Rincon and Paoletti, 2012; Rezig *et al.*, 2022). The process of separating cellular components to create two daughter cells is known as cytokinesis (Figure 1-4), progression of these events is controlled by mechanisms and proteins that are evolutionary conserved in eukaryotes (Rezig *et al.*, 2022).

The development and subsequent constriction of an actomyosin contractile ring, as the ring constricts, facilitate furrow formation and abscission (Hercyk *et al.*, 2019). Cytokinesis nodes are assemblies of stoichiometric proportions of proteins linked with the plasma membrane, which act as basics for the contractile ring during cytokinesis by fission yeast (Sayyad and Pollard, 2022). The actomyosin ring is assembled during cytokinesis in fission yeast, where it undergoes constriction concurrently as the septum and the membrane furrow are formed (Pollard 2010; Sayyad and Pollard, 2022).

Cell division facilitated by a contractile ring is common in all cellular organism, the cleavage furrow assembled at the division site where the actomyosin ring (actin, myosin, and other protein) called the contractile ring causes a furrow (Cheffings *et al.*, 2016). The ring then contracts to create a membrane barrier between the cytoplasmic contents of each daughter cell. The ingression furrow constricts the spindle midzone components into a dense structure called the midbody. The furrow seals generation complete separate cells in a process called abscission (Green *et al.*, 2012). During cytokinesis Figure 1-4, a contractile ring generates the constricting force to separate a cell into two daughters. This ring is composed of filamentous actin, the motor protein myosin, and additional structural and regulatory proteins, including anillin (Kim *et al.*, 2017).

Fission yeast cells divide by medial cleavage using actin-based contractile rings, prior to anaphase, the ring develops in the centre of the cell during mitosis (Figure 1-4). The actin ring compresses as the septum establishes the place designated by the actin ring at the conclusion of mitosis. The two daughter cells are separated by the septum's digestion process (Rezig *et al.*, 2022). Cellular mechanisms are associated with the progression of mitosis to ensure the copying and equal distribution of genetic materials amongst the two daughter cells before physical separation (Green *et al.*, 2012). Cytokinesis by fission yeast is compromised by the loss of anillin/Mid1p function, because cytokinesis organizing centres, called nodes, are misplaced and fail to acquire myosin-II, so they assemble slowly into abnormal contractile rings (Chatterjee and Pollard, 2019).

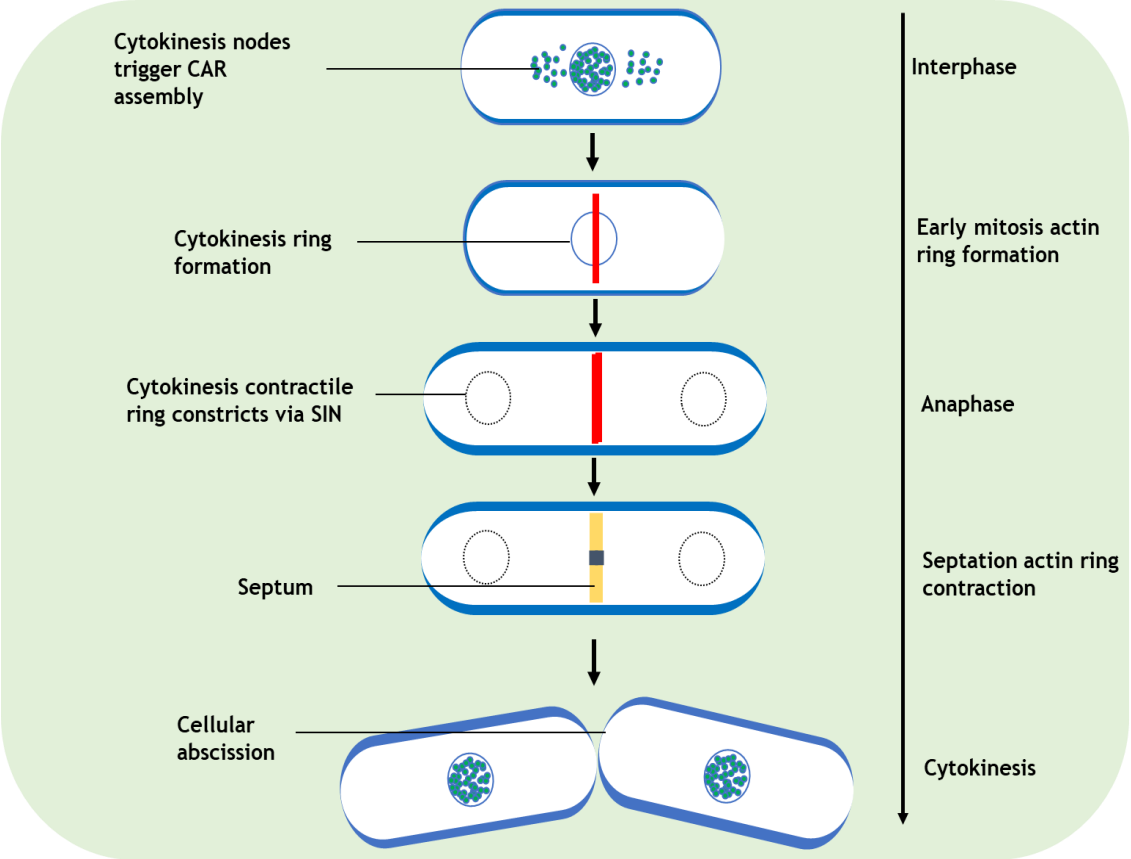

Figure 1-4 Cell division in *S. pombe*. During interphase cells localized to the cortical patches, in early mitosis contractile in (red) forms in the middle of the cell. The ring denotes the position of septum formation and contracts the cell wall septum (yellow) develops from the surface. The septum advanced and absorbed away leading to separation of the two daughter cells having separate nuclei and cytoplasm.

1.2.1 Mid1p in spatiotemporal control of CR formation

In fission yeast, Mid1p (also known a Dmf1p) plays an important role in positioning the division site by inducing the formation and progression of contractile (CR). Mid1p, emanating from the nucleus located in the cell centre forms many of nodes in the cell cortex ahead of mitosis, and actin filaments and myosin II accumulate at each node to interact and assemble the CR in metaphase (Yasuda *et al.*, 2016). During the CR-dependent cytokinesis of eukaryotes organism, the interaction of filamentous actin (F-actin) and myosin II in the CR are thought to generate forces to constrict the cell just beneath the cleavage furrow, enabling them to divide into two daughter cells. The molecular mechanism of the mitosis-specific assembly of F-actin and myosin II in CR formation at the proper region beneath the plasma is not entirely clear (Yasuda *et al.*, 2016).

S. pombe has shown that the nucleocytoplasmic shuttling protein Mid1p plays a central role in the spatiotemporal control of CR formation (Rincon and Paoletti, 2012). Mid1p has a nuclear localization signal (NLC), a nuclear exclusion signal (NES), and an amphipathic sequence followed by a pleckstrin homology (PH) domain located at the C-terminal which is considered important for its function Rezig *et al.*, 2021). During interphase (Figure 1-5), most Mid1p is located in the nucleus, but the residual amount of Mid1p from cortical dots called interphase nodes by interacting with the Cdr2p kinase and other proteins associated with the nodes (Rincon *et al.*, 2014). This distribution of interphase nodes is restricted to the middle of the cell by exclusion from cell tips by the Pom1p kinases.

As the G2 phase progresses, the amount of Mid1p at the equatorial cortex, a region proximal to the nucleus positioning in the centre of interphase cells, increases and other components such as Gef2p, Blt1p, and Klp8p localizes to the interphase nodes (Akamatsu *et al.*, 2014). Just after a cell enters mitosis, Cdr2p and other proteins are released from the interphase nodes, and Mid1p and its associated protein form cytokinetic nodes together with an IQGAP-like protein Rng2p, myosin II consisting of the heavy chain Myo2p and light chains Rlc1p and Cdc4p, an F-BAR domain protein Cdc15p and formin Cdc12p (Wu *et al.*, 2003; Wu *et al.*, 2006). The cytokinesis nodes induce a cortical actin-myosin meshwork

encircling the future division site in the cell middle and are merged and as result, the CR assembled before the onset of anaphase (Yasuda *et al*., 2016). Figure 1-5 represent a schematic of Sib2 temporal regulates Cdr2p-Mid1p associate for successful cell division.

In *S. pombe,* gene disruption of *mid1* is detrimental for cell proliferation at high temperatures and causes severe defects in the spatiotemporal control of the CR formation. This position and orientation of the CR are frequently disturbed in *mid1* deletion cells (Paoletti and Chang, 2000), and the timing of CR components accumulation is delayed in the mutants than that in the wild-type cells (Motegi *et al*., 2004; Huang *et al*., 2008). This discordance on the timing of CR construction between the two *Schizosaccharomyces species* may entail that the molecular mechanism controlling CR formation and development differ between the two fission yeast, because *Schizosaccharomyces japonicus* cells without Mid1p function still carried out symmetrical binary division (Yasuda *et al*., 2016). Thus, Mid1p plays a central role in the spatiotemporal control of CR formation in *S. pombe*.

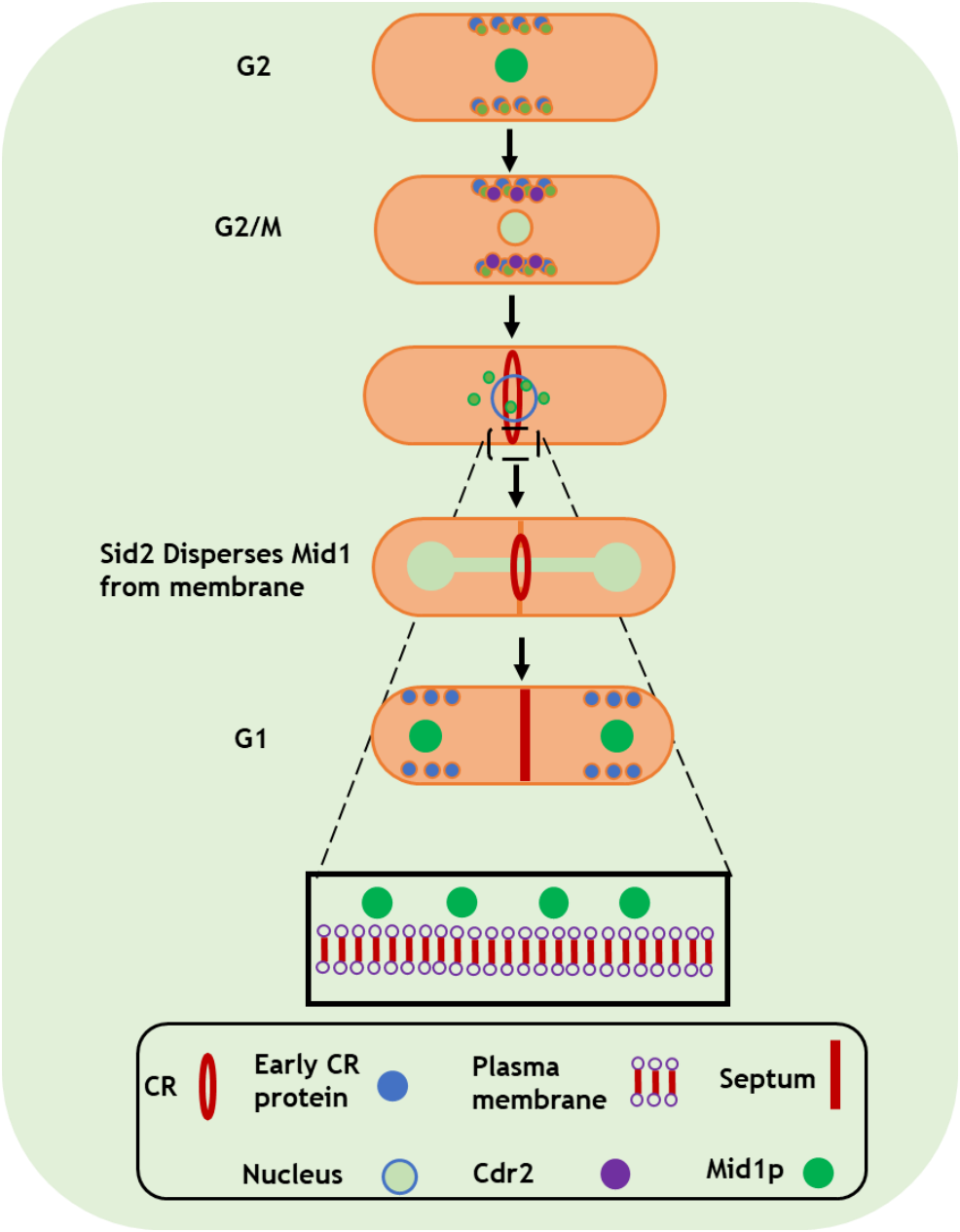

Figure 1-5 A schematics of Sid2p temporally regulates Cdr2p-Mid1p association. CR forms mid-cell during mitosis from clusters of protein at the medial cell cortex**.** Anillin-like Mid1p is a substrate of SIN kinase Sid2 and localizes to the nodes, SIN signalling controls Mid1p membrane localization and Sid2p temporally regulates Cdr2p-Mid1p association while Cdr2p and Mid1p are key SIN substrates for resetting cell division site placement, CR represent contractile ring (Adapted and modified from Willet *et al*., 2019).

1.2.2 Structure and molecular function of Mid1p

Mid1p has a structural similarity to anillin, which plays an important role in animal cell cytokinesis (Piekny and Maddox, 2010). To ensure the progression of cytokinesis, anillin functionally interacts with F-actin, myosin II, septin, and the plasma membrane, under the control of Roh-type small GTPases (Piekny and Glotzer, 2008). Both Mid1p and anillin share a conserved sequence called an anillin homology domain (AHD) that forms a C2 domain-like structure with a lipid-binding amphipathic region followed by a PH domain at the C-terminal (Sun *et al.*, 2015). However, it is still unclear whether anillin and Mid1p share a common ancestral gene.

Mid1p is crucial for the biological functions of septa and is required for their precise positioning and orientation during the *S. pombe* cell cycle. Although necessary but insufficient for the localization of full-length Mid1p to cortical nodes, are the residues 1-149 (Saha and Pollard, 2012). However, residues 1–452 facilitate Mid1p roles including localization and accumulation in cortical nodes during mitosis, while residues 1–578 are essential for the assembly of several node elements comprising Myo2p and Cdc15, and residues 579–797 look like the insoluble domain of Mid1p that enable the condensation of nodes into the actin-myosin contractile ring (ACR). Residues 798–920 of Mid1p comprise the C-terminal PH domain (Sohrmann *et al.*, 1996; Saha and Pollard 2012). Both the C2 lipid-attachment domain and the PH domain are two membrane anchoring components found in the Mid1p structure (Sun *et al.*, 2015).

The Mid1p-N452 domain is composed of the Mid1p N-terminal residues (1-452), largely disordered, and this flexible nature may enable the export of Mid1p from the nucleus through early mitosis (Chatterjee and Pollard, 2019). Interestingly, this domain of Mid1p comprises many residues that are phosphorylated. This appears to control the self-association of Mid1p-N452. Current examples indicate that phosphorylation by Plo1p might regulate Mid1p export from the nucleus by “solubilizing” the protein, as non-phosphorylated Mid1p-N452 has an enhanced tendency to accumulate. Of note, this domain does not interact with Myso2p (Chatterjee and Pollard, 2019). Figure 1-6 represents schematics of Mid1p domains and their role during mitosis and cytokinesis in *S. pombe*.

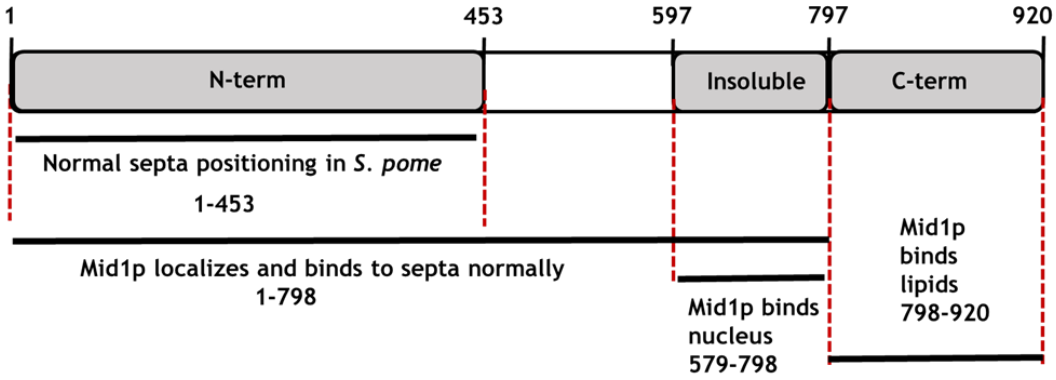

Figure 1-6 A schematic of Mid1p domains and their role during mitosis and cytokinesis in *S. pombe*. Mid1p residues 1-453 resemble the N-terminal domain, Mid1p residues 579-797 resemble the insoluble domain and Mid1p residues 798-920 resemble the C-terminal PH domain. Red broken lines represent Mid1p domain boundaries. Black lines represent fragments of Mid1p sufficient for the role denoted below in each line (Adapted and modified from Saha and Pollard, 2012)

It is important to note that both mammalian anillin and *S. pombe* Mid1p share functional and operational similarities, thus both are multi-domain scaffolding proteins and connect the cell cortex with the ACR during mammalian cell development (Piekny and Glotzer, 2008), and during cytokinesis in *S. pombe* respectively (Akamatsu *et al.*, 2014). Likewise, effective analysis of mammalian anillin and *S. pombe* Mid1p revealed that proteins have cryptic membrane-associating components and bind to membrane lipids through a C2 cryptic domain (Sun *et al.*, 2015).

1.2.3 Phospho-regulation of Mid1p

Phospho-regulation of Mid1p is necessary to control *S. pombe* events beginning with Mid1p free from the nucleus to promote the interaction of Mid1p with interphase nodes moving into the mitotic entry. Mid1p association with interphase node, and final removal of Mid1p from cell cortex during the late stage of cytokinesis (Almonacid *et al.*, 2011; Willet *et al.*, 2019; Magliozzi *et al.*, 2020). The phosphorylation of Mid1p N-terminal region which contains residues (1-452): Mid1p-N452. Researchers utilized two techniques: the disorder-enhanced phosphorylation predictor (DISPHOS) device to estimate phosphorylation sites, and matrix-assisted laser desorption/ionization (MALDI)

mass spectrometry which identifies phosphorylated residues (Chatterjee and Pollard, 2019). Such evaluations validated Mid1pN452 phosphorylation by six of the nine accepted consensus Sid2p phosphorylation sites (Chen *et al.*, 2008), three of four minimal consensus Cdk1p phosphorylation sites. (Swaffer *et al.*, 2016), and one of the eight accepted consensus Plo1p phosphorylation sites (Suzuki *et al.*, 2015).

Early primary studies explained a physical collaboration between the *S. pombe* polo-like kinase Plo1p and Mid1p proteins and this interaction was necessary for the correct and proper localization of Mid1p to the actin-myosin contractile ring (ACR) (Bähler *et al.*, 1998). It was afterward corroborated that phosphorylation of residues within the first 100 amino acids of the N-terminal region of Mid1p by Plo1p activates Mid1p release from the nucleus and promotes the interaction of Mid1p with interphase nodes leading to mitotic entry (Almonacid *et al.*, 2011). Thus, such phosphorylation also enables Myo2p recruitment to medial cortical nodes. Even though Mid1p has a regulatory role in ACR medial assembly, the NDR-family kinase Sid2p has a regulatory obligation during the later stages of cytokinesis to promote ring constriction and septation leading to the end of cell division. However, Mid1p leaves from the site of division at ACR constriction onset (Sohrmann *et al.*, 1996) this event occurs concurrently with precise translocation of Sid2p from spindle pole bodies (SPBs) to the ACR, Sid2p consensus phosphorylation motifs are discovered in Mid1p amino acid sequence (Sparks *et al.*, 1999; Chen *et al.*, 2008).

According to research by Willet *et al.* (2019), Mid1p phospho-deficient mutant is unable to be phosphorylated by Sid2p kinase and remains strongly tied and attached to the plasma membrane throughout cytokinesis. Additionally, after completion of cell division, this mutant over-assembles in interphase nodes and triggers too early recruitment of ACR proteins to interphase nodes. The finding also confirmed and demonstrated that phosphorylation of Mid1p by Sid2p on amino acid residues within the N-terminal domain 1–578; furthermore, it provided evidence that the removal of Mid1p from the cell cortex is determined by this phosphorylation event (Willet *et al.*, 2019).

According to research by Magliozzi *et al*. (2020), Cdc42-triggered polarity kinase (Pak1p) is localized to the assembly ACR and retains this localization throughout septation. In this research, large-scale phospho-proteomic testing and screening identified Mid1p and Cdc15p as Pak1p substrates. Disrupting the Pak1p/Mid1p signaling pathway and mechanism created damaged, defective, and misplaced ACRs; nevertheless, such damaged and defective phenotypes are rescued by synthetic tethering of Mid1p to cortical nodes. Thereby suggested that Pak1p phosphorylation of the N-terminal region of Mid1p stimulates its association with interphase nodes (Magliozzi *et al*., 2020). Remarkably, the N-terminal region of Mid1p is phospho-regulated and controlled by three kinases. Phosphorylation by Plo1p stimulates Mid1p nuclear transfer and the commencement of mitosis (Almonacid *et al*., 2011), phosphorylation by Pak1p promotes Mid1p interaction with interphase nodes (Magliozzi *et al*., 2020), and phosphorylation by Sid2p stimulates Mid1p removal from the cell cortex (Willet *et al*., 2019). Figure 1-7 represents the schematic of Mid1p phospho-regulation sites identified in different research findings.

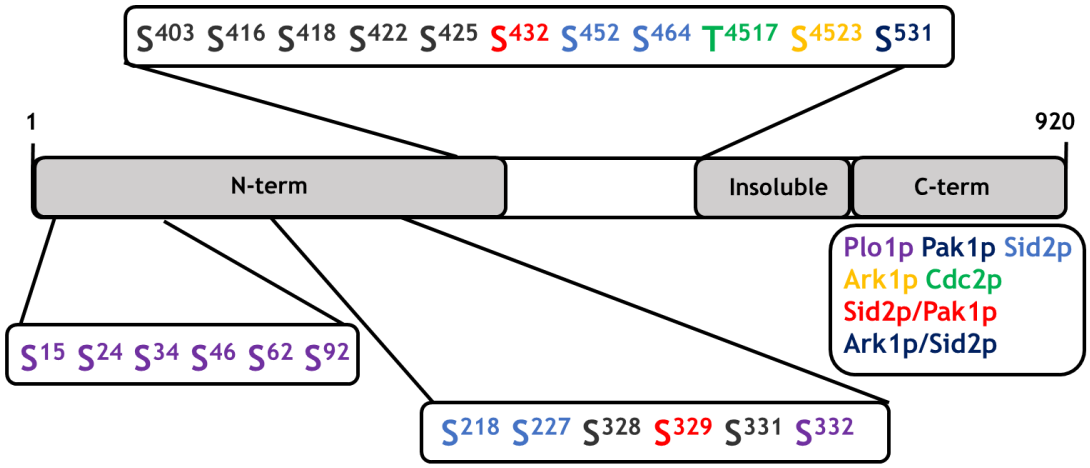

Figure 1-7 Schematic of *S. pombe* Mid1p phospho-regulation sites. Identified and mapped phosphorylation sites of Mid1p domain structure by Plo1p (Almonacid *et al*., 2011; Rezig *et al*., 2021), Cdc2p (Almonacid *et al*., 2011), Pak1p (Magliozzi *et al*., 2020), Ark1p (Rezig *et al*., 2021) and Sid2p (Willet *et al*., 2019). These phospho-sites play a crucial role and function during cell cycle events in *S. pombe*.

Recent fascinating findings revealed the genetic interactions in *S. pombe* between classes of genes: *mid1*, *vps4*, and aurora kinase *ark1*. Genetic interactions were identified among the *mid1* gene, *vps4* gene, and *ark1* gene, such interactions imply a relationship between the regulation of Mid1p's function by both Vps4p and Ark1p (Bhutta *et al.*, 2014; Rezig *et al.*, 2021). Additionally, it was discovered that Vps4p physically interacts with the C-terminal region of Mid1p, which is important for the localization of Mid1p cell cycle. It emerges that the function of Mid1p is partially controlled by interaction with Vps4p, with this interaction directly or indirectly with Mid1p PH domain cell cortex anchorage to control Mid1p-dependent node cortical attachment to promote medial division (Rezig *et al.*, 2021). Mid1p phospho-regulation was investigated by three approaches: *in vitro* phosphorylation studies, mass spectrometry (nLC-MS/MS) evaluation and probing published *S. pombe* global proteomic data. Such methods identified numerous amino acid residues as possible phospho-acceptor sites in Mid1p by aurora and polo-like kinases with S332, S523, and S531 needed for the absolute function of Mid1p in *S. pombe* (Rezig *et al.*, 2021).

1.3 ESCRT complex and cytokinesis

ESCRT (endosomal sorting complexes required for transport) are highly conserved protein machinery that drives a diverse set of physiological and pathological membrane remodelling processes (Azad *et al.*, 2023). ESCRT system was first characterized in yeast giving the scenario of how this system is structured to drive the sorting of endocytosed receptors meant to degrade in the lysosome (Sadoul *et al.*, 2018). The ESCRT complex catalyses many divergent membrane remodelling processes including the formation of multivesicular endosomes (MVEs), cytokinesis, nuclear envelope formation, membrane repair, autophagy, and enveloped virus budding yeast (Sadoul *et al.*, 2018; Azad *et al.*, 2023). Similarly, ESCRT complex encompasses multiple proteins and subcomplexes, and is important for membrane remodelling in eukaryotic cells, in processes that include ubiquitin-mediated multivesicular body formation, membrane repair, cytokinetic abscission, and virus exit from host cells (Hatano *et al.*, 2022).

The ESCRT complex consists of ESCRT-0, ESCRT-I, ESCRT-II, and ESCRT-III complexes, and associate protein ALIX, and the AAA^+ ATPase Vps4. All except ESCRT-III contain at least one ubiquitin-binding subunit. Studies on the assembly of ESCRT in yeast and later structural studies have indicated a sequential function of ESCRT-I, ESCRT-II, and ESCRT-III, a mechanism that seems to be conserved across the eukaryotic lineages (Paez Valencia *et al.*, 2016). These proteins act in sequence to bind, bend, deform, and cut membranes during membrane trafficking, cell division, viral ingress, and other important topologically similar membrane remodelling events in eukaryotes (Olmos *et al.*, 2015; Hatano *et al.*, 2022).

When driving the formation of multivesicular bodies (MVBs), the role of ESCRT in membrane trafficking and cellular transport has been best characterized, the ESCRT complex is recruited to endosomal membranes by ubiquitylated trans-membrane proteins that are targeted to the vesicles (Raiborg and Stenmark, 2009). The ubiquitin moiety is identified by ESCRT-0 and ESCRT-I sub-complex (Katzmann *et al.*, 2001). The ESCRT-III undergoes assembly and disassembly cycles, which involve the activity of the AAA-ATPase SKD1/VPS4 for the disassembly of the complex (Paez Valencia *et al.*, 2016). To complete cytokinesis events, cells need to cleave the intercellular bridge, a membrane structure enriched in microtubules linking the two daughter cells (Merigliano *et al.*, 2021). This cleavage step named abscission is primarily operated and regulated by the ESCRT complexes and ESCRT-associates such as AAA-ATPase Vps4 (Carlton, 2010; Schoneberg *et al.*, 2017).

1.3.1 ESCRT complex sub-divisional function

The ESCRT-0 complex is required to sort plasma membrane proteins into MVB pathways in animal cells and for MVB biogenesis in yeast. ESCRT-0 attaches to and clusters ubiquitinated cargo for delivery into MVBs and recruits clathrin, ubiquitin ligases, and de-ubiquitinating enzymes (Hurley, 2010). ECSRT-0 is recruited on endosomes on the cytoplasmic side of trans-membrane proteins becoming confined to small membrane domains where recruitment of ESCRT-I and ESCRT-II occurs (Sadoul *et al.*, 2018). ESCRT-0 is a complex of Vps27, Hse 1 and (hepatocyte growth factor regulated tyrosine kinase substrate HRS) and

(signal transducing adaptor molecule STAM-I/STAM-II) in eukaryotic cells, Vps27/HRS domain localizes ESCRT-0 and thus the entire machinery through Ptdlns(3)-rich endosomes (Ren *et al.*, 2009; Stoten and Carlton, 2017). Vps27/HRS and Hse1/STAM both contain ubiquitin interacting motifs (UIMs), highlighting ESCRT-0 as a critical endosomal ubiquitin cargo receptor (Shields and Piper, 2011). The ESCRT machinery performs both the cargo and membrane remodelling functions (Stoten and Carlton, 2018).

ESCRT-I complex is a rod-shaped hetero-tetrameric complex that co-assembles with ESCRT II on the membrane to interact with a variety of adaptor proteins to localize this machinery to subcellular localizations (Kostelansky *et al.*, 2007; Hurley, 2010). ESCRT-I appears to be able to act independently of ESCRT-II, however, ESCRT-I and ESCRT-II contain ubiquitin-binding domains that participate in the transfer of ubiquitinated cargo onto nascent intraluminal vesicles (Alam *et al.*, 2004; Slagsvold *et al.*, 2005). These complexes act at the bud neck of invaginating vesicles and are localized to endosomal membranes through interaction with ubiquitinated cargo binding complex (Wollert and Hurley, 2010). Figure 1-8 represents schematics of ESCRT-II-mediate coupling of IVL formation with cargo sorting role. Physical sequestration of the transmembrane cargoes that will be bundled into IVL and demarcation of the membrane surface section that is sculpted into the cargo filled ILV. ESCRT-0 and ESCRT-I concentrates transmembrane cargo along the lipid interacting with the cargoes. Subsequent recruitment and activation of ESCR-II cause ESCRT-III polymerization. Vps4-mediated constriction of ESCRT-III results in the deepening of the membrane invagination and ultimately fission of the IVL neck (Mageswaran *et al.*, 2014).

The ESCRT-II complex can bind directly to the charged multivesicular proteins CHMP6 subunit of ESCRT-III and so links upstream ESCRT activity with the proposed membrane remodelling complex and is noteworthy to state that ESCRT-II is the vital partner of ESCRT-I in MVB biogenesis, bud formation, and functions in MVB sorting in yeast (Babst *et al.*, 2002; Henne *et al.*, 2012). ESCRT-II is the most important of the two complexes involved in MVB biogenesis since overexpression of ESCRT-II can rescue deletions of ESCRT-I genes in yeast, but not vice versa (Babst *et al.*, 2002). Despite its central role in MVB biogenesis and membrane budding, ESCRT-II happens to be non-essential for cytokinesis (Morita

et al., 2007b). Recent data suggest an interesting alternative explanation that ESCRT-II behaves as an assistive linker between ESCRT-I and ESCRT-III during cytokinesis (Goliand *et al.*, 2014; Christ *et al.*, 2016).

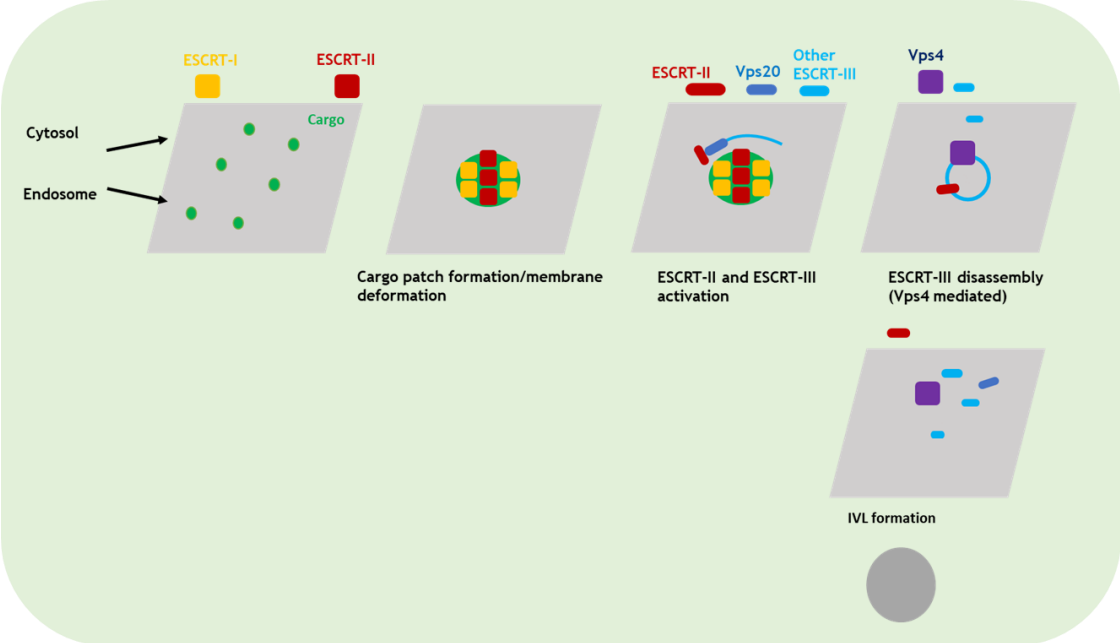

Figure 1-8 Schematic of ESCRT-II-mediated coupling of IVL formation with cargo sorting. The early ESCRT complex (ESCRT-0 and ESCRT-I) concentrates transmembrane cargo along with lipids interacting with the cargoes. The resulting cargo-lipid patch deforms the endosomal membrane. Subsequent recruitment and activation of ESCR-II cause ESCRT-III polymerization. Vps4-mediated constriction of ESCRT-III results in the deepening of the membrane invagination and ultimately fission of the IVL neck. In the absence of ESCRT-0 and ESCRT-I, ESCRT-II randomly initiates ESCRT polymerization. However, in the absence of a cargo patch, Vps4-mediated remodelling of ESCRT-III does not result in IVL formation (Adapted and modified from Mageswaran *et al.*, 2014).

The ESCRT-III complex is the principal membrane scission machine at the heart of the ESCRT system (Azad *et al.*, 2023). ESCRT-III shapes membranes and in most cases cooperates with VPS4 ATPase to facilitate fission membrane necks from the inside (Sadoul., *et al.*, 2023). ESCRT-III comprises a polymer of small self-assembling proteins which in mammalian cells are known as CHMPs (charged multivesicular body proteins/chromatin remodelling proteins) and the CHMP-like protein, increased sodium tolerance-1 (IST1) (Stauffer *et al.*, 2001; Howard *et al.*, 2001; Babst *et al.*, 2002). CHMPs contain 5 to 6 recognizable alpha helices and occur in soluble or filament-forming conformations, the transition between states is controlled by the dislocation of a C-terminal controlling helix which is

thought to drive assembly and membrane remodelling (Saksena *et al.*, 2009; Henne *et al.*, 2012). Remarkably, ESCRT-III proteins comprise C-terminal peptide states called MIT-domain interaction motifs (MIMs) that engage the microtubule interaction and trafficking (MIT)-domain of an evolutionarily conserved AAA-ATPase called Vps4 (Scott *et al.*, 2005; Bauer *et al.*, 2015).

Vps4 signifies the sole energy-consuming component of this pathway and is required for recycling and disassembling ESCRT-III filaments (Stoten and Carlton 2018). The particular mechanism of ESCRT-III-dependent membrane separation remains a matter of intense debate, in recent finding that ESCRT-III spirals force individual CHMP subunits to assume energetically unfavourable confirmations has permitted the proposal that these spiral filaments procedures an elastic spring that can store energy and later release it for membrane deformation or scission (Shen *et al.*, 2014; Chiaruttini *et al.*, 2015; Carlson *et al.*, 2015). Similarly, ATP consumption by Vps4 has been suggested to disassemble and remodel the ESCRT-III filament, which may contribute to its activity in membrane fission (Alonso *et al.*, 2016; Mierzwa *et al.*, 2017).

A variety of suggestions for Vps4-depending on the regulation of ESCRT-III have been proposed, culminating in biophysical models such as “dome” or “reverse dome” where the progressive constriction of an ESCRT-III filament, capped by dome-shaped subcomplex of CHMP2/CHMP3 is thought to reduce the energetic barrier of severing the membranous stalk and achieving membrane fission (Fabrikant *et al.*, 2009; Schoneberg *et al.*, 2017). Vtal is an ESCRT protein that binds to Vps4 and promotes its oligomerization activity and ESCRT-III binding (Yeo *et al.*, 2003; Shestakova *et al.*, 2010). Although Vtal is not constitutively associated with Vps4 in the cytosol as are the subunits of ESCRT 0-II, for practical purposes Vps4 and Vtal function together as a complex in MVB biogenesis and other Vps4-dependent pathways. Deletion of Vtal does not have as severe a defect in cargo sorting as deletion of Vps4 (Yeo *et al.*, 2003; Shiflett *et al.*, 2004).

1.3.2 Abscission

Abscission is the final stage of cytokinesis, Cep55 a coiled protein is thought to engage ESCRTs complex, specifically ECSRT-III is recruited to the midbody to complete abscission (Little and Dwyer, 2021). Furrow ingression contracts the central spindle microtubules inside the intercellular bridge, forming a midbody with a central bulge and two flanks (Figure 1-9). Within the midbody narrowing and severing of the bridge continue, midbody is enriched with hundreds of proteins, many of which facilitate and regulate abscission (Addi *et al.*, 2020). As the midbody continues and matures, the flanks thin constriction sites from each flank adjacent to the central bulge, and scission usually occurs sequentially at the constriction sites on both sides (McNeely and Dwyer, 2020).

Abscission involves the disassembly of microtubules and plasma membrane remodelling at the constriction sites. These disassembly and membrane remodelling occur concurrently, a conserved membrane remodelling system applied in diverse cellular processes and pathways. Assembly of the ESCRT complex continues as a recruitment cascade through site-specific targeting factors, ESCRT-III complex components assemble into spiral filaments that progressively remodel and constrict the membrane (Stoten and Carlton, 2018). In the final stage of abscission, CEP55 accumulates in a disk at the midbody centre by attaching KIF23/MKLP1. CEP55 attaches and recruits ALIX and the ESCRT-I TSG101, both ALIX and TSG101 in turn recruit ESCRT-III elements through two parallel pathways (Morita *et al.*, 2007, Christ *et al.*, 2016; Stoten and Carlton 2018). Figure 1-9 represents a schematic of cytokinetic abscission and the specific role of CEP-55, Tsg101, and ALIX during abscission.

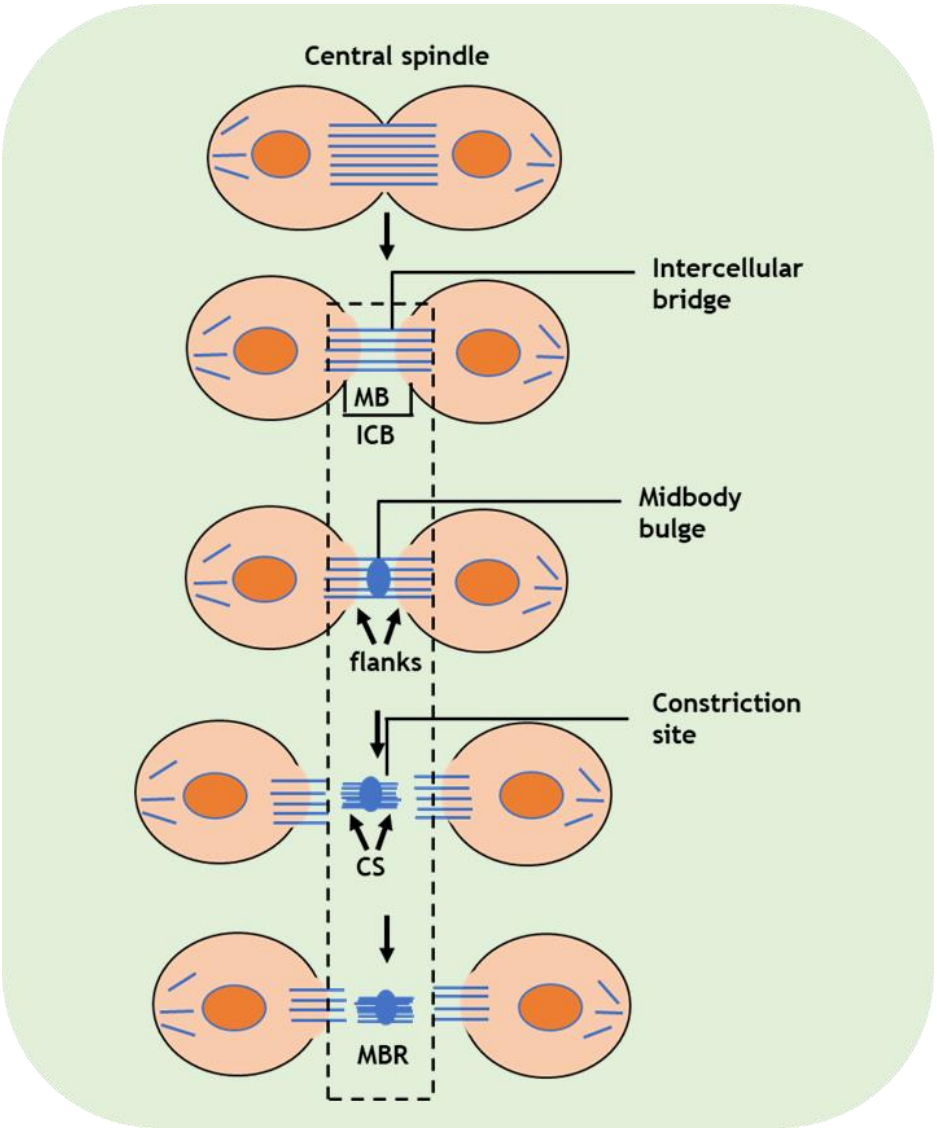

Figure 1-9 Schematic of cytokinetic abscission. Typically, both flanks are severed sequentially but, in some cells, only one side may be cut. CEP-55 recruits the ESCRT-I Tsg101 and ALIX which form a ring, and both Tsg101 and ALIX interact to recruit ESCRT-III components in a parallel pathway. ESCRT-III then forms filaments that progressively narrow the midbody at the constriction sites to mediate abscission. Microtubules must be removed, and the plasma membrane remodelled. MB, midbody, ICB intercellular bridge, CS constriction site, MBR midbody remnant (Adapted and modified from Little and Dwyer, 2021).

1.3.3 ESCRTs traffic during abscission

Endocytic membrane transport has emerged as a crucial process required for effective completion of cytokinesis, specific endocytic membranes act with the cytoskeleton and ESCRT proteins to regulate the various stages of cytokinesis (Schiel and Prekeris, 2013). The end of the cell cycle terminates in a very complex and vastly arranged physical separation of daughter cells, known as cytokinesis. It was originally thought that plant and animal cells divide by completely different means, however recent studies showed a lot of molecular and mechanistic similarities (Pollard and O'Shaughnessy, 2019).

Studies demonstrate that membrane trafficking and subsequent membrane fusion is an important step during cytokinesis in eukaryotic cells, numerous organisms have shown that membranes originating from the Golgi apparatus and endosomes are trafficked to the intracellular bridge (ICB) of dividing cells and are required for both early and late steps of cytokinesis (Schiel and Prekeris, 2013). Membrane transport has been shown to be important in regulating the early phases of cytokinesis, the identity, and spatiotemporal properties of identified organelles during late cell division remain unclear (Schiel *et al.*, 2011).

The membrane cleavage during abscission happens at sites in the intercellular bridge that are observed to "thin" just before abscission. Through the abscission, one side of the midbody bulge narrows and tightens, the microtubules are severed, and the membrane is entirely cleaved (Neto and Gould, 2011). Both Tsg101 and the ESCRT-III subunit CHMP4B are sequentially recruited into the centre of the intercellular bridge where they develop a series of cortical rings (Elia *et al.*, 2011; Stoten and Carlton, 2018). Later during cytokinesis, CHMP4B accumulates at the narrow constriction zones, Vps4 then follows CHMP4B to this site and abscission takes place almost immediately (Elia *et al.*, 2011).

At the sites of microtubule assembly in HeLa cells, the cortex of the intercellular bridge ingression to a thin stalk (presumably analogous to the thinned secondary ingression or constriction zone) and is deformed by regular spaced electron-dense "ripple" at either side of the midbody. The ESCRT-III subunits including

CHMP4B extend on the way to these sites of cortical constriction, suggesting that the polymerization of ESCRT-III facilitates the formation of these constriction zones (Guizetti *et al.*, 2011). ESCRT-III complex or CHMP2A is necessary for the formation of filaments, these filaments are intertwined around the sites of constriction thus offering the view that these filaments generate the contractile force needed for membrane scission (Elia *et l.*, 2011; Guizetti *et al.*, 2011). Figure 1-10 represents a schematic molecular mechanism of ESCRTs within the midbody and how they interact with other classes of proteins to drive abscission.

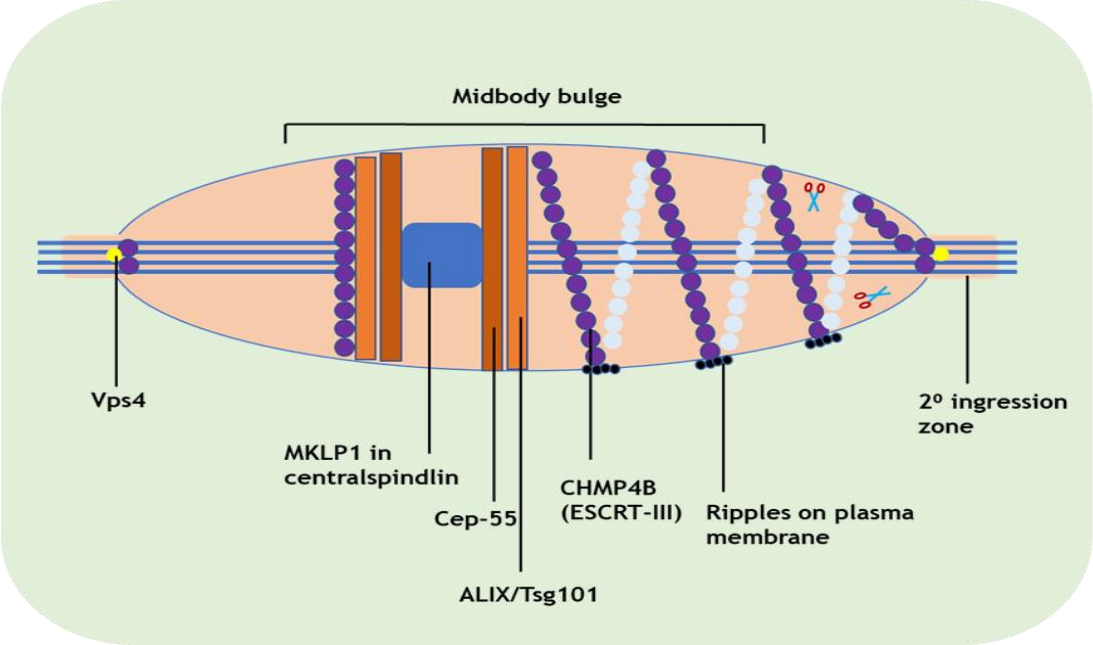

Figure 1-10 ESCRTs drives abscission. The centralspindlin element recruits Cep-55 to the midbody. Cep-55 then interacts with ESCRT-I protein Tsg101/ALIX which in turn recruits ESCRT-III elements. Both Tsg101 and ESCRT-III subunit CHMP4B are shown as purple spheres and are sequentially recruited into the centre of the intercellular bridge where they create a sequence of cortical rings. Later during cytokinesis, CHMP4B accumulates at the narrow secondary abscission zones closely followed by Vps4 shown in yellow spheres which leads to abscission at these sites. CHMP4B creates two narrow cortical rings adjacent to the midbody before the assembly of the microtubules. ESCRT-III subunits (CHMP4B) continue towards these sites of the vital constriction forming a series of intertwined, regularly spaced, filaments that extend towards the site of secondary ingression. These rings also give rise to the emergence of a “ripple” on the plasma membrane, ESCRT-III then recruits the microtubule-severing enzyme spastin (Adapted and modified from Neto and Gould, 2011).

1.3.4 Actin-microtubule interactions during cell division

The post-anaphase array (PAA) of microtubules in fission yeast accumulates along the plane of the contractile ring, and its accumulation relies on the Myp2p-dependent recruitment of Mto1p, a part of equatorial microtubule organizing centers (eMTOCs). The general structure of this array of microtubules and the impact on their physical attachment to the contractile ring and the actin-microtubule interactions are critical for cell division (Bellingham-Johnstun *et al.*, 2023). Microtubules construct the mitotic spindle during cell division while the actin network gathers and accumulates the contractile ring at the division plane. Actin-microtubule interactions during cell division are well-established in higher eukaryotes. Interactions between the cortical actin complex that lines the inside of the plasma membrane, and the spindle microtubules position the spindle within the cell while the spindle determines the location of the assembly of the contractile ring (Laan *et al.*, 2012; Bringmann and Hyman, 2005).

Contrary to research and findings, our understanding of the function and effects of actin-microtubule interactions during cell division in fission yeast, a popular model organism for research on cell division is restricted. During cytokinesis in fission yeast, the PAA microtubules polymerize from specialized eMTOCs connected to the actin network of the contractile ring (Pardo and Nurse, 2003, Samejima *et al.*, 2010). Mto1p and its dimerization partner Mto2p, gamma-tubulin complex linker proteins and important components of eMTOCs, promote the polymerization of different microtubule networks all through the cell cycle. The recruitment of Mto1p to the contractile ring depends on the presence of myosin-II Myp2p and the activation of both the Septation Initiation Network and the Anaphase Promoting Complex (Samejima *et al.*, 2010). The physical interactions between the stiff PAA microtubules and the more flexible actin filaments may impact the mechanical properties of the contractile ring and affect cytokinesis (Bellingham-Johnstun *et al.*, 2023).

The PAA microtubules have different purported functions including attaching the contractile ring to the plasma membrane/cell wall and positioning the separated daughter nuclei after anaphase (Mana-Capelli *et al.*, 2012). Therefore, if PAA microtubules anchor the contractile ring, these physical interactions between

microtubules and actin filaments may influence cytokinesis. Alternatively, the PAA microtubules may utilize the contractile ring for their assembly as a positional scaffold without any functional gain for the contractile ring (Bellingham-Johnstun *et al.*, 2023). The PAA microtubules impact the mechanical properties of the contractile ring by granting stiffness to the ring during constriction. Although they correct the stiffness of the contractile ring, the ring is assembled and constricted naturally in the absence of PAA microtubules. Contrary to previously proposed models, the PAA microtubules do not anchor the ring at the division plane. Therefore, PAA microtubules exploit the contractile ring to scaffold their assembly (Bellingham-Johnstun *et al.*, 2023).

Actin and microtubules frequently interact, these physical interactions alter their mechanical properties and influence their cellular functions (Dogterom and Koenderink, 2019; Preciado *et al.*, 2014). The microtubule and actin cytoskeleton physically interact during cytokinesis in fission yeast, recently discoveries showed the molecular organization of the contractile ring and its mechanical properties (Bellingham-Johnstun *et al.*, 2021; McDargh *et al.*, 2021; Bellingham-Johnstun *et al.*, 2022; Moshtohry *et al.*, 2022). Such an extensive understanding of cytokinesis in fission yeast enables us to dig into the actin-microtubule crosstalk's impact in *vivo* cytokinesis. Fission yeast was used to investigate the impact of PAA microtubules on the actin contractile ring and cytokinesis. The study was leveraged on a particular mutation in *mto1*, *mto1-427*, to specifically eliminate PAA microtubules and test the outcome on cytokinesis. The timing analysis supports the sequential assembly of the PAA microtubule following Myp2p recruitment to the contractile ring with Myp2p arriving at the ring first, rapidly followed by Mto1p/eMTOCs, PAA microtubules and eventually Ase1p crosslinkers (Bellingham-Johnstun *et al.*, 2023). This progressive assembly is consistent with the previous observation that the actin network and Myp2p are required for Mto1p and eMTOCs recruitment to the contractile ring (Samejima *et al.*, 2010).

Myp2p and Mto1p assemble into a protein complex and may directly interact, according to co-immunoprecipitation studies using yeast two-hybrids and whole-cell extracts (Bellingham-Johnstun *et al.*, 2023). This remarkable finding establishes that the presence of Myp2p is required for Mto1p recruitment, but

this recruitment may not be dependent on the concentration of Myp2p in the ring. Collectively, the results propose that Myp2p facilitates the recruitment of Mto1p without forming a specific complex with Mto1p. One possible mechanism for Myp2p to facilitate Mto1p recruitment could be that Myp2p modifies the actin network in a way that enables the local recruitment of Mto1p to the inner face of the contractile ring. Alternatively, if Mto1p forms a protein complex with Myp2p, this complex would only assemble locally, on the inside portion of the Myp2p ring, which may spatially restrict the localization of Mto1p and limit the total amount of Mto1p recruitment. (Bellingham-Johnstun *et al.*, 2023).

1.3.5 Relevance of the cell cycle to diseases

Cell division and cell mortality are important predominant physiological processes that regulate homeostasis in eukaryotic organisms, anillin is vital for cell division, development, and homeostasis in metazoans (Zhivotoskiy and Orrenius, 2010). Recent findings revealed that levels of anillin correlate to the metastatic potential of human and eukaryotes tumours (Rezig *et al.*, 2022). The importance of dysregulation of these in the pathogenesis of major diseases such as cancer, and neurodegenerative disorder is becoming increasingly evident (Zhivotoskiy and Orrenius, 2010; Chuang *et al.*, 2014). The modification of the protein sequence and protein kinases involved in cytokinesis affects the natural cell processes and progression during cell division that may lead to the failure of cytokinesis.

In eukaryotic cells, positive signals produced by the central spindle with anillin linking the ACR to the cell cortex ensure the medial placement of the ACR (Piekny *et al.*, 2008). The scaffold protein anillin is vital for cytokinesis regulation and inhibition resulting in cytokinesis failure and cell multi-nucleation (Oegema *et al.*, 2000). Anillin is composed of two functional regions, one the N-terminal region, which triggers actin polymerization and myosin-II stimulation progressing to the assemblage of a steady ACR (Piekny and Maddox, 2010), and two the C-terminal region connected with RhoA, septins, and $PI(2,4)P_2$ linking the ARC to the cell cortex (Field *et al.*, 2005; Sun *et al.*, 2015). Anillin are substrates for mitotic kinases and their enrolment to the equatorial membrane is controlled by phosphorylation. Kim and associates discovered phosphorylation of

a single residue, S635, as a vital determinant facilitating cytokinesis controlling anillin's recruitment to the equatorial cortex and facilitating stabilization of the cleavage furrow (Kim *et al.*, 2017). After its discovery, anillin was explored mainly by cell and developmental biologists to find out the sequential events of cell separation, without being associated with human disease (Rezig *et al.*, 2021)

S. pombe offered data on the role of membrane lipids during cytokinesis. First, the proper localization of the PI4 kinase Stt4p by its scaffold subunit Efr3p was shown to play a vital function in the spatial regulation of cytokinesis by blocking the CR from sliding to one cell tip during anaphase (Baird *et al.*, 2008). Likewise, defects in the spatial regulation of cytokinesis at the start of mitosis have been described in the PI-5 kinase *its3-1* mutant, characterized by decreasing levels of phosphatidylinositol 3, 5-bisphosphate (Snider *et al.*, 2018). Secondly, defects during cytokinesis, as well as cell morphology and cell wall organization, were observed in mutants of Pps1p, involved in phosphatidylserine (PS) synthesis (Matsuo *et al.*, 2007). Lastly, defects during sphingolipid hydrolysis into ceramide in *css1* mutant were displayed to induce defects in the cell wall and septum formation, due to the accumulation of α and ß-glucans in the periplasmic space with cell division arrest and a lethal outcome (Feoktisova *et al.*, 2001).

The defective control of this step can either lead to cell death or aneuploidy, and can gradually promote cancer progression (Maddox *et al.*, 2012). Cell division either cytokinesis is a vital process required for the proliferation of unicellular organisms as well as for the development of multicellular organisms and renewal within tissues, the final step cytokinesis ensures the physical separation of the two daughter cells with equal nucleus and cytoplasm (Rincon and Paoletti, 2017).

1.4 Aims and objectives

This study aimed to investigate the important processes using a range of molecular and biological methods to understand the roles, interactions, and functions of Mid1p using *S. pombe*. This project explored a genetic approach to analyse the potential interaction between gene encoding *mid1* and ESCRT-associate *vps4* genes in fission yeast, as both classes of proteins are universally conserved and when mutated cause growth defect in fission yeast and diseases in humans. This study focused on understand the role of anillin/Mid1p and ESCRT-Vps4p associated protein in the regulation of cytokinesis in fission yeast. We belief that this study will provide valuable information in fission yeast genetics and biochemistry using a range of molecular biology techniques.

Specific objectives include:

- To investigate and characterize the genetic interactions between *mid1* and *vps4* genes during cytokinesis in *S. pombe*, and to identify important phosphorylation sites that regulate Mid1p during cytokinesis in *S. pombe* cell division.

- To identify the physical interaction between the N-terminal, Middle, and C-terminal domains of the Mid1p and Vps4p proteins using an *in vitro* biochemical approach.

- Quantify and analyse the different cell septation phenotypes, localization frequency, and distribution of Mid1p in GFP-*mid1* phospho-mutants in *S. pombe* strains.

Chapter 2 Materials and Methods

2. 1 Materials

2.1.1 Media and strains

All *S. pome* and *Escherichia coli* (*E. coli*) media were prepared in one litre of distilled water and autoclaved before use. Solid media were prepared by adding 20 g/l Bacto agar to one litre of medium (*S. pombe*. YE, ME or EMM, or LB) before autoclaving. They were then poured into 90 mm Petri dishes and allowed to room temperature to solidify. For the typical solid medium ~ 20 ml per Petri dish was poured, while for the thin solid YE medium for micro-manipulation of tetrads ~10 ml per Petri dish was poured.

2.1.2 *S. pombe* media

S. pombe cells were cultured and maintained as previously described (Moreno *et al.*, 1991; Rezig *et al.*, 2019).

Mating medium (limiting for nitrogen): Malt Extract (ME)
30 g Bacto malt extract

Rich complete medium: Yeast Extract (YE)
30 g D-glucose, 5 g Bacto yeast extract, 225 mg adenine, and 225 mg uracil.

Selective medium: Edinburgh Minimum Medium (EMM)
20 g D-glucose, 5 g NH_4CL, 0.1 g Na_2SO_4, 0.1 g $MgCL_2$, 15 mg $CaCL_2$, 3 g $C_8H_5KO_4$, 1.8 g Na_2HPO_4, 1 ml vitamins (per litre of distilled H_2O: 10 g inositol, 10 g nicotinic acid, 1 g calcium pantothenate, and 10 mg biotin) and 0.1 ml trace minerals (per litre of distilled H_2O: 5 g boric acid, 5.2 g $MnSO_4$, 4 g $ZnSO_4$, 2 g $FeCL_3$, 1.44 g molybdic acid, 0.4 g $CuSO_4$, 10 g citric acid and 0.1 g KI).

2.1.3 *S. pombe* strains

Each *S. pombe* (fission yeast) strain produced during this research was provided with a University of Glasgow laboratory reference "GG" annotation number and stored long-term in 30% glycerol at -80ºC (Table 2-1).

GG No.	Genotype	Annotation
1	h- 972	wild-type (W-T)
397	h+ *ade6-210 leu1-32 ura4-D18*	
400	h- *ade6-216 leu1-32 ura4-D18*	
1129	h- *mid1*::*ura4*+ *ura4-D18 leu1-32*	*mid1*Δ
1167	h- *plo1-ts35 ura4-D18 leu1-32*	*plo-ts35*
1347	pmid-*mid1*-4GFP (integrated; pAP221; *leu1*+) h- *dmf1*::*ura4*+ *ura4*-D18 *leu1-32*	Mid1p-GFP
1349	pmid-NLS*-*mid1*-GFP (integrated; pAP167#2; *leu1*+) h- *dmf1*::*ura4*+ *ura4-D18 leu1-32*	
1384	pAM19 (D450-506 *mid1*:*12myc*:*leu1*+) h- *dmf1*::*ura4*+*ura4-D18 leu1-32*	
1388	pAM23 (*NLS*mid1*:*12myc*:*leu1*+) h- *dmf1*::*ura4*+ *ura4-D18 leu1-32*	
1554	h+ *dmf1*::*kanMX4 ura4-D18 leu1-32 ade*+	*mid1*Δ
1622	h- *vps4*::*ura4*+ *leu1-32 ura4-D18 ade*+	*vps4*Δ
2417	h+ *ark1-T11*<<kanR *leu1-32 ade*+	*ark1-T11*
2432	h+ *ark1*-T8<<kanR *leu1-32 ade*+	*ark1*-T8
2451	h+ *ark1-T11*<<kanR *ura4-C190T leu1-32*	*ark1-T11*
2673	h+ *vps4*::*ura4*+ *leu1-32 ura4-D18 ade*+	*vps4*Δ
2674	pmid-*mid1*-4GFP (integrated; pAP221; *leu1*+) h- *dmf1*::*ura4*+*ura4-D18? leu1-32 vps4*::*ura4*+	*vps4*Δ Mid1p-GFP
2709	pmid-*mid1*-4GFP (integrated; pAP221; *leu1*+) h- *dmf1*::*ura4*+*ura4-D18? leu1-32 vps4*::*ura4*+	*vps4*Δ Mid1p-GFP
2886	pmid-*mid1*-4GFP (integrated; pAP221; *leu1*+) h- *dmf1*::*ura4*+*ura4-D18? leu1-32 ark1-T11*<<kanR	*ark1-T11* Mid1p-GFP
2922	pmid-mid1-4GFP (integrated; pAP221; *leu1*+) h+ *dmf1*::*ura4*+ *ura4-D18 leu1-32 ark1*-T8<<kanR	*ark1-T8* Mid1p-GFP
3100	NLS* *mid1*:*12myc*:*leu1*+ h- *dmf1*::*ura4*+ *vps4*::*ura4*+ *ura4-D18 leu1-32*	
3107	D450-506 *mid1*:*12myc*:*leu1*+ h- *dmf1*::*ura4*+ *vps4*::*ura4*+ *ura4-D18 leu1-32*	
3181	pJK148:*mid1*+ (wild-type) *mid1*ΔpJK148:*mid1*+h- *mid1*::*ura4*+ *ura4-D18 leu1-32*	
3185	pJK148:*mid1* S523 to A523 h- *mid1*::*ura4*+ *ura4-D18 leu1-32*	
3189	pJK148:*mid1* S523 to D523 h- *mid1*::*ura4*+ *ura4-D18 leu1-32*	
3193	pJK148:*mid1* S531 to A531 h- *mid1*::*ura4*+ *ura4-D18 leu1-32*	

GG No.	Genotype Annotation
3197	pJK148:*mid1* S531 to D531 h⁻ *mid1*::*ura4*⁺ *ura4-D18 leu1-32*
3201	pJK148:*mid1* S523+S531 to A523+A531 h⁻ *mid1*::*ura4*⁺ *ura4-D18 leu1-32*
3205	pJK148:*mid1* S523+S531 to D523+D531 h⁻ *mid1*::*ura4*⁺ *ura4-D18 leu1-32*
3218	pJK148:*mid1* S523 to A523 h? *mid1*::*ura4*⁺ *ark1-T11*<<kanR *ade*⁺
3224	pJK148:*mid1* S523 to A523 h? *mid1*::*ura4*⁺ *vps4*::*ura4+ura4-D18 leu1-32*
3230	pJK148:*mid1* S523 to D523 h? *mid1*::*ura4*⁺ *ark1-T11*<<kanR *ura4-C190T leu1-32*
3235	pJK148:*mid1* S531 to A531 h? *mid1*::*ura4*⁺ *ark1-T11*<<kanR *ura4-C190T leu1-32*
3239	pJK148:*mid1* S531 to D531 h? *mid1*::*ura4*⁺ *ark1-T11*<<kanR *ura4-C190T leu1-32*
3242	pJK148:*mid1* S523 to A523+S531 to A531 h? *mid1*::*ura4*⁺ *ark1-T11*<<kanR *ura4-C190T leu1-32*
3246	pJK148:*mid1* S523+S531 to D523+D531 h? *mid1*::*ura4*⁺ *ark1-T11*<<kanR *ura4-C190T leu1-32*
3249	pJK148:*mid1* S523 to A523 h? *mid1*::*ura4*⁺ *vps4*::*ura4+ura4-D18 leu1-32*
3250	pJK148:*mid1* (wild-type) *mid1*Δ pJK148:*mid1*⁺ *ark1-T11* h? *mid1*::*ura4*⁺ *ark1-T11*<<kanR *ura4-C190T leu1-32*
3255	pJK148:*mid1* S523 to A523 h? *mid1*::*ura4*⁺ *vps4*::*ura4+ura4-D18 leu1-32*
3256	pJK148:*mid1* S523 to A523 h? *mid1*::*ura4*⁺ *vps4*::*ura4+ura4-D18 leu1-32*
3257	pJK148:*mid1* S523+S531 to D523+D531 h⁻ *mid1*::*ura4*⁺ *vps4*::*ura4+ ura4-D18 leu1-32*
3258	pJK148:*mid1* S523+S531 to D523+D531 h⁻ *mid1*::*ura4*⁺ *vps4*::*ura4+ ura4-D18 leu1-32*
3260	pJK148:*mid1* S523+S531 to A523+A531 h? *mid1*::*ura4*⁺ *vps4*::*ura4*⁺ *ura4-D18 leu1-32*
3264	pJK148:mid1 S531 to D531 h? *mid1*::*ura4*⁺ *vps4*::*ura4*⁺ *ura4-D18 leu1-32*
3267	pJK148:*mid1* S167 to A167 h⁻ *mid1*::*ura4*⁺ *ura4-D18 leu1-32*
3271	pJK148:*mid1* S167 to D167 h⁻ *mid1*::*ura4*⁺ *ura4-D18 leu1-32*

GG No.	Genotype Annotation
3275	pJK148:*mid1* S328 to A328 h⁻ *mid1*::*ura4*⁺ *ura4-D18 leu1-32*
3280	pJK148:*mid1* S328 to D328 h⁻ *mid1*::*ura4*⁺ *ura4-D18 leu1-32*
3283	pJK148:*mid1* S331 to A331 h⁻ *mid1*::*ura4*⁺ *ura4-D18 leu1-32*
3290	pJK148:*mid1* S331 to D331 h⁻ *mid1*::*ura4*⁺ *ura4-D18 leu1-32*
3291	pJK148:*mid1* S332 to A332 h⁻ *mid1*::*ura4*⁺ *ura4-D18 leu1-32*
3295	pJK148:*mid1* S332 to D332 h⁻ *mid1*::*ura4*⁺ *ura4-D18 leu1-32*
3299	pJK148:*mid1* S167+S328+S331+S332 to A167+A328+A331+A332 h⁻ *mid1*::*ura4*⁺ *ura4-D18 leu1-32*
3305	pJK148:*mid1* S167+S328+S331+S332 to D167+D328+D331+D332 h⁻ *mid1*::*ura4*⁺ *ura4-D18 leu1-32*
3307	pJK148:*mid1* S167+S328+S331+S332+S523+S531 to A167+A328+A331+A332+A523+A531 h⁻ *mid1*::*ura4*⁺ *ura4-D18 leu1-32*
3311	pJK148:*mid1* S167+S328+S331+S332+S523+S531 to D167+D328+D331+D332+D523+D531 h⁻ *mid1*::*ura4*⁺ *ura4-D18 leu1-32*
3315	pJK148:*mid1* S523 to D523 h? *mid1*::*ura4*⁺ *vps4*::*ura4+ ura4-D18 leu1-32*
3316	pJK148:*mid1* S523 to D523 h? *mid1*::*ura4*⁺ *vps4*::*ura4+ ura4-D18 leu1-32*
3317	pJK148:*mid1* S523 to D523 h? *mid1*::*ura4*⁺ *vps4*::*ura4+ ura4-D18 leu1-32*
3318	pJK148:*mid1* S531 to A531 h? *mid1*::*ura4*⁺ *vps4*::*ura4+ ura4-D18 leu1-32*
3319	pJK148:*mid1* S531 to A531 h? *mid1*::*ura4*⁺ *vps4*::*ura4+ ura4-D18 leu1-32*
3320	pJK148:*mid1* S531 to A531 h? *mid1*::*ura4*⁺ *vps4*::*ura4+ ura4-D18 leu1-32*
3321	pJK148:*mid1* S167 to A167 h? *mid1*::*ura4*⁺ *ark1-T11*<<kanR ura4-C190T *leu1-32*
3322	pJK148:*mid1* S167 to A167 h? *mid1*::*ura4*⁺ *ark1-T11*<<kanR ura4-C190T *leu1-32*
3323	pJK148:*mid1* S167 to A167 h? *mid1*::*ura4*⁺ *ark1-T11*<<kanR ura4-C190T *leu1-32*

GG No.	Genotype Annotation
3324	JK148:*mid1* S167 to D167 h? *mid1*::*ura4*+ *ark1-T11*<<kanR *ura4-C190T leu1-32*
3325	JK148:*mid1* S167 to D167 h? *mid1*::*ura4*+ *ark1-T11*<<kanR *ura4-C190T leu1-32*
3326	JK148:*mid1* S167 to D167 h? *mid1*::*ura4*+ *ark1-T11*<<kanR *ura4-C190T leu1-32*
3327	pJK148:*mid1* S328 to A328 h? *mid1*::*ura4*+ *ark1-T11*<<kanR *ura4-C190T leu1-32*
3328	pJK148:*mid1* S328 to A328 h? *mid1*::*ura4*+ *ark1-T11*<<kanR *ura4-C190T leu1-32*
3329	pJK148:*mid1* S328 to A328 h? *mid1*::*ura4*+ *ark1-T11*<<kanR *ura4-C190T leu1-32*
3330	pJK148:*mid1* S328 to D328 h? *mid1*::*ura4*+ *ark1-T11*<<kanR *ura4*-C190T *leu1-32*
3331	pJK148:*mid1* S328 to D328 h? *mid1*::*ura4*+ *ark1-T11*<<kanR *ura4*-C190T *leu1-32*
3332	pJK148:*mid1* S328 to D328 h? *mid1*::*ura4*+ *ark1-T11*<<kanR *ura4*-C190T *leu1-32*
3333	pJK148:*mid1* S331 to A331 h? *mid1*::*ura4*+ *ark1-T11*<<kanR *ura4-C190T leu1-32*
3336	pJK148:*mid1* S331 to D331 h? *mid1*::*ura4*+ *ark1-T11*<<kanR *ura4-C190T leu1-32*
3339	pJK148:*mid1* S332 to A332 h? *mid1*::*ura4*+ *ark1-T11*<<kanR *ura4-C190T leu1-32*
3340	pJK148:*mid1* S332 to A332 h? *mid1*::*ura4*+ *ark1-T11*<<kanR *ura4-C190T leu1-32*
3341	pJK148:*mid1* S332 to A332 h? *mid1*::*ura4*+ *ark1-T11*<<kanR *ura4-C190T leu1-32*
3342	pJK148:*mid1* S332 to D332 h? *mid1*::*ura4*+ *ark1-T11*<<kanR *ura4-C190T leu1-32*
3343	pJK148:*mid1* S332 to D332 h? *mid1*::*ura4*+ *ark1-T11*<<kanR *ura4-C190T leu1-32*
3344	pJK148:*mid1* S332 to D332 h? *mid1*::*ura4*+ *ark1-T11*<<kanR *ura4-C190T leu1-32*
3345	pJK148:*mid1* S167+S328+S331+S332 to A167+A328+A331+A332 h? *mid1*::*ura4*+ *ark1-T11*<<kanR *ura4-C190T leu1-32*
3346	pJK148:*mid1* S167+S328+S331+S332 to A167+A328+A331+A332 h? *mid1*::*ura4*+ *ark1-T11*<<kanR *ura4-C190T leu1-32*
3347	pJK148:*mid1* S167+S328+S331+S332 to A167+A328+A331+A332 h? *mid1*::*ura4*+ *ark1-T11*<<kanR *ura4-C190T leu1-32*

GG No.	Genotype Annotation
3349	pJK148:*mid1* S167+S328+S331+S332 to D167+D328+D331+D332 h? *mid1*::*ura4*+ *ark1-T11*<<kanR *ura4-C190T leu1-32*
3350	pJK148:*mid1* S167+S328+S331+S332 to D167+D328+D331+D332 h? *mid1*::*ura4*+ *ark1-T11*<<kanR *ura4-C190T leu1-32*
3351	pJK148:*mid1* S167+S328+S331+S332 to D167+D328+D331+D332 h? *mid1*::*ura4*+ *ark1-T11*<<kanR *ura4-C190T leu1-32*
3352	pJK148:*mid1* S167+S328+S331+S332+S523+S531 to A167+A328+A331+A332+A523+A531 h? *mid1*::*ura4*+ *ark1-T11*<<kanR *ura4-C190T leu1-32*
3353	pJK148:*mid1* S167+S328+S331+S332+S523+S531 to A167+A328+A331+A332+A523+A531 h? *mid1*::*ura4*+ *ark1-T11*<<kanR *ura4-C190T leu1-32*
3354	pJK148:*mid1* S167+S328+S331+S332+S523+S531 to A167+A328+A331+A332+A523+A531 h? *mid1*::*ura4*+ *ark1-T11*<<kanR *ura4-C190T leu1-32*
3355	pJK148:*mid1* S167+S328+S331+S332+S523+S531 to D167+D328+D331+D332+D523+D531 h? *mid1*::*ura4*+ *ark1-T11*<<kanR *ura4-C190T leu1-32*
3356	pJK148:*mid1* S167+S328+S331+S332+S523+S531 to D167+D328+D331+D332+D523+D531 h? *mid1*::*ura4*+ *ark1-T11*<<kanR *ura4-C190T leu1-32*
3357	pJK148:*mid1* S167+S328+S331+S332+S523+S531 to D167+D328+D331+D332+D523+D531 h? *mid1*::*ura4*+ *ark1-T11*<<kanR *ura4-C190T leu1-32*
3375	pJK148:*mid1* S167 to A167 h? *mid1*::*ura4*+ *plo1-ts35 ura4-D18 leu1-32*
3376	pJK148:*mid1* S167 to A167 h? *mid1*::*ura4*+ *plo1-ts35 ura4-D18 leu1-32*
3378	pJK148:mid1 S167 to D167 h? *mid1*::*ura4*+ *plo1-ts35 ura4-D18 leu1-32*
3377	pJK148:mid1 S167 to D167 h? *mid1*::*ura4*+ *plo1-ts35 ura4-D18 leu1-32*
3378	pJK148:mid1 S167 to D167 h? *mid1*::*ura4*+ *plo1-ts35 ura4-D18 leu1-32*
3379	pJK148:*mid1* S167 to A167 h? *mid1*::*ura4*+ *plo1-ts35 ura4-D18 leu1-32*
3381	pJK148:*mid1* S167 to A167 h? *mid1*::*ura4*+ *plo1-ts35 ura4-D18 leu1-32*
3383	pJK148:*mid1* S167 to A167 h? *mid1*::*ura4*+ *vps4*::*ura4*+ *ura4-D18 leu1-32*

GG No.	Genotype Annotation
3384	pJK148:*mid1* S167 to A167 h? *mid1*::*ura4*+ *vps4*::*ura4*+ *ura4-D18 leu1-32*
3452	pJK148:*mid1* S167 to A167 h? *mid1*::*ura4*+ *vps4*::*ura4*+ *ura4-D18 leu1-32*
3386	pJK148:*mid1* S328 to D328 h? *mid1*::*ura4*+ *plo1-ts35 ura4-D18 leu1-32*
3387	pJK148:*mid1* S328 to D328 h? *mid1*::*ura4*+ *plo1-ts35 ura4-D18 leu1-32*
3388	pJK148:*mid1* S328 to D328 h? *mid1*::*ura4*+ *plo1-ts35 ura4-D18 leu1-32*
3392	pJK148:*mid1* S328 to A328 h? *mid1*::*ura4*+ *plo1-ts35 ura4-D18 leu1-32*
3393	pJK148:*mid1* S328 to A328 h? *mid1*::*ura4*+ *plo1-ts35 ura4-D18 leu1-32*
3394	pJK148:*mid1* S328 to A328 h? *mid1*::*ura4*+ *plo1-ts35 ura4-D18 leu1-32*
3397	pJK148:*mid1* S331 to A331 h? *mid1*::*ura4*+ *plo1-ts35 ura4-D18 leu1-32*
3398	pJK148:*mid1* S331 to A331 h? *mid1*::*ura4*+ *plo1-ts35 ura4-D18 leu1-32*
3399	pJK148:*mid1* S331 to A331 h? *mid1*::*ura4*+ *plo1-ts35 ura4-D18 leu1-32*
3400	pJK148:*mid1* S332 to A332 h? *mid1*::*ura4*+ *plo1-ts35 ura4-D18 leu1-32*
3401	pJK148:*mid1* S332 to A332 h? *mid1*::*ura4*+ *plo1-ts35 ura4-D18 leu1-32*
3402	pJK148:*mid1* S332 to A332 h? *mid1*::*ura4*+ *plo1-ts35 ura4-D18 leu1-32*
3403	pJK148:*mid1* S523 to D523 h- *mid1*::*ura4*+ *plo1-ts35 ura4-D18 leu1-32*
3404	pJK148:*mid1* S523 to D523 h- *mid1*::*ura4*+ *plo1-ts35 ura4-D18 leu1-32*
3405	pJK148:*mid1* S523 to D523 h- *mid1*::*ura4*+ *plo1-ts35 ura4-D18 leu1-32*
3407	pJK148:*mid1* S523 to A523 h- *mid1*::*ura4*+ *plo1-ts35 ura4-D18 leu1-32*
3408	pJK148:*mid1* S523 to A523 h- *mid1*::*ura4*+ *plo1-ts35 ura4-D18 leu1-32*
3409	pJK148:*mid1* S523 to A523 h- *mid1*::*ura4*+ *plo1-ts35 ura4-D18 leu1-32*

GG No.	Genotype Annotation
3411	pJK148:*mid1* S332 to D332 h⁻ *mid1*::*ura4*⁺ *plo1-ts35 ura4-D18 leu1-32*
3412	pJK148:*mid1* S332 to D332 h⁻ *mid1*::*ura4*⁺ *plo1-ts35 ura4-D18 leu1-32*
3413	pJK148:*mid1* S332 to D332 h⁻ *mid1*::*ura4*⁺ *plo1-ts35 ura4-D18 leu1-32*
3415	pJK148:*mid1* S531 to A531 h⁻ *mid1*::*ura4*⁺ *plo1-ts35 ura4-D18 leu1-32*
3416	pJK148:*mid1* S531 to A531 h⁻ *mid1*::*ura4*⁺ *plo1-ts35 ura4-D18 leu1-32*
3417	pJK148:*mid1* S531 to A531 h⁻ *mid1*::*ura4*⁺ *plo1-ts35 ura4-D18 leu1-32*
3419	pJK148:*mid1* S167+S328+S331+S332 to A167+A328+A331+A332 h⁻ *mid1*::*ura4*⁺ *plo1-ts35 ura4-D18 leu1-32*
3420	pJK148:*mid1* S167+S328+S331+S332 to A167+A328+A331+A332 h⁻ *mid1*::*ura4*⁺ *plo1-ts35 ura4-D18 leu1-32*
3421	pJK148:*mid1* S167+S328+S331+S332 to A167+A328+A331+A332 h⁻ *mid1*::*ura4*⁺ *plo1-ts35 ura4-D18 leu1-32*
3422	pJK148:*mid1* S167+S328+S331+S332 to D167+D328+D331+D332 h⁻ *mid1*::*ura4*⁺ *plo1-ts35 ura4-D18 leu1-32*
3423	pJK148:*mid1* S167+S328+S331+S332 to D167+D328+D331+D332 h⁻ *mid1*::*ura4*⁺ *plo1-ts35 ura4-D18 leu1-32*
3424	pJK148:*mid1* S167+S328+S331+S332 to D167+D328+D331+D332 h⁻ *mid1*::*ura4*⁺ *plo1-ts35 ura4-D18 leu1-32*
3425	pJK148:*mid1* S167+S328+S331+S332+S523+S531 to A167+A328+A331+A332+A523+A531 h⁻ *mid1*::*ura4*⁺ *plo1-ts35 ura4-D18 leu1-32*
3426	pJK148:*mid1* S167+S328+S331+S332+S523+S531 to A167+A328+A331+A332+A523+A531 h⁻ *mid1*::*ura4*⁺ *plo1-ts35 ura4-D18 leu1-32*
3427	pJK148:*mid1* S167+S328+S331+S332+S523+S531 to A167+A328+A331+A332+A523+A531 h⁻ *mid1*::*ura4*⁺ *plo1-ts35 ura4-D18 leu1-32*
3428	pJK148:*mid1* S531 to D531 h⁻ *mid1*::*ura4*⁺ *plo1-ts35 ura4-D18 leu1-32*
3429	pJK148:*mid1* S531 to D531 h⁻ *mid1*::*ura4*⁺ *plo1-ts35 ura4-D18 leu1-32*
3430	pJK148:*mid1* S531 to D531 h⁻ *mid1*::*ura4*⁺ *plo1-ts35 ura4-D18 leu1-32*
3437	pJK148:*mid1*⁺ (wild-type) *mid1*Δ pJK148:*mid1*⁺ *plo1-ts35*

GG No.	Genotype	Annotation
	h- *mid1::ura4+ plo1-ts35 ura4-D18 leu1-32*	
3438	pJK148:*mid1+* (wild-type) h- *mid1::ura4+ plo1-ts35 ura4-D18 leu1-32*	*mid1*Δ pJK148:*mid1+ plo1-ts35*
3439	pJK148:*mid1+* (wild-type) h- *mid1::ura4+ plo1-ts35 ura4-D18 leu1-32*	*mid1*Δ pJK148:*mid1+ plo1-ts35*
3441	pJK148:*mid1* S167+S328+S331+S332+S523+S531 to D167+D328+D331+D332+D523+D531 h- *mid1::ura4+ plo1-ts35 ura4-D18 leu1-32*	
3442	pJK148:*mid1* S167+S328+S331+S332+S523+S531 to D167+D328+D331+D332+D523+D531 h- *mid1::ura4+ plo1-ts35 ura4-D18 leu1-32*	
3443	pJK148:*mid1* S167+S328+S331+S332+S523+S531 to D167+D328+D331+D332+D523+D531 h- *mid1::ura4+ plo1-ts35 ura4-D18 leu1-32*	
3444	pJK148:*mid1* S523 to A523 + S531 to A531 h- *mid1::ura4+ plo1-ts35 ura4-D18 leu1-32*	
3445	pJK148:*mid1* S523 to A523 + S531 to A531 h- *mid1::ura4+ plo1-ts35 ura4-D18 leu1-32*	
3446	pJK148:*mid1* S523 to A523 + S531 to A531 h- *mid1::ura4+ plo1-ts35 ura4-D18 leu1-32*	
3447	pJK148:*mid1* S523 to D523 + S531 to D531 h- *mid1::ura4+ plo1-ts35 ura4-D18 leu1-32*	
3448	pJK148:*mid1* S523 to D523 + S531 to D531 h- *mid1::ura4+ plo1-ts35 ura4-D18 leu1-32*	
3449	pJK148:*mid1* S523 to D523 + S531 to D531 h- *mid1::ura4+ plo1-ts35 ura4-D18 leu1-32*	
3450	pJK148:*mid1* S167 to A167 h? *mid1::ura4+ vps4::ura4+ ura4-D18 leu1-32*	
3451	pJK148:*mid1* S167 to A167 h? *mid1::ura4+ vps4::ura4+ ura4-D18 leu1-32*	
3452	pJK148:*mid1* S167 to A167 h? *mid1::ura4+ vps4::ura4+ ura4-D18 leu1-32*	
3456	pJK148:*mid1* S328 to A328 h? *mid1::ura4+ vps4::ura4+ ura4-D18 leu1-32*	
3457	pJK148:*mid1* S328 to A328 h? *mid1::ura4+ vps4::ura4+ ura4-D18 leu1-32*	
3458	pJK148:*mid1* S328 to A328 h? *mid1::ura4+ vps4::ura4+ ura4-D18 leu1-32*	
3461	pJK148:*mid1* S167+S328+S331+S332 to D167+D328+D331+D332 h? *mid1::ura4+ vps4::ura4+ ura4-D18 leu1-32*	

GG No.	Genotype Annotation
3463	pJK148:*mid1* S167+S328+S331+S332+S523+S531 to D167+D328+D331+D332+D523+D531 h? *mid1*::*ura4*+ *vps4*::*ura4+ ura4-D18 leu1-32*
3464	pJK148:*mid1* S167+S328+S331+S332+S523+S531 to D167+D328+D331+D332+D523+D531 h? *mid1*::*ura4*+ *vps4*::*ura4+ ura4-D18 leu1-32*
3465	pJK148:*mid1* S167+S328+S331+S332+S523+S531 to D167+D328+D331+D332+D523+D531 h? *mid1*::*ura4*+ *vps4*::*ura4+ ura4-D18 leu1-32*
3467	pJK148:*mid1* S167+S328+S331+S332+S523+S531 to A167+A328+A331+A332+A523+A531 h? *mid1*::*ura4*+ *vps4*::*ura4+ ura4-D18 leu1-32*
3468	pJK148:*mid1* S167+S328+S331+S332+S523+S531 to A167+A328+A331+A332+A523+A531 h? *mid1*::*ura4*+ *vps4*::*ura4+ ura4-D18 leu1-32*
3469	pJK148:*mid1* S332 to D332 h? *mid1*::*ura4*+ *vps4*::*ura4+ ura4-D18 leu1-32*
3470	pJK148:*mid1* S167+S328+S331+S332+S523+S531 to A167+A328+A331+A332+A523+A531 h? *mid1*::*ura4*+ *vps4*::*ura4+ ura4-D18 leu1-32*
3473	pJK148:*mid1* S332 to A332 h? *mid1*::*ura4*+ *vps4*::*ura4+ ura4-D18 leu1-32*
3474	pJK148:*mid1* S332 to A332 h? *mid1*::*ura4*+ *vps4*::*ura4+ ura4-D18 leu1-32*
3475	pJK148:*mid1* S332 to A332 h? *mid1*::*ura4*+ *vps4*::*ura4+ ura4-D18 leu1-32*
3478	pJK148:*mid1* S332 to D332 h? *mid1*::*ura4*+ *vps4*::*ura4+ ura4-D18 leu1-32*
3479	pJK148:*mid1* S332 to D332 h? *mid1*::*ura4*+ *vps4*::*ura4+ ura4-D18 leu1-32*
3481	pJK148:*mid1* S328 to D328 h? *mid1*::*ura4*+ *vps4*::*ura4+ ura4-D18 leu1-32*
3482	pJK148:*mid1* S328 to D328 h? *mid1*::*ura4*+ *vps4*::*ura4+ ura4-D18 leu1-32*
3483	pJK148:*mid1* S328 to D328 h? *mid1*::*ura4*+ *vps4*::*ura4+ ura4-D18 leu1-32*
3485	pJK148:*mid1* S331 to A331 h? *mid1*::*ura4*+ *vps4*::*ura4+ ura4-D18 leu1-32*
3486	pJK148:*mid1*+ (wild-type) *mid1*Δ pJK148:*mid1*+ *vps4*Δ h? *mid1*::*ura4*+ *vps4*::*ura4+ ura4-D18 leu1-32*
3488	pJK148:*mid1*+ S167+S328+S331+S332 to A167+A328+A331+A332

GG No.	Genotype Annotation
	h? *mid1*::*ura4*+ *vps4*::*ura4+ ura4-D18 leu1-32*
3489	pJK148:*mid1* S331 to A331 h? *mid1*::*ura4*+ *vps4*::*ura4+ ura4-D18 leu1-32*
3493	pJK148:*mid1*+ S167+S328+S331+S332 to A167+A328+A331+A332 h? *mid1*::*ura4*+ *vps4*::*ura4+ ura4-D18 leu1-32*
3494	pJK148:*mid1*+ S167+S328+S331+S332 to A167+A328+A331+A332 h? *mid1*::*ura4*+ *vps4*::*ura4+ ura4-D18 leu1-32*
3496	pJK148: *mid1* S331 to A331 *h? mid1 ::ura4+ vps4*::*ura4+ ura4-D18 leu1-32 ade6-216*
3497	pJK148: *mid1* S331 to A331 *h? mid1 ::ura4+ vps4*::*ura4+ ura4-D18 leu1-32 ade6-216*
3498	pJK148: *mid1* S331 to A331 *h? mid1 ::ura4+ vps4*::*ura4+ ura4-D18 leu1-32 ade6-216*
3499	pJK148: *mid1* wild-type+4GFP h- mid1::ura4+ ade6-216 ura4-D18 leu1-32
3500	pJK148: *mid1* wild-type+4GFP *h- mid1*::*ura4+ ade6-216 ura4-D18 leu1-32*
3501	pJK148: *mid1* wild-type+4GFP *h- mid1*::*ura4+ ade6-216 ura4-D18 leu1-32*
3502	pJK148: *mid1* wild-type+4GFP *h- mid1*::*ura4+ ade6-216 ura4-D18 leu1-32*
3503	pJK148: *mid1* wild-type+4GFP *h- mid1*::*ura4+ ade6-216 ura4-D18 leu1-32*
3504	pJK148: *mid1* wild-type+4GFP *h- mid1*::*ura4+ ade6-216 ura4-D18 leu1-32*
3505	pJK148: *mid1* wild-type+4GFP *h- mid1*::*ura4+ ade6-216 ura4-D18 leu1-32*
3506	pJK148: *mid1* wild-type+4GFP *h- mid1*::*ura4+ ade6-216 ura4-D18 leu1-32*
3507	pJK148 :*mid1* wild-type+4GFP *h- mid1*::*ura4+ ade6-216 ura4-D18 leu1-32*
3508	pJK148: *mid1* wild-type+4GFP *h- mid1*::*ura4+ ade6-216 ura4-D18 leu1-32*
3509	pJK148: *mid1* wild-type+4GFP *h- mid1*::*ura4+ ade6-216 ura4-D18 leu1-32*
3510	pJK148: *mid1* wild-type+4GFP *h- mid1*::*ura4+ ade6-216 ura4-D18 leu1-32*
3511	pJK148: *mid1* wild-type+4GFP *h- mid1*::*ura4+ ade6-216 ura4-D18 leu1-32*
3512	pJK148: *mid1* wild-type+4GFP

GG No.	Genotype Annotation
	h- mid1::ura4+ ade6-216 ura4-D18 leu1-32
3513	pJK148: *mid1* S332D+4GFP *h- mid1::ura4+ ade6-216 ura4-D18 leu1-32*
3514	pJK148: *mid1* S523A+S531A+4GFP *h- mid1::ura4+ ade6-216 ura4-D18 leu1-32*
3515	pJK148: *mid1* S523A+S531A+4GFP *h- mid1::ura4+ ade6-216 ura4-D18 leu1-32*
3516	pJK148: *mid1* S523A+S531A+4GFP *h- mid1::ura4+ ade6-216 ura4-D18 leu1-32*
3517	pJK148: *mid1* S523A +S531A+4GFP *h- mid1::ura4+ ade6-216 ura4-D18 leu1-32*
3518	pJK148: *mid1* S523A +S531A+4GFP *h- mid1::ura4+ ade6-216 ura4-D18 leu1-32*
3519	pJK148: *mid1* S523A S531A+4GFP *h- mid1::ura4+ ade6-216 ura4-D18 leu1-32*
3520	pJK148: *mid1* S523D+S531D+4GFP *h- mid1::ura4+ ade6-216 ura4-D18 leu1-32*
3521	pJK148: *mid1* S523D+S531D+4GFP *h- mid1::ura4+ ade6-216 ura4-D18 leu1-32*
3522	pJK148: *mid1* S523D+S531D+4GFP *h- mid1::ura4+ ade6-216 ura4-D18 leu1-32*
3523	pJK148: *mid1* S523D+S531D+4GFP *h- mid1::ura4+ ade6-216 ura4-D18 leu1-32*
3524	pJK148: *mid1* S531D+4GFP *h- mid1::ura4+ ade6-216 ura4-D18 leu1-32*
3525	pJK148: *mid1* S531D+4GFP *h- mid1::ura4+ ade6-216 ura4-D18 leu1-32*
3526	pJK148: *mid1* S531D+4GFP *h- mid1::ura4+ ade6-216 ura4-D18 leu1-32*
3527	pJK148: *mid1* S531D+4GFP *h- mid1::ura4+ ade6-216 ura4-D18 leu1-32*
3528	pJK148: *mid1* S531D+4GFP *h- mid1::ura4+ ade6-216 ura4-D18 leu1-32*
3529	pJK148: *mid1* S531D+4GFP *h- mid1::ura4+ ade6-216 ura4-D18 leu1-32*
3530	pJK148: *mid1* S167A+S328A+S331A+S332A+S523A+S531A+4GFP *h- mid1::ura4+ ade6-216 ura4-D18 leu1-32*
3531	pJK148: *mid1* S167A +S328A+S331A+S332A+S523A+S531A+4GFP *h- mid1::ura4+ ade6-216 ura4-D18 leu1-32*
3532	pJK148: *mid1* S167A +S328A+S331A+S332A+S523A+S531A+4GFP

GG No.	Genotype Annotation
	h- mid1::ura4+ ade6-216 ura4-D18 leu1-32
3533	pJK148: *mid1* S167A +S328A+S331A+S332A+S523A+S531A+4GFP *h- mid1::ura4+ ade6-216 ura4-D18 leu1-32*
3534	pJK148: *mid1* S167A +S328A+S331A+S332A+S523A+S531A+4GFP *h- mid1::ura4+ ade6-216 ura4-D18 leu1-32*
3535	pJK148: *mid1* S167A +S328A+S331A+S332A+S523A+S531A+4GFP *h- mid1::ura4+ ade6-216 ura4-D18 leu1-32*
3536	pJK148: *mid1* S328A+4GFP *h- mid1::ura4+ ade6-216 ura4-D18 leu1-32*
3537	pJK148: *mid1* S328A+4GFP *h- mid1::ura4+ ade6-216 ura4-D18 leu1-32*
3538	pJK148: *mid1* S328A+4GFP *h- mid1::ura4+ ade6-216 ura4-D18 leu1-32*
3539	pJK148: *mid1* S328A+4GFP *h- mid1::ura4+ ade6-216 ura4-D18 leu1-32*
3540	pJK148: *mid1* S328A+4GFP *h- mid1::ura4+ ade6-216 ura4-D18 leu1-32*
3541	pJK148: *mid1* S328A+4GFP *h- mid1::ura4+ ade6-216 ura4-D18 leu1-32*
3542	pJK148: *mid1* S328D+4GFP *h- mid1::ura4+ ade6-216 ura4-D18 leu1-32*
3543	pJK148: *mid1* S328D+4GFP *h- mid1::ura4+ ade6-216 ura4-D18 leu1-32*
3544	pJK148: *mid1* S328D+4GFP *h- mid1::ura4+ ade6-216 ura4-D18 leu1-32*
3545	pJK148: *mid1* S328D+4GFP *h- mid1::ura4+ ade6-216 ura4-D18 leu1-32*
3546	pJK148: *mid1* S332A+4GFP *h- mid1::ura4+ ade6-216 ura4-D18 leu1-32*
3547	pJK148: *mid1* S332A+4GFP *h- mid1::ura4+ ade6-216 ura4-D18 leu1-32*
3548	pJK148: *mid1* S332A+4GFP *h- mid1::ura4+ ade6-216 ura4-D18 leu1-32*
3549	pJK148: *mid1* S332A+4GFP *h- mid1::ura4+ ade6-216 ura4-D18 leu1-32*
3550	pJK148: *mid1* S332A+4GFP *h- mid1::ura4+ ade6-216 ura4-D18 leu1-32*
3551	pJK148: *mid1* S332A+4GFP *h- mid1::ura4+ ade6-216 ura4-D18 leu1-32*
3552	pJK148: *mid1* S167D+S328D+S331D+S332D+S523D+S531D+4GFP

GG No.	Genotype	Annotation
	h- mid1::ura4+ ade6-216 ura4-D18 leu1-32	
3553	pJK148: *mid1* S167D+S328D+S331D+S332D+S523D+S531D+4GFP *h- mid1::ura4+ ade6-216 ura4-D18 leu1-32*	
3554	pJK148: *mid1* S167D+S328D+S331D+S332D+S523D+S531D+4GFP *h- mid1::ura4+ ade6-216 ura4-D18 leu1-32*	
3555	pJK148: *mid1* S167D+S328D+S331D+S332D+S523D+S531D+4GFP *h- mid1::ura4+ ade6-216 ura4-D18 leu1-32*	
3556	pJK148: *mid1* S531A+4GFP *h- mid1::ura4+ ade6-216 ura4-D18 leu1-32*	
3557	pJK148: *mid1* S531A+4GFP *h- mid1::ura4+ ade6-216 ura4-D18 leu1-32*	
3558	pJK148: *mid1* S531A+4GFP *h- mid1::ura4+ ade6-216 ura4-D18 leu1-32*	
3559	pJK148: *mid1* S531A+4GFP *h- mid1::ura4+ ade6-216 ura4-D18 leu1-32*	
3560	pJK148: *mid1* S531A+4GFP *h- mid1::ura4+ ade6-216 ura4-D18 leu1-32*	
3561	pJK148: *mid1* S332D+4GFP *h- mid1::ura4+ ade6-216 ura4-D18 leu1-32*	
3562	pJK148: *mid1* S332D+4GFP *h- mid1::ura4+ ade6-216 ura4-D18 leu1-32*	
3563	pJK148: *mid1* S332D+4GFP *h- mid1::ura4+ ade6-216 ura4-D18 leu1-32*	
3564	pJK148: *mid1* S332D+4GFP *h- mid1::ura4+ ade6-216 ura4-D18 leu1-32*	
3565	pJK148: *mid1* S332D+4GFP *h- mid1::ura4+ ade6-216 ura4-D18 leu1-32*	
3566	pJK148: *mid1* S332D+4GFP *h- mid1::ura4+ ade6-216 ura4-D18 leu1-32*	
3567	h$^-$ *mid1*::*ura4*$^+$ *ura4-D18 leu1-32*	*mid1*Δ

Table 2-1 List *S. pombe* (fission yeast) strains used in this study. "GG" The number refers to the University Glasgow laboratory reference collection. All strains *ade*$^-$, unless indicated.

2.1.4 *E. coli* media

All *E. coli* cells were cultured and maintained, as previously described (Green and Sambrook 2012).

Complete medium. Yeast Extract Tryptone (2YT)

15 g tryptone, 5 g NaCl, and 10 g yeast extract.

Bacterial antibiotics

Ampicillin was added to a solid LB medium to a final concentration of 100 μg ml^{-1}

2.1.5 Plasmid DNA constructs

Each plasmid vector DNA construct synthesized by GenScript used during this research was provided a University of Glasgow laboratory reference "GB" annotation number and stored long-term in *E. coli* in 30% glycerol at -80ºC (Table 2-2).

GB No.	Abbreviated plasmid vector description
880	pET-14b – His tagged + ampicillin, Vps4, Cloned with *Nde* I/*Bam* HI transformed into *E. coli* BL21. Invitrogen – 13AB6ZFP
881	pGEX4T1 – GST tagged + ampicillin, Mid1p amino acid 1-453, cloned with *Bam* HI/*Xho* I GeneScript order number U2640BJ110 – Transformed into BL21 (same for GB 882-884)
882	pGEX4T1 – GST tagged + ampicillin, Mid1p amino acid 452-579, cloned with *Bam* HI/*Xho* I transformed into *E. coli* BL21.
883	pGEX4T1 – GST tagged + ampicillin, Mid1p amino acid 478-799, cloned with *Bam* HI/*Xho* I transformed into *E. coli* BL21.
884	pGEX4T1 – GST tagged + ampicillin, Mid1p amino acid 798-920, cloned with *Bam* HI/*Xho* I transformed into *E. coli* BL21.
889	pET-14b – His tagged + ampicillin, Myo2p C-terminal amino acid 1394-1526, cloned with *Nde* I/*Bam* HI GeneScript order number U9540CD270_2-Transformed into BL21
923	*mid1* mutant gene full length + 1 kb upstream of ORF-3,853 bp in total Polo sites S167 to A167 pJK148-Transformed into XL1-Blue. *Kpn* I/*Sac* I fragment from cloned into same sites of pJK148 by GeneScript order number U894VEB050. To linearise for yeast integration use *Nde* I to cut in *leu1*$^{+}$ (same for GB 924-934).
924	*mid1* mutant gene full length + 1 kb upstream of ORF-3,853 bp in total Polo sites

GB No.	Abbreviated plasmid vector description
	S167 to D167 Transformed into XL1-Blue.
925	*mid1* mutant gene full length + 1 kb upstream of ORF-3,853 bp in total Aurora/Polo sites S328 to A328 Transformed into XL1-Blue.
926	*mid1* mutant gene full length + 1 kb upstream of ORF-3,853 bp in total Aurora/Polo sites S328 to D328 Transformed into XL1-Blue.
927	*mid1* mutant gene full length + 1 kb upstream of ORF-3,853 bp in total Polo sites S331 to A331 Transformed into XL1-Blue.
928	*mid1* mutant gene full length + 1 kb upstream of ORF-3,853 bp in total Polo sites S331 to D331 Transformed into XL1-Blue.
929	*mid1* mutant gene full length + 1 kb upstream of ORF-3,853 bp in total Polo sites S332 to A321 Transformed into XL1-Blue.
930	*mid1* mutant gene full length + 1 kb upstream of ORF-3,853 bp in total Polo sites S332 to D332 Transformed into XL1-Blue.
931	*mid1* quadruple (4) mutant gene full length + 1 kb upstream of ORF-3,853 bp in total Aurora/Polo sites S167 to A167 + S328 to A328 + S331 to A331 + S332 to A332 Transformed into XL1-Blue.
932	*mid1* quadruple (4) mutant gene full length + 1 kb upstream of ORF-3,853 bp in total Aurora/Polo sites S167 to D167 + S328 to D328 + S331 to D331 + S332 to D332 Transformed into XL1-Blue.
933	*mid1* hexa (6) mutant gene full length + 1 kb upstream of ORF-3,853 bp in total Aurora/Polo sites S167 to A167 + S328 to A328 + S331 to A331 + S332 to A332 + S523 to A523 + S531 to A531 Transformed into XL1-Blue.
934	*mid1* hexa (6) mutant gene full length + 1 kb upstream of ORF-3,853 bp in total Aurora/Polo sites S167 to D167 + S328 to D328 + S331 to D331 + S332 to D332 + S523 to D523 + S531 to D531 Transformed into XL1-Blue.
959	pGEX4T1 GST tagged + ampicillin, Mid1p amino acids 448-90 – DNA synthesized and cloned *Bam* HI/*Xho*-I into the vector by GenScript order number -U4921GD120 Transformed into DH5 alpha (same as GB 959 - 962)
961	pGEX4T1 tagged - GST + ampicillin, Mid1p amino acids 448-90 cloned *Bam* HI/*Xho*-I Transformed into BL21
963	pJK148 Mid1p – tagged 4GFP Mid1p full length + 1kb upstream of ORF – 3,853 synthesized by GenScript order number U6016GK010, cloned in frame downstream of Mid1p in pJK148 and transformed into XL1-Blue
964	pJK148 *mid1* S328A – tagged 4GFP Mid1p full length + 1kb upstream of ORF – 3,853 synthesized by GenScript order number U058BHB090, cloned in frame downstream of Mid1p in pJK148 and Transformed into NED 5α GB 964-973
965	pJK148 *mid1* S328D – tagged 4GFP Mid1p full length + 1kb upstream of ORF – 3,853 synthesized by GenScript order number U058BHB090, cloned in frame downstream of Mid1p in pJK148 and Transformed into NED 5α
966	pJK148 *mid1* S332A – tagged 4GFP Mid1p full length + 1kb upstream of ORF – 3,853

GB No.	Abbreviated plasmid vector description
	synthesized by GenScript order number U058BHB090, cloned in frame downstream of Mid1p in pJK148 and Transformed into NED 5α
967	pJK148 *mid1* S332D – tagged 4GFP Mid1p full length + 1kb upstream of ORF – 3,853 synthesized by GenScript order number U058BHB090, cloned in frame downstream of Mid1p in pJK148 and Transformed into NED 5α
968	pJK148 *mid1* S523 + D531 – tagged 4GFP Mid1p full length + 1kb upstream of ORF – 3,853 synthesized by GenScript order number U058BHB090, cloned in frame downstream of Mid1p in pJK148 and Transformed into NED 5α
969	pJK148 *mid1* S523 + D531 – tagged 4GFP Mid1p full length + 1kb upstream of ORF – 3,853 synthesized by GenScript order number U058BHB090, cloned in frame downstream of Mid1p in pJK148 and Transformed into NED 5α
970	pJK148 *mid1* S531A – tagged 4GFP Mid1p full length + 1kb upstream of ORF – 3,853 synthesized by GenScript order number U058BHB090, cloned in frame downstream of Mid1p in pJK148 and Transformed into NED 5α
971	pJK148 *mid1* S531D – tagged 4GFP Mid1p full length + 1kb upstream of ORF – 3,853 synthesized by GenScript order number U058BHB090, cloned in frame downstream of Mid1p in pJK148 and Transformed into NED 5α GB 964-973
972	pJK148 *mid1* D167 + D328 + D331 + D332 + D523 + D531 – tagged 4GFP Mid1p full length + 1kb upstream of ORF – 3,853 synthesized by GenScript order number U058BHB090, cloned in frame downstream of Mid1p in pJK148 and Transformed into NED 5α
973	pJK148 *mid1* A167 + A328 + A331 + A332 + A523 + A531 – tagged 4GFP Mid1p full length + 1kb upstream of ORF – 3,853 synthesized by GenScript order number U058BHB090, cloned in frame downstream of Mid1p in pJK148 and Transformed into NED 5α

Table 2-2 List bacterial plasmids used in this study. "GB" The number refers to the University Glasgow laboratory reference collection.

2.1.6 Standard solutions and reagents

List of standard solutions

Unless stated otherwise, all buffers and reagents were made up of distilled water.

Bradford's reagents

30 mg/ml Coomassie Brilliant Blue, 5.0% (v/v) orthophosphoric acid

Note: Bradford's reagent was filtered and stored in the dark

Coomassie Brilliant Blue solution

1 g/l Coomassie Brilliant Blue, 50% (v/v) methanol, 10% (v/v) acetic acid

Note: Coomassie Brilliant Blue solution was filtered before use

Phosphate buffer saline (PBS)

137 mM NaCl, 2.7 mM KCl, 10 mM Na_2HPO_4 and 1.8 mM KH_2PO_4, pH 7.4.

Calcofluor-white

1 g l^{-1} distilled H_2O.

HEPES buffer

25 mM HEPES, 400 mM KCl, and 10% (v/v) glycerol, pH 7.4.

Glutathione beads elution buffer 1

1 mM reduced GST in PBS, pH 8.

Glutathione beads elution buffer 2

20 mM reduced GST in PBS, pH 8.

Glutathione beads elution buffer 3

20 mM reduced GST and 1% (w/v) octyl glucoside in PBS, pH 8.

Ni-NTA beads washing buffer

25 mM imidazole in HEPES buffer, pH 6.5.

Ni-NTA beads elution buffer 1

250 mM imidazole in HEPES buffer, pH 4.5.

Ni-NTA beads elution buffer 2

500 mM imidazole in HEPES buffer, pH 4.5.

Laemmli sample buffer (LSB) 4X

375 mM Tris pH 6.8, 12% (w/v) SDS, 60% (v/v) glycerol, 600 mM DTT, and 0.6% (w/v) bromophenol Blue.

SDS PAGE sample buffer (4X)

200 mM Tris-HCl, pH 6.8, 8% (w/v) SDS, 40% (v/v) glycerol, 0.4% (w/v) bromophenol blue, 200 mM DTT. Note: DTT was added on the day of use

SDS-polyacrylamide gel electrophoresis (SDS-PAGE) running buffer

25 mM Tris-HCl, 250 mM glycine and 0.1% (w/v) SDS.

TE buffer

0.1 M Tris-HCl, pH 7.5, 0.1 M EDTA

Transfer buffer

190 mM glycine, 62 mM Tris base

Tris-buffered saline (TBS)

20 mM Tris-HCl, pH 7.5, 137 mM NaCl

Tris-buffered saline + Tween 20 (TBST)

20 mM Tris-HCl, pH 7.5, 137 mM NaCl, 0.1% (v/v) Tween 20

P1 solution

50 mM Tris, 10 mM EDTA and 100 μl^{-1} RNAse A, pH 8.

P2 solution

0.2 M NaOH and 1% (w/v) SDS.

P3 solution

2.55 M KOAc, pH 4.8

Tris-acetate-EDTA (TAE) buffer

40 mM Tris, 20 mM acetic Acid, and 1 mM EDTA, pH 8.5.

DNA loading dye 6X

Bromophenol Blue 0.25% (w/v) xylene cyanol FF and 30% (v/v) glycerol.

2.1.6.1 List of reagents and kits

Acrylamide

Severn Biotech

Ampicillin

SIGMA-ALDRICH

Bacto agar

BD Biosciences

EDTA-free protease inhibitors

A complete protease inhibitor, ROCHE

Glutathione Sepharose beads

GE Healthcare Bio-Sciences

Isopropyl B-D-1 thiogalactopyranoside (IPTG)

SIGMA-ALDRICH

Nickel-nitro acetic (Ni-NTA) beads

SIGMA-ALDRICH

Octylglucoside

SIGMA-ALDRICH

Precision Plus Protein Standards All Blue
Bio-Rad

Tetramethyl ethylenediamine (TEMED)
SIGMA-ALDRICH

Triton X-100
SIGMA-ALDRICH

Ultrapure water
SIGMA-ALDRICH

Ponceau S stain
0.2% (w/v) Ponceau S, 1% (v/v) acetic acid

2.2 Methods

2.2.1 *S. pombe* methods

All *S. pombe* methods used were as described in Moreno *et al*. (1991) and Rezig *et al*. (2019, 2021).

2.2.2 General yeast methods

Strains of suitable genotypes were collected from the laboratory frozen stock at -80ºC. The strains were inoculated on solid yeast extract (YE) medium plates and allowed to grow at an appropriate temperature of 28ºC. Strains of opposite mating types were mated on solid malt extract (ME) medium and the double mutants were screened on solid Edinburgh minimum medium (EMM) medium provided with the supplement. The strains generated in this study were assigned a GG number by laboratory stock.

2.2.3 Tetrad dissection

Tetrad analysis allows the unambiguous identification and selection of individual meiotic products. It is an immensely effective tool in yeast genetics. Asci are arranged in a line about 3 mm apart on a solid YE plate using a Singer MSM Ascus Dissector with a micromanipulator needle. Opposite mating type h^+ and h^- parent strains were freshly grown at 28^{0}C for 24 hours; approximately an equal amount of the parent strains were mixed with 50µl sterile distilled H_2O on a solid ME medium. The mating mixture was allowed to air dry for about 10-15 minutes and was incubated at 25^{0}C for up to two days. After the formation of asci tetrads, a small amount of the mating mixture was transferred from solid ME to solid YE medium. Each ascus is then micro-manipulated using Singer MSM Ascus Dissector to give a line of four isolated spores, separated by 3-5 mm. The spores are incubated at 28^{0}C until colonies form.

2.2.4 Genotype screening

After colonies are made on YE solid media, replica plating onto selective media EMM was used for genotype screening of colonies. Sterile scalpel was used to remove the solid YE medium area with the grown mating mixture and a sterile velvet material was assembled over the replica-plating device. The YE medium was placed on the sterile velvet and the colonies were transferred to the EMM medium and incubated at 28^{0}C for 2 days.

2.2.5 Serial dilution/growth rate analysis

Small numbers of cells were collected from wild-type, parent strains, *mid1* deletion, and the newly created double mutant isolates; suspended at 1.5x10^6 cell/ml of sterile distilled water and subjected to 10-fold serial dilution (100-1000 µl) in 1.5 ml test tubes. Using a calibrated pipette 10-15 µl of cell suspension from each strain was pipetted sequentially in the marked areas on solid YE media, allowed to air dry for 10 minutes, and incubated at four different temperatures (25^{0}C, 28^{0}C, 32^{0}C and 37^{0}C) for 2 days to assess the growth rate. Scans of the growing cells on a solid YE medium at the above temperature were taken on the second day using a photo scanner.

2.2.6 Septation analysis

Septation analyses were carried out by imagining *S. pombe* septa using calcofluor-white stain and fluoresce microscopy, as described (Bhutta *et al.*, 2014; Rezig *et al.*, 2019 and Rezig *et al.*, 2021). 50 ml YE cultures were incubated overnight in a soaking water bath at 25^{0}C shaking. Cells were examined for septa formation using confocal microscopy. 1 ml of the cell culture was transferred to a micro-centrifuge tube and the cells were pelleted at 17,550 g for 30 seconds. The pellet was re-suspended in 1 ml PBS and 30 µl of calcofluor-white stain was added, tube was incubated in the dark for 5 minutes. The cells were then centrifuged at 17,550 g for 30 seconds and the pellet was re-suspended in 20 µl PBS; cells were then visualized using the bright field and DAPI filters of a Zeiss LSM 880 Microsystem with a Zeiss 63X oil-immersion objective lens. The image was processed using ZEN 3.4 (Blue Edition) and PowerPoint.

2.2.7 Confocal microscopy

Confocal microscopy analysis was used to study fission yeast strains containing an EGFP tag on the Mid1p gene used to analyse EGFP-Mid1p localization. *S. Pombe* cells were cultured in 50 ml YE in a water bath shaking at 28^{0}C overnight. Cells were viewed under a light microscope system, with 10 µl samples used for examination using a Zeiss LSM 880 Microsystem with a Zeiss 63X oil-immersion objective lens. Cell images were collected using and processed using ZEN 3.4 (Blue Edition) and PowerPoint.

2.2.8 Lithium acetate transformation

Grow up cells in YE to a density of 10^{7}/ml, harvest cells by centrifugation at 3000 rpm for 5 minutes at room temperature, and the pellet was with 30 ml sterile water at 3000 rpm for 5 minutes. The pellet was re-suspended and transferred to 1 ml sterile water in a microcentrifuge tube and centrifuged at 4000 rpm for 1 minute. The pellet was washed once with 1 ml 1X TE/LiAC (filter sterilized). Cell pellet was resuspended in 500 µl TE/LiAC and 100 µl cells with 2 µl Salmon sperm DNA (10 mg/ml) and 10 µl transforming DNA. After 10 minutes at room temperature, 260 µl PEG/LiAC/TE was added. Mix gently and incubate for 30-60 minutes at 30^{0}C rocking. 43 µl of DMSO was added and cells were heat

shocked at 42ºC for 50 minutes. The cells were washed with sterile water, resuspended in 500 µl sterile water, and plated onto a minimal drop medium.

2.2.9 *In vivo S. pombe* integration

Phospho-mimetic/resistant mutant versions of the *mid1* gene were designed to test for their functional relevance. These *mid1* gene versions were designed to have the wild-type *mid1* endogenous promoter and 1 kb upstream of the *mid1*$^{+}$ reading frame were all synthesized by GenScript and cloned into the pJK148 integrative vector. Integration of the *mid1* gene into *mid1Δ S. pombe* (GG 1129) was performed via homologous recombination. The pJK148 integrative vector has a *leu*$^{+}$ selective marker that includes an *Nde* I restriction site. The plasmid was digested with *Nde* I to linearize in the *leu1*$^{+}$ gene and then it was transformed into a *mid1Δ* S. pombe strain (GG 1129) with a *leu1-32* point mutation, where it integrates at the *leu1*$^{+}$ locus. The resulting *S. pombe* strain is subjected to cell morphology analysis through confocal microscopy with 10 µl samples used for examination using a Zeiss LSM 880 Microsystem with a Zeiss 63X oil-immersion objective lens. Cell images were collected using and processed using ZEN 3.4 (Blue Edition) and PowerPoint.

2.3 *E. coli* methods

2.3.1 General methods

E. coli cells (5-alpha) were stored in 30% glycerol stocks for the long-term purpose at -80ºC. While (BL21) competent cells were used for protein expression and purification. Cells were recovered from glycerol stock by streaking on a solid LB medium and incubated at 37ºC overnight. *E. coli* cells were grown in LB solid medium and cultured in LB liquid medium and protein expression was conducted in LB liquid medium. A laboratory reference number was assigned to all *E. coli* strains using the annotation ‘’GB’’.

2.3.2 DNA constructs designed for recombinant protein expression

Two approaches to designing *mid1*$^{+}$ DNA constructs for bacterial expression were carried out. DNA constructs used in this study were synthesized by GenScript and transformed into *E. coli* assigned laboratory GB number and stored at -80^{0}C.

The first approach used three domains of the *mid1* gene cloned into *Sma* I and *Sal* I restriction sites of the pGEX-4T-1 vector with an N-terminal glutathione S-transferase (GST) tag to express the corresponding Mid1p domains. The plasmid encoding Mid1p N-terminus 1-422 amino acids were designed GB 824, Mid1p middle 331-531 amino acids were designed GB 825, and Mid1p amino acids 478-799 designated GB 883, and Mid1p amino acids 798-920 designated GB 884.

The full-length *vps4* gene was cloned into *Nde* I and *Bam* HI restriction sites of the pET-14b vector with a 6His tag to express Vps4p and designated GB 880. The C-terminal domain of the *myo2*$^{+}$ gene was cloned into *Nde* I and *Bam* HI restriction sites of the pET-14b vector with a 6His tag to express the C-terminal domain of Myo2p and designated GB 889.

2.3.3 Plasmid DNA extraction for bacterial transformation

Plasmid DNA was extracted using the Qiagen Minipreps where *E. coli* 5-alpha and XL-1 blue cells were cultured in 10 ml LB medium (100 µg/ml^{-1} ampicillin shaking overnight). 1.5 ml of the bacterial culture was centrifuged at 12000 g for 1 minute and the bacterial pellet was resuspended in 150 µl of P2 solution was added followed by 5 minutes of incubation at room temperature. After that, 150 µl of P3 solution was added and the mixture was centrifuged at 12000 g for 5 minutes. The supernatant was transferred into a new microfuge tube followed by adding 1 ml of ethanol. The mixture was centrifuged at 12000 g for 5 minutes and the pellet was dissolved in 40 µl RNase-free water.

2.3.4 DNA transformation

1 µl of DNA was mixed with 50 µl BL21 or XL1-blue competent cells and the mixture was incubated on ice for 30 minutes. The cells were then transferred to a water bath at 42ºC for 42 seconds and then placed back on the ice for 2 minutes. 750 µl of SOC medium were added and cells were incubated at 37ºC for exactly 1 h. The cells were then streaked onto LB solid plates with ampicillin 100 µg/ml^{-1} at 37ºC overnight.

2.3.5 Recombinant protein expression (small-scale expression)

After DNA transformation, different colonies were tested for the expression of recombinant proteins. From the transformation plate, five random colonies were inoculated into 5 ml LB cultures and were incubated at 37ºC overnight with shaking. The cultures were then diluted into 50 ml LB culture and incubated at 37ºC with shaking until OD reached 0.6-0.8; after that, 500 µl of the culture were centrifuged at 12000 *g* for 5 minutes (sample 1: -IPTG). 1mM ml-1 IPTG was added to the cultures which was incubated at 37ºC with shaking for 2 h. 500 µl of the culture were centrifuged at 12000 *g* for 5 minutes (sample 2: +IPTG). Protein expression was compared in samples 1 and 2 using SDS-PAGE.

2.3.5.1 Recombinant protein expression (large scale expression)

E. coli BL21 cells were cultured in 10 ml LB medium (100 µg ml-1 ampicillin, shaking; 37ºC; overnight). GST-Mid1p, 6His-Vps4p, or 6His-C-term myo2p recombinant proteins were expressed in 1 L LB cultures supplied with 100 µg/ml-1 ampicillin (shaking; 37ºC; overnight) until the optical density reached 0.6-0.8; then, protein production was induced by adding 1 mM IPTG, and the cultures were incubated with shaking (210 rpm for 2 h at 37ºC).

2.4 *In vitro* biochemical methods

2.4.1 Recombinant protein purification

Bacterial pellets were produced by centrifugation (3750 rpm at 4ºC for 30 min). The pellets were then re-suspended in 20 ml re-suspension buffer with EDTA-free protease inhibitors; For GST-Mid1p fusion protein, PBS was used, whereas, for 6His-Vps4p protein, HEPES buffer was used. The cells were then lysed using either sonication, where a final concentration of 1 mg ml-1 lysozyme was added for cell wall digestion followed by sonication 4 x 30 sec using a Sanyo Soniprep 150 sonicator (with an amplitude of 15 microns) with a 30-second pause between sonication. A clear lysate was produced by centrifugation (20000 rpm; 4ºC; 1 h) of the lysed cells. GST-tagged fusion proteins were purified using 1ml L-1 Glutathione beads in PBS buffer, while 6His-tagged Vps4p or C-term Myo2p were purified using 500 µl L-1 Ni-NTA beads in HEPES buffer either for 2 h or overnight at 4ºC using a rotating platform. Mid1p was eluted from glutathione beads using three conditions (Glutathione beads elution buffer 1, 2, and 3 respectively (1 mM reduced-GST in PBS pH 8.0, 20 mM reduced-GST in PBS pH 8.0, and 20 mM reduced-GST and 1% w/v octyl glucoside in PBS pH 8.0). Vps4p or C-term Myo2p were washed and eluted from Ni-NTA beads using washing Ni-NTA beads washing buffer (25 mM imidazole in HEPES buffer pH 6.5) and elution buffer (250mM imidazole in HEPES buffer, pH 4.5 and 500 mM imidazole in HEPES pH 4.5). Elution was carried out for 2 h at 4ºC using a rotating platform. Three samples (B+: protein bound to glutathione or Ni-NTA beads, E: eluted protein, and B-: glutathione or Ni-NTA beads after protein is eluted) were subjected to SDS-PAGE to determine elution efficiency.

2.4.2 Pull-down assay

Pull-down experiments make use of Ni-NTA beads-immobilized bait proteins (6His-Vps4p or Myo2p) and prey-eluted proteins (Mid1p: N-terminus, middle or C-terminus, or GST) to analyse protein-protein interactions. Bait proteins were loaded onto Ni-NTA beads by incubation in PBS containing 0.01% (v/v) Triton X-100 for 1 h (4ºC) on a rotating wheel. Following loading, the mixture was washed with PBS containing 0.01% (v/v) Triton X-100, and beads were blocked for non-specific binding by incubation in PBS comprising 0.2% fish-skin gelatin on a

rotating wheel (4ºC) for 1 h. The beads mixture was again incubated with the prey protein in PBS with 0.01% (v/v) Triton X-100 on a rotating wheel (4ºC) for 2 h. Accordingly, beads were washed with PBS containing 0.01% (v/v) Triton X-100 three times, 0.5% (v/v) glycerol, and 0.2% (w/v) fish skin gelatin three times, and with PBS only four times. Thereafter, 4X Laemmli Sample Buffer (LSB) was added to elute the proteins from beads, and the samples were subjected to sodium dodecyl sulphate-polyacrylamide gel electrophoresis (SDS-PAGE).

2.4.3 Gel electrophoresis (SDS-PAGE)

SDS-PAGE was used to resolve the size and identify specific proteins, 2X Laemmli sample buffer (LSB) was added to protein samples in a ratio of 1:1; the samples were heated to 95ºC for 5 minutes and loaded on a 12-15% 1 mm Tris-HCl SDS gel composed of 30% (w/v) acrylamide, 10% SDS, 10% ammonium persulphate and tetramethyl ethylenediamine (TEMED). Bio-Rad gel casting units were used. A Precision Plus Protein Standards All Blue protein marker was run together with the proteins to determine molecular weights. SDS-PAGE running buffer was used to run the gels at 90 V initially followed by 110 V using the Bio-Rad Protean III system.

2.4.4 Agarose gel electrophoresis

Sample was subjected to agarose gel electrophoresis to verify the presence of plasmid DNA. 10% agarose gel was prepared in TAE buffer by dissolving 0.8 g agarose in 80 ml TAE buffer with heating. Once cooled, but still liquid, 8 µl ethidium bromide was added before pouring into Bio-Rad gel casting units. DNA samples were mixed with 6X DNA loading dye in a ratio of 6:1 and the gel was run in TAE buffer at 80 V for 1 hour. Trackit 1 kb DNA Ladder was run alongside the DNA samples to determine molecular weights.

2.5 Western blotting of proteins

2.5.1 Preparation of protein extracts for western blotting

0.5-1 l of *S. pombe* cells grown to mid-exponential phase in YE media, were collected in 50 ml centrifuge tubes by centrifugation at 2000 rpm for 5 minutes at 4ºC. The supernatant was discarded, and cell pellets were washed once with sterile dH_2O. Once the supernatant was discarded, the cells were resuspended in ice-cold HB extraction buffer (25 mM Tris-HCl pH 7.5, 60 mM ß-glycerophosphate, 15 mM p(4)-nitrophenylphosphate (pNPP), 15 mM EGTA, 15 mM, $MgCl_2$, 5 mM DTT, 0.5 mM Na_3VO_4 0.1 mM NaF, 0.1% NP-40, 1mM PMSF, 1 µg/ml leupeptin, 10 µg/ml aprotinin) at 3 x 10^{10} cells/ml and transferred to screw top microcentrifuge tubes. In each case, the cell suspension was mixed with equal volume of acid-washed glass beads and the tubes were chilled on ice for 2-3 minutes before cell lysis using an HYBRAID Ribolyser (4 x 20 second at setting 4). During cell lysis, the cells were chilled on ice for 2-3 minutes between each disruption step. Following cell breakage, cell lysates were spun at 3000 rpm for 5 minutes at 4ºC and supernatant was transferred into fresh tubes which were spun at 13000 rpm for 30 minutes at 4ºC. Following centrifugation, all clarified materials referred to as crude lysate were transferred into a 15 ml tube on ice and its protein concentration was measured using the Bradford method. The protein concentration of the crude lysate was adjusted to 5 µg/µl with HB extraction buffer before storing at -80ºC.

2.5.2 Electrophoretic transfer of proteins onto nitrocellulose membrane

Gels were placed on a nitrocellulose membrane and layered between two sheets of 3 mm filter paper. Sponges were placed outside the filter paper and then carefully placed in a gel holder cassette. The electrophoretic transfer was carried out at 60 V for 2.25 h or 30 mA overnight. The nitrocellulose membrane was stained with Ponceau S to determine the efficiency and equal loading of the protein.

2.5.3 Blocking of the membrane and primary antibodies incubation

To block the non-specific binding of antibodies to the membrane, the nitrocellulose was incubated in 5% (w/v) Marvel milk powder in TBS for 30 minutes at room temperature. Membranes were washed three times at 5 minutes each with TBS three times and then incubated with primary antibodies overnight at 4^{0}C shaking.

2.5.4 Secondary antibodies and immunodetection of proteins

After incubating with primary antibodies overnight, membranes were washed three times at 5 minutes with TBST and incubated with appropriated secondary antibodies for 1 hour at room temperature shaking. Membranes were washed again three times at 5 minutes with TBST and the secondary antibodies were detected using the Li-COR Odyssey system.

2.5.5 Statistical analysis

All statistical analysis and results are shown as mean ± standard error of the mean (SEM). Statistical significance was measured by two-way analysis of variance (ANOVA) with $p<0.05$ regarded significant.

Chapter 3 Vps4p, Plo1p kinase, Ark1p kinase and Mid1p genes interact to control cell division in *S. pombe*

3.1 Introduction

3.1.1 Anillin and ESCRT complex are involved in the control of cytokinesis

After successful DNA replication during mitosis and separation of cell components into two daughter cells, the membrane link between the two daughter cells must be cleaved. This appears late in telophase in response to signals arising from mitotic spindle microtubules and the spindle midzone (Neto and Gould, 2011). Mammalian cells assemble a contractile ring comprising the motor protein myosin II, actin filaments and other proteins, the interaction between myosin and actin drives constriction of the contractile forming a cleavage furrow between the daughter nuclei which demarcates the scission point (Figure 3-1) (Guizetti and Gerlich, 2010). After the completion of furrowing, the two daughter cells remain attached by a thin cytoplasmic bridge known as the midbody. The structure is filled with densely packed matrix of proteins that surround a tightly compressed bridge of two opposite arrays of microtubules (Schiel and Prekeris, 2010). Membrane trafficking involves several functionally separable steps namely, cargo selection, the movement of vesicles towards their correct cellular destination, the tethering of the vesicles and their subsequent fusion (Neto and Gould, 2011).

During telophase (Figure 3-1), endosomal vesicles traffic bidirectionally into and out of the intercellular bridge, recycling endosomal vesicles interact with exocyst components in the intercellular bridge (Gromley *et al.*, 2005). Vesicles accumulate in the intercellular bridge during telophase, centrioles ring and microtubule buckling might demarcate a specialized plasma membrane domain known as the secondary ingression zone to which the endosomal vesicle within the intercellular bridge is directed to fuse (Prekeris and Gould, 2008). Abscission zones are functionally distinct regions of the plasma membrane at which the terminal session events occur (Neto and Gould, 2011). Cep-55 interacts with Tsg101 which is, in turn, proposed to recruit ESCRT-III components. Tsg101 and CHMP4B are sequentially recruited into the centre of the intercellular bridge where they form a series of cortical rings within the midbody (Elia *et al.*, 2011). Later in cytokinesis, CHAMP4B concentrates at the narrow secondary abscission zones, closely followed by Vps4 which leads to abscission at these sites,

CHAMP4B forms two narrow cortical rings adjacent to the midbody before disassembly of the microtubule (Guizetti *et al.*, 2011).

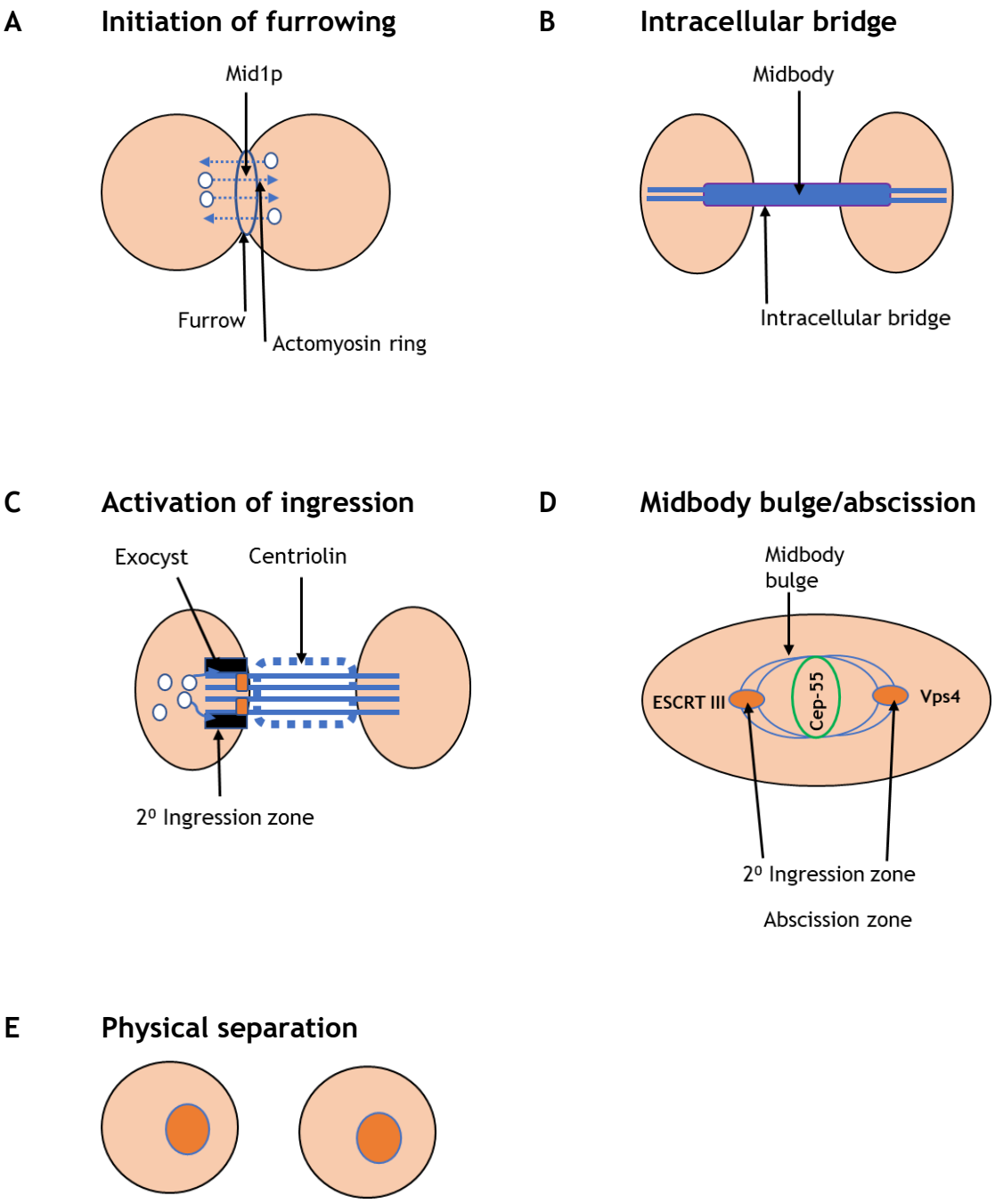

Figure 3-1 Schematic phases of cytokinesis. (A) During telophase endosomal vesicles move in and out of the intercellular bridge as highlighted in blue arrows, recycling endosomal vesicles interact with exocyst elements into the intercellular bridge. **(B)** Furrowing advances until the daughter membrane move through interaction with portions of the exocyst complex. **(C)** Centriolin ring demarcate a specific plasma membrane domain which the endosomal vesicles within the intercellular bridge are directed to fuse. **(D)** Tightening of intercellular bridge and the establishment of the midbody bulge in turn enables the final abscission results to produce two daughter cells. **(E)** Physical separation of the cell to produce two daughter cells via distribution of tethering complexes such as exocyst elements, plasma membrane and endosomal vesicles activities.

3.1.2 Mid1p and Vps4p genes interact to regulate cell division

After the initiation of cytokinesis by the activity of endosomal vesicles, Endosomal sorting complex required for transport (ESCRT) mediates cellular processes that are similar to membrane remodelling such as multivesicular body and cytokinesis (Horväth and Müller-Reichert, 2020). ESCRT proteins play a role in abscission, the final stage of cytokinesis (Bhutta *et al.*, 2014). Cep-55 is proposed to initiate the recruitment of the ESCRT complex and mediates the final abscission events to yield two daughter cells, during the establishment of the secondary ingression zones, the distribution of tethering complexes, such as exocyst components between the plasma membrane and the endosomal vesicles assists in the directionality of exocytosis and thus the specialization of the fusion machinery at these sites (Neto and Gould, 2011) (Figure 3-1). Cep-55 interacts sequentially with ESCRT-I protein which is, in turn, proposed to recruit ESCRT-III components respectively. ESCRT-I and ESCRT-III subunit CHMP4B are recruited into the centre of the intercellular bridge where they procedure a series of cortical rings within the midbody (Elia *et al.*, 2011).

Abnormality in the regulation of cytokinesis has been recognized as a mechanism in the pathogenesis of cancers and neurogenerative disorders. Endosomal sorting complex required for transport, polo-like kinase, aurora kinase, and anillin-like proteins are established key regulators of cell cycle-related events in both fission yeast (*Schizosaccharomyces pombe*) and higher eukaryotes such as humans.

We hypothesized that the *vps4* (ESCRT), *ark1* (aurora kinase), *plo1* (polo-like kinase) and *mid1* (anillin-like) genes interact through phosphorylation to mediate cytokinesis during the cell cycle. In this study,

3.2 Aims

The control of cytokinesis is a universal process common to all eukaryotes during cell division, protein phosphorylation is a common mechanism regulating timing events during cellular processes specifically cytokinesis. This study aims to investigate the potential interactions between *mid1*, *vps4*, *plo1*, and *ark1* genes in the regulation of cytokinesis during cell division and identification of the phosphorylation site essential for this event in *S. pombe*. To this end, here we investigated the genetic interactions between *mid1* phospho-mutant, *vps4Δ, plo1-ts35,* and *ark1-ts11* genes using tetrad dissection, growth viability and morphological studies as the first step in this process. This work will describe:

- Investigation and characterization of genetic interactions between *mid1* phospho-mutant, *vps4Δ, plo1-ts35,* and *ark1-ts11* genes during cytokinesis in *S. pombe* using tetrad dissection.

- Characterization of synthetic viable and morphology defect phenotypes expressed in the double mutant strains of *mid1* phospho-mutant, *vps4Δ, plo1-ts35,* and *ark1-ts11* genes by growth assay and microscopy analysis.

- Identification of important phosphorylation sites important for the regulation of Mid1p during cytokinesis in *S. pombe* in cell division.

3.3 Results

3.3.1 An *in vivo* integration strategy to study Mid1p function

This study was concerned with understanding the regulation of Mid1p through the cell cycle of *S. pombe*. To achieve this an *S. pombe* integration experiment was designed which involved introducing single, double, or multiple mutations of potential phospho-sites in Mid1p to yield phospho-mimetic versions by converting serine (S) to aspartic acid (D), and phospho-resistant by converting from serine (S) to alanine (A). These amino acid changes were made because alanine cannot be phosphorylated (phospho-deficient), whereas the negative charge of aspartic acid mimics permanent phosphorylation (phospho-mimetic).

An *S. pombe* plasmid pJK148 was used to integrate mutated *mid1* DNA sequences into the *leu1*$^{+}$ chromosome locus of fission yeast (Figure 3-2). The plasmid was first linearized and then transformed into an *S. pombe* strain with a point mutation in the *leu1*$^{+}$ gene (Siam *et al.*, 2004). We used this approach to produce *S. pombe* strains with phospho-mimetic (S>D) and phospho-resistant (S>A) versions of the *mid1* gene to test the effect of such mutations on Mid1p function by examining cell growth defects and morphology formation. Single-point, double-point, and multiple-point mutants of the *mid1* gene were designed with the *mid1* endogenous promoter contained in 1k bp upstream of the *mid1* open reading frame and were synthesized by GenScript (Chapter 2). Following the successful integration of each of the *mid1* mutant genes, the strains were subjected to *in vivo* growth and morphological analysis.

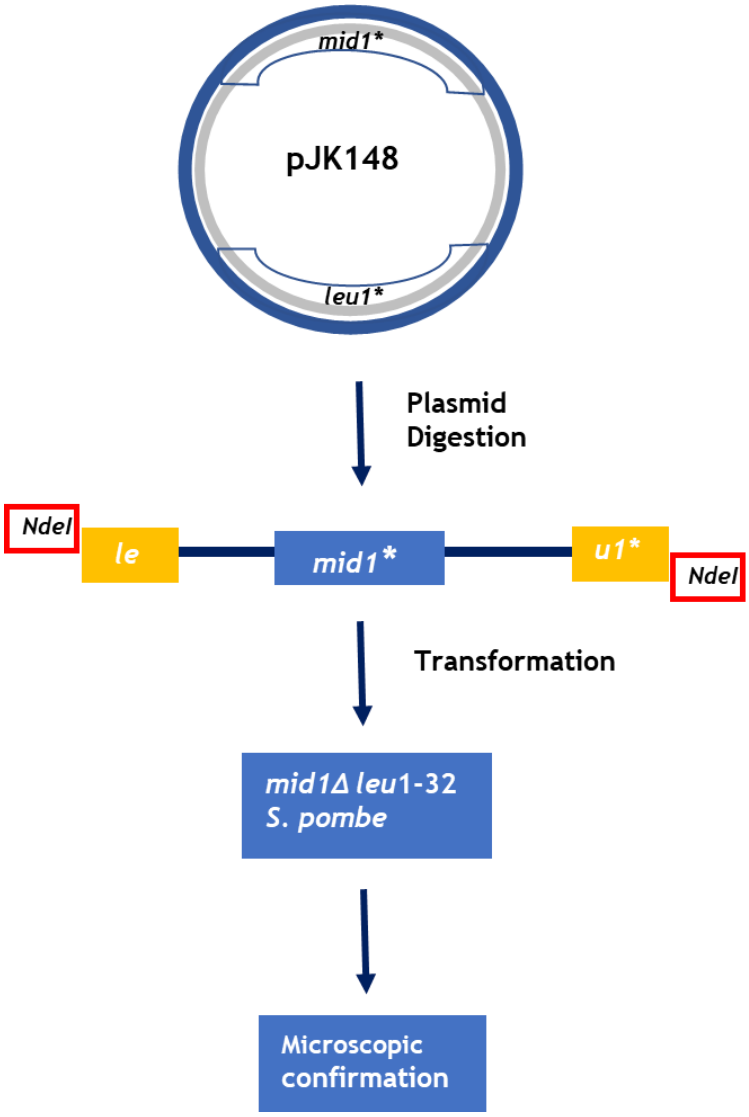

Figure 3-2 Design of construct and integration of *mid1* phospho-resistant and a phospho-mimetic mutant version of a gene. The endogenous *mid1* gene is replaced with phospho-resistant and phospho-mimetic mutant versions using an interactive vector. *S. pombe in vivo* integration experiment was designed to evaluate the functional significance of Mid1p phosphorylation sites. The *mid1* phospho mimetic and phospho resistant mutant versions of the gene are contained in the pJK148 integrative vector with a *leu*$^{+}$ selective marker and a *Nde I* restriction site. *mid1** represents the Mid1p wild-type and *mid1* gene mutants. The plasmid is linearized in *leu*$^{+}$ with *Nde I* and then transformed into a Mid1p *S. pombe* strain with a *leu1*-32 point mutation, where it integrates at the *leu1*$^{+}$ locus. Cell growth defects, colony formation, morphology, and confocal imaging are performed on the resulting *S. pombe* strain.

3.3.2 Genetic interactions between *vps4*△, *plo1-ts35, ark1-ts11* and *mid1* phospho-mutants

To study the role of the six phospho-acceptor sites identified in Mid1p through mass spectrometric analysis, we examined the genetic interaction and the effect of their mutation *in vivo*. Previous data from our Laboratory showed that *S. pombe* cells exhibit synthetic lethality without the Mid1p function *(vps4Δ mid1Δ)*. Therefore, we tested the effect of mutations of Mid1p phospho-acceptor sites in fission yeast by creating double mutants to evaluate their genetic relevance. Mid1p is a phosphoprotein, and previous studies from this group have mapped phospho-acceptor sites by protein kinases assays and proteomics, revealing six serine residues of notable importance shown in Figure 3-3 (Rezig *et al.*, 2021). To explore the phosphorylation of Mid1p by aurora and polo kinases, a mass spectrophotometry approach was utilized to identify and map out phospho-acceptor sites. The N-terminal and Middle domains of Mid1p were discovered to have 35 potential Mid1p residues phosphorylated by both polo 1 and aurora A kinases. These phospho-sites consist of S167, S328, S331, S332, S523 and S531 where theses six sites were identified (Rezig *et al.*, 2021). Moreover, other studies were examined on fission yeast phospho-proteomes to confirm the number of Mid1p phospho-sites (Koch *et al.*, 2011; Carpy *et al.*, 2014; Kettenbach *et al.*, 2015; Swaffer *et al.*, 2018).

Versions of the *mid1* gene containing phospho-acceptor site mutations were generated and integrated into a single copy of the chromosomal DNA of *S. pombe mid1*Δ cells. Each version of the *mid1* gene had either a phospho-mimetic (S>D) or a phospho-resistant (S>A) point mutation(s) of the residues S167, S328, S331, S332, S523, or S531 to create a panel of mutant *S. pombe* strains (Figure 3-3). These amino acid modifications were made from serine to alanine (phospho-deficient) and serine to aspartic acid (phospho-mimetic). Additionally, as a positive control, a wild-type version of the *mid1* gene was integrated into *mid1Δ* cells; this resulted in cells that behaved and looked identical to wild-type, in solid medium and liquid culture, indicating that the integration process restored Mid1p function (Rezig *et al.*, 2021).

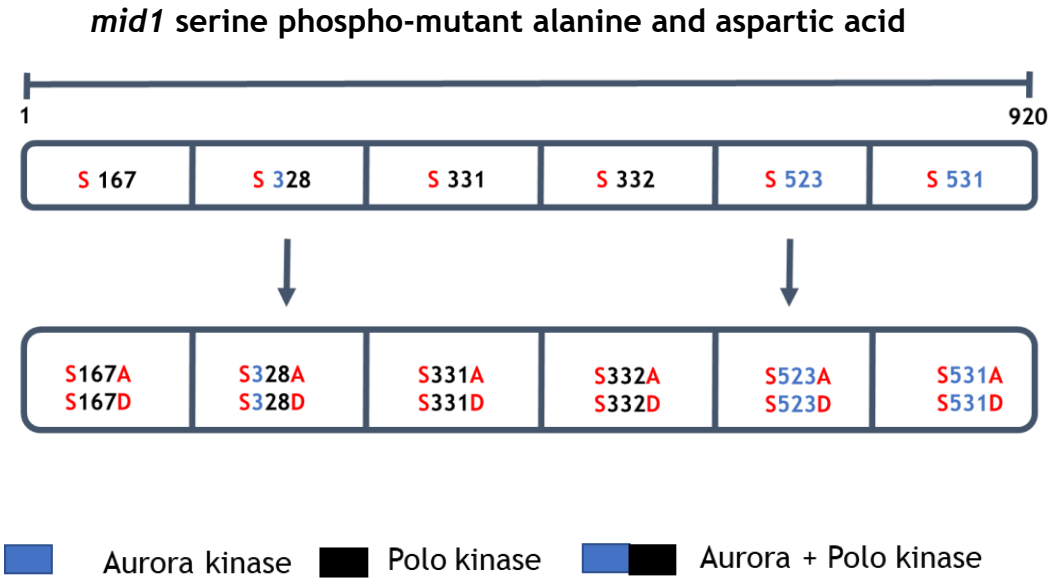

Figure 3-3 *mid1* serine phospho-mutant alanine (A) and aspartic acid (D). Mid1p phosphorylated amino acid residues mapped by protein kinases assays and proteomic (Rezig et al., 2021). The six identified serine residues were mutated to either *mid1* phospho-mutant alanine (A) and phospho-mimetic aspartic acid (D). *mid1* serine phospho-mutant alanine and aspartic acid are illustrated in black and blue, the black indicates polo kinase, blue showed aurora kinase and blue-black showed polo and aurora kinase.

3.3.2.1 Classical genetic approach

A yeast genetic approach was chosen to study the interaction between *vps4*, *plo1*, *ark1*, and anillin *mid1* genes. Tetrad analysis is a technique for analyzing meiotic product phenotypes to identify genetic interactions and is widely used for mapping and identifying genetic interaction between two genes (Moreno *et al.*, 1991; Rezig *et al.*, 2019). Hence, we created *mid1* phospho-mutant and *vps4Δ* double mutants by mating two *mid1* phospho-mutant and *vps4Δ* genes. Double mutants were identified using a micromanipulator and selective media (Figure 3-4). It has been previously shown in fission yeast that double chromosome deletions of the *vps4 and mid1 genes (vps4Δ mid1Δ)* are synthetically lethal, studies have identified physical interaction between the encoded Vps4p and Mid1p proteins (Rezig *et al.*, 2021).

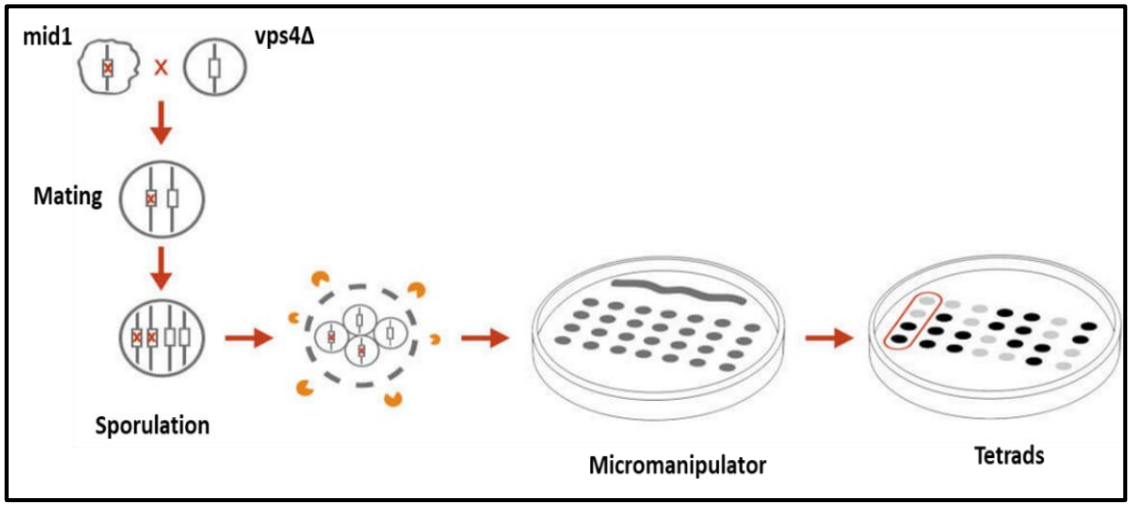

Figure 3-4 Schematic description of tetrad analysis and identification of double mutants in *S. pombe*. Yeast strains were mated on a mating medium at 25ºC for two days and then transferred to a solid YE medium for ascus dissection. Individual spores from each tetrad were placed with a micromanipulator at sequential horizontal grid positions and allowed to form colonies, then replica plated to two solid media: EMM lacking uracil (EMM -ura) and EMM lacking leucine (EMM -leu).

3.3.3 Generation of *mid1* phospho-mutant *vps4*Δ double mutants

To continue this study, we made double mutants of *mid1* phospho-mutant and *vps4Δ* where a serine residue has been replaced by either alanine or aspartic acid in search of a synthetic phenotype. Two fission yeast strains were crossed, one containing a chromosome deletion of *vps4Δ* and the other a *mid1* phospho-mutant. Double mutants were produced by tetrad dissections of ascospores produced by sexual mating and were identified by growing them on an appropriate selective medium (Figure 3-5). The crosses completed between *vps4Δ* and *mid1* phospho-mutants are summarised in Table 3-1.

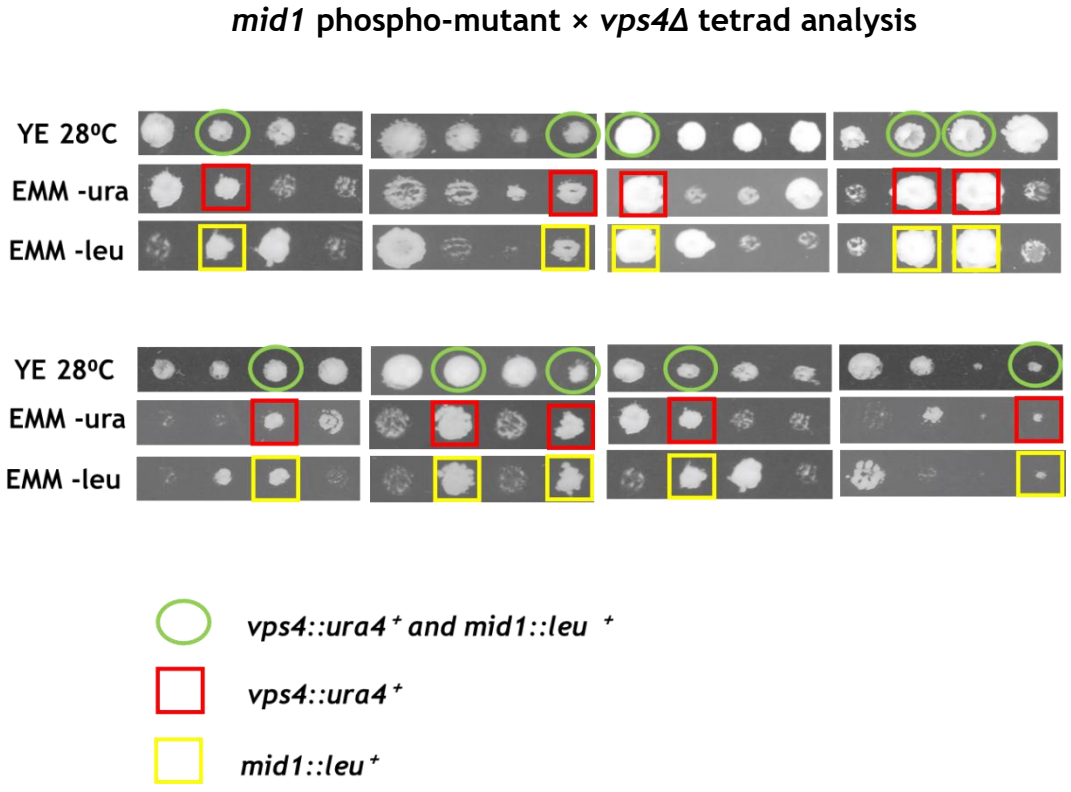

Figure 3-5 Identification of fission yeast double *mid1* phospho-mutant *vps4*Δ generated by ascus dissection. Yeast strains were mated on solid ME medium at 25ºC for two days and then transferred to solid YE medium for ascus dissection using a Singer MSM Ascus Dissector. Spores from each tetrad were placed at sequential horizontal grid positions and allowed to form colonies, then replica plated to two solid media: EMM lacking uracil (EMM -ura) and EMM lacking leucine (EMM -leu). This was incubated at 28ºC until the growth of colonies, the double mutants are boxed in green, red, and yellow. The double mutants were created in three (n=3) independent experiment for each genotype, given a GG number respectively and stored in 30% glycerol in the Glasgow yeast collection at -80ºC.

After strains of *mid1* phospho-mutant were mated with *vps4Δ*, the ascus micromanipulator microscope was used to transfer four spores from each tetrad and allow them to develop colonies. The four yeast colonies were subjected to genotype screening using selective media. EMM -leu identify *mid1* phospho-mutant and EMM -ura identifies *vps4Δ* (Rezig *et al*., 2019, Rezig *et al*., 2021). This result allows for the identification of double mutants of *mid1* phospho-mutant and *vps4Δ*. The double mutants m*id1* phospho-mutant *vps4Δ* genotype are predicted to have viable growth and colonies on both selective plates. Hence, the double mutants are identified by identifying growth and colonies at the same spot on both EMM -leu and EMM -ura selective media. In all instances, double mutants *mid1* phospho-mutant *vps4Δ* showed viable growth and colonies on both selective media suggesting a successful creation and identification of double mutants. In all cases no synthetic lethality was observed: all the double mutants created are listed in Table 3-1, with an example shown in Figure 3-5 and the remainder of the Figures illustrating the identification of the double mutants shown in Appendix I.

3.3.4 Synthetic viable phenotypes of *mid1* phospho-mutants *vps4*∆

To further investigate the double *mid1* phospho *vps4*Δ mutant for synthetic phenotypes, we studied the growth defects phenotypes compared with the single mutant strains by examining growth rates defects. Cells were collected from wild-type, parent strains, *mid1*Δ, and the newly formed double mutant isolates; these were suspended at $1.5x10^6$ cell/ml of sterile distilled water and subjected to 10-fold serial dilution. Using a calibrated pipette 10-15 µl of cell suspension from each strain was pipetted sequentially on solid YE media, allowed for 20-30 minutes to dry, and incubated at four different temperatures (25^oC, 28^oC, 32^oC, and 37^oC) for two days to assess the growth rate.

Initial experiments showed that wild-type (WT) cells and all *mid1* phospho mutants formed viable colonies with similar growth rate patterns and colony morphology to the wild-type yeast strain in all temperatures (25^oC, 28^oC, 32^oC, and 37^oC. However, the *vps4Δ* cells grew slower similar to *mid1Δ*, viable growth was observed between wild-type, integrated wild-type and most of the *mid1* phospho-mutant strains (Figure 3-7). The double mutants showed defective and impaired growth rate in the *vps4Δ* and *mid1* phospho-mutants double mutants implying a strong genetic interaction between the encoded *mid1* phospho-mutant and *vps4Δ* genes are required for cell growth. Some mutants exhibit partial loss of integrity and function, reduced activity, and increased cell width under tolerant conditions (Figure 3-7).

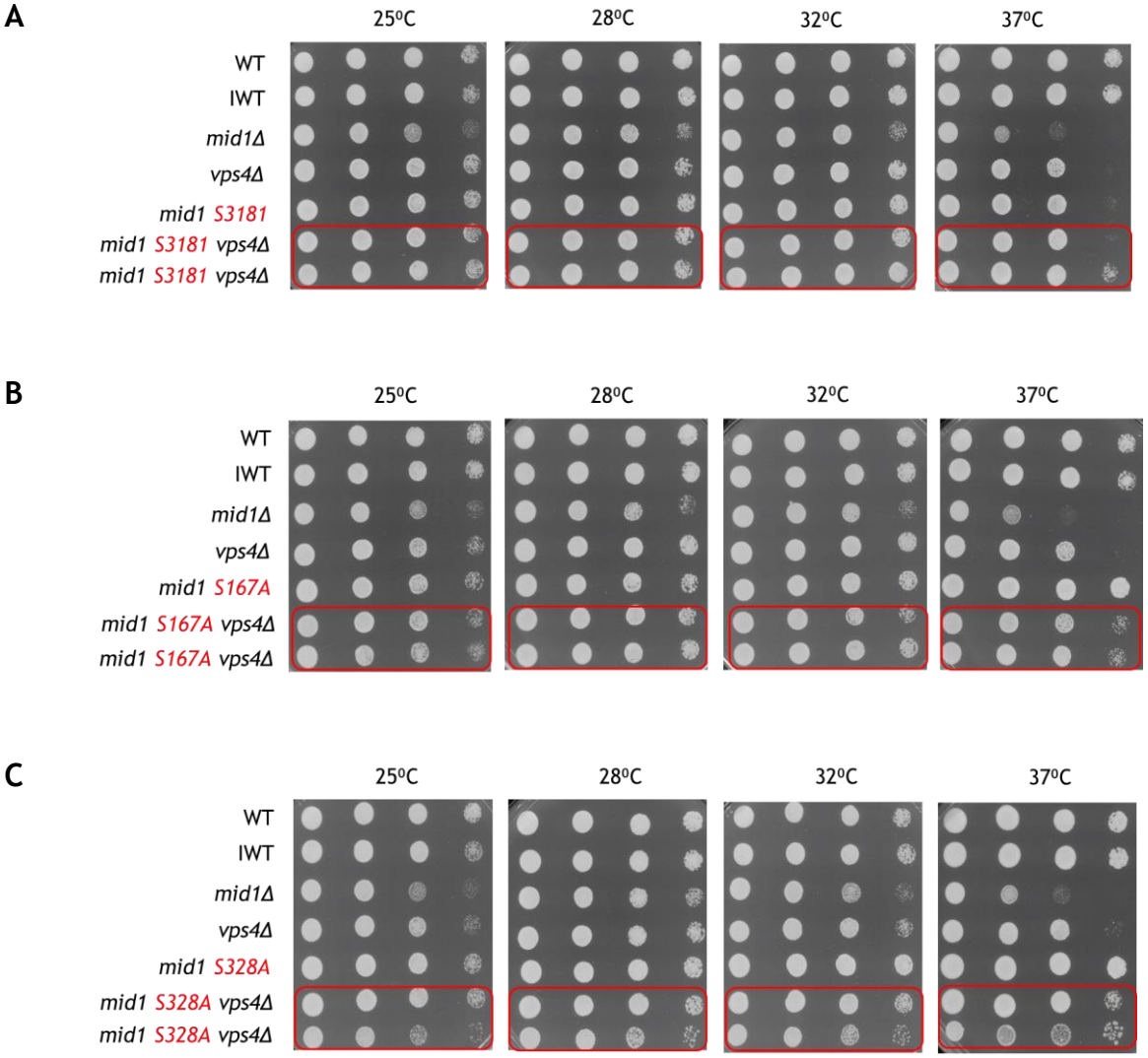

Figure 3-6 *mid1* phospho-mutant shows synthetic viable phenotypes with *vps4*Δ. Synthetic viable phenotypes and colony analysis of wild-type, parent cells, *mid1*Δ, and double mutant isolates. All the cells were suspended at 1.5x10^6 cells/ml and subjected to 10-fold serial dilution. Cells suspended were pipetted onto solid YE media and incubated at four different temperatures (25ºC, 28ºC, 32ºC, and 37ºC). The analysis of growth phenotype was captured and interpreted after two days of cell growth on a solid YE medium. **A** double mutant wild-type and *vps4*Δ (GG 3486), **B** double mutant of *mid1* phospho-mutant *S167A* and *vps4*Δ (GG 3450), and **C** double mutant of *mid1* phospho-mutant *S328A* and *vps4*Δ (GG 3456). WT is wild-type, IWT is integrated wild-type, *mid1*Δ is Mid1p deletion, and *vps4*Δ is Vps4p deletion.

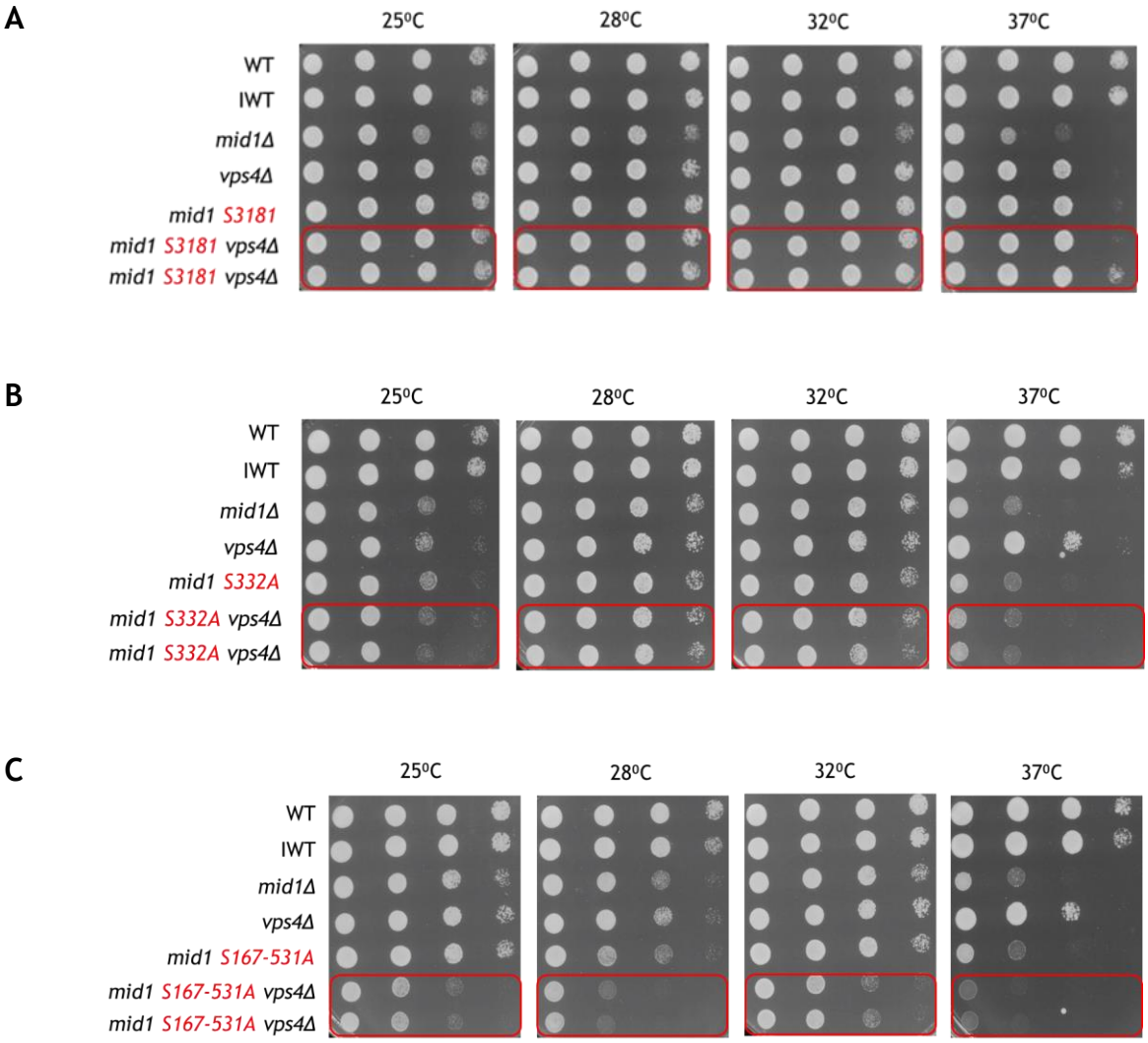

Figure 3-7 *mid1* phospho-mutant shows synthetic viable phenotypes with *vps4*Δ. Synthetic viable phenotypes and colony analysis of wild-type, parent cells, *mid1*Δ, and double mutant isolates. All the cells were suspended at 1.5x10^6 cells/ml and subjected to 10-fold serial dilution. Cells suspended were pipetted onto solid YE media and incubated at four different temperatures (25ºC, 28ºC, 32ºC, and 37ºC). The analysis of growth phenotype was captured and interpreted after two days of cell growth on a solid YE medium. A double mutant wild-type and *vps4*Δ (GG 3487), B double mutant of *mid1* phospho-mutant *S332A* and *vps4*Δ (GG 3469), and C double mutant of *mid1* phospho-mutant *S167-531A* and *vps4*Δ (GG 3467). WT is wild-type, IWT is integrated wild-type, *mid1*Δ *is* Mid1p deletion, and *vps4*Δ is Vps4p deletion. Double mutants indicating growth rate defects are represented in red circles.

Nearly all the double mutants *mid1* phospho *vps4Δ* created in previous results showed viable growth at 25ºC, 28ºC, and 32ºC while at 37ºC the double mutants, single mutants, and *vps4Δ* did not grow. Only wild-type and integrated wild-type grow at 37ºC. The double *mid1* phospho *vps4Δ* mutants serine positions S332A and S523-531A were observed to have similar growth rate patterns with *mid1Δ* across the four temperatures at S332A and S523-531A serine positions (Figure 3-7). However, wild-type and integrated wild-type cells grow well at 37ºC. The double *mid1* phospho *vps4Δ* mutants S332A and S167-531A, *vps4Δ*, and *mid1Δ* colonies showed defective growth rates. S523-531A are observed to have a slow growth, with temporarily defective cells as the cells eventually grow over a period of time. We could suggest that Mid1p S523-531 serine position have the mechanism to rescue the impact of phosphorylation during cytokinesis. This was observed and noted during growth assay of single and double mutant cells.

Compared with the two parents' single mutants and wild-type strains, the double mutant strains were unable to grow and form large colonies at 37ºC but were observed to have a defective growth phenotypes. *mid1* phospho *vps4Δ* double mutants showed defective growth phenotypes similar to *mid1Δ* phenotypes.

3.4 Morphology and colony formation of *mid1* phospho-mutants *vps4*Δ

The observed impaired growth of the double mutants *mid1* phospho *vps4Δ* compared to the wild-type, integrated wild-type, and parent strains suggests that these two genes interact in the cell cycle of *S. pombe*. To understand the genetic interaction between the phenotypes with impaired growth, we examined the colony formation and morphology between double mutant *mid1* phospho-mutants *vps4Δ*, and the morphology and colony formation of the *mid1* phospho-mutants and the double mutants during the cell cycle. To achieve this, strains were grown on solid media alongside wild-type, *mid1Δ, mid1* phospho-mutants, and double mutants of *mid1* phospho-mutants *vps4Δ*. The strains were grown for 24-48 hours on YE solid medium and colony morphology visualized microscopically.

Results from the morphology experiment showed that wild-type and most *mid1* phospho-mutants formed viable colonies with similar colony and morphological patterns to the wild-type yeast strain (Figure 3-8). However, we observed that *mid1* phospho-mutant *vps4Δ* double colony and morphology revealed a phenotype similar to *mid1Δ*. This study also revealed that S332A and S167-531A showed defective irregular colony formation (Figure 3-9). Viable colonies and morphology were observed in wild-type and integrated wild-type yeast strain compared with the double mutants generated. However, S332A and S167-531A revealed defective colony and morphology in the *mid1* phospho-mutant *vps4Δ* double mutant compared with wild-type cells.

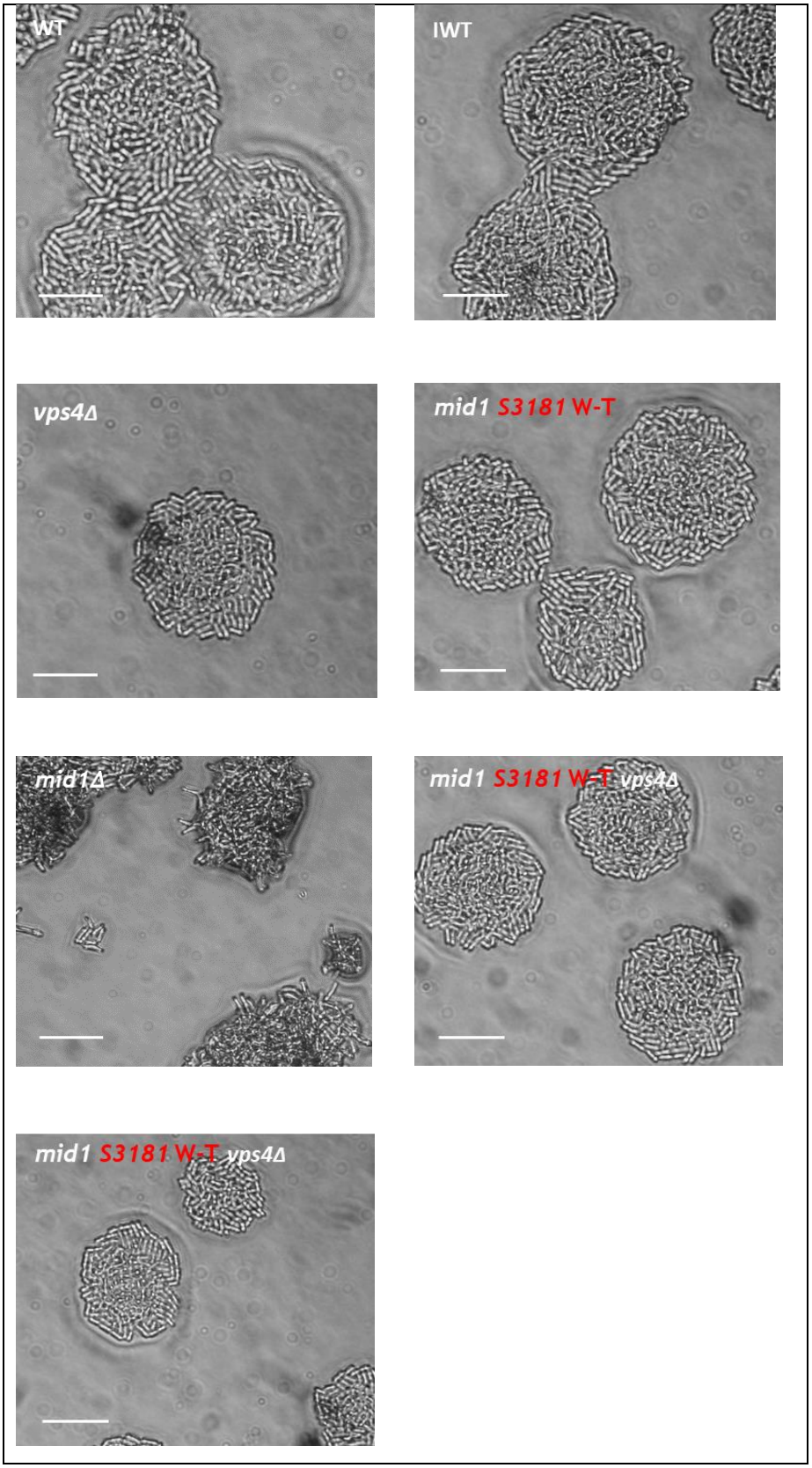

Figure 3-8 The *vps4*Δ integrated wild-type reveals no morphological defects. Analysis of the morphological defect of double mutant *vps4*Δ (GG 2673) and integrated wild-type (GG 3181), strains grown at 28ºC on solid YE medium and suspended at a concentration of $1.5x10^6$ cells/ml, cells were subjected to serial dilution. Pipetted cells were placed on solid YE media and incubated, after two days of cell growth on a solid YE medium, the wild-type, *mid1* phospho-mutants, and double mutants were examined and interpreted. The colony was captured using Sony DSC-75 camera, scale bar represents 50 µm. WT is wild-type, IWT is integrated wild-type, *mid1*Δ *is* Mid1p deletion, and *vps4*Δ is Vps4p deletion.

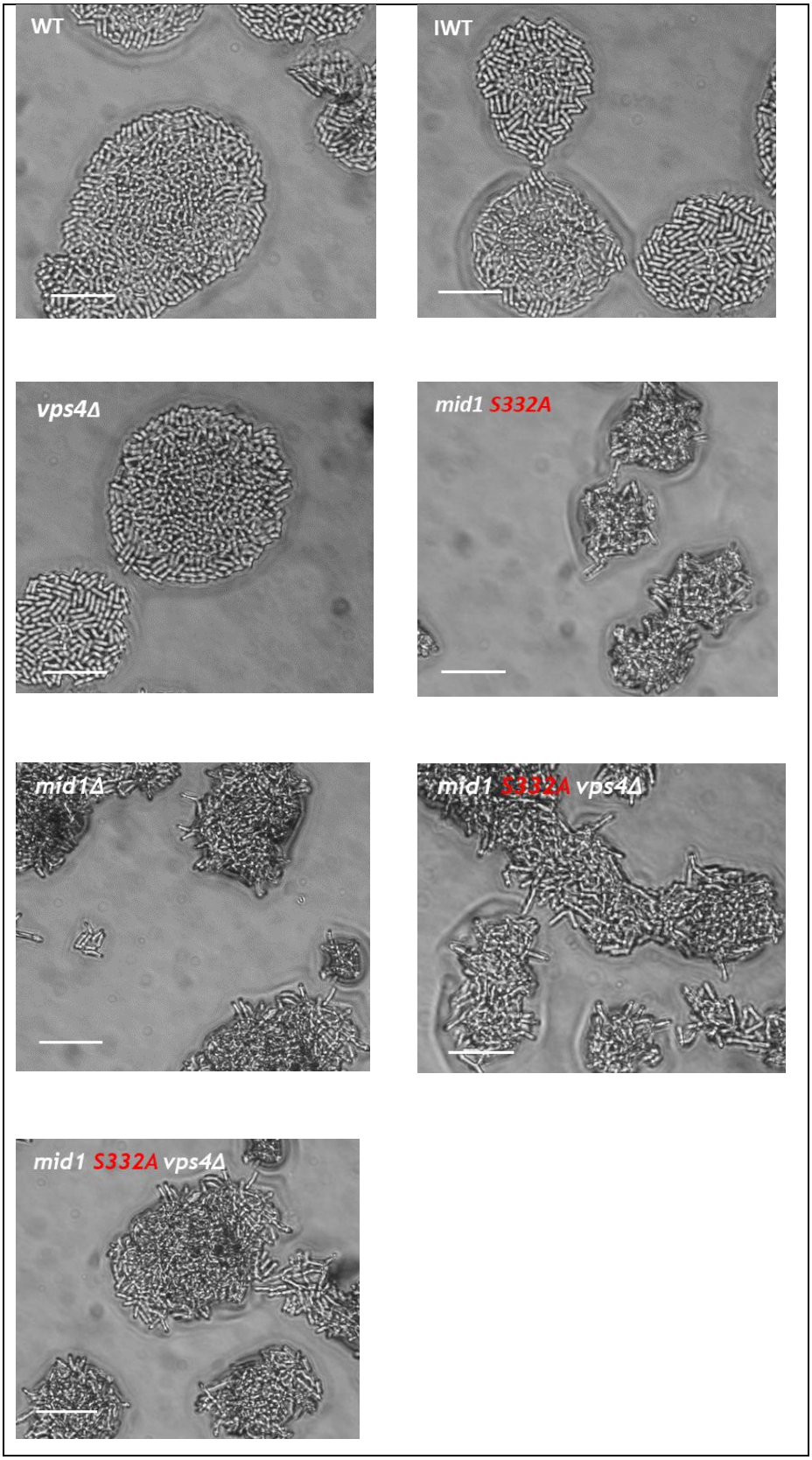

Figure 3-9 The *vps4*Δ *mid1* phospho-mutant reveals morphological defects. Analysis of the morphological defect of double mutant *vps4*Δ (GG 2673) and *mid1* phospho-mutant (GG 3291), strains grown at 28ºC on solid YE medium and suspended at a concentration of $1.5x10^6$ cells/ml, cells were subjected to serial dilution. Pipetted cells were placed on solid YE media and incubated, after two days of cell growth on a solid YE medium, the wild-type, *mid1* phospho-mutants, and double mutants were examined and interpreted. The colony was captured using Sony DSC-75 camera, scale bar represents 50 µm. WT is wild-type, IWT is integrated wild-type, *mid1*Δ *is* Mid1p deletion, and *vps4*Δ is Vps4p deletion.

The wild-type, *mid1* phospho-mutant, and *vps4Δ mid1* phospho double mutants showed a viable and normal colony formation in *S. pombe* cells. Nearly all the double mutant phenotypes showed no colony and morphological changes compared with the wild-type. In contrast, *mid1Δ* differs from the wild-type and *mid1* phospho-mutant with defective colony formation and morphology. Double mutants of *vps4Δ mid1* phospho S332A and S523-531A showed impaired, defective colony formation and morphology compared with wild-type and *mid1* phospho mutants Figure 3-9). In comparison with the two parents and the wild-type, the double mutants formed impaired defective colonies and morphological changes in size and shape similar to *mid1Δ*, and serine positions S332A and S523-531A exhibited defective colony formation similar to *mid1Δ*. All double mutants showed changes in the colony and morphology as the temperature increased. The observed defective colony and morphology phenotypes in the *vps4Δ mid1* phospho double mutants illustrate a strong genetic interaction between *vps4* and *mid1* genes, this further suggests a strong interaction of the encoded *vps4* and *mid1* genes is required for *S. pombe* viable growth, colony formation, and function.

3.5 Generation of double *mid1* phospho-mutants with *ark1-ts11* and *plo1-ts35*

To further understand the genetic interaction between proteins associated with the cycle in *S. pombe* in this study, we created double mutants of *plo1-ts35* and *ark1-ts11* with *mid1* phospho-mutants by crossing with various strains. Both *plo1-ts35* and *ark1-ts11* proteins were used as a control to validate the genetic interaction between *mid1* phospho-mutant *vps4Δ* as both *plo1-ts35* and *ark1-ts11* proteins were previously established to genetically interact with the classes of ESCRT proteins during cytokinesis (Bhutta *et al.*, 2014; Rezig *et al.*, 2019; Rezig *et al.*, 2021). Double mutants with *mid1* phospho-mutants, *plo1-ts35* and *ark1-ts11* were created as it was hypothesized that these cell cycle protein kinases may have a role in phosphorylating Mid1p.

Double mutants were created for the various *mid1* phospho-mutants, both single mutants and multiple (S>A) or (S>D). Table 3-1 shows all the generated double mutants created with *plo1-ts35,* or *ark1* and *mid1* phospho-mutants in this study. In each case fission yeast strains temperature-sensitive mutants of *plo1-ts35*, *ark1-ts11,* and the other *mid1* phospho-mutant were crossed. Double mutants were created, identified, and isolated by tetrad dissections of ascospores produced by sexual mating and the identification was possible by growing them on an appropriate selective medium. An example of such a cross is between *ark1-ts11 mid1* phospho-mutant is shown in Figure 3-10 *plo1-ts35* and *mid1* phospho-mutant shown in Figure 3-11. There was no synthetic lethality recorded at any stage of the study: all double mutants created are listed in Table 3-1 with the remainder of the Figures illustrating the identification of the double mutants shown in Appendix I.

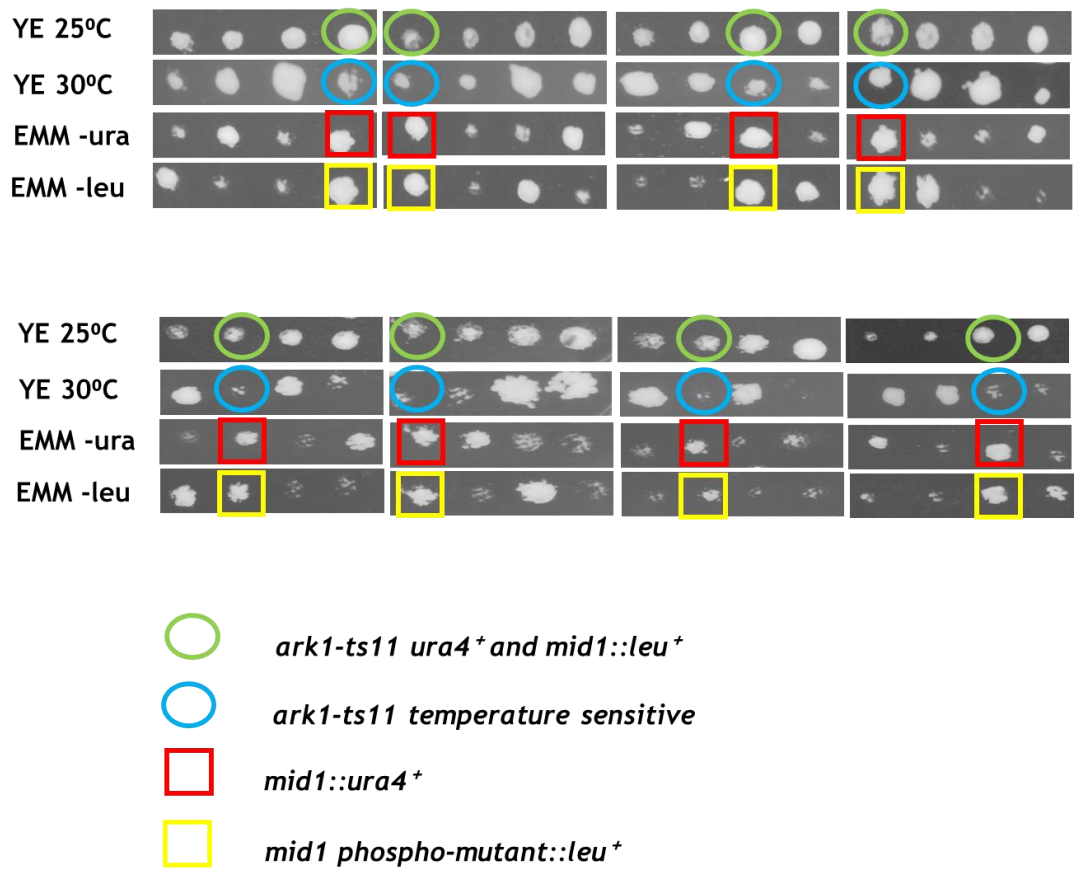

Figure 3-10 Identification of fission yeast double *mid1* phospho *ark1-ts11* mutants generated by ascus dissection. Yeast strains were mated on solid ME medium at 25ºC for two days and then transferred to solid YE medium for ascus dissection using a Singer MSM Ascus Dissector. Spores from each tetrad were placed at sequential horizontal grid positions and allowed to form colonies, then replica plated to two solid media: EMM lacking uracil (EMM -ura) and EMM lacking leucine (EMM -leu). This was incubated at 28ºC until the growth of colonies, the double mutants are boxed in green, blue, red, and yellow. The double mutants were created in three (n=3) independent experiment for each genotype, given a GG number respectively and stored in 30% glycerol in the Glasgow yeast collection at -80ºC.

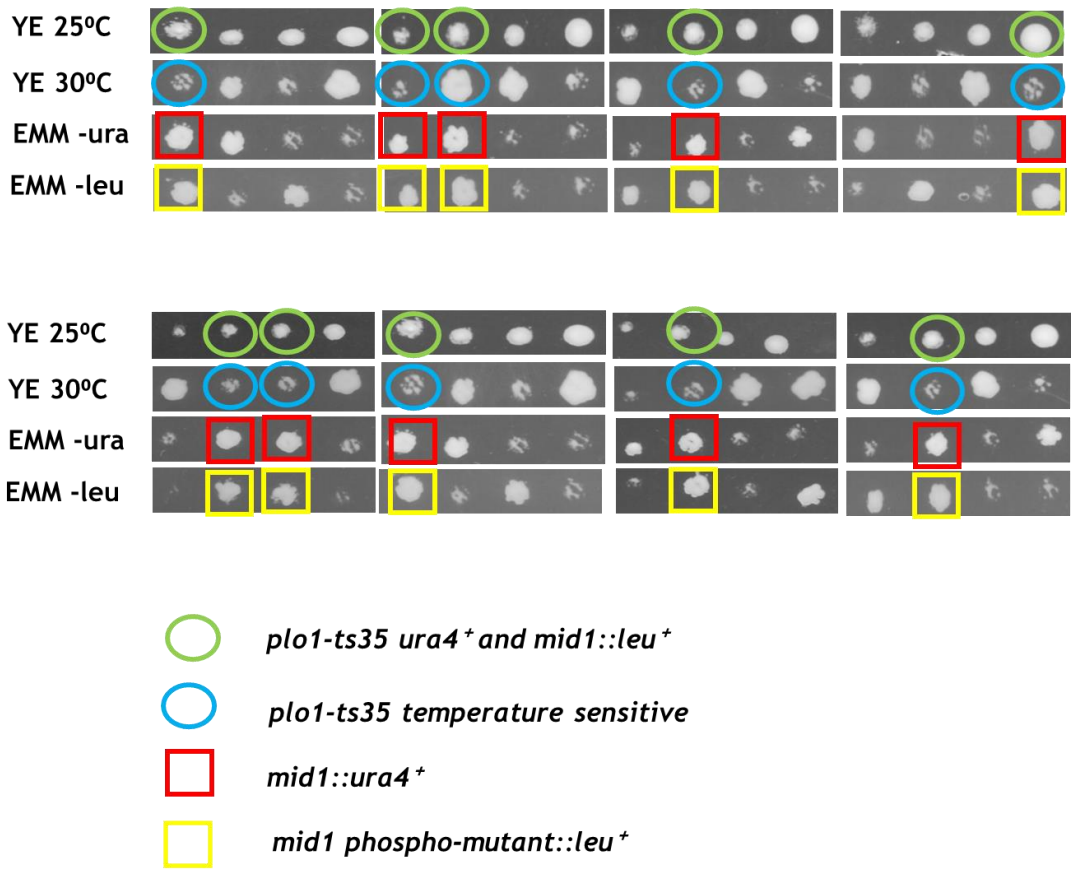

Figure 3-11 Identification of fission yeast double *mid1* phospho *plo1-ts35* mutants generated by ascus dissection. Yeast strains were mated on solid ME medium at 25ºC for two days and then transferred to solid YE medium for ascus dissection using a Singer MSM Ascus Dissector. Spores from each tetrad were placed at sequential horizontal grid positions and allowed to form colonies, then replica plated to two solid media: EMM lacking uracil (EMM -ura) and EMM lacking leucine (EMM -leu). This was incubated at 28ºC until the growth of colonies, the double mutants are boxed in green, blue, red, and yellow. The double mutants were created in three (n=3) independent experiment for each genotype, given a GG number respectively and stored in 30% glycerol in the Glasgow yeast collection at -80ºC.

In each *S. pombe* yeast strain case, one containing temperature-sensitive *ark1-ts11* and *plo1-ts35*, and *mid1* phospho-mutant were crossed. Double mutants were created by tetrad dissections of ascospores produced by sexual mating and were identified by growing them on an appropriate selective medium EMM -ura and EMM -leu. EMM -leu identify *mid1* phospho-mutant and EMM -ura *ark1-ts11* and *plo1-ts35* (Rezig *et al.*, 2019, Rezig *et al.*, 2021).

However, all the generated double mutants were viable showing that none of the double *mid1* phospho *ark1-ts11* (Figure 3-10) and *mid1* phospho *plo1-ts35* **(**Figure 3-11**)** mutants were synthetically lethal. The double mutants m*id1* phospho-mutant *ark1-ts11* and *plo1-ts35* genotypes are predicted to have growth and colonies on both selective plates. Hence, the double mutants are identified by spotting growth and colonies at the same position on both EMM -leu and EMM -ura selective media. In all instances, double mutants *mid1* phospho-mutant *ark1-ts11* and *plo1-ts35* showed viable growth and colonies on both selective media suggesting a successful creation and identification of double mutants.

***mid1* serine phospho-mutants** **(A) alanine (D) aspartic acid** **167 328 331 332 523 531**	***ark1-ts11*** **GG Number**	***plo1-ts35*** **GG number**	***vps4Δ*** **GG number**
GG 3181 wild-type, no mutation	3250 3251 3252	3437 3438 3439	3486 3487 3490
A	3321 3322 3323	3375 3376 3379	3450 3451 3452
D	3324 3325 3326	3377 3378 3380	3383 3384 3453
A	3327 3328 3329	3392 3393 3394	3456 3457 3458
D	3330 3331 3332	3386 3387 3388	3481 3482 3483
A	3333 3334 3335	3397 3398 3399	3485 3489 3495
D	3339 3340 3341	3400 3401 3402	3473 3474 3475
A	3342 3343 3344	3411 3412 3413	3469 3478 3479
D	3218 3219 3220	3407 3408 3409	3224 3249 3255
A	3230 3231 3232	3403 3404 3405	3315 3316 3317
D	3235 3236 3237	3415 3416 3417	3318 3319 3320
A	3239 3240 3241	3428 3429 3430	3264 3265 3366
D	3345 3346 3347	3419 3420 3421	3488 3493 3494
D D D D	3349 3350 3351	3422 3423 3424	3461 3462 3476
A A	3242 3243 3244	3444 3445 3446	3260 3261 3262
D D	3246 3247 3248	3447 3448 3449	3257 3258 3259
A A A A A A	3352 3353	3425 3426	3467 3468

***mid1* serine phospho-mutants (A) alanine (D) aspartic acid**						***ark1-ts11***	***plo1-ts35***	***vps4Δ***
167	**328**	**331**	**332**	**523**	**531**	**GG Number**	**GG number**	**GG number**
						3354	3427	3470
D	D	D	D	D	D	3355	3441	3463
						3356	3442	3464
						3357	3443	3465

Table 3-1. Double mutants of vps4Δ, *ark1-ts11, plo1-ts35 and mid1* phospho-mutant *S. pombe* strains were isolated during this study. In each fission yeast strain case, one containing *vps4*Δ, temperature-sensitive *ark1-ts11,* and *plo1-ts35*, and *mid1* phospho-mutants were crossed. The double mutants were created in triplicate, assigned a laboratory GG number respectively, and stored in 30% glycerol in the Glasgow yeast collection at -80ºC.

3.5.1 Synthetic viable phenotypes of *mid1* phospho-mutants in *ark1-ts11*

To further corroborate our initial tetrad analysis findings, double mutants of temperature-sensitive *ark1-ts11* with *mid1* phospho-mutants were subjected to growth rate defects analysis in the search for defective phenotypes. We examined the growth phenotypes compared with the single mutant strains by observing growth rate defects, cells were suspension from each strain was pipetted sequentially on solid YE media, allowed on the bench for 20-30 minutes, then incubated at four different temperatures (25^{0}C, 28^{0}C, 32^{0}C, and 37^{0}C) for two days to assess the growth rate (explained in detail in *section 2.2.2*). However, in this instance, *mid1* phospho-mutant and *ark-ts11* were analysed for synthetic viable phenotypes.

Wild-type cells and most of the *mid1* phospho mutants formed viable growth with similar growth rate patterns to the wild-type yeast strain in all temperatures (25^{0}C, 28^{0}C, and 32^{0}C). Temperature-sensitive *ark1-ts11* cells grew slower similar to *mid1Δ* and, as expected, did not survive under high temperatures (37^{0}C). However, when *ark1-ts11* were crossed with *mid1* phospho-mutant, the double mutants tended to survive under high temperatures. Serine position S332A and S167-531A double mutant of *mid1* phospho-mutant and *ark1-ts11* showed a defective growth rate (Figure 3-13). This was observed as the double mutants showed defective growth similar to *mid1Δ*. We also observed slow growth but not defective growth patterns in *mid1* phospho-mutant cells with changes at serine position S523-531A and S532-531D, but when allowed to grow longer the cells recovered to normal growth, similar to wild-type. However, a viable growth was observed in wild-type and integrated wild-type yeast strain compared with the double mutants generated, the double mutants showed a viable growth (Figure 3-13).

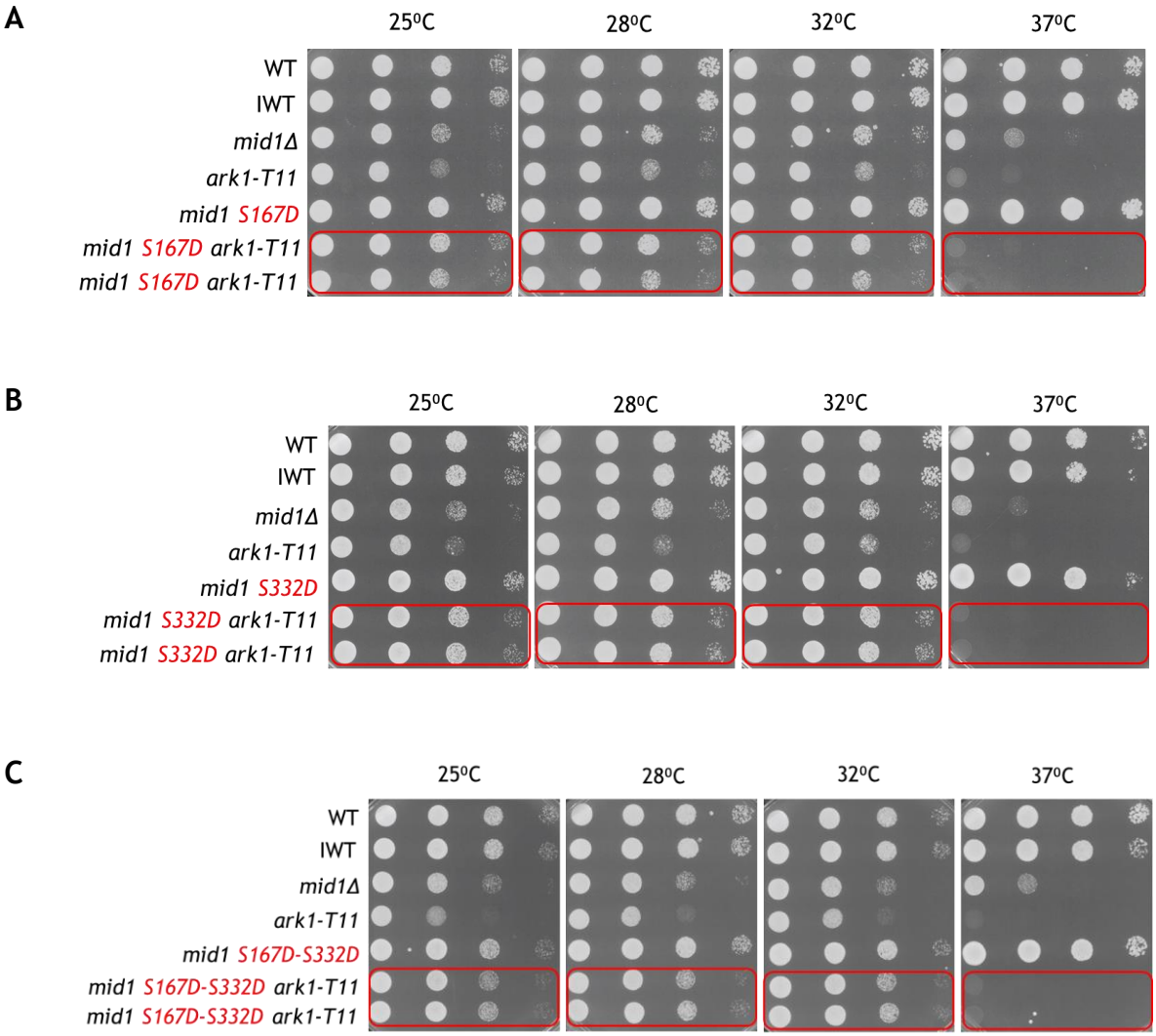

Figure 3-12 *mid1* phospho-mutant shows synthetic viable phenotypes with *ark1-T11.* Synthetic viable phenotypes and colony analysis of wild-type, parent cells, *mid1*Δ, and double mutant isolates. All the cells were suspended at 1.5x10^6 cells/ml and subjected to 10-fold serial dilution. Cells suspended were pipetted onto solid YE media and incubated at four different temperatures (25ºC, 28ºC, 32ºC, and 37ºC). The analysis of growth phenotype was captured and interpreted after two days of cell growth on a solid YE medium. **A** double mutant of *mid1* phospho-mutant *S167D* and *plo1-ts35* (GG 3324), **B** double mutant of *mid1* phospho-mutant *S332D* and *plo1-ts35* (GG 3218), and **C** double mutant of *mid1* phospho-mutant *S167-531D* and *plo1-ts35* (GG 3355). WT is wild-type, IWT is integrated wild-type, and *mid1*Δ *is* Mid1p deletion.

As *ark1-ts11* is a temperature-sensitive strain with a permissive temperature of 25ºC and a restrictive temperature of 37ºC, it was hypothesized that combining this with *mid1* phospho-mutant may result in reducing the restrictive temperature sensitivity. Therefore, yeast strains were also grown at 25ºC, 28ºC, 32ºC, and 37ºC to search for growth differences. (Figure 3-12 and Figure 3-13) of *mid1* phospho-mutant and double mutants illustrate the identification of such a viable growth phenotype in doubles of *ark1-ts11 mid1* phospho-mutant at various temperatures. The results of the growth rate study of all *mid1* phospho-mutant strains with *ark1-ts11 mid1* phospho-mutant strains are shown and summarised in Table 3-2 *ark1-ts11* showed genetic interactions with *mid1* phospho-mutants, as they exhibited viable growth phenotypes.

Double mutant of *ark1-ts11 mid1* phospho-mutant strains also showed viable colonies, whereas wild-type, integrated wild-type, and *mid1* phospho-mutant revealed normal growth rate with the cells growing like normal yeast cells (Figure 3-12 and Figure 3-13) respectively. On the other hand, *mid1Δ* and *ark1-ts11* revealed defective growth rate phenotypes. The double mutant of *mid1* phospho-mutant serine positions S332A and S167-531A showed similar growth phenotypes to *mid1Δ* with impaired growth and a reduced number of viable cells compared to the wild-type. There was no growth at 37ºC of either *ark1-ts11* and *ark1-ts11 mid1* phospho mutant.

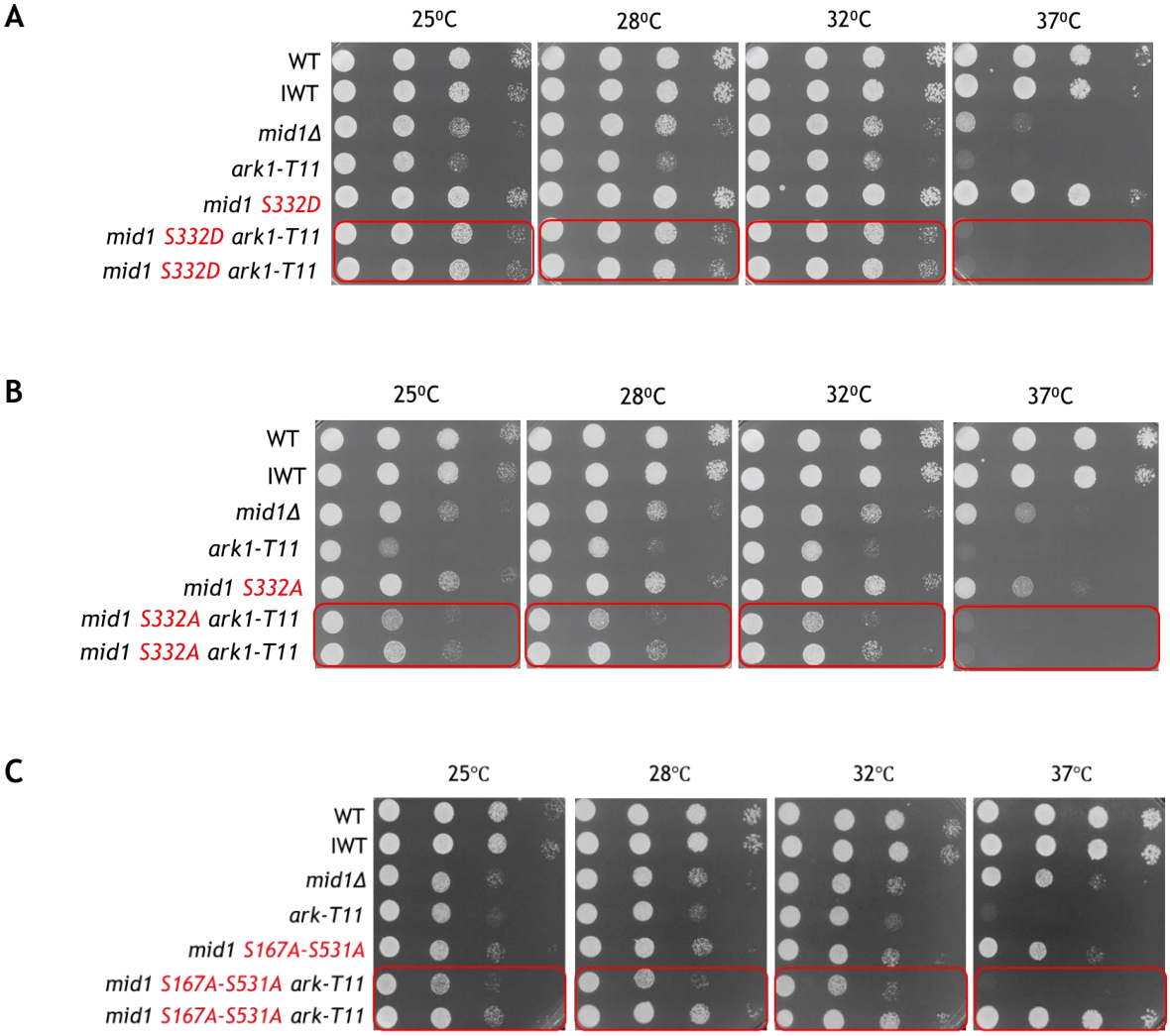

Figure 3-13 *mid1* phospho-mutant shows synthetic viable phenotypes with *ark1-T11.* Synthetic viable phenotypes and colony analysis of wild-type, parent cells, *mid1*Δ, and double mutant isolates. All the cells were suspended at 1.5x10^6 cells/ml and subjected to 10-fold serial dilution. Cells suspended were pipetted onto solid YE media and incubated at four different temperatures (25ºC, 28ºC, 32ºC, and 37ºC). The analysis of growth phenotype was captured and interpreted after two days of cell growth on a solid YE medium. **A** double mutant of *mid1* phospho-mutant *S332D* and *plo1-ts35* (GG 3218), **B** double mutant of *mid1* phospho-mutant *S332A* and *plo1-ts35* (GG 3342), and **C** double mutant of *mid1* phospho-mutant *S167-531A* and *plo1-ts35* (GG 3352). WT is wild-type, IWT is integrated wild-type, and *mid1*Δ *is* Mid1p deletion. Double mutants indicating growth rate defects are represented in red circles.

3.5.2 Synthetic viable phenotypes of *mid1* phospho-mutants in *plo1-ts35*

Similar growth rate defects were observed for double mutants of temperature-sensitive *plo1-ts* with *mid1* phospho-mutants suggesting defective phenotypes. We examined the growth phenotypes of single mutant strains by observing growth rate defects. Wild-type cells and most of the *mid1* phospho-mutants formed viable growth phenotype with similar growth rate patterns at various temperatures (Figure 3-14 and Figure 3-15). Temperature-sensitive *plo1-ts35* cells grew slower similar to *mid1Δ and* did not survive under high temperatures (37^0C).

However, when *plo1-ts35* were crossed with *mid1* phospho-mutant, the double mutants tend to survive under high temperatures. Serine position S332A and S167-531A double mutant of *mid1* phospho-mutant and *plo1-ts35* showed defective growth rate (Figure 3-15). This was observed as the double mutants did not grow viably and in some instances grew worse than *mid1Δ*. We also observed slow growth but not defective growth patterns on serine position S523-531A and S532-531D, but when allowed to grow longer the cells were rescued and recovered back to normal growth like the wild-type. However, a viable growth phenotype was observed in wild-type and integrated wild-type yeast strain compared with the double mutants generated, the double mutants showed a viable growth phenotype (Figure 3-14). However, S332A and S167A-S531A revealed a defective growth pattern compared with wild-type cells (Figure 3-15).

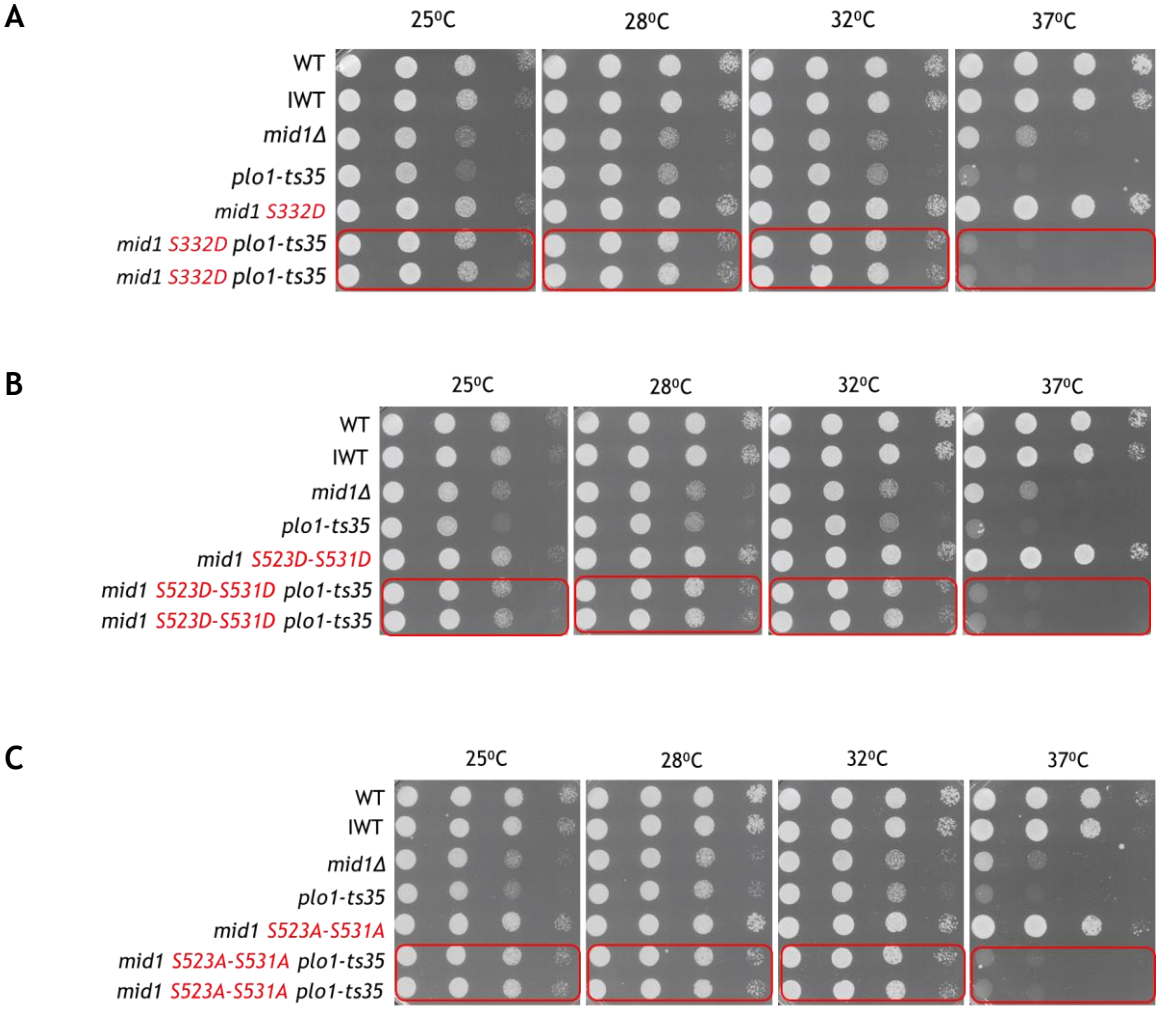

Figure 3-14 *mid1* phospho-mutant shows synthetic viable phenotypes with *plo1-ts3535.* Synthetic viable phenotypes and colony analysis of wild-type, parent cells, *mid1*Δ, and double mutant isolates. All the cells were suspended at 1.5x10^6 cells/ml and subjected to 10-fold serial dilution. Cells suspended were pipetted onto solid YE media and incubated at four different temperatures (25ºC, 28ºC, 32ºC, and 37ºC). The analysis of growth phenotype was captured and interpreted after two days of cell growth on a solid YE medium. **A** double mutant of *mid1* phospho-mutant *S332D* and *plo1-ts35* (GG 3407), **B** double mutant of *mid1* phospho-mutant *S523-531D* and *plo1-ts35* (GG 3447), and **C** double mutant of *mid1* phospho-mutant *S523-531A* and *plo1-ts35* (GG 3444). WT is wild-type, IWT is integrated wild-type, and *mid1*Δ *is* Mid1p deletion.

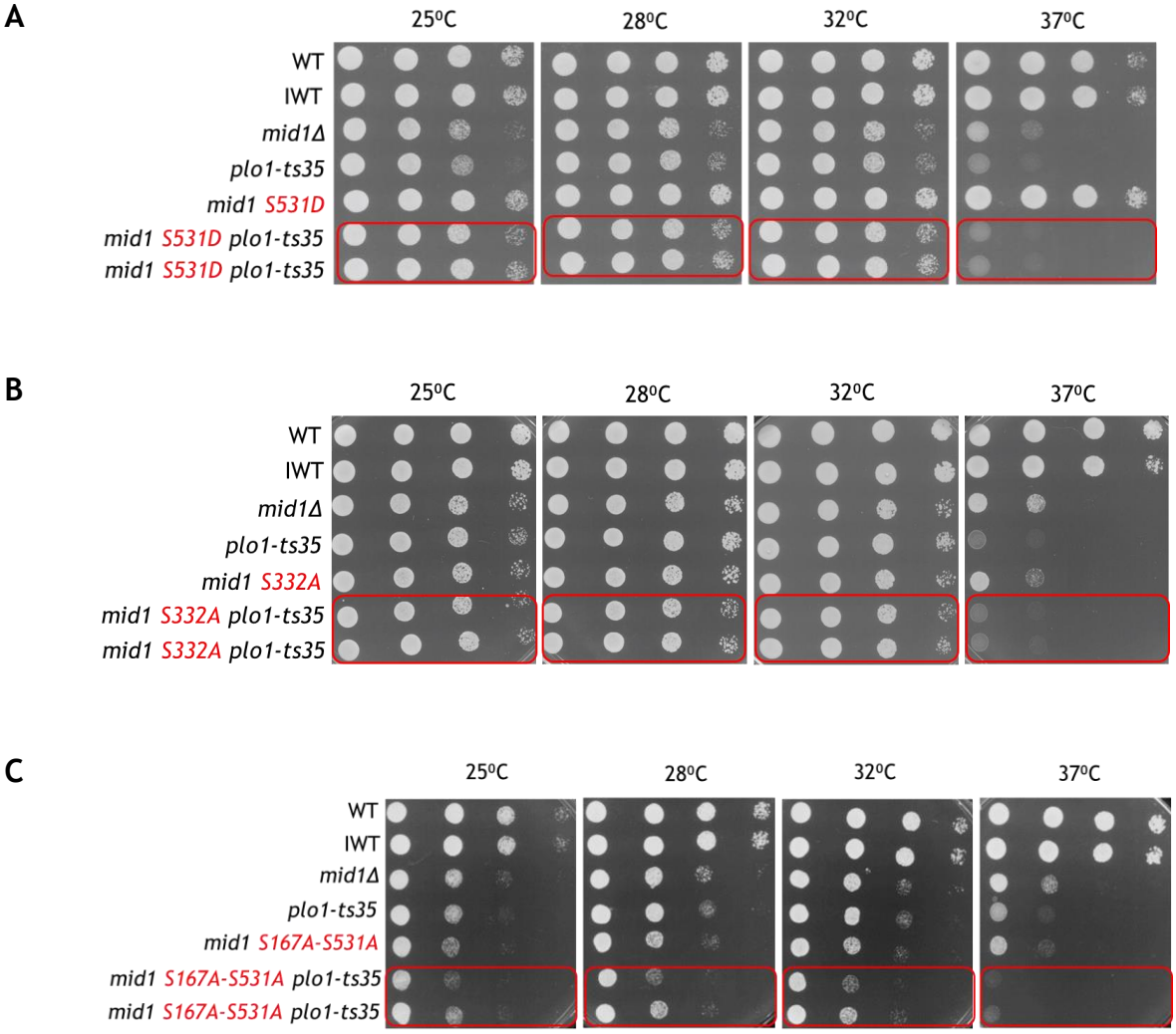

Figure 3-15 *mid1* phospho-mutant shows synthetic viable phenotypes with *plo1-ts3535*. Synthetic viable phenotypes and colony analysis of wild-type, parent cells, *mid1*Δ, and double mutant isolates. All the cells were suspended at 1.5x10^6 cells/ml and subjected to 10-fold serial dilution. Cells suspended were pipetted onto solid YE media and incubated at four different temperatures (25ºC, 28ºC, 32ºC, and 37ºC). The analysis of growth phenotype was captured and interpreted after two days of cell growth on a solid YE medium. **A** double mutant of *mid1* phospho-mutant *S531D* and *plo1-ts35* (GG 3419), **B** double mutant of *mid1* phospho-mutant *S332A* and *plo1-ts35* (GG 3411), and **C** double mutant of *mid1* phospho-mutant *S167-531A* and *plo1-ts35* (GG 3425). WT is wild-type, IWT is integrated wild-type, and *mid1*Δ *is* Mid1p deletion. Double mutants indicating growth rate defects are represented in red circles.

The reduction in the growth colonies of the double mutants, unlike the parent strain and wild-type, suggests that these two genes interact in the cell cycle of *S. pombe*. The observed impaired growth phenotypes in the *plo1-ts35 mid1* phospho-mutant illustrate a strong genetic interaction between *plo1ts* and *mid1* genes, which suggest an interaction of the encoded *plo1* genes is required for cell growth. This could be due to the possibility that phosphorylation of Mid1p during cytokinesis affects the stability and function of Mid1p. The genetic interactions observed in crosses between the *mid1* phospho-mutant and *plo1-ts35* strains are summarised in Table 3-2. This shows a global perspective of the genetic interactions observed between these strains, as the represented genetic interactions may refer to one or more observations of synthetic phenotype in the conditions explored for each gene was analyzed at four temperatures 25^{0}C, 28^{0}C, 32^{0}C, and 37^{0}C.

3.5.3 Morphology and colony formation of *mid1* phospho-mutants in *ark1-ts11* and *plo1-ts35*

Having identified the of growth rate defects in *mid1* phospho-mutant *ark1-ts11* and *mid1* phospho-mutant *plo1-ts35* double mutants, suggests that these two genes interact in the cell cycle of *S. pombe*. To further understand the genetic interaction between different phenotypes, we investigated the colony formation between *mid1* phospho-mutants and *ark1-ts11 and plo1-ts35* double mutants, we examine the morphology and colony formation of the phospho-mutants and the double mutants during the cell cycle. This was also examined in *mid1* phospho-mutant *vps4Δ* revealing an irregular colony and morphology. The strain was grown on solid media alongside wild-type, *mid1Δ*, *mid1* phospho-mutants, and double of mutants of *mid1* phospho-mutants *ark1-ts11 and plo1-ts35*. The strains were grown for 24-48 hours on a solid YE media plate and visualized microscopically.

Results from the morphology experiments showed that wild-type cells and most *mid1* phospho-mutants formed viable colonies with similar colony and morphological patterns to the wild-type yeast strain (Figure 3-16). However, we observed that *mid1* phospho-mutant *ark1-ts11* double colony and morphology revealed a phenotype similar to *mid1Δ,* the study identified particular serine positions S332A and S167-531A with defective irregular colony formation. Viable colonies and morphology were observed in wild-type and integrated wild-type yeast strain compared with the double mutants generated (Figure 3-16). However, defective colony and morphology were observed in *mid1* phospho-mutant S332A *vps4Δ* double mutant compared with wild-type cells (Figure 3-17).

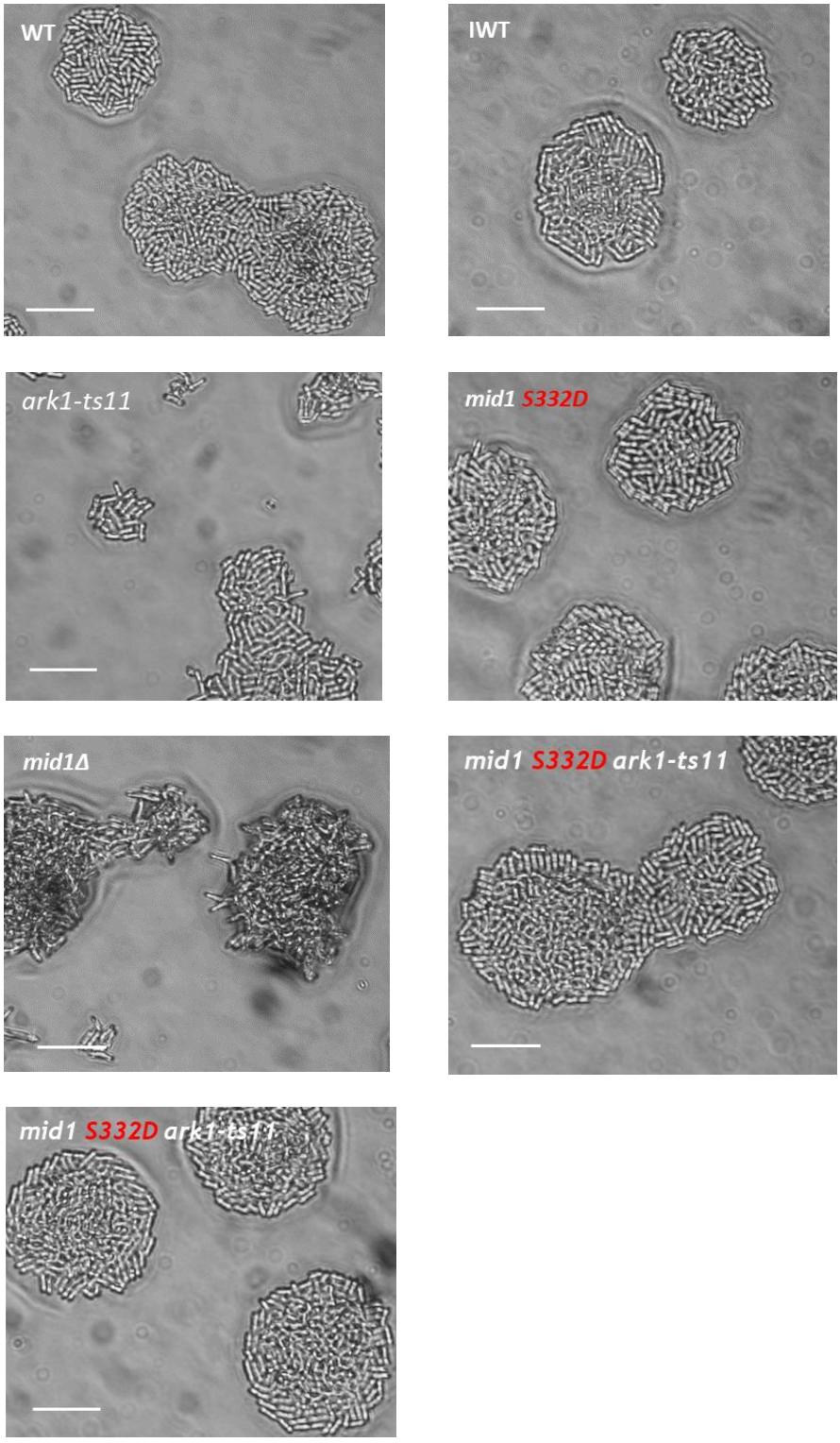

Figure 3-16 The *ark1-ts11* wild-type reveals morphological defects. Analysis of the morphological defect of double mutant *ark1-ts11* (GG 2451) and *mid1* phospho-mutant (GG 3295), strains grown at 25ºC on solid YE medium and suspended at a concentration of $1.5x10^6$ cells/ml, cells were subjected to serial dilution. Pipetted cells were placed on solid YE media and incubated, after two days of cell growth on a solid YE medium, the wild-type, *mid1* phospho-mutants, and double mutants were examined and interpreted. The colony was captured using Sony DSC-75 camera, scale bar represents 50 µm. WT is wild-type, IWT is integrated wild-type, and *mid1*Δ *is* Mid1p deletion.

Both double mutants of *ark1-ts11, plo1-ts35,* and *mid1* phospho-mutant at serine position S332A and S167-531A phenotype showed defective and irregular colony and morphology in *S. pombe* cells. We observed vivid colony and morphological modifications compared with the wild-type (Figure 3-17). Double mutants of *plo1-ts35, ark1-ts11,* and *mid1* phospho at serine position showed a substantial change in shape and colony formation compared with the other *mid1* phospho mutants (Figure 3-17 and Figure 3-18). In comparison with the two parents and the wild-type, the double mutants formed colonies similar to *mid1Δ*, serine positions S332A and S523-531A that have defective colony formation similar to *mid1Δ*. All double mutants showed changes in the colony morphology as the temperature increased.

The reduction in the colony size of the double mutants suggests that these two genes interact in the cell cycle of *S. pombe*. The observed impaired morphology in the double mutants of *plo1-ts35, ark1-ts11,* and *mid1* phospho-mutant illustrate a strong genetic interaction between the genes, which suggests an interaction of the encoded *plo1*, *ark1*, and *mid1* genes are required for cell growth. This potential lost of function observed could be due to the possible effect of phosphorylation of Mid1p during cytokinesis which affects the stability and function of Mid1p.

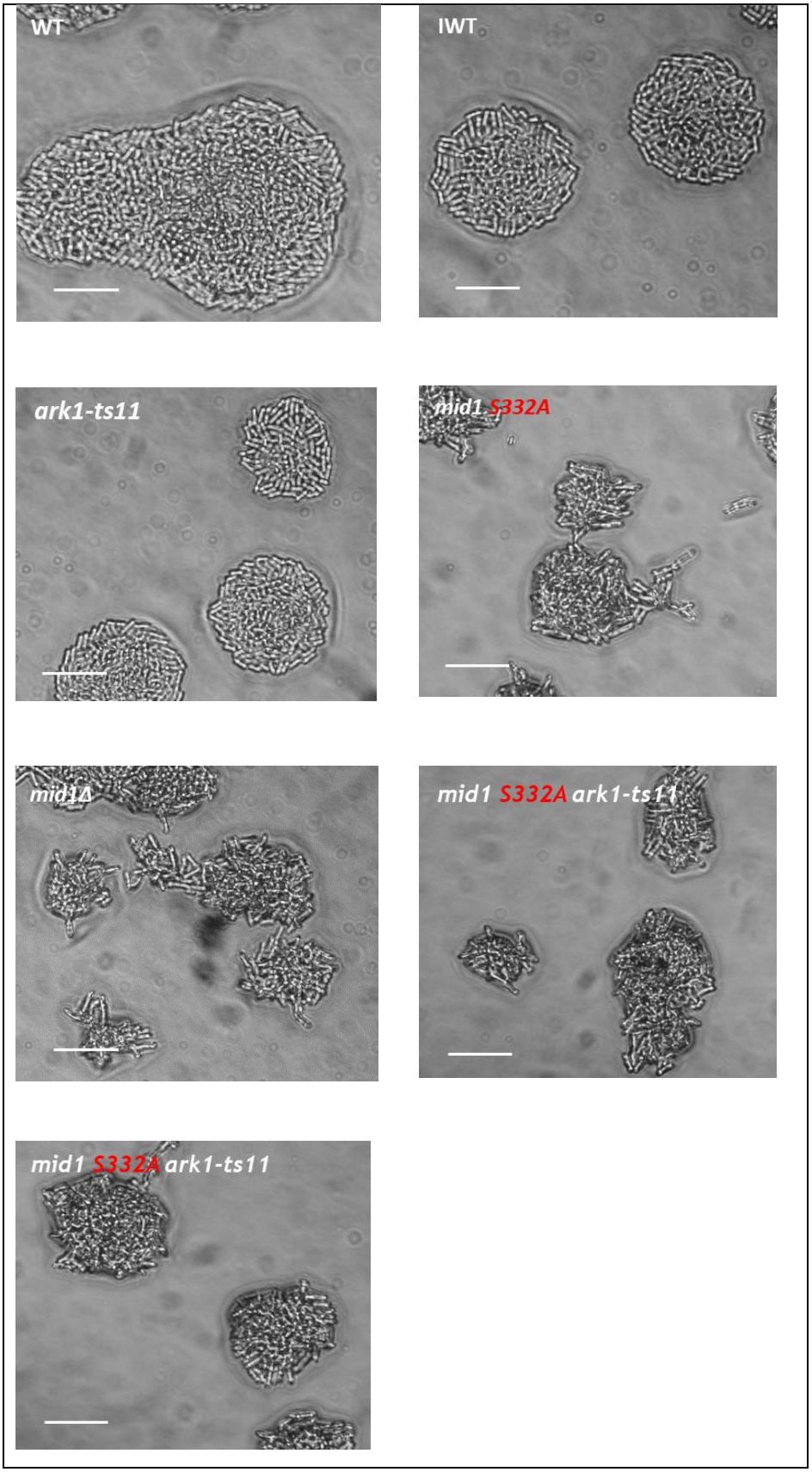

Figure 3-17 The *ark1-ts11 mid1* phospho-mutant reveals morphological defects. Analysis of the morphological defect of double mutant *ark1-ts11* (GG 2451) and *mid1* phospho-mutant (GG 3291), strains grown at 25ºC on solid YE medium and suspended at a concentration of $1.5x10^6$ cells/ml, cells were subjected to serial dilution. Pipetted cells were placed on solid YE media and incubated, after two days of cell growth on a solid YE medium, the wild-type, *mid1* phospho-mutants, and double mutants were examined and interpreted. The colony was captured using Sony DSC-75 camera, scale bar represents 50 µm. WT is wild-type, IWT is integrated wild-type, *mid1*Δ *is* Mid1p deletion.

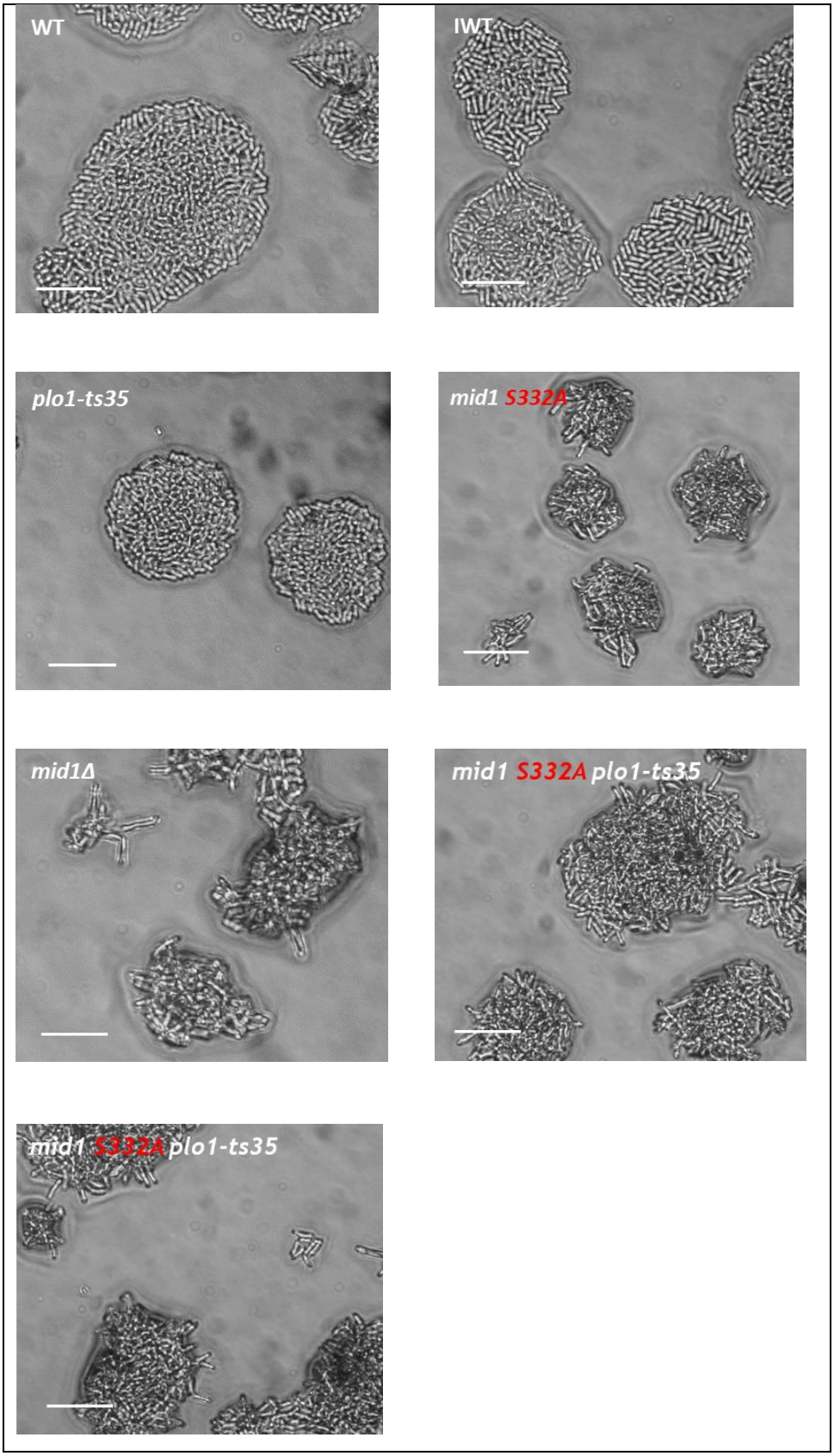

Figure 3-18 The *plo1-ts35 mid1* phospho-mutant reveals morphological defects. Analysis of the morphological defect of double mutant *plo1-ts35* (GG 1167) and *mid1* phospho-mutant (GG 3291), strains grown at 25ºC on solid YE medium and suspended at a concentration of $1.5x10^6$ cells/ml, cells were subjected to serial dilution. Pipetted cells were placed on solid YE media and incubated, after two days of cell growth on a solid YE medium, the wild-type, *mid1* phospho-mutants, and double mutants were examined and interpreted. The colony was captured using Sony DSC-75 camera, scale bar represents 50 µm. WT is wild-type, IWT is integrated wild-type, *mid1*Δ *is* Mid1p deletion.

mid1 mutations S = serine A = adenine D = aspartic acid		*mid1* single/double phospho-receptor mutant synthetic phenotypes Morph= cell morphology, WT = wild-type, *mid1*Δ = *mid1* deletion, *ark1* = *ark1*-T11, Int. = intermediate between WT and *mid1*Δ								GG No.
		mid1 single mutant		*mid1 plo1-ts35* double mutant		*mid1 ark1-T11* double mutant		*mid1 vps4*Δ double mutant		
Single or in combination		Morph	Growth	Morph	Growth	Morph	Growth	Morph	Growth	
mid1 wild-type		WT	WT	WT	Int.	WT	WT	WT	WT	3181
mid1 S167 (1)	A	WT	WT	WT	WT	WT	WT	WT	WT	3267
	D	WT	WT	WT	WT	WT	Int.	WT	WT	3271
mid1 S328 (1)	A	WT	slow	WT	WT	WT	WT	WT	WT	3275
	D	WT	WT	WT	WT	WT	Int.	WT	WT	3280
mid1 S331 (1)	D	WT	WT	WT	WT	WT	Int.	WT	WT	3283
mid1 S332 (1)	A	*mid1*Δ	*mid1*Δ	*mid1*Δ	*mid1*Δ	*mid1*Δ	*mid1*Δ	*mid1*Δ	*mid1*Δ	3291
	D	WT	WT	Int.	WT	WT	WT	WT	WT	3295
mid1 S523 (1)	A	WT	WT	WT	WT	WT	Int.	WT	WT	3185
	D	WT	WT	WT	WT	WT	WT	WT	WT	3189
mid1 S531 (1)	A	WT	WT	WT	Int.	*ark1*	*mid1*Δ	WT	WT	3193
	D	WT	WT	WT	Int.	*ark1*	*mid1*Δ	WT	WT	3197
mid1 S167-S332 (4)	A	*mid1*Δ	*mid1*Δ	*mid1*Δ	*mid1*Δ	*mid1*Δ	*mid1*Δ	*mid1*Δ	*mid1*Δ	3299
	D	WT	WT	Int.	WT	WT	WT	WT	WT	3305
mid1 S523-S531 (2)	A	*mid1*Δ	*mid1*Δ	*mid1*Δ	*mid1*Δ	*mid1*Δ	*mid1*Δ	*mid1*Δ	slow	3201
	D	WT	WT	Int.	WT	WT	Int.	WT	WT	3205
mid1 S167-S531 (6)	A	*mid1*Δ	*mid1*Δ	*mid1*Δ	*mid1*Δ	*mid1*Δ	*mid1*Δ	*mid1*Δ	*mid1*Δ	3307
	D	WT	WT	WT	WT	WT	WT	WT	WT	3311

Table 3-2 A summary of synthetic viable and morphology defects of mutation in *vps4*Δ, *ark1-ts11, plo1-ts35,* and *mid1* phospho-mutant. Summary of *S. pombe* cell growth and morphology synthetic phenotypes of single/double *mid1* phospho-mutants combined with *plo1-ts3535*, *ark1-T11,* and *vps4*Δ mutants. In each case, strains with serine residues (S167, S328, S331, S332, S523, or S531) in Mid1p were mutated to either a phospho-mimetic (S>D) or a phospho-resistant (S>A) point mutation(s) of the residues to create a panel of mutants of *S. pombe* strains. Such *mid1* mutations were made both singly and in combination. Each was then combined individually with the mutants *plo1-ts35*, *ark1-T11,* and *vps4*Δ with cell growth and morphology analysis of the double mutants when grown on a solid medium to identify synthetic phenotypes. Double mutants displaying phenotypes mentioned in the text are circled in red. Note that the *mid1* S331A mutant was not created as cells were found to be sterile.

We utilized the genetic interaction results to identify and map out potential amino acids important for genetic interaction in *S. pome*. Double mutants between *vps4Δ, plo1-ts35, ark1-ts11,* and *mid1* phospho-mutants were created by mating two single mutants generating a double mutant and characterized through growth and morphological defects. The impaired growth phenotype indicates a strong genetic interaction between the *vps4Δ, plo1-ts35, ark1-ts11,* and *mid1* phospho mutant, which further suggests an interaction of the encoded *vps4* and *mid1* proteins required for cell growth and function.

Phosphorylated amino acid residues in Mid1p protein were mapped by protein kinases assays and proteomics, revealing six serine residues which were utilized in this study. Serine positions S332A and S523-531A revealed defective growth and changes in the colony morphology (Figure 3-19).

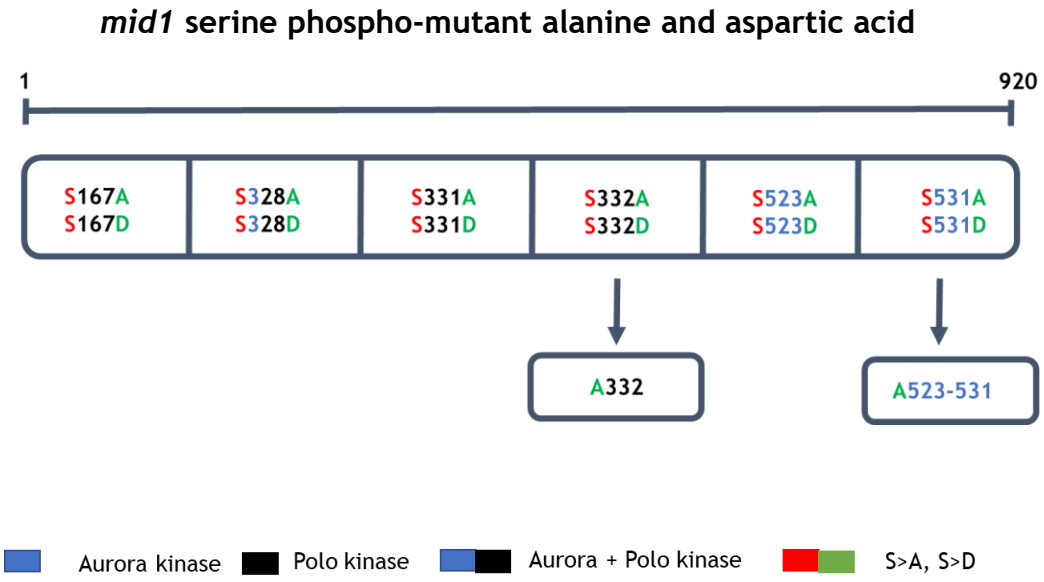

Figure 3-19 Identification of phospho-sites of interaction in Mid1p. Mid1p phosphorylated amino acid residues showing serine resides phospho-mutant alanine and aspartic acid with sites suggesting an interesting genetic interaction with *vps4Δ, plo1, ark1,* and *mid1* phospho-mutant at serine positions S332A, S167-531A and S523-531A are observed to have significant genetic interaction with *vps4Δ, plo1, ark1,* and *mid1* phospho-mutant observed to have impaired growth and deformed colony orientation analyzed microscopically. (A) is *mid1* phospho-mutant alanine, (D) is *mid1* phospho-mutant aspartic acid, *mid1* phospho-mutant alanine and aspartic acid are illustrated in black and blue, black indicate polo kinase, blue indicate aurora kinase, blue-black indicate polo and aurora kinase while red-green indicate *mid1* phosphorylation from either alanine or aspartic acid.

3.6 Summary

In this chapter, we showed that *mid1* phospho-mutant, *vps4Δ, ark1-ts11,* and *plo1-ts35* genes interact genetically to regulate cytokinesis in *S. pombe*. It has been shown that *mid1* genes are required for cell division in *S. pombe*, implying that *mid1*, *vps4*, *plo1*, and *ark1* genetically interact to regulate cell division. First, we illustrated the presence of genetic interaction between *mid1* phospho-mutant and *vps4Δ* through tetrad analysis and further validated our findings by establishing the same interactions with *plo1-ts35*, and *ark1-ts11 mid1* phospho-mutant genes, indicated by growth defective phenotypes in double mutants of *vps4Δ mid1 phospho mutant*s, *plo1-ts35 mid1 phospho mutant*s, and *ark1-ts11 mid1 phospho mutant*s.

S. pombe double mutants were created by crossing strains containing *mid1* phospho-mutants, *vps4Δ* (Figure 3-5), *plo1-ts35* (Figure 3-10), and *ark1-ts11* (Figure 3-11). All double mutants created in this study were found to be viable, and synthetic interactions were identified by examining the growth rate defects among the single-parent mutants and the double mutants on YE solid medium at various temperatures. Genetic interactions between various mutants may suggest synthetic lethality among progeny (Papadopoulou *et al.*, 2010; Rezig *et al.*, 2019). On several occasions, double mutants of *plo1-ts35* and *ark1-ts11* showed growth rate defects at 28^{0}C 32^{0}C and 37^{0}C suggesting temperature sensitivity of *plo1-ts35* and *ark1-ts11* 32^{0}C and 37^{0}C. However, when crossed with a non-temperature sensitive *mid1*phospho-mutant the double mutant exhibited temperature endurance and survived under 28^{0}C and 32^{0}C. The principle of temperature sensitivity was previously established between *plo1* and *clp1* where *clp1 D257A* mutant reduced the restrictive temperature of *plo1-ts35* indicating impaired cell stress because of genetic interaction (Papadopoulou *et al.*, 2010; Bhutta *et al.*, 2014).

Second, nearly all the double mutants *mid1 phospho vps4Δ* created in previous results showed viable growth at 25^{0}C, 28^{0}C, and 32^{0}C while at 37^{0}C the double mutants, single mutants, and *vps4Δ* did not grow. The double *mid1 phospho vps4Δ* mutants serine positions S332A and S523-531A were observed to have similar defective growth rate patterns with *mid1Δ* across the four temperatures at S332A and S523-531A serine positions. The double *mid1 phospho vps4Δ*

mutants S332A and S167-531A, *vps4Δ*, and *mid1Δ* colonies showed defective growth rates, double *mid1 phospho vps4Δ* mutants serine positions S523-531A are observed to have a slow growth rate, but not defective as the cells eventually grow over a period of time. We may suggest that it can rescue the effect of phosphorylation at that double-point (S523-531) mutation.

Double mutants of *vps4Δ mid1* phospho-mutants, *plo1 mid1* phospho mutants, and *ark1 mid1* phospho mutants revealed defective growth rate, indicating that *vps4, plo1, ark1, and mid1* genes are required for cell growth and progression. As *ark1-ts11 and plo1-ts35* are temperature-sensitive strains with a permissive temperature of 25^{0}C and a restrictive temperature of below 37^{0}C, it was hypothesized that combining this with *mid1* phospho-mutant may result in the decrease of restrictive temperature. Therefore, yeast strains were also grown at 25^{0}C, 28^{0}C, 32^{0}C, and 37^{0}C to search for growth differences. Figure 3-13 and Figure 3-15 illustrate the identification of such a viable growth defects phenotype in doubles mutants of *ark1-ts11 mid1* phospho-mutant and *plo1-ts35 mid1* phospho-mutant at various temperatures at seine positions S332A and S167-531A. The results of the growth rate study of all *mid1* phospho-mutant strains with *ark1-ts11 and plo1-ts35* mutant strains are shown and summarised in Table 3-2. Strikingly, it was observed that *ark1-ts11* and *plo1-ts35* showed genetic interactions with *mid1* phospho mutant, as they exhibited defective phenotypes during this study.

Third, double mutants showed a defective and impaired morphology in the *vps4Δ mid1* phospho-mutants, *plo1 mid1* phospho-mutants and *ark1 mid1 phospho mutant*s double mutants further imply a strong genetic interaction between the encoded *vps4, plo1, ark1, and mid1* genes are required for cell growth. Some mutants exhibit partial loss of integrity and function, reduced activity, and increased cell width under tolerant conditions. Growth rate and morphological defects were observed in double mutants with *mid1* phospho-mutants, *plo1-ts35,* and *ark1-ts11* this is also in tandem with Bhutta *et al*. (2014) where *plo1*, *clp1,* ESCRT genes, and *vps4* show defective growth rate.

The fission yeast is an ideal organism to study the molecular mechanisms controlling cytokinesis events during cell cycle (Rezig *et al.*, 2022). It has been showed that the shuttling protein Mid1p plays a significant role in the

spatiotemporal mechanism of CR formation (Rincon and Paoletti, 2012). In *S. pombe* Mid1p protein is released from the nucleus, which is situated at the cell center to the proximal cell cortex during G2 phase and forms nodes by interacting with Cdr2 and other functional associated proteins (Akamatsu *et al.*, 2014; Rincon *et al.*, 2014). Mid1p-achored nodes play a significant role for CR positioning in the cell center, numerous mechanisms function cooperatively to ensure Mid1p localization to the center of the cortex in *S. pombe* (Huang *et al.*, 2007). During interphase, most Mid1p is located in the nucleus but residual amounts of Mid1p form cortical dots called interphase nodes by interacting with the Cdr2 kinase and other proteins associated with the nodes (Rincon *et al.*, 2014). The distribution of interphase nodes is limited to the middle of the cell by exclusion from cell tips by the Pom1 kinase. As the G2 phase continues, the amount of Mid1p at the equatorial cortex a region proximal to the nucleus positioning in the center of interphase cells (Akamatsu *et al.*, 2014). The cytokinetic nodes induces a cortical actin-myosin meshwork encircle the future division site in the cell middle and are merged with each other. As a result, the CR is assembled before the onset of anaphase (Yasuda *et al.*, 2016).

In *S. pombe*, a gene disruption of *mid1* is lethal for cell proliferation at high temperatures and causes severe defects in the spatiotemporal control of CR formation, the position and orientation of the CR is disturbed in *mid1* deletion cells (*mid1* null cells) (Paoletti and Chang, 2000). Hence, the growth and timing of CR components accumulation is delayed in the mutants than in the wild-type cells, thus Mid1p plays a central role in the spatiotemporal control of CR formation during cell cycle in *S. pombe* (Motegi *et al.*, 2004; Huang *et al.*, 2008). Similarly, the genome of *S. pombe* contains *mid2* which encodes a protein that has an AHD and a PH domain at its C-terminus and localizes to the cell division site during cytokinesis, moreover, Mid1p functionally interacts with the septin cytoskeleton (Tasto *et al.*, 2003; Martin-Cuadrado *et al.*, 2005). Cells lacking *mid2* form a normal CR but have defective cell separation after cytokinesis in *S. pombe* and *mid2* homologues are conserved among yeast and fungi (Berlin *et al.*, 2003; Si *et al.*, 2012).

3.7 Conclusions

These results, in addition to the observation that *mid1*, *vps4Δ*, *ark1-ts11*, and *plo1-ts35* genes interact genetically through phosphorylation of Mid1p phospho-sites. The result further suggests that phosphorylation of Mid1p protein is important for the coordination and regulation of cell cycle events in *S. pombe*. As with *mid1* and *vps4* genes, such a strong genetic interaction might be explained in relation to strong genetic interaction between *mid1*, *ark1*, and *plo1* genes. Thus, these results combined suggest that *mid1*, *vps4*, *plo1*, and *ark1* genes interact to regulate cytokinesis events in *S. pombe*.

Chapter 4 Physical interaction between Mid1p and Vps4p proteins

4.1 Introduction

4.1.1 Anillin/Mid1p proteins

Anillin is an actin-binding protein that plays an important factor in cell division, and it is a multi-domain protein that plays a vital role in cell proliferation and migration during cytokinesis (Tuan and Lee, 2020). Both the actin and myosin proteins are vital components of cytokinesis as they are essential to provide structural support and signal contraction of the contractile ring, which initiates the processes of anaphase (Robert-Paganin *et al.*, 2020). Additionally, anillin can regulate the position of myosin to promote the assembly of the contractile ring, meaning that cellular division can continue its process (Piekny and Glotzer, 2008). Anillin/Mid1p also plays a role of a recruiter of actin complexes by modifying actin and encouraging greater contractility of the contractile ring (Hercyk *et al.*, 2019).

Anillin in fission yeast cells is referred to as Mid1p, and here anillin/Mid1p plays an essential role in the positioning of the cytokinetic furrow by promoting the structure of a contractile ring around the point of the nucleus (Rezig *et al.*, 2022). Shuttling between the nucleus and the cortical medial broadband, Mid1p forms nodes that recruit additional Mid1p, and Myosin II forms a contractile ring. At this point, the interaction between Myosin II and actin filaments leads to the formation of the ring, which causes it to constrict, leading to cleavage and subsequent division of the cell into two daughter cells (Rezig *et al.*, 2021).

4.1.2 Endosomal sorting complexes required for transport (ESCRT)

The ESCRT proteins play a significant role in the transformation of cell membranes, ESCRT proteins consisting of ESCRT-0, ESCRT-I, ESCRT-II, and ESCRT-III (Horvath and Muller-Reichert, 2020). Through sequence of steps, cytosolic protein complexes transport ubiquitinated cargo to the plasma membrane (McCullough *et al.*, 2018). ESCRT-0 is responsible for the assembly of ubiquitinated cargo that requires transport to the plasma membrane of multivesicular endosomes (MVEs), whereas ESCRT-I and ESCRT-II work to form a compact in the plasma membrane into which the ubiquitinated cargo will be transported. (Werner *et al.*, 2011; McCullough *et al.*, 2018). The regulator of ESCRT-III, known as Vps4p AAA+ ATPASES promote dynamic ESCRT-III subunit

exchange, constriction, membrane fission and cell separation (Wenzel *et al.*, 2022).

In cytokinesis, approximately 30 human ESCRT factors consist of five subcomplexes: ALIX, ESCRT-I, ESCRT-II, ESCRT-III and Vps4 assemble sequentially to constrict and sever membranes (McCullough *et al.*, 2018). The ESCRT-associated proteins accumulate in the midbody, the process results in ESCRT-III accumulating at the cell cleavage site, in which the microtubules are cleaved, and the two daughter cells are split apart (Bhutta *et al.*, 2014). ESCRT-III can then be broken down by Vps4p protein and salvaged back into the cytosol (Yang *et al.*, 2015). The process can serve as the modulation of receptors indicated in the plasma membrane, a principal factor of cytokinesis in the cell cycle (Werner *et al.*, 2011).

4.1.3 Interactions between Mid1p and ESCRT

Mid1p has been shown to interact genetically and physically with ESCRT-associated protein Vps4p *in vitro*. A pull-down experiment of full-length bacterial recombinant Vps4p and three GST-tagged domains of Mid1p resulted in the C-terminal domain of Mid1p being pulled down by the recombinant Vps4p, providing evidence of a physical interaction existing between the two. Aurora and polo kinases both phosphorylate Mid1p, and one method used to study this was by *in vivo* mutation of their Mid1p phospho-acceptor sites. Mid1p phospho-mutants in *mid1* mutant cells and *vps4* mutant cells were all investigated, and their sites were mapped (Rezig *et al.*, 2021).

For the *mid1* phospho-mutant cells, the effects of the phosphorylation indicated that serine position 523 of Mid1p produced defective growth and defective morphology and this was also observed with *plo1-ts*35 and *ark1-ts11* cells (Rezig *et al.*, 2021). Cytokinesis in fission yeast requires the anillin-related protein Mid1p which is important for forming and accurately placing the contractile ring at the cell equator (Paoletti and Chang, 2000; Saha and Pollard, 2012).

In this study, S523 and S531 serine residues were mutated to aspartic acid to investigate the effect of mutations on the interaction between Mid1p and Vps4p.

4.2 Aims

Several proteins have been identified that control cytokinesis in fission yeast, but it is unclear how they interact, coordinate, and regulate each other. Similarly, the role of the ESCRT-associated regulator Vps4p in yeast membrane scission and cytokinesis is well established. However, it is unknown how Mid1p and ESCRT-associated Vps4p interact, coordinate, and regulate cytokinesis in *S. pombe*. In this Chapter, we specifically explore the biochemical/physical interactions between Mid1p domains and full length Vps4p proteins. We determine whether the phosphorylation of Mid1p is required for Vps4p to attach to Mid1p and whether the phosphorylation of Mid1p's "middle" terminal enhances its function or capacity to interact with Vps4p. Our specific aims of this chapter are:

- Expression, purification, and quantification of the N-terminal, Middle, and C-terminal domains of Mid1p (prey proteins), Vps4p, and Myo2p (bait proteins).

- Identification of the physical interaction between the N-terminal, Middle, and C-terminal domains of the Mid1p and Vps4p proteins using an *in vitro* biochemical approach.

- Expression, purification, and quantification of wild-type Mid1p and *mid1* phospho-mutant Vps4p, and Myo2p proteins.

- Identification of the physical interaction between wild-type Mid1p, *mid1* phospho-mutant (prey proteins), and Vps4p (bait proteins) proteins using an *in vitro* biochemical approach.

4.3 Results

4.3.1 Physical interaction between Mid1p and Vps4p proteins

In Chapter 3, we demonstrated that *mid1* gene genetically interacts with other proteins including protein kinases that are essential in the regulation of cytokinesis in *S. pombe*. Here we build upon this existing knowledge to explore the functional significance of this genetic interaction in *S. pombe*. For clarity, the biochemical/physical interaction between the Mid1p and Vps4p protein was examined. To do this, Mid1p was expressed in *E. coli* as fusion protein with glutathione S-transferase (GST) to be purified in three different domains, and the interaction of each of the Mid1p domains was tested for pull-down experiment with full-length Vps4p protein. We did not purify full-length Mid1p because Rezig *et al*. (2021) indicated that full-length Mid1p is so large that cannot be expressed and purified in *E. coli*.

Previous work to understand the function of Mid1p and Vps4p proteins has shown that the *mid1* and *vps4* genes interact genetically in *S. pombe* to regulate the cell cycle. To gain more profound knowledge, understanding and functional importance of these novel genetic interactions, Mid1p interactive domains were mapped to enable an *in vitro* biochemical analysis to understand the physical interactions of the encoded Mid1p and Vps4p proteins. GST-fusion proteins of these domains were employed together with full-length Vps4p protein in pull-down experiments. Positive and negative controls, the Myo2p and GST proteins, respectively, were used.

4.3.2 Design of the *in vitro* pull-down experiment

Positive and negative controls were utilized for the experiment, with the positive control substituting the baits protein Vps4p with Myo2p, a known Mid1p interacting protein (Motegi *et al*., 2004). To create the negative control, the prey GST-Mid1p domain was replaced with GST alone - see Figure 4-1. For each pull-down experiment, the bait protein was immobilized on Ni-NTA agarose beads, and prey protein was added in equal amounts. Several washes were performed to remove the non-specific binding, and the bait-prey complex was eluted from the beads to identify the protein-protein interaction using SDS-PAGE.

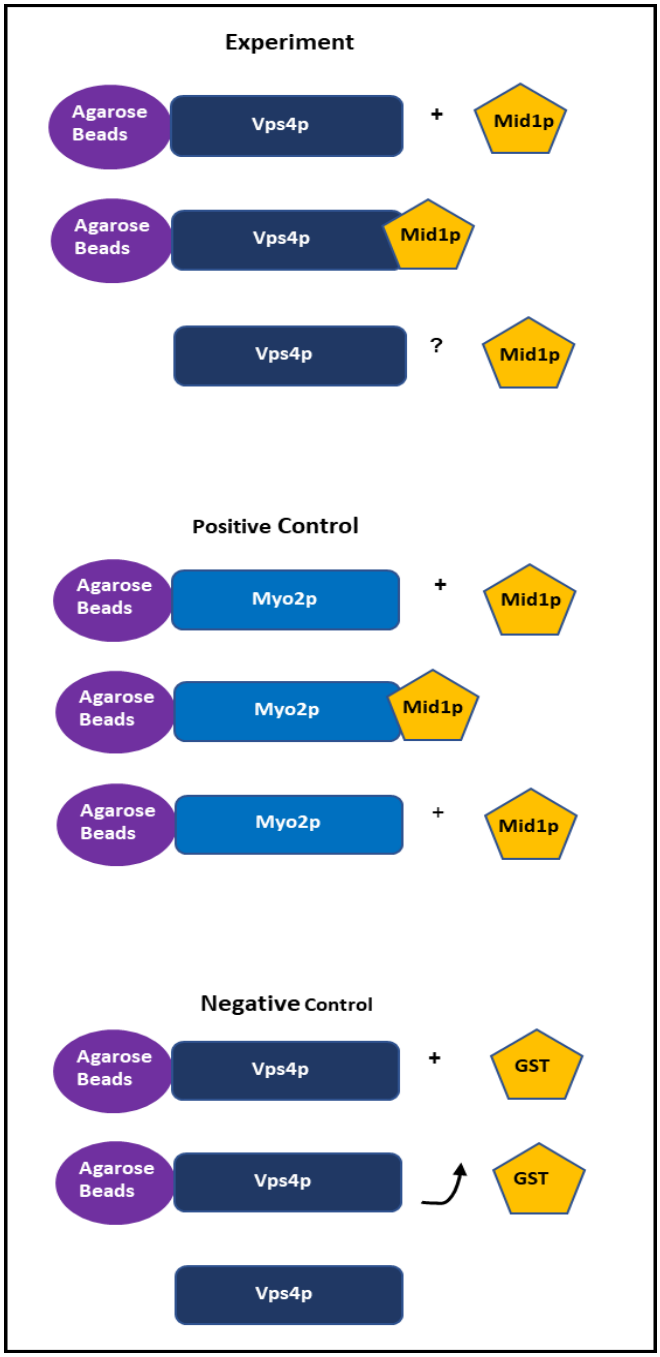

Figure 4-1 Design of *in vitro* pull-down assay to test for the physical interactions between various Mid1p domains and full-length Vps4p. The positive control was designed by substituting the bait Vps4p protein with the C terminal domain of Myo2p protein, a known interacting domain of Mid1p protein (Motegi *et al*., 2004). The negative control was designed by replacing the prey Mid1p domains with purified GST proteins which are predicted not to interact with Vps4p and for the experiment, His-6-tagged Vps4p protein bait protein was immobilized to Ni-NTA agarose beads and different domains of prey Mid1p protein were separate.

4.3.3 Purification of *S. pombe* Mid1p (prey) proteins from *E. coli* for *in vitro* pull-down assay experiments

To simplify the biochemical experiments, we adapted and modified the molecular method used by Saha and Pollard (2012). The study revealed the biological function of Mid1p domains during cell cycle in *S. pombe* and found out that amino acid residues (1-149) of Mid1p are important for the correct orientation and accurate placement of septa during cytokinesis. Similarly, residues (1-149) are essential but not sufficient for the correct localization of full-length Mid1p to the nodes. However, residues (1-452) enable Mid1p functions through localization and concentration of nodes during mitosis, while residues (1-578) are required for assembly of nodes, Myosin-II and Cdc15. Residues (579-797) represent the insoluble domain of Mid1p and facilitates condensation of nodes into the actomyosin contraction ring (ACR). Residues (798-920) of Mid1p contain the C-terminal domain which consist of lipid binding PH domain. In the study, Saha and Pollard (2012) characterize the functional domains of the Mid1p protein using a complementary experiment with *mid1Δ* cells and identified the biological functions of six putative domains accounting for the full-length Mid1p protein as shown in Table 4-1.

Name	**Amino acid residues (aa)**	**Localization in *S. pombe***
M1-1	1-149	Localized to the nodes
M1-2	150-308	Partial localization to the nucleus
M1-3	309-452	Partial localization inside the nucleus
M1-4	453-578	Strong localization inside the nucleus
M1-5	579-797	Associated with the nuclear envelope
M1-6	798-920	Partial localization inside the nucleus

Table 4-1. Description and localization of Mid1p putative domains in *S. pombe* cells. Identification and description of the six (M1-1), (M1-2), (M1-3), (M1-4), (M1-5) and (M1-6) structural and functional of six domains according to Saha and Pollard (2012). Each representing amino acid residue with their localized micro domain and function (1-149), (150-308), (309-452), (453-578), (579-797) and (798-920) respectively.

Saha and Pollard (2012b) combine all together M1-1, M1-2, and M1-3 domains of Mid1p in an M1-13 into a collective domain (aa 1-452) (Table 4-1). However, the M1-13 collective domain was able to complete the known functions of the full-length Mid1p including the assembly of node components in the equatorial cortex. Therefore, we decided to use the M1-13 domain in the pull-down experiment instead of using the M1-1, M1-2, and M1-3 Mid1p domains separately. The insoluble domain (aa 579-797: M1-5) was found to facilitate the condensation of the noses to the contractile ring (Saha and Pollard, 2012b). However, in our laboratory purification of this domain was unsuccessful. Therefore, it was not included in any experiments presented here. For clarity, we will refer to the domains as the ‘’N-terminal’’ (M1-13), ‘’Middle (M1-4), and “C-terminal” (M1-6) domains (Table 4-2). These three domains of Mid1p were cloned into the pGEX-4T-1 vector and tagged with glutathione S-transferase (GST) (Rezig *et al.*, 2021).

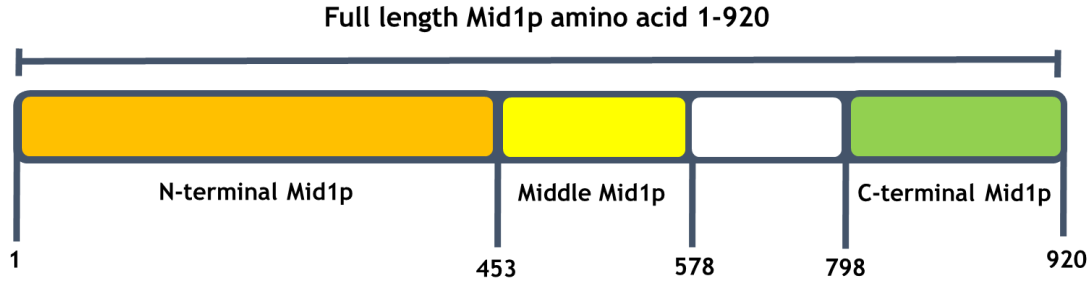

Figure 4-2 Design of Mid1p domains and their role during cytokinesis in *S. pombe*. (A) Mid1p residues 1-453 representing the N-terminal domain. (B) Mid1p residues 453-578 representing Middle terminal. (C) Mid1p residues 579-997 representing the insoluble domain. (E) Mid1p residues 798-920 representing the C-terminal domain. Figure adapted and modified from Saha and Pollard (2012).

Name	**Amino acid residues (aa)**	**Localization in *S. pombe***
N-terminal domain	1-453	Localized to the nodes, partial localization inside the nucleus
Middle	453-578	Strong localization inside the nucleus
C-terminal domain	798-920	Partial localization inside the nucleus

Table 4-2. Description and localization of different Mid1p remodel putative domains in *S. pombe* cells. For clarity, in this study we refer to the domains as N-terminal (M1-13), Middle (M1-4), and C-terminal (M1-6) with amino acid (1-452), (453-578), and (798-920) respectively. The three domains of Mid1p protein were cloned into the pGEX-4T-1 vector and tagged with glutathione S-transferase (GST) (Rezig *et al*., 2021).

4.3.4 Recombinant protein expression of N-terminal, Middle, and C-terminal Domain of Mid1p

To further investigate the biochemical relationship between Mid1p and Vps4p, DNA constructs were designed and ordered from (GenScript) comprising the various domains of Mid1p as stated N-terminal (M1-13), Middle (M1-4), and C-terminal (M1-6) fragments. These three domains of Mid1p domains were cloned into the pGEX-4T-1 vector in-frame with the glutathione S-transferase (GST) gene to generate fusion proteins which were purified as outlined in (*section 2.3.1.1*). Samples of bacteria expressing the recombinant proteins incubated with or without IPTG, and run on SDS PAGE to determine the level of protein expression.

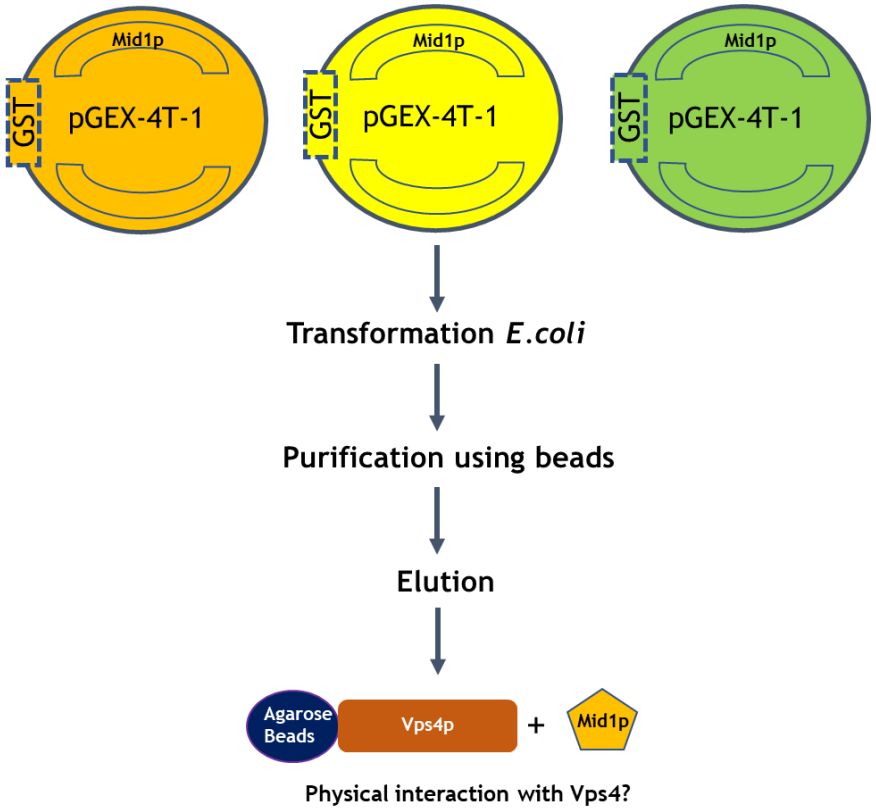

Figure 4-3 Design of Mid1p protein N-terminal, Middle, and C-terminal domain constructs to test their physical interaction with Vps4p protein. (A) The three domains of Mid1p are represented in different colours. (B) The recombinant GST-tagged with Mid1p domains were expressed in BL21 *E coli* followed by purification, elution, and quantification of proteins. Recombinant 6His-tagged Vps4p and C-terminal Myo2p were also expressed in BL21 *E coli*, followed by purification and quantification. The eluted Mid1p domains were subjected to a pull-down assay with Vps4p and Myo2p proteins.

E. coli expressed proteins of the expected size for both the Mid1p N-terminal terminal, Middle and C-terminal fission yeast protein in *E. coli* following the induction with IPTG. The proteins were found to be suitable for Mid1p N-terminal, Middle and C-terminal GST-Mid1p protein purification experiments and purified (Figure 4-4 and Figure 4-5).

4.3.5 Purification of S. *pombe* Mid1p (prey) proteins from *E. coli* for *vitro* pull-down assay experiments

After the expression of the GST-Mid1p recombinant proteins, the various Mid1p domains were purified by affinity binding to GST- Sepharose beads as outlined in *section 2.4.1.1.* GST-tagged proteins were eluted from the beads as outlined in *section 2.4.1.1* (Figure 4-4 and Figure 4-5). The initial protein purification of N-terminal, Middle and C-terminal for the first time was partially successful, we saw protein sizes that was ambiguous and unspecific, with some protein not eluting and remaining attached to the beads. Henece a different approach was used to increase protein's efficiency of expression.

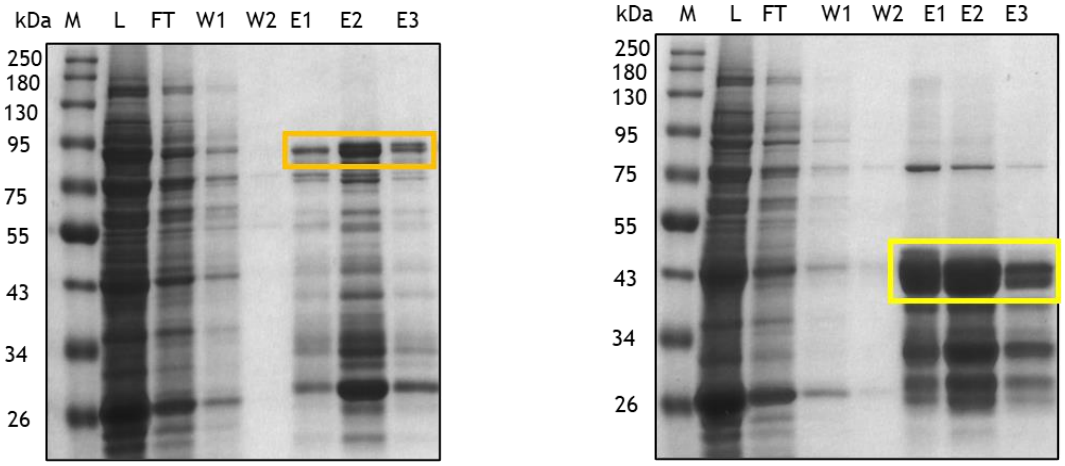

Figure 4-4 Purification of GST-tagged N-terminal and Middle Mid1p protein. Purification of 76 kDa N-terminal Mid1p domain and 40 kDa middle Mid1p domain. GST-tagged with N-terminal recombinant Mid1p was loaded on 1 mM L^{-1} GST Sepharose beads in PBS buffer and incubated overnight at 4ºC beads were washed three times with PBS. After the purification of the N-terminal Mid1p protein recombinant domain, they were eluted from the GST Sepharose beads by adding reduced glutathione transferase which competes with the recombinant protein for GST binding. M, protein marker; L, lysate; FT, flow-through; W1, wash 1; W2, wash 2; W3, E, elution. Orange and yellow boxes highlight the N-terminal terminal domain of Mid1p proteins, respectively.

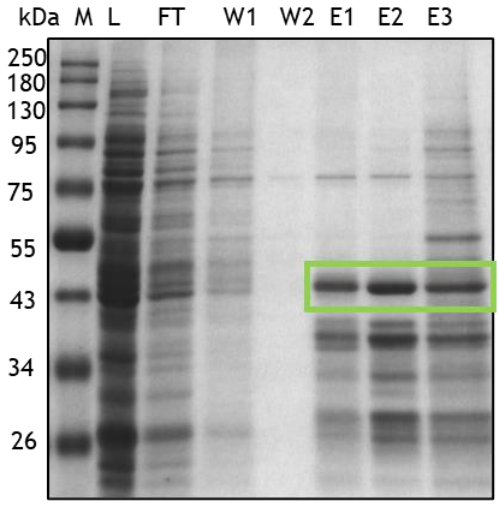

Figure 4-5 Purification of GST-tagged N-terminal Mid1p protein. Purification of 39 kDa C-terminal Mid1p domain. GST-tagged C-terminal recombinant Mid1p was loaded on 1 mM L^{-1} GST Sepharose beads in PBS buffer and incubated overnight at 4ºC beads were washed three times with PBS. After the purification of the C-terminal Mid1p protein recombinant domain, they were eluted from the GST Sepharose beads by adding reduced glutathione transferase which competes with the recombinant protein for GST binding. M, protein marker; L, lysate; FT, flow-through; W1, wash 1; W2, wash 2; W3, wash 3; E, elution. Green boxes highlight the C-terminal domain of the Mid1p protein.

4.3.6 Purification of S. *pombe* Mid1p (prey) proteins from *E. coli* for the *vitro* pull-down assays with 1% octylglucoside

After the initial protein purification with ambiguous and unspecific protein sizes, with some remaining attached to the beads; therefore, we increased the protein's efficiency of expression. To enhance protein yield, the pH of the elution buffer was raised from 8.0 to 9.0. To elute the protein, 1% octylglucoside detergent was added to the elution buffer (Figure 4-6 and Figure 4-7). Octylglucoside is a valuable detergent used for purification of proteins and can promptly catalyze the removal of unspecific bands during protein extraction without necessarily denaturing the targeted protein of interest.

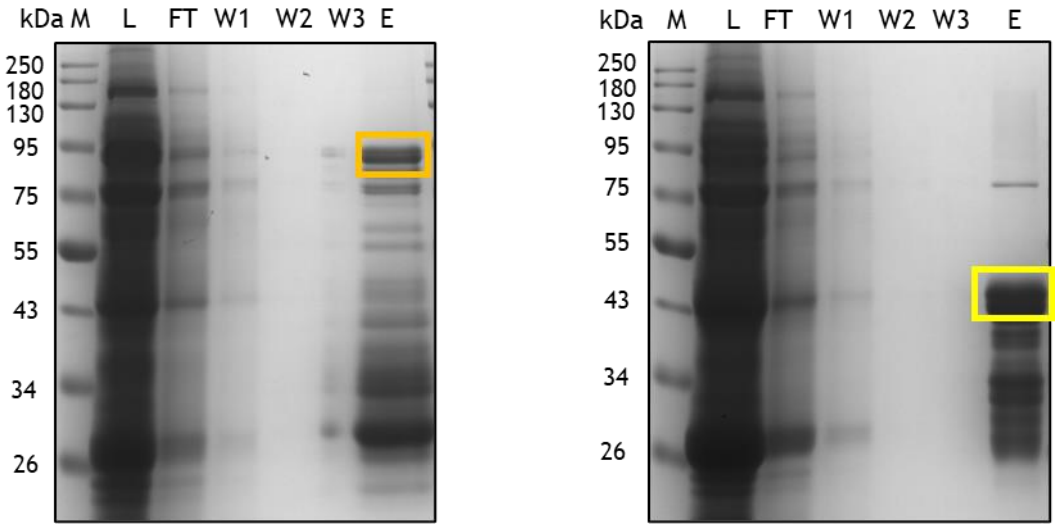

Figure 4-6 Purification of GST-tagged N-terminal and Middle Mid1p proteins. Purification of 76 kDa N-terminal Mid1p domain and 40 kDa middle Mid1p domain. GST-tagged N-terminal recombinant Mid1p was loaded on 1 mM L^{-1} GST Sepharose beads in PBS buffer and incubated overnight at 4ºC beads were washed three times with PBS. After the purification of the N-terminal and middle Mid1p recombinant domain, they were eluted from the GST Sepharose beads by adding reduced glutathione transferase which competes with the recombinant protein for GST binding. M, protein marker; L, lysate; FT, flow-through; W1, wash 1; W2, wash 2; W3, wash 3; E, elution. Orange and yellow boxes highlight the N-terminal terminal domain of Mid1p proteins, respectively.

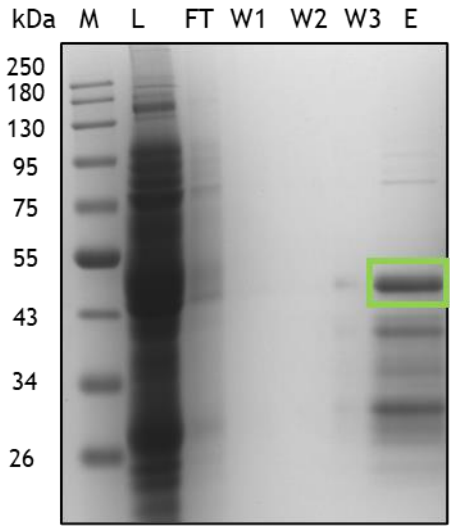

Figure 4-7 Purification of GST-tagged C-terminal Mid1p protein. Purification of 39 kDa C-terminal Mid1p domain. GST-tagged C-terminal recombinant Mid1p was loaded on 1 mM L^{-1} GST Sepharose beads in PBS buffer and incubated overnight at 4ºC beads were washed three times with PBS. After the purification of the C-terminal Mid1p recombinant domain, they were eluted from the GST Sepharose beads by adding reduced glutathione transferase which competes with the recombinant protein for GST binding. M, protein marker; L, lysate; FT, flow-through; W1, wash 1; W2, wash 2; W3, wash 3; E, elution. Green boxes highlight the C-terminal domain of the Mid1p protein.

4.3.7 Purification of Vps4p and Myo2p (bait) proteins for the pull-down assay experiments

To investigate the potential interaction between Vps4p and the purified different Mid1p domains, a full-length *vps4* gene was designed to encode a 6His-tag by being cloned into a pET-14b vector. Myosin 2 protein is known to interact with Mid1p, most likely through the C-terminal domain of Myo2p amino acid 1394-1526 (Motegi *et al.*, 2004; Rezig *et al.*, 2021). We utilized previously known findings and data to create a parallel pull-down test with this positive control. The 6His-C-term Myo2p construct was designed in the same manner as the 6His-Vps4p construct. Both 6His-tagged Vps4p and C-terminal Myo2p recombinant proteins were expressed in BL21 *E. coli,* and their production was induced by the addition of IPTG and purified by binding to Ni-NTA-agarose beads. Biochemical pull-down assay used prey and bait proteins, the prey Mid1p different domain proteins were designed, expressed, purified, and eluted.

To purify the 6His-Vps4p and 6His-Myo2p proteins employed as baits, Ni-NTA beads were utilized, 6His-tagged proteins were eluted twice with 250 mM imidazole in HEPES buffer, and 500 mM imidazole in HEPES. The elution was allowed to proceed for 2 hours at rotating at 4^{0}C. The samples were obtained from different washes and elution of the purification experiment and were analyzed on SDS-PAGE to see the efficiency of the elution. The gel images showed the different concentrations of proteins during the purification (Figure 4-8).

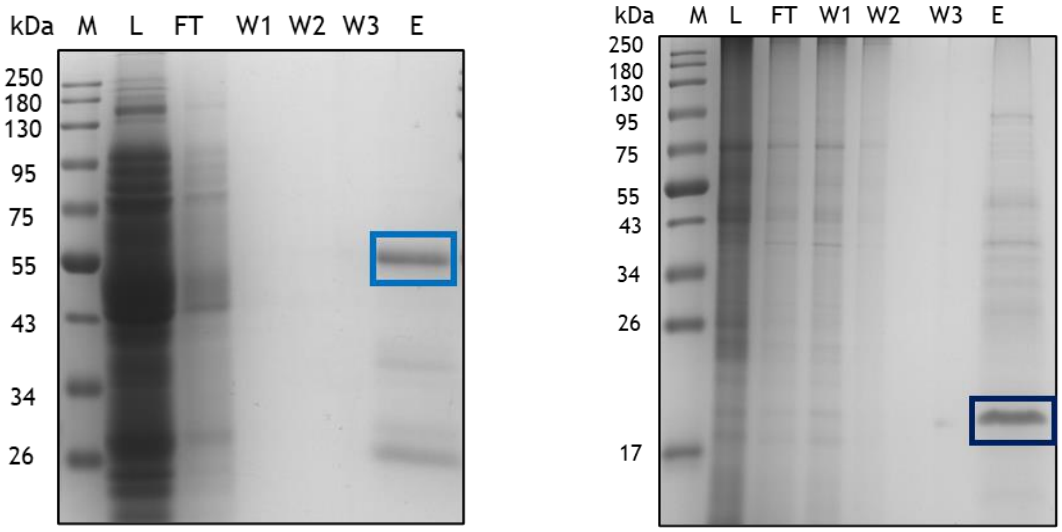

Figure 4-8 Purification of 48 kDa 6His-tagged Vps4p and 14 kDa 6His-tagged C-terminal Myo2p for *in vitro* biochemical pull-down experiment to determine the physical interactions between Mid1p and Vps4p. Both proteins were purified using 1 ml L^{-1} Ni-NTA beads in HEPES buffer and incubated overnight at 4ºC. The proteins were washed three times with 25 mM imidazole in HEPES buffer pH 6.5 and were eluted two times for two 2 hours with 250 mM and 500 mM imidazole in HEPES pH 4.5, respectively. Protein samples were analyzed by subjecting them to SDS-PAGE. M, protein marker; L, lysate; FT, flow-through; W1, wash 1; W2, wash 2; W3, wash 3; E, elution. Blue and purple boxes highlight Vps4p and Myo2p, respectively.

4.3.8 Quantification of purified *S. pombe* Mid1p, Vps4p, and Myo2p for pull-down assay experiments

To determine the total amount of proteins that would be used for the pull-down assay to investigate the interaction between Mid1p domains and Vps4p, different volumes of GST-Mid1p N-terminal, Middle, and C-terminal domain, 6His-Vps4p and 6His-Myo2p were run using SDS-PAGE, alongside with different known concentrations of BSA. Consequently, 10 µl, 5 µl, and 2.5 µl of GST-Mid1p N-terminal, Middle, and C-terminal domains were measured against 10 µg, 5 µg, and 2.5 µg of BSA (Figure 4-9). The same method was used for 10 µl, 5 µl, and 2.5 µl Vps4p, Myo2p, and GST-protein and various concentrations of BSA, the samples were used for the pull-down assay (Figure 4-10).

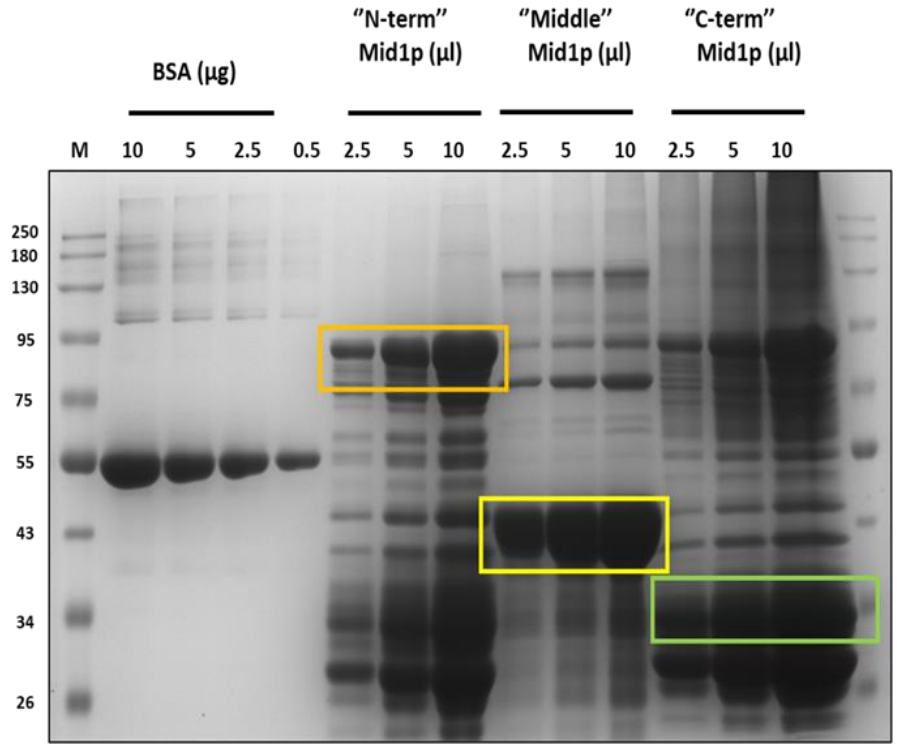

Figure 4-9 Quantification of purified GST-tagged N-terminal, Middle, and C-terminal Mid1p proteins. Different volumes of prey GST-purified N-terminal, Middle, and C-terminal Mid1p domains were subjected to SDS-PAGE alongside the known concentrations of bovine serum albumin (BSA) 10 µg ml^{-1}, 5 µg ml^{-1}, 2.5 µg ml^{-1}, and 0.5 µg ml^{-1}, for the quantification. Orange, yellow, and green boxes highlight the N-terminal terminal, Middle, and C-terminal domains of Mid1p, respectively.

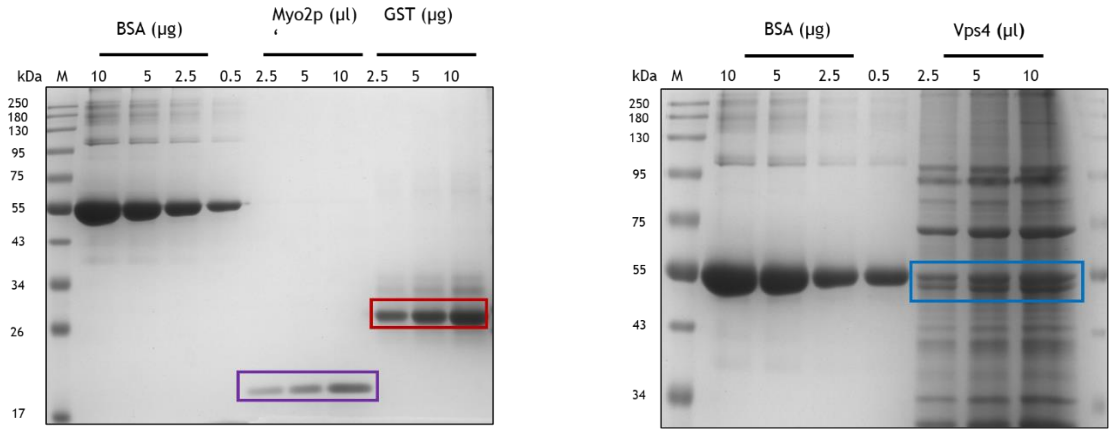

Figure 4-10 Quantification of purified C-terminal Myo2p, and Vps4p. Different volumes of baits 6His C-terminal Myos2p, GST, and Vps4p were subjected to SDS-PAGE alongside the known concentrations of bovine serum albumin (BSA) 10 µg ml^{-1}, 5 µg ml^{-1}, 2.5 µg ml^{-1}, and 0.5 µg ml^{-1}, for the quantification. Purple, red and blue boxes highlight Myo2p, GST, and Vps4p, respectively.

4.4 A pull-down assay reveals a physical interaction between Vps4p and the C-terminal domain of Mid1p

4.4.1 Protein affinity pull-down assay

In this study, a pull-down assay was performed three times using various batches of purified proteins. The pull-down assay was to test for the biochemical/physical interaction between Mid1p N-terminal, Middle terminal, C-terminal and full length Vps4p proteins. The outcome of the experiment is shown in Figure 4-11. The data showed various level of interactions between the three domains of Mid1p and was interpreted as follows:

i. Bait Vps4p pulled-down the C-terminal domain of Mid1p but not the N-terminal and the Middle terminals.

ii. No pull-down (physical interaction) was observed between Vps4p and GST alone.

iii. Myosin was used as a positive control demonstrating a interaction between the N-terminal, Middle and C-terminal domains of Mid1p (Figure 4-11).

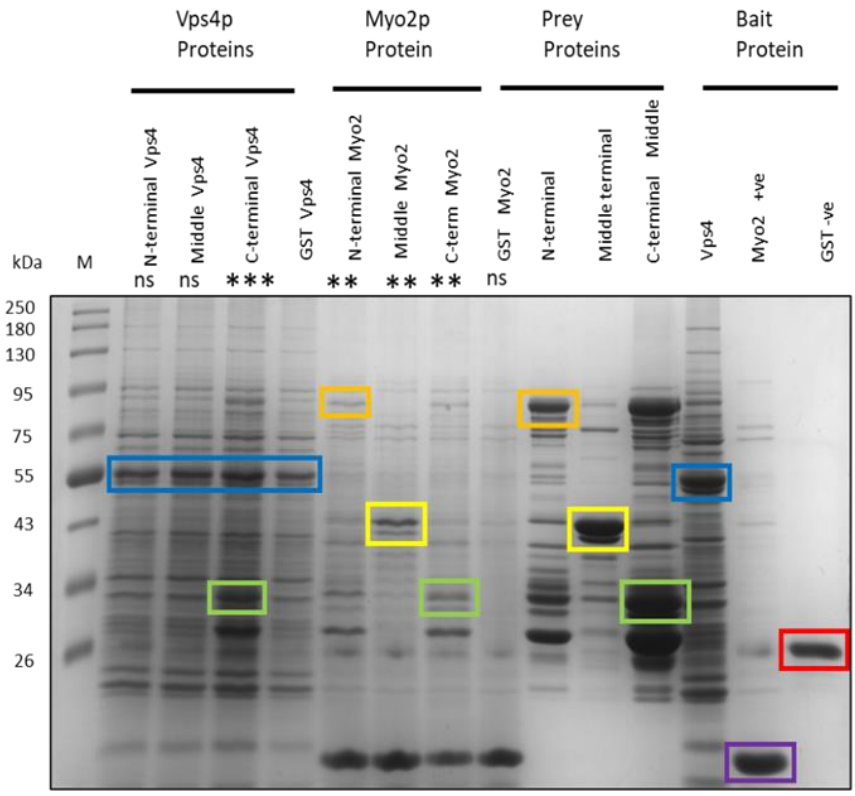

Figure 4-11 Direct physical interaction between Vps4p and C-terminal domain of Mid1p. The recombinant GST-tagged (Mid1p domains: ''N-term'' aa 1-453, ''Middle'' aa 452-579 and ''C-term'') and 6His-tagged (Vps4p and ''C-term'' Myo2p) proteins were expressed in *E coli* and purified using GST-Sepharose beads and Ni-NTA agarose beads, respectively. The purified proteins were utilized for pull-down assay where eluted prey proteins (N-term, Middle, and C-term) were added to baits proteins (6His-Vps4p and 6His Myo2p) that were bound to Ni-NTA beads, protein samples were subjected to SDS-PAGE. Myo2p bait protein was used as positive control while GST prey protein was used as a negative control. M, protein marker; blue boxes represent Vps4p, the yellow boxes represent Middle, orange boxes represent N-terminal, red boxes represent GST, green boxes represent C-terminal, the purple box represents Myo2p, (***) represents physical interaction between C-terminal Mid1p and Vps4p (**) represents physical interaction between Myo2p and Vps4p. Data from a typical experiment is shown, replicated using three independent batches of proteins for each condition.

A pull-down assay to determine the physical interaction between the N-terminal domain, middle and C-terminal domains of Mid1p with Vps4p protein using Ni-NTA agarose beads. The eluted prey protein was loaded to the bait protein that is bound to Ni-NTA agarose beads. We did not detect physical interactions between the N-terminal, and middle, with Vps4p but positive physical interaction between the C-terminal domains of Mid1p with Vps4p suggesting biochemical interaction between C-terminal domains of Mid1p with Vps4p as observed and represented by the asterisk above (Figure 4-11).

4.4.2 *mid1* phospho-mutant protein does not interact with Vps4p

To determine whether the *mid1* phospho-mutant protein is required for its interaction with Vps4p, a pull-down assay was performed using a wild-type version of Mid1p as a positive control and a mutant form of Mid1p in which the phospho-acceptor sites have been mutated from a serine residue to aspartic acid (S>D). The fragment of Mid1p employed will have both the "C-terminus" in which Vps4p interacts and the "middle" that contains the phosphorylation sites. Mutated phospho-sites are hypothesized to result in a lack of interaction between the two proteins, an indication that phosphorylation of these sites must be essential for the Mid1p and Vps4p protein to interact with one another to carry their role in cytokinesis.

To examine protein-protein interactions between wild-type Mid1p, *mid1* phospho-mutant, and Vps4p in detail. We examined the effects of phosphorylation of Mid1p concerning its physical interaction with Vps4p, and a large C-terminal fragment of Mid1p was inserted into a plasmid vector. The large segment contains the two phospho-sites that were mutated from serine (S) to aspartic (D) acid and incorporated into the "C-term" domain which interacts with Vps4p (Rezig *et al.*, 2021), in addition to the two phospho-sites that we believe are essential for cytokinesis in fission yeast.

Name	**Amino acid residues (aa)**	**Localization in *S. pombe***
Wild-type	S453-S920	Strong localization inside the nucleus and partially localized
mid1 phospho-mutant	S453-S920 (D523 and D531)	Strong localization inside the nucleus and partially localized

Table 4-3. Description and localization of wild-type and *mid1* phospho-mutant *S. pombe* cells. Mid1p wild-type and *mid1* phospho-mutant with amino acid (S453-S920) and (D453-D531) respectively. The phospho-mutant (D523-D531) contains Middle terminal which has the phosphorylation sites and the C-terminal domain that interact with Vps4p. Both Mid1p wild-type and *mid1* phospho-mutant protein were cloned into the pGEX-4T-1 vector and tagged with glutathione S-transferase (GST).

Mid1p wild-type S523 S531

HPSMQPVPGTKRTYSNYCENEPNKSSQSLVSSESHNVEGWNYSETGTVGFYDPSAEISAS
IDELRQSTPVARD**S**ELLSRAH**S**FDLNRLDLPSQDKSTSYEVPNGTENQSPRPVTSLGFVN
ETFFEEKPKAPLPLGRFYIHLNSILNISISEVHSPIKIIVNTPTQNMQLPWQAVNGNNRL
DHDFAFHVDDNFKVSFMFLDIPIEDKSNGSKGVSATKDVSNGKPAETKSKARKFFDKLFN
RRKKRKLNKAAAVENSKAKKSVVIKKVSGTATLNLGNVKDSCFGKAFNVEIPIISRGFLE
AIPVKINSIGKRTLGNLTLTCLYIPELSVPEQELPFTLEQATMDLRHVRSNYLYNEGYLY
RLEDSSIRRRFVVLRSKQLNFYAEKGGQYLDTFQLSKTVVSIPMVNFSEAVSNLGLVAGI
LATSVDRRHVQLFADSKKVCQKWLQVMNSRSFALDRGTEKLWLQEYVNFMA*

***mid1* phospho-mutant D523 D531**

HPSMQPVPGTKRTYSNYCENEPNKSSQSLVSSESHNVEGWNYSETGTVGFYDPSAEISAS
IDELRQSTPVARD**D**ELLSRAH**D**FDLNRLDLPSQDKSTSYEVPNGTENQSPRPVTSLGFVN
ETFFEEKPKAPLPLGRFYIHLNSILNISISEVHSPIKIIVNTPTQNMQLPWQAVNGNNRL
DHDFAFHVDDNFKVSFMFLDIPIEDKSNGSKGVSATKDVSNGKPAETKSKARKFFDKLFN
RRKKRKLNKAAAVENSKAKKSVVIKKVSGTATLNLGNVKDSCFGKAFNVEIPIISRGFLE
AIPVKINSIGKRTLGNLTLTCLYIPELSVPEQELPFTLEQATMDLRHVRSNYLYNEGYLY
RLEDSSIRRRFVVLRSKQLNFYAEKGGQYLDTFQLSKTVVSIPMVNFSEAVSNLGLVAGI
LATSVDRRHVQLFADSKKVCQKWLQVMNSRSFALDRGTEKLWLQEYVNFMA*

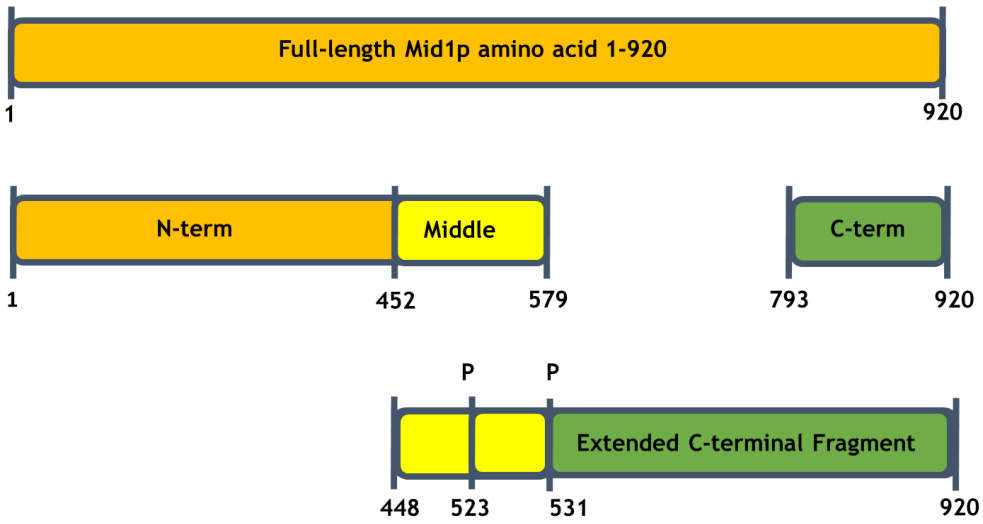

Figure 4-12 Schematic design of wild-type Mid1p and *mid1* phospho-mutant construct fragments. Mid1p contains 920 amino acids, these fragments contain most of the C-terminus, larger than the C-terminus fragment used in Rezig *et al.*, 2021. Wild-type Mid1p contains 448-920 amino acids and has the phosphorylation sites S523 and S531, while *mid1* phospho-mutant has the amino acid sequences 448-920 and S523D, S531D mutated residues.

4.4.3 *S. pombe* wild-type Mid1p and *mid1* phospho-mutant expression in *E. coli*

The first step to establishing the interaction between *mid1* phospho-mutant with Vps4p, Mid1p DNA constructs were designed and created by GenScript, containing a larger fragment of Mid1p than previously used by Rezig *et al*. (2021) allowing both the C-terminus and the potential phosphorylation sites to be present in the same fragment of the protein, with these expressed and purified in *E. coli*. Both wild-type and phospho-mutant forms of the Mid1p larger fragment were created, with the form containing mutations in phosphorylation sites serine (S) S523 and S531 to aspartic acid (D) of the middle phospho-sites.

To determine whether wild-type GST-Mid1p and phospho-mutant GST-Mid1p interact with Vps4p, wild-type GST-Mid1p and phospho-mutant GST-*mid1* plasmids were successfully expressed in bacteria (Figure 4-13).

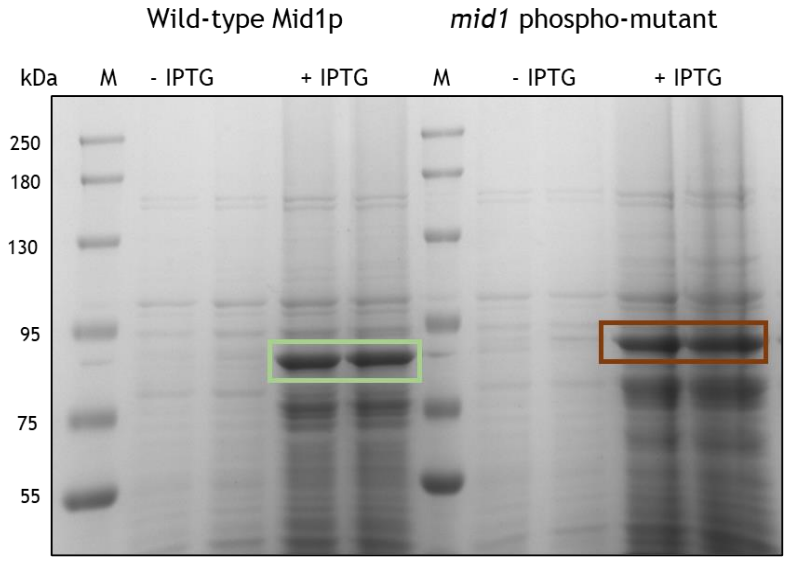

Figure 4-13 Expression of GST-tagged wild-type Mid1p and GST-tagged *mid1* phospho-mutant fission yeast proteins in *E. coli*. Wild-type Mid1p and mid*1* phospho-mutant plasmids were grown in BL21 *E. coli* competent cells to OD 0.6-0.8 and protein production was induced by the addition of 1 mM IPTG. The protein extracts were prepared and separated by SDS-PAGE. Wild-type Mid1p and *mid1* phospho-mutant proteins were expressed in BL21 *E. coli* before and after the induction with IPTG for 2 hours. Wild-type and phospho-mutant proteins were expressed in both samples at (79.99 kDa. Green and brown highlight the wild-type and phospho-mutant of the Mid1p protein, respectively.

4.4.4 Purification of S. *pombe* wild-type and *mid1* phospho-mutant (prey) proteins from *E. coli* for *in vitro* pull-down assay experiments

Following the expression of the GST-wild-type and *mid1* phospho-mutant recombinant proteins, the two fragments were purified using GST- Sepharose beads together with 6His-Vps4p and 6His-Myo2p proteins as outlined in Figure 4-14 and Figure 4-15 show different concentration of proteins so obtained.

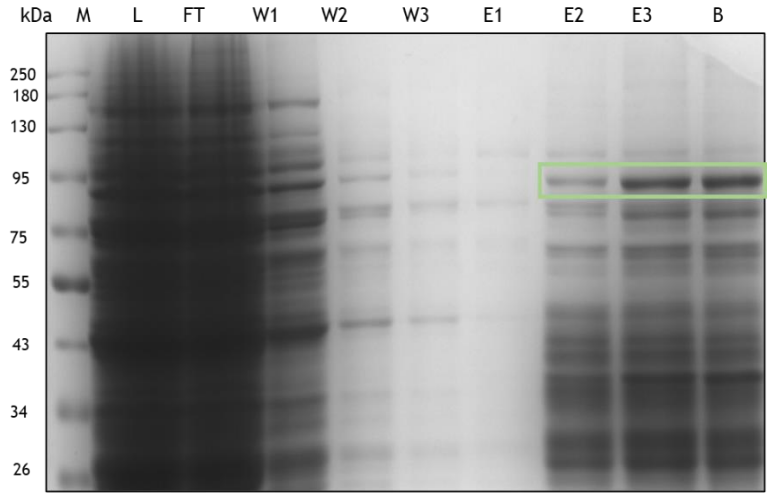

Figure 4-14 Purification of GST-tagged wild-type Mid1p fission yeast protein in *E. coli*. Purification of 79 kDa wild-type Mid1p protein. GST-tagged wild-type recombinant Mid1p was immobilized on 1mML^{-1} GST Sepharose beads in PBS buffer and incubated overnight at 4ºC and washed three times with PBS. After the purification of the wild-type Mid1p protein recombinant, they were eluted from the GST Sepharose beads by adding reduced glutathione transferase which competes with the recombinant protein for GST binding. M, protein marker; L, lysate; FT, flow-through; W1, wash 1; W2, wash 2; W3, wash 3; E, elution. Green boxes highlight wild-type Mid1p protein.

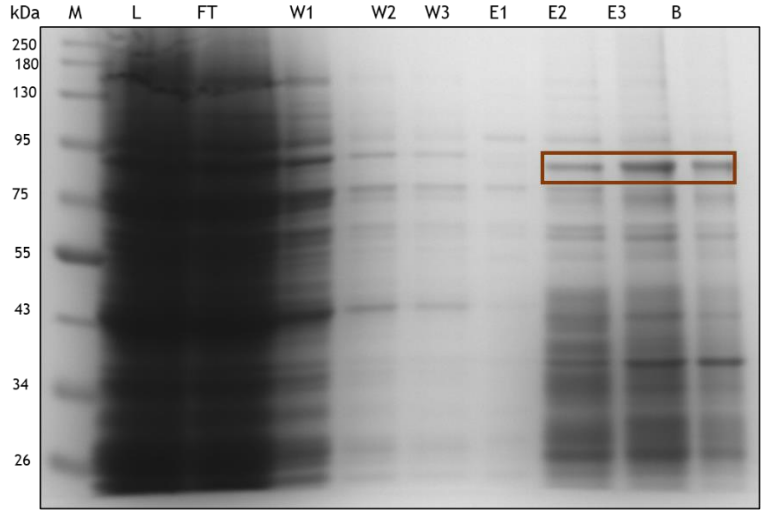

Figure 4-15 Purification of GST-tagged *mid1* phospho-mutant fission yeast protein in *E. coli*. Purification of 79 kDa *mid1* phospho-mutant protein. GST-tagged *mid1* phospho-mutant recombinant protein was immobilized on 1mML^{-1} GST Sepharose beads in PBS buffer and incubated overnight at 4ºC and washed three times with PBS. After the purification of the *mid1* phospho-mutant recombinant protein, they were eluted from the GST Sepharose beads by adding reduced glutathione transferase which competes with the recombinant protein for GST binding. M, protein marker; L, lysate; FT, flow-through; W1, wash 1; W2, wash 2; W3, wash 3; E, elution. Brown boxes highlight phospho-mutant Mid1p protein.

4.4.5 Quantification of purified *S. pombe* wild-type (WT) Mid1p and *mid1* phospho-mutant (MT) proteins

Proteins were quantified by comparison with BSA as outlined in Figure 4-16. Three different volumes of GST-purified and 6His-purified proteins were subjected to SDS-PAGE, along with various concentrations of bovine serum albumin (BSA) as indicated.

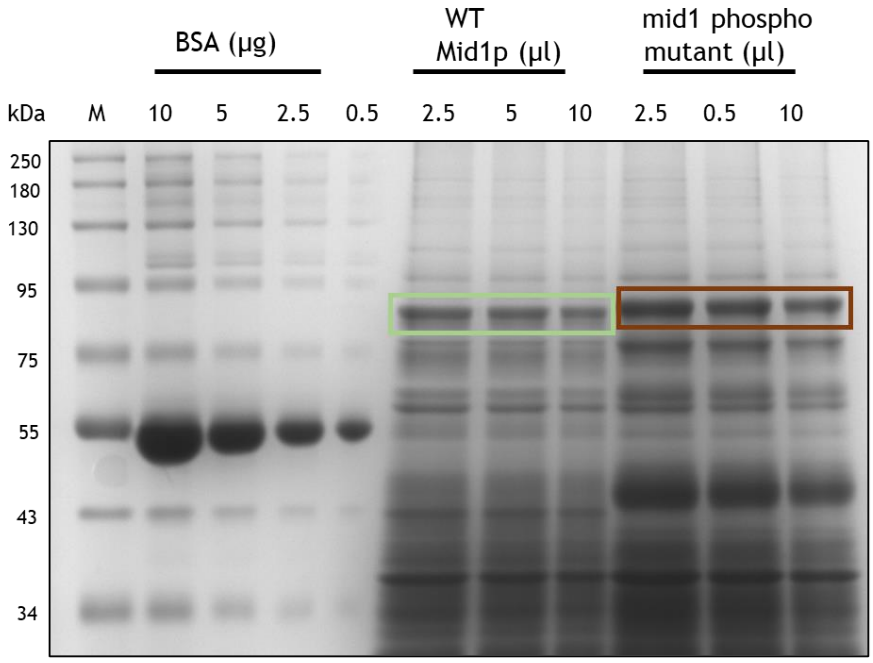

Figure 4-16 Quantification of purified GST-tagged wild-type Mid1p and *mid1* phospho-mutant. Different volumes of GST-purified wild-type Mid1p and *mid1* phospho-mutant proteins were subjected to SDS-PAGE alongside various concentrations of bovine serum albumin (BSA) 10 µg ml^{-1}, 5 µg ml^{-1}, 2.5 µg ml^{-1}, and 0.5 µg ml^{-1}, for the quantification of purified GST-tagged wild-type and *mid1* phospho-mutant. M, protein marker (kDa). Coloured boxes highlight predicted proteins: Green and brown boxes highlight wild-type and phospho-mutant Mid1p proteins.

4.5 A pull-down assay reveals no physical interaction between Vps4p and *mid1* phospho-mutant

A pull-down assay was performed three times, the result of the experiment is shown in Figure 4-17. From these data we can draw the following general conclusions:

i. Bait Vps4p pulled down Mid1p wild-type protein but didn't pull-down *mid1* phospho-mutant.

ii. No pull-down (physical interaction) was observed between Vps4p and GST alone.

iii. Myosin was used as a positive control demonstrating interaction with Mid1p wilt-type.

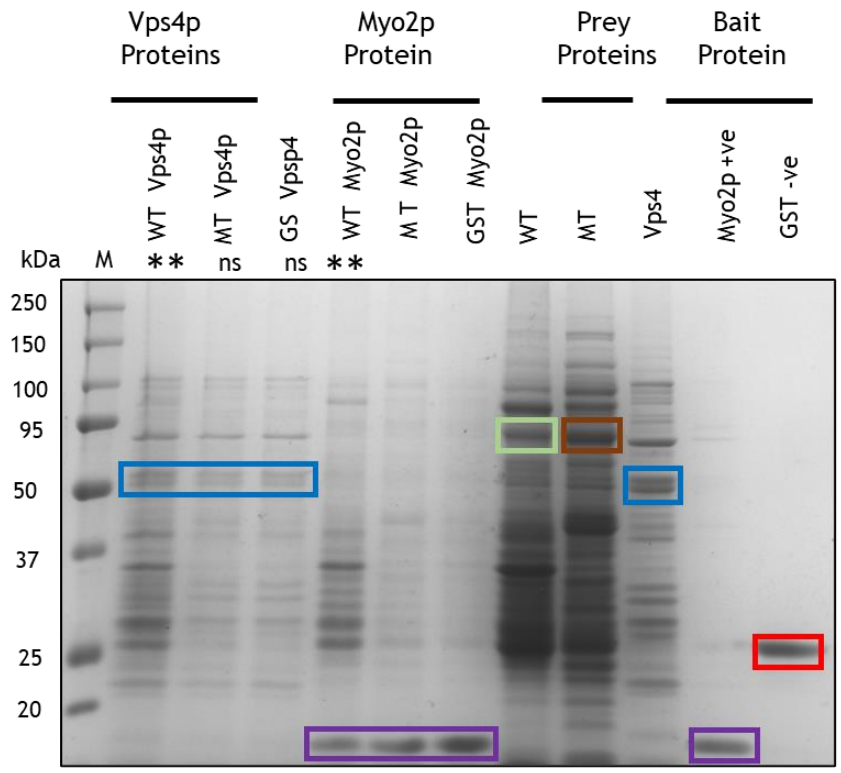

Figure 4-17 Direct physical interaction between wild-type Mid1p and Vps4p and non-physical interaction between *mid1* phospho-mutant and Vps4p. The recombinant GST-tagged (Mid1p wild-type and *mid1* phospho-mutant) and (Vps4p and ''C-term'' Myo2p) proteins were expressed in *E Coli* and purified using GST-Sepharose beads and Ni-NTA agarose beads and Ni-NTA beads proteins, respectively. The purified proteins were subsequently used in pull-down studies where prey proteins (wild-type or phospho-mutant GST-Mid1p or GST) were added to bait proteins (6His-Vps4p or 6His-Myo2p) that were bound to Ni-NTA beads, protein samples were subjected to SDS-PAGE. Myo2p bait protein was used as positive control while GST prey protein was used as a negative control. M, protein marker; WT, wild-type; MT; *mid1* phospho-mutant, Coloured boxes highlight predicted proteins: green boxes represent Vps4p; Red boxes represent wild-type Mid1p boxes represent orange boxes represent *mid1* phospho-mutant; Blue boxes represent Myo2p; Purple boxes represent GST. (***) represents a physical interaction between wild-type Mid1p and Vps4p.

4.6 Summary

Rezig *et al*. (2021) investigated the interaction between Mid1p and the ESCRT-associated protein Vps4p in fission yeast, and their role in cytokinesis. Initially, various double mutant strains were created and screened in fission yeast: *mid1* and ESCRT-0 to ESCRT-III and *mid1Δ* and *vps4Δ*, each of which had been chromosomally deleted. Viability was observed in all double mutants except for that of the *mid1Δ* and *vps4Δ* double mutants. With this cross, viable colonies failed to thrive and instead yielded to synthetic lethality after only a few divisions. This provided evidence that *mid1*$^{+}$ and *vps4* genes genetically interact with one another and suggest that this interaction may be an important and essential for cellular function.

In this chapter a pull-down assay was used to determine the physical interaction between the N-terminal domain, middle and C-terminal domains of Mid1p with Vps4p and also pull-down between wild-type and *mid1* phospho-mutant of Mid1p with Vps4p protein using Ni-NTA agarose beads. The eluted prey protein was loaded to the bait protein that is bound to Ni-NTA agarose beads. We observed a positive physical interaction between C-terminal domain with Vps4p suggesting biochemical interaction between C-terminal and Vps4p. However, we observed a negative physical interaction between N-terminal and Middle with Vps4p.

We observed no physical interactions between the *mid1* phospho-mutant and Vps4p but positive physical interaction between the wild-type of Mid1p and Vps4p was observed. These observations suggest a direct physical interaction between wild-type Mid1p which comprises amino acid 448-920 which was hypothesized to pull-down Vps4p. This observation is consistent with the published observation that C-term amino acid 798-920 of Mid1p pull-down Vps4p (Rezig *et al*., 2021), Furthermore, the same amino acid 448-920 fragment of Mid1p when mutated in certain phosphorylated amino acids, did not pull-down Vps4p.

4.7 Conclusions

The pull-down study focused on the physical interaction between the prey and bait proteins using Ni-NTA agarose beads. The eluted prey protein was loaded onto the Ni-NTA agarose bead-bound bait protein. The principal outcomes of the chapter are:

- Negative physical interactions were observed between the N-terminal and middle of Mid1p proteins and Vps4p, indicating that there are no biochemical interactions between the N-terminal and middle of Mid1p proteins and Vps4p.

- A positive physical interaction was observed between the C-terminal domain of Mid1p and Vps4p, indicating a biochemical interaction.

- We observed negative physical interactions between the *mid1* phospho-mutant and Vps4p, but positive physical interactions between the wild-type of Mid1p and Vps4p, suggesting a biochemical interaction between the two proteins that require the phosphorylation in Mid1p.

Chapter 5 Investigating the role of phosphorylation of Mid1p during cytokinesis in fission yeast

5.1 Introduction

5.1.1 Mid1p plays an important role during cytokinesis in *S. pombe*

Although the cytokinesis contractile ring (CR) was initially described more than 50 years ago, we still do not fully understand how eukaryotic cells construct CRs (Garno *et al.*, 2021). In *Schizosaccharomyces pombe*, two essential phases of cytokinesis are division site selection and contractile ring assembly. Fission yeast has revealed significant aspects of medial division including proteins participating throughout cytokinesis, mechanisms of division site specification, and medial actin-myosin contractile ring ACR assembly. The scaffold proteins, anillin, and Mid1p play key roles during the mammalian and fission yeast cell cycle, respectively (Rezig *et al.*, 2022).]

Mid1p/anillin localizes to nodes and is required for CR assembly in the mid-cell region (Rincon and Paoletti 2012; Rincon and Paoletti, 2016). When CR constriction is initiated, Mid1p migrates to the division site; however, it is unknown how Mid1p migrates and disassociates. However, through a signalling cascade, the septation initiation network (SIN) triggers node dispersals, CR assembly, constriction, and septum development (Sparks *et al.*, 1999; Johnson *et al.*, 2015). *S. pombe* Mid1p shuttles back and forth between the cortical nodes and late interphase nodes (Paoletti and Chang, 2000; Akamatsu *et al.*, 2014). The cortical nodes spread to the equator of the cell, where they are captured at the beginning of mitosis to become cytokinesis. Then, Mid1p attracts additional cytokinesis node proteins, including myosin II (Celton-Morizur *et al.*, 2004; Wu *et al.*, 2006; Almonacid *et al.*, 2011).

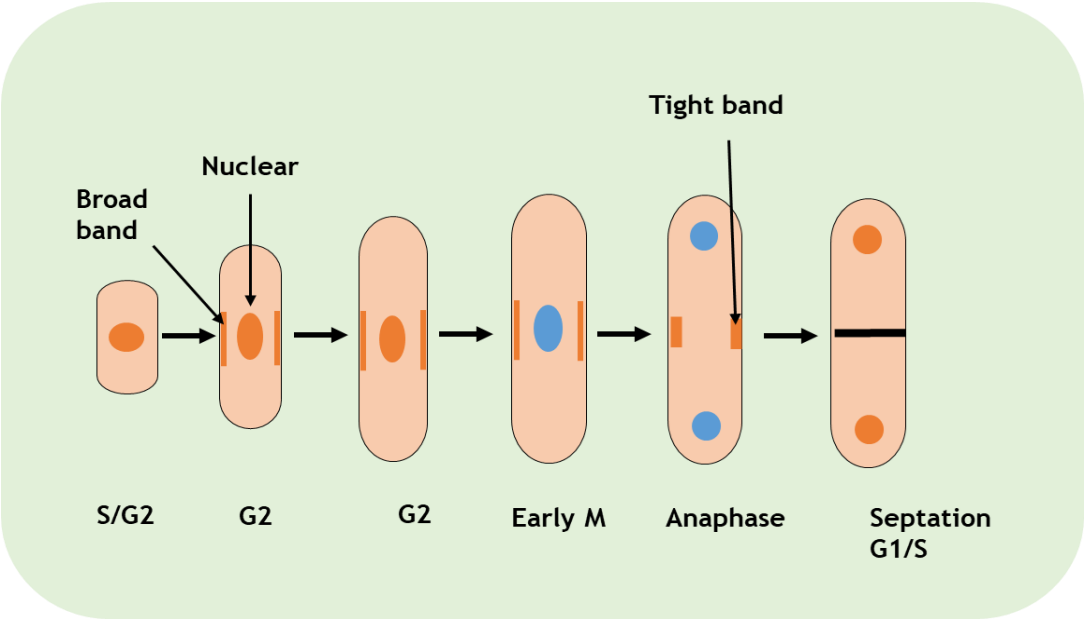

Figure 5-1 Schematic diagram of Mid1p localization pattern during the cell cycle. Mid1p is shown in orange, whereas the nucleus without Mid1p is shown in blue. In early mitosis, before nuclear division, the contractile ring forms at the predicted location of the nucleus. During interphase, Mid1p was concentrated at the nucleus's periphery and on a broad, central cell surface that covered the nucleus in the bulge region. During mitosis, nuclear disappeared, but the broadband remained at the end of anaphase, with two bands atop each nucleus (adapted and modified from Paoletti and Chang, 2000).

The node proteins remain in the CR, and the nodes are reset to daughter cell equators in preparation for medial cell division in the subsequent cell cycle. Mid1p exits the CR and re-accumulates in the nucleus as constriction commences (Akamatsu *et al.*, 2014; Rincon *et al.*, 2017). Even though Mid1p's ability to attach to the plasma membrane and other protein interactions controlled by polo-like kinase Plo1 and Cdk are required for localization to type 1 and cytokinetic nodes, Mid1p's ability to attach to the plasma membrane is not necessary (Sohrmann *et al.*, 1996; Bähler *et al.*, 1998; Moseley *et al.*, 2009). Mid1p/anillin displays phosphorylation-induced band retardation in SDS-PAGE, and large-scale phospho-proteomics identified numerous phosphorylation sites. Protein phosphorylation is a common mechanism for regulating localization and function in mitosis (Gnad *et al.*, 2011).

Previous work by Kim *et al.* (2017) demonstrated that phosphorylation regulates the efficient recruitment of human anillin to the equatorial membrane, they have shown that phosphorylation enhances anillin recruitment to the equatorial cortex at the onset of anaphase and promotes successful cytokinesis. Progression of these events is regulated by mechanisms and proteins that are evolutionarily conserved in eukaryotes from fungi to humans. Genetic and molecular findings in

different model organisms recognized essential cytokinesis genes, with numerous conserved proteins, including the anillin/Mid1p proteins, constituting the core cytokinetic machinery. The fission yeast *Schizosaccharomyces pombe* represents a well-established model organism to study eukaryotic cell cycle regulation (Rezig *et al.*, 2022).

5.2 Aims

Anillin is a central integrator of cytokinesis that is recruited in a ring-like structure on the membrane of dividing cells, understanding how mitosis and cytokinesis are coordinated may provide insight into human diseases. Protein phosphorylation is a common mechanism for regulating the timing of mitotic events, but the functional significance of anillin's phosphorylation sites is unknown (Kim *et al.*, 2017).

Previously, we reported that *S. pombe* Mid1p is phosphorylated during cytokinesis and that phosphorylation is necessary for correct cytokinesis (Rezig *et al.*, 2021). Our aim in this chapter is to characterize the localization phenotypes of GFP-Mid1p in wild-type and GFP-*mid1* phospho-mutant cells. We will study the relationship between phosphorylation and GFP-Mid1p nuclear-shuttling distribution and nuclear localization phenotypes in *S. pombe* cell components. Our specific objectives are:

- Determine the growth defects of *mid1* phospho-mutants and GFP-*mid1* phospho-mutants in *S. pombe* strains.

- Report the cell morphology defects of *mid1* phospho-mutants and GFP-*mid1* phospho-mutants in *S. pombe* strains.

- Examine and quantify the septation defects of *mid1* phospho-mutants in *S. pombe* strains.

- Assay the cell localization frequency and distribution of Mid1p in GFP-*mid1* phospho-mutants in *S. pombe* strains.

5.3 Results

5.3.1 Mid1p phosphorylation has a role during cytokinesis in *S. pombe*

5.3.2 An *in vivo* integration strategy for *S. pombe*

This study was concerned with understanding the regulation of Mid1p through the cell cycle of *S. pombe*. To do this an *S. pombe* integration experiment was completed which involved introducing single, double, or multiple mutations of potential phospho-sites in Mid1p to yield phospho-mimetic versions by converting serine (S) to aspartic acid (D) phospho-resistant by converting from serine (S) to alanine (A) as described in Chapter 3, *section 3.3.1*. An *S. pombe* plasmid pJK148 was used to integrate mutated *mid1* DNA sequences into the *leu1*$^{+}$ chromosome locus of fission yeast, with the plasmid first linearized and then transformed into an *S. pombe* strain with a point mutation in the *leu1*$^{+}$ gene (Siam *et al.*, 2004). We used this approach to produce *S. pombe* strains with phospho-mimetic (S>D) and phospho-resistant (S>A) versions of the *mid1* gene to test the effect of such mutations on Mid1p function by examining cell growth defects, colony and morphology formation. Single-point, double-point, and multiple-point mutants of the *mid1* gene were designed to have the *mid1* endogenous promoter and 1K bp upstream of the *mid1* open reading frame and were synthesized by GenScript (Chapter 2, *section 2.3.2*). Following the successful integration of each of the *mid1* mutant genes, the strains were subjected to *in vivo* growth and morphological analysis.

5.3.3 *mid1* phospho-resistant mutants and phospho-mimetic mutants reveal growth defects phenotypes

Following a successful design and integration experiment, *mid1* phospho-mutant strains were subjected to a growth defect analysis to determine the growth characteristics of the strain. For these experiments, two control strains were used: a Mid1p wild-type W-T *mid1Δ*pJK148: *mid1*$^{+}$ (GG 2673) and *mid1Δ* deletion strain (GG 1129). Additionally, five *mid1* phospho-resistant and phospho-mimetic strains were examined. The five phospho-resistant and phospho-mimetic strains were identified and selected based on my previous results in Chapter 3 which revealed the striking genetic interaction between *mid1* phospho-mutants, *vps4Δ*, *plo1-ts35*, *ark1-ts11*, and other important cytokinesis-associated proteins that regulate cell division processes in S. *pombe*. The striking genetic interaction observed in *mid1* phospho-mutant, and cytokinesis-associated strains *vps4Δ* (328, 332, 523 and 531) also indicate that it could be a potential site for regulating Mid1p function during cytokinesis (Rezig *et al.*, 2021).

To examine the effect of phosphorylation during cytokinesis on *mid1* phospho-mutants, serial dilutions of the various *mid1* phospho-mutant strains were performed on a solid YE medium and incubated at 28°C for two days to determine if any of the *mid1* phospho-mutants exhibit a defective or delayed growth phenotype.

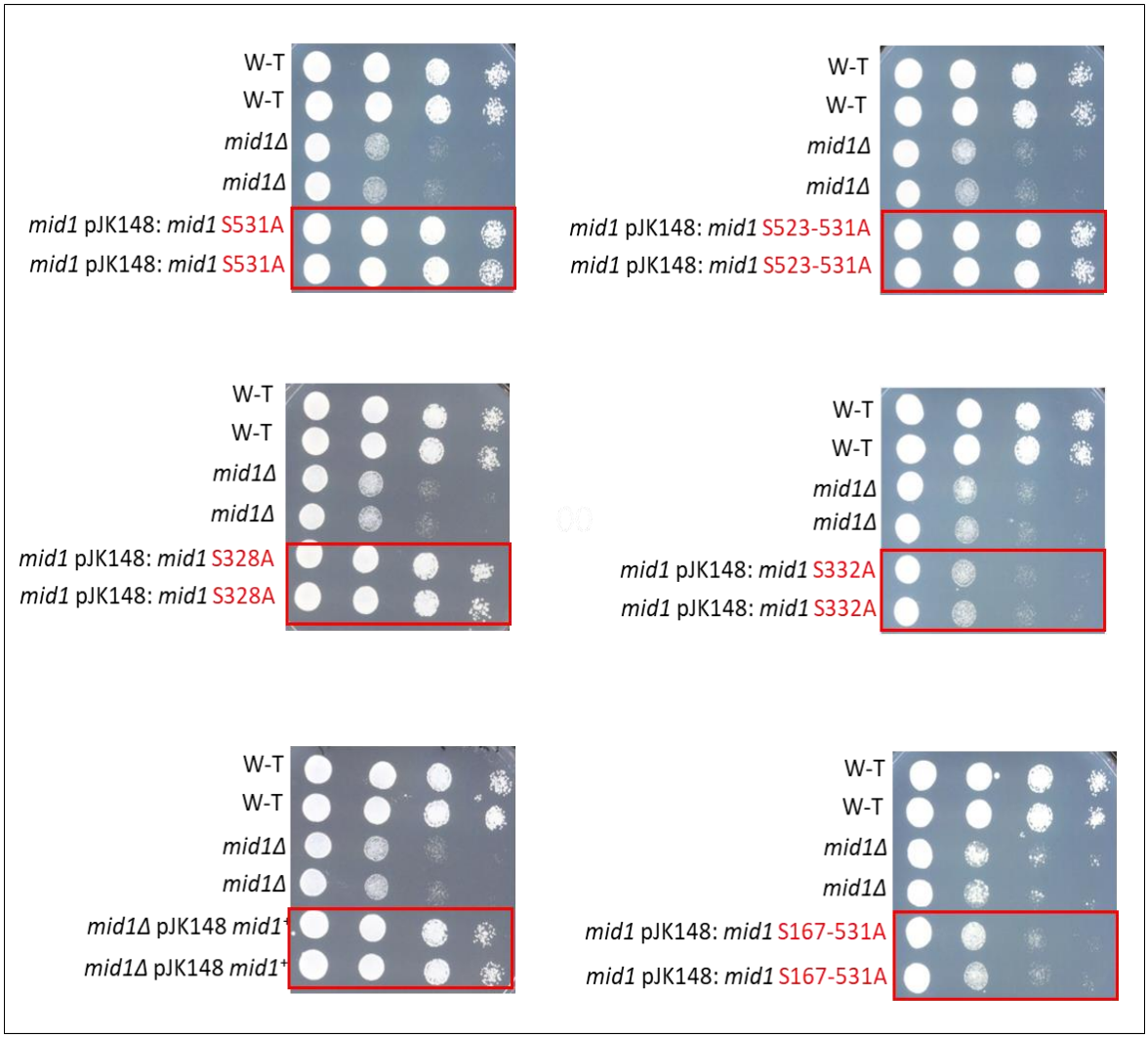

Figure 5-2 The *mid1* phospho-resistant mutants (S>A) reveal growth defects phenotypes. Analysis of the growth defects phenotypes of wild-type (W-T) *mid1*ΔpJK148: *mid1*$^{+}$ (GG 1347), *mid1*Δ (GG 1129), *mid1*ΔpJK148: *mid1*S328A (GG 3536), *mid1*ΔpJK148: *mid1*S332A (GG 3551), *mid1*ΔpJK148: *mid1*S531A (GG 3336) *mid1*ΔpJK148: *mid1*S523-531A (GG 3514) and *mid1*ΔpJK148: *mid1*S167-531A (GG 3533). Two isolates of each strain were grown at 28ºC on solid YE medium and suspended at a concentration of 1.5x10^{6} cells/ml, cells were subjected to a 10-fold serial dilution. Pipetted cells were placed on solid YE media and incubated. After two days of cell growth on a solid YE medium, the phospho-mutants were examined and interpreted.

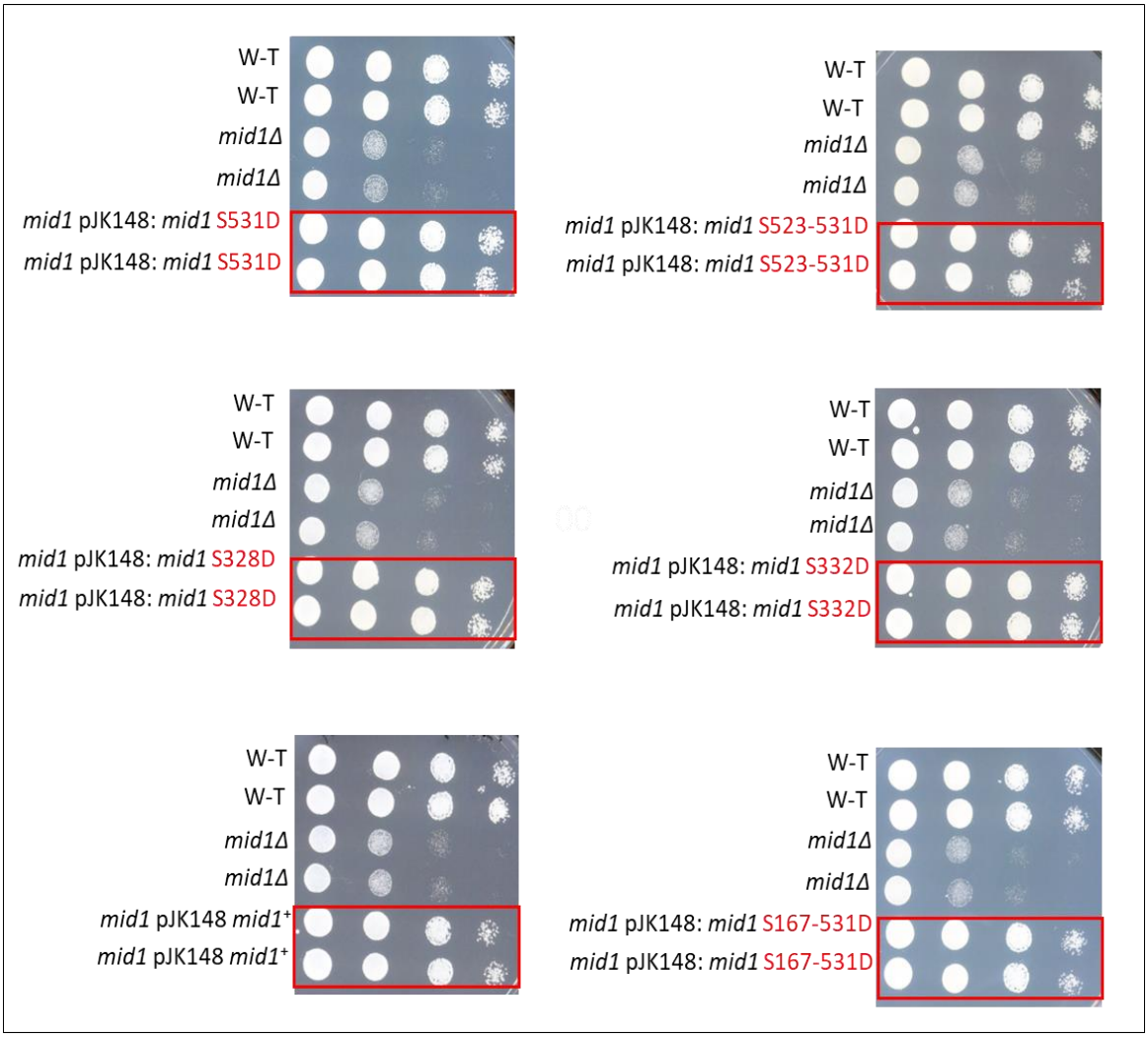

Figure 5-3 The *mid1* phospho-mimetic mutants (S>D) reveal growth defects phenotypes. Analysis of the growth defects phenotypes of wild-type (W-T) *mid1*ΔpJK148: *mid1*$^{+}$ (GG 1347), *mid1*Δ (GG 1129), *mid1*ΔpJK148: *mid1*S328D (GG 3542), *mid1*ΔpJK148: *mid1*S332D (GG 3564), *mid1*ΔpJK148: *mid1*S531D (GG 3525), *mid1*ΔpJK148: *mid1*S523-531D (GG 3520), and *mid1*ΔpJK148: *mid1*S167-531D (GG 3552). Two isolates of each strain were grown at 28ºC on solid YE medium and suspended at a concentration of 1.5x10^{6} cells/ml, cells were subjected to a 10-fold serial dilution. Pipetted cells were placed on solid YE media and incubated. After two days of cell growth on a solid YE medium, the *mid1* phospho-mutants were examined and interpreted.

All single, double, and multiple S328D, S332D, S532D, S523D-531D, and S167-531D phospho-mimetic mutations showed no defective growth phenotypes vividly showing normal rod-shaped, growth colonies and normal growth phenotypes similar to wild-type (Figure 5-3). However, the phospho-resistant strains S332A and S167-531A shown in (Figure 5-3) exhibit defective and delayed growth phenotypes among the phospho-resistant mutant strains. The strains displayed a disorganized growth colonies and disoriented cell formation, while other strains S328A, S523A, and S531A (Figure 5-3) exhibited rod-shaped, normal growth and dividing phenotypes similar to wild-type, these strains share the same viable phenotype as the wild-type. Mid1p wild-type W-T, iW-T integrated wild-type, and *mid1Δ* were used as controls for the experiment.

5.3.4 The *mid1* phospho-resistant mutants and phospho-mimetic mutants reveal colony and morphological defects phenotypes

After establishing preliminary information on the growth properties of *mid1* phospho-resistant and phospho-mimetic strains through growth defect experiments. To further investigate *mid1* phospho-mutant strains, we examined their mutation *in vivo*. In the absence of the Mid1p function, *S. pombe* cells exhibited morphological defects. Therefore, we examined the relevance of mutations of *mid1* phospho-mutants on the morphology of *S. pombe* strains. As a control for the experiment, again we maintain wild-type (GG 2673) and *mid1* deletion *mid1Δ* (GG 1129).

We examined five each of the phospho-resistant and phospho-mimetic strains, to determine the effect of phosphorylation during cytokinesis on *mid1* phospho-mutants, serial dilutions of various *mid1* phospho-mutant strains were performed on a solid YE medium and incubated at 28^{0}C for two days. Individual colonies were observed using a Sony camera and Zeiss Axioscope microscope.

All single, double, and multiple mutants S328D, S332D, S532D, S523D-531D, and S167-531D *mid1* phospho-mimetic mutations reveal a normal phenotype similar to wild-type phenotypes with rod-shaped colonies with no morphology defects phenotypes observed (Figure 5-5). However, the phospho-resistant mutant strains (S>A) S332A and S167-531A have defective colonies on solid medium with slow growth rate and impaired morphology when compared to wild-type. Nonetheless, the remaining strains (S328A, S523A, and S531A) exhibited normal rod-shaped colonies and morphology phenotype as the wild-type phenotype, which have normal rod-shaped colonies and morphology (Figure 5-4).

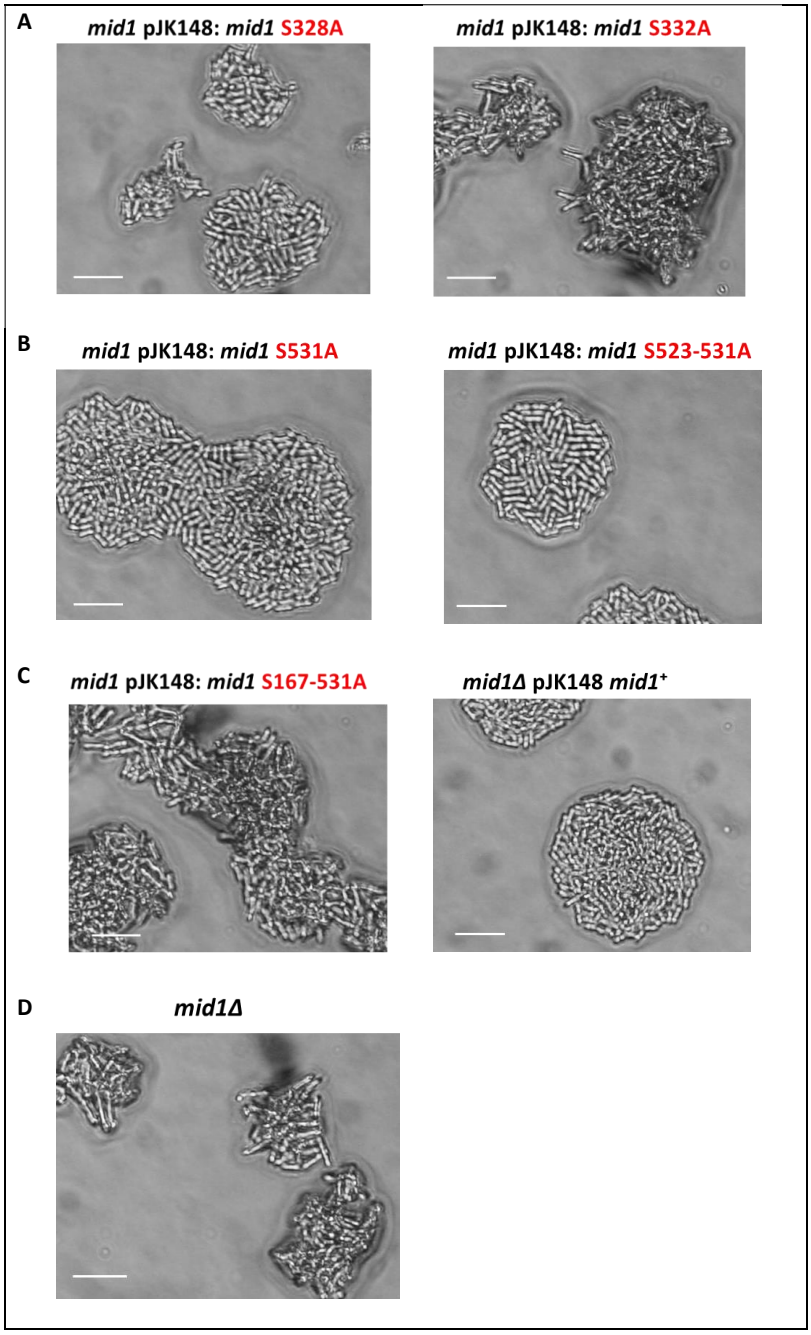

Figure 5-4 The *mid1* phospho-resistant mutants (S>A) reveal morphological defects. Analysis of the morphological defect of wild-type (W-T) *mid1*$^{+}$ (GG 1347), *mid1*Δ (GG 1129), *mid1* S328A (GG 3536), *mid1* S332A (GG 3551), *mid1* S531A (GG 3336) *mid1* S523-531A (GG 3514) and *mid1* S167-531A (GG 3533). Strains grown at 28ºC on solid YE medium and suspended at a concentration of 1.5x10^{6} cells/ml, cells were subjected to a 10-fold serial dilution Pipetted cells were placed on solid YE media and incubated. After two days of cell growth on a solid YE medium, the *mid1* phospho-mutants were examined and interpreted. The scale bar represents 50 µm.

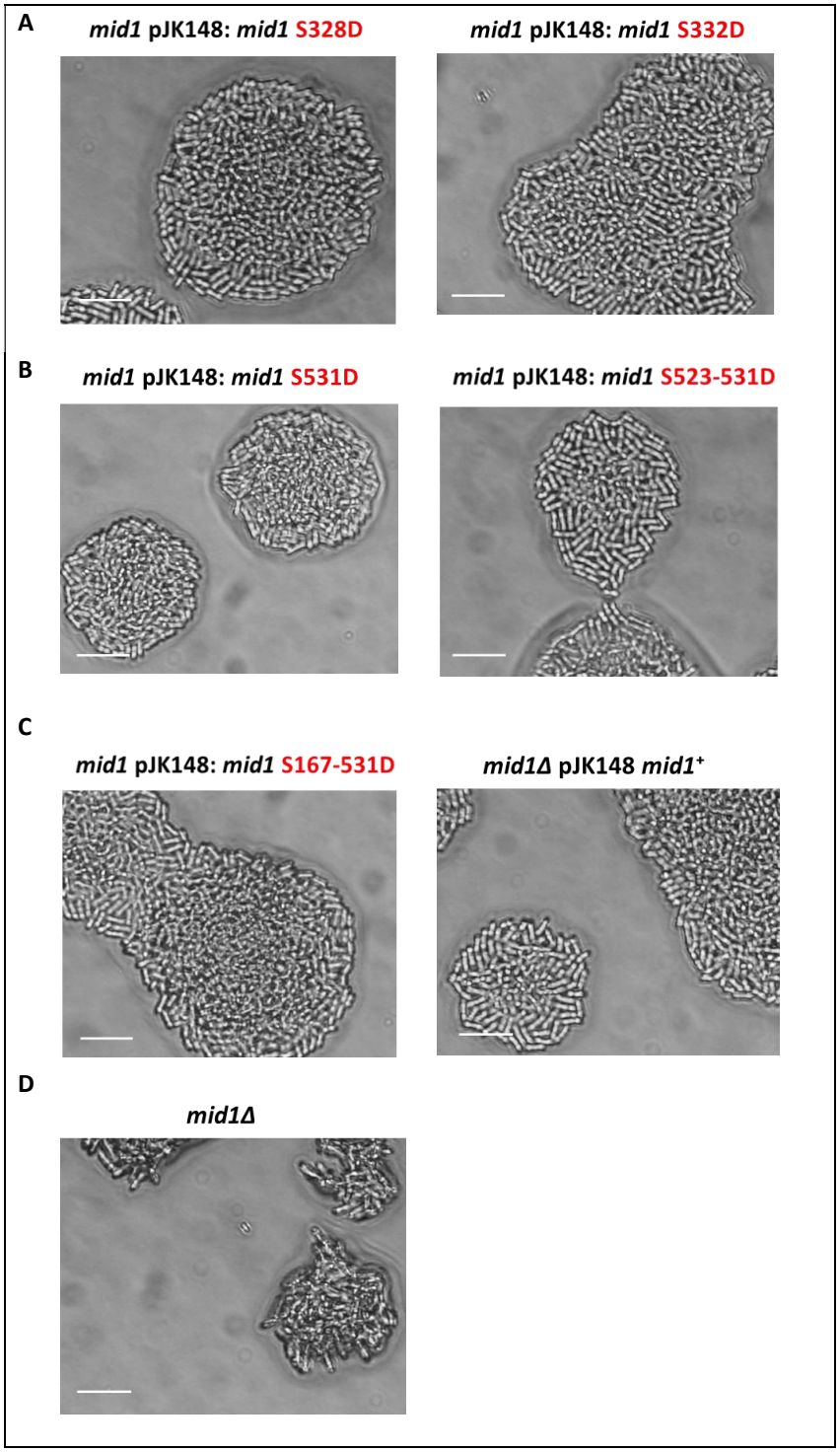

Figure 5-5 The *mid1* phospho-resistant mutants (S>D) reveal morphological defects. Analysis of the morphological defect of wild-type (W-T) *mid1*$^{+}$ (GG 1347), *mid1*Δ (GG 1129), *mid1* S328D (GG 3542), *mid1* S332D (GG 3564), *mid1* S531D (GG 3525), *mid1* S523-531D (GG 3520), and *mid1* S167-531D (GG 3552). Strains grown at 28ºC on solid YE medium and suspended at a concentration of 1.5x10^{6} cells/ml, cells were subjected to a 10-fold serial dilution Pipetted cells were placed on solid YE media and incubated. After two days of cell growth on a solid YE medium, the *mid1* phospho-mutants were examined and interpreted. The scale bar represents 50 µm.

Observing certain *mid1* phospho-mutant, and double mutant phenotypes revealed defective colony. We investigated the phenotype of synthetic colony defects caused by *mid1* phospho-resistant and phospho-mimetic mutations. In each instance where strains were grown on a solid YE medium, colonies were formed. In the majority of serine-to-alanine or serine-to-aspartic acid mutated strains, rod-shaped cells with colonies resembling wild-type were observed. However, it was observed that S332A and S167-531A (Figure 5-4) cells had slow growth, defective colonies, and similar morphology to *mid1Δ* cells.

The S332A and S167-531A mutants were compared to the wild-type cells, and disoriented colonies were observed in the S332A and S167-531A mutants. In contrast, S332D and S167-531D (Figure 5-5) exhibited no significant change in terms of colonies and morphological defect, with normal rod-shaped sizes and an organized colony phenotype comparable to the wild-type, S332D and S167-531D exhibited no significant change in terms of colonies and morphological defect. These observations revealed that S328A, S531A, S523-531A (Figure 5-4) and S328D, S332D, S531D, S523-531D, and S167-531D in (Figure 5-5) have rod-shaped sizes and organized colony phenotypes comparable to those of the wild-type, suggesting that these amino acid residues do not play have an impact in colony formation and morphology during cytokinesis.

5.3.5 The role of Mid1p phosphorylation during septation

After the identification and characterization of the growth defect and colony formation of the *mid1* phospho-resistant and phospho-mimetic strains, the same strains were used for septation studies to determine the importance of phosphorylation during septation. Septation was evaluated using calcofluor-white staining to examine how phosphorylation of Mid1p may influence *S. pombe* during cytokinesis. The frequency of septation in each *mid1* phospho-mutant train was quantified and analyzed. *S. pombe* strains grown in liquid YE media were stained with calcofluor-white to visualize newly deposited septa using an LSM 880 confocal microscope.

The septation phenotypes of wild-type (GG 1273), *mid1Δ* (GG 1129), and *mid1* phospho-mutant cells were characterized, and the statistical frequency of each septation phenotype for each strain was determined. Then, the phenotype frequencies of wild-type *mid1Δ*, and *mid1* phospho-mutant strains were compared to those of the wild-type strain Figure 5-8, and Figure 5-9. The following is the classification of the relative frequency of previously described septation phenotypes Class A-F as described in Bhutta *et al*. (2014) and Rezig *et al*. (2019):

- Class A - normal septum
- Class B - misaligned septum
- Class C - multiple septa
- Class D - delayed separation after septation
- Class E - absent of septa

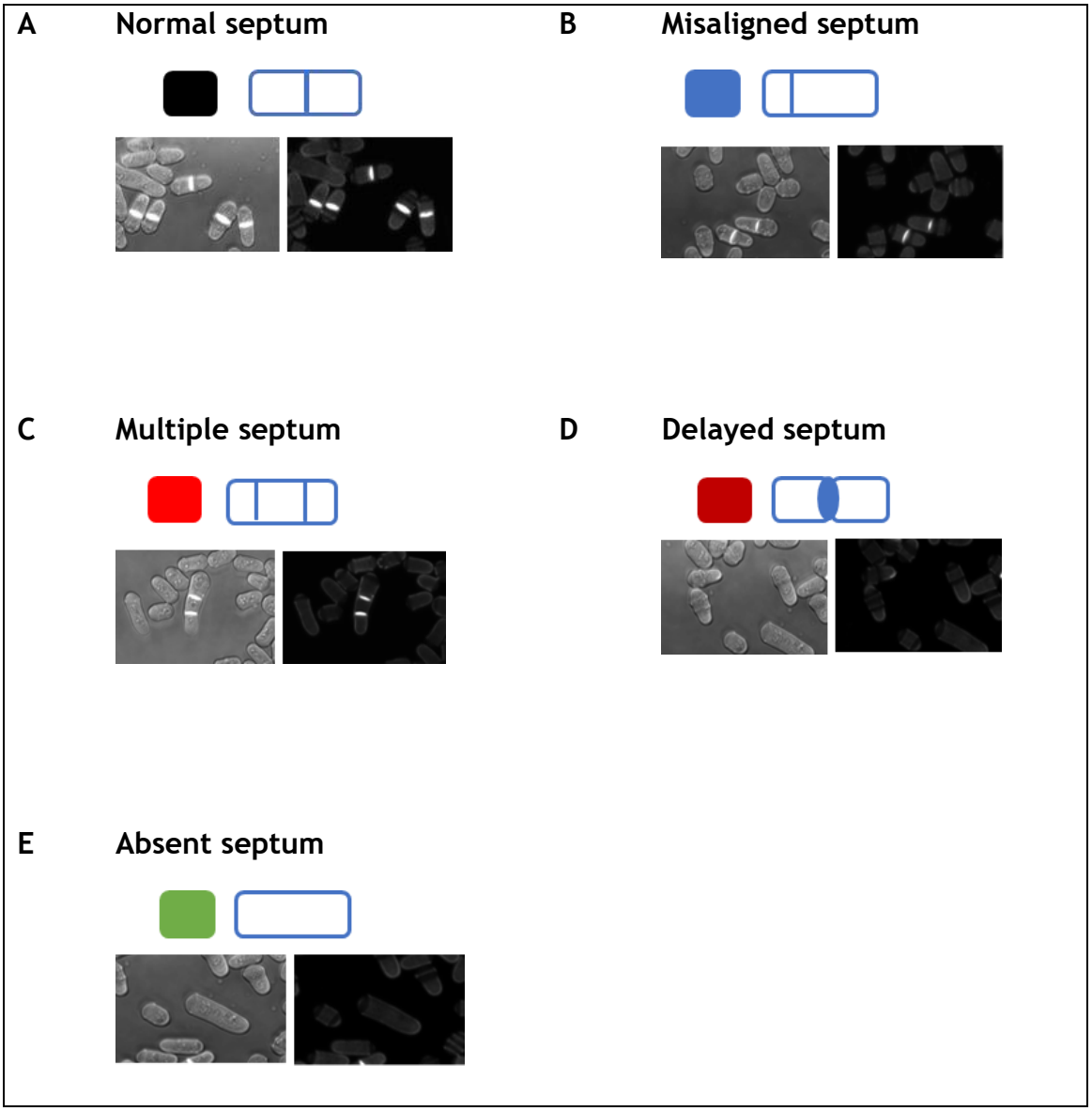

Figure 5-6 Defective septation in fission yeast strains containing *mid1* phospho-mutants. Wild-type Mid1p and *mid1* phospho-mutant strains were grown at 28ºC in a liquid medium harvested. Cells were stained with calcofluor white and visualized using LSM 880 confocal microscope. Both fluorescence and bright field images are shown. Panels A-E show representative cells illustrating observed septation phenotypes. Schematic diagrams above panels represent each phenotype: (A) a normal septum, (B) a misaligned septum, (C) multiple septa, (D) delayed separation of daughter cells following septation, and (E) absence of septa.

The results presented in (Figure 5-7) showed that wild-type cells predominantly revealed the Class A phenotype with ~ 80% of cells having normal septum separation, followed by Class E phenotype with ~20% of cells having the absence of septa. No other classes of septation phenotype that was observed in wild-type cells. However, *mid1Δ* cells revealed an increase in the proportion of cells with Class E phenotypes with ~ 50% of cells having the absence of septa, the percentage of cells not dividing, and a significant decrease in the proportion of cells with Class A phenotypes with ~ 39% of cells having normal septum. Similarly, ~7% of cells revealed Class B phenotypes misaligned with d septum ~1% of cells revealed Class C phenotypes which is multiple septa, and ~ 5% of cells showed Class D phenotype which is delayed separation after septation.

A similar result was observed with *mid1* phospho-mutant S332A and S167-531A where the percentage number of cells having normal septum Class A decreases significantly when compared with the wild-type, while the percentage number of cells having Class E phenotypes which are delayed separation after septation increases significantly. For S332A (Figure 5-8) we observed an increase in the proportion of cells with class E phenotypes absence of septa with ~ 51% of cells of the cells not dividing and a significant decrease in the proportion of cells with class A phenotypes with ~27% of cells having normal cell division. About ~ 6.8% of cells of the cells are having Class B phenotypes with a misaligned septum ~2% of cells showed Class C phenotypes which multiple septa and ~12% of cells showed Class D phenotypes with delayed separation after septation.

S167-531A (Figure 5-9) revealed a significant increase in the proportion of cells with class E phenotypes, with approximately ~ 52% of cells having an absence of septa while a significant decrease was observed with Class A phenotypes with 26% of cells having normal septum. About ~ 5% of cells were observed with Class B phenotypes with a misaligned septum, ~ 2% of cells showed Class C phenotypes which multiple septa and ~14% of cells showed Class D phenotypes that delayed separation after septation.

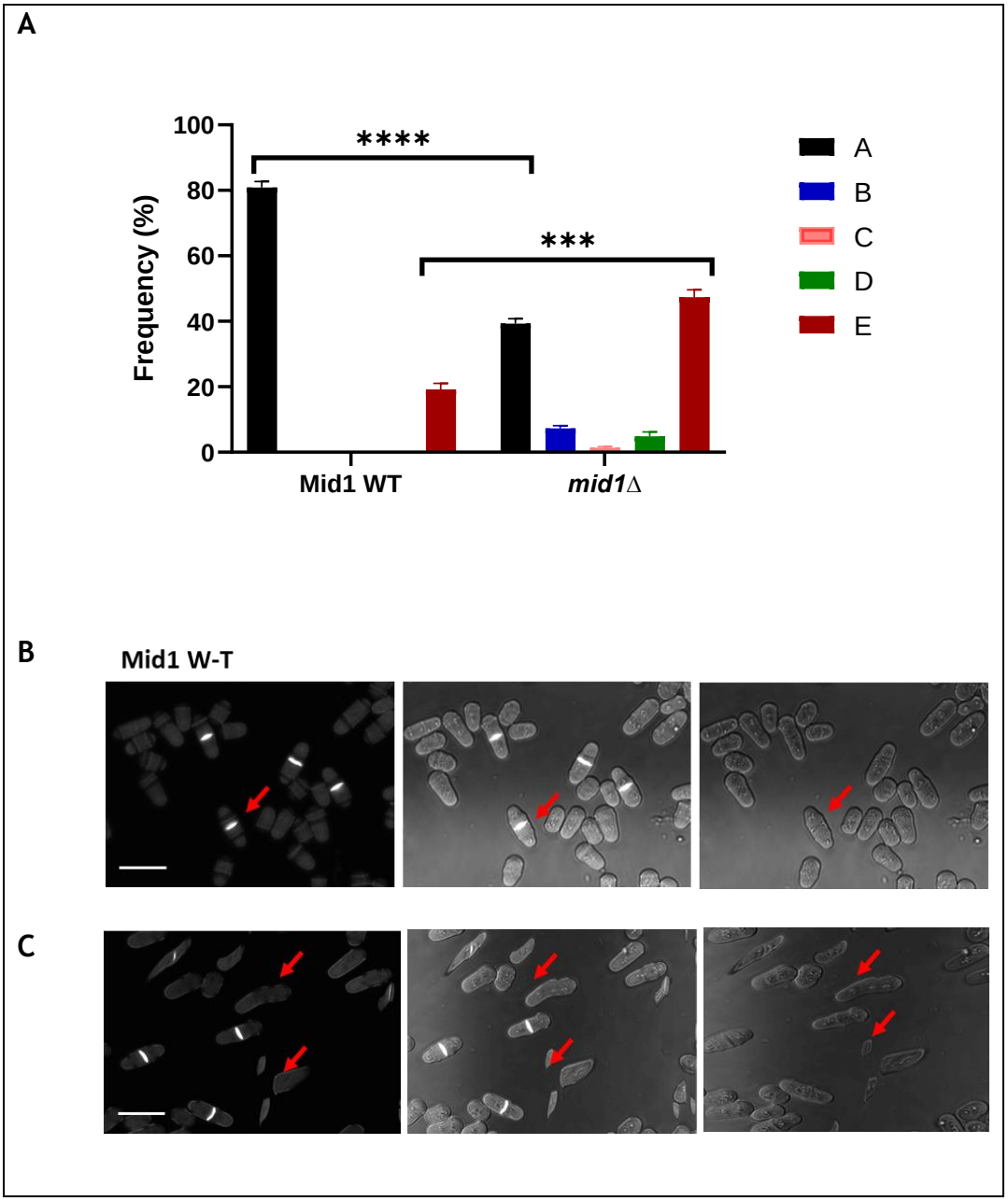

Figure 5-7 Classification and quantification of synthetic septation defects in Mid1p wild-type and *mid1*Δ cells. Division septa were visualized using calcofluor-white, examined by the fluorescence confocal microscope, and each phenotype's frequency was recorded. 400 cells in total were counted over three technical replicates, performed on three independent biology replication occasions for each genotype. Wild-type (GG1276) and *mid1*Δ (GG 1129) strains were cultured in liquid YE media at 28ºC for 18 hours. (A) is a 2-way ANOVA statistical analysis for the quantification of frequencies of the localization phenotypes in Mid1p W-T and *mid1*Δ cells, the frequencies were compared. Asterisks (****) denote a p-value <0.0001, (***) denote a p-value =0.0008, and Error bars represent SEM. representative images of calcofluor-white stained cells. The scale bar represents 30 µm. (B and C) Characterized representative images of septation phenotypes.

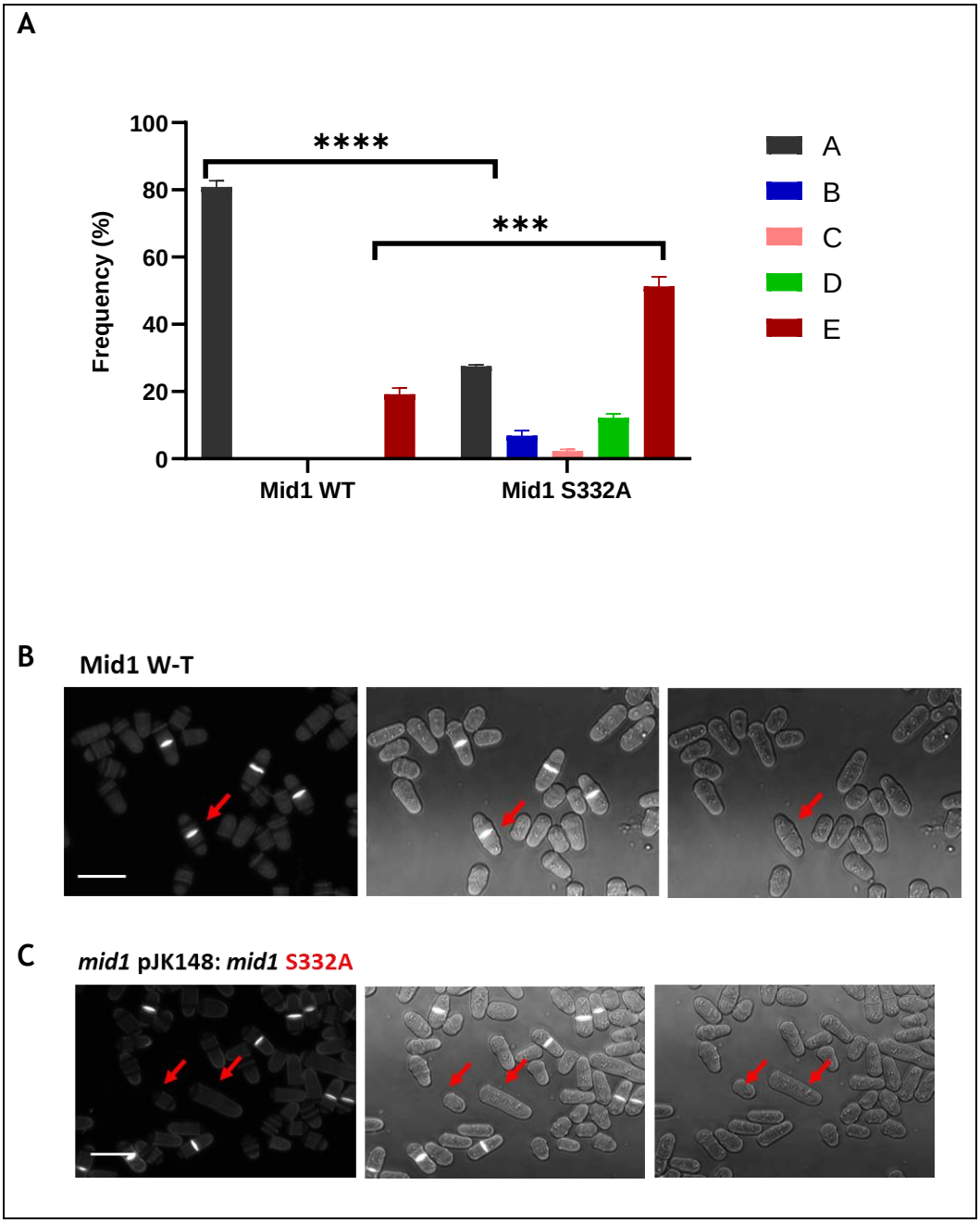

Figure 5-8 Classification and quantification of synthetic septation defects in Mid1p wild-type and *mid1* phospho-mutant S332A cells. Division septa were visualized using calcofluor-white, examined by the fluorescence confocal microscope, and each phenotype's frequency was recorded. 400 cells in total were counted over three technical replicates, performed on three independent occasions for each genotype. Wild-type (GG1276) and *mid1* phospho-mutant S332A (GG 3291) strains were cultured in liquid YE media at 28ºC for 18 hours. (A) 2-way ANOVA statistical analysis for the quantification of frequencies of the localization phenotypes in Mid1p W-T and *mid1* S332A cells, the frequencies were compared. Asterisks (****) denote a p-value <0.0001, (***) denote a p-value =0.0007, and Error bars represent SEM. representative images of calcofluor-white stained cells. The scale bar represents 30 µm. (B and C) Characterized representative images of septation phenotypes.

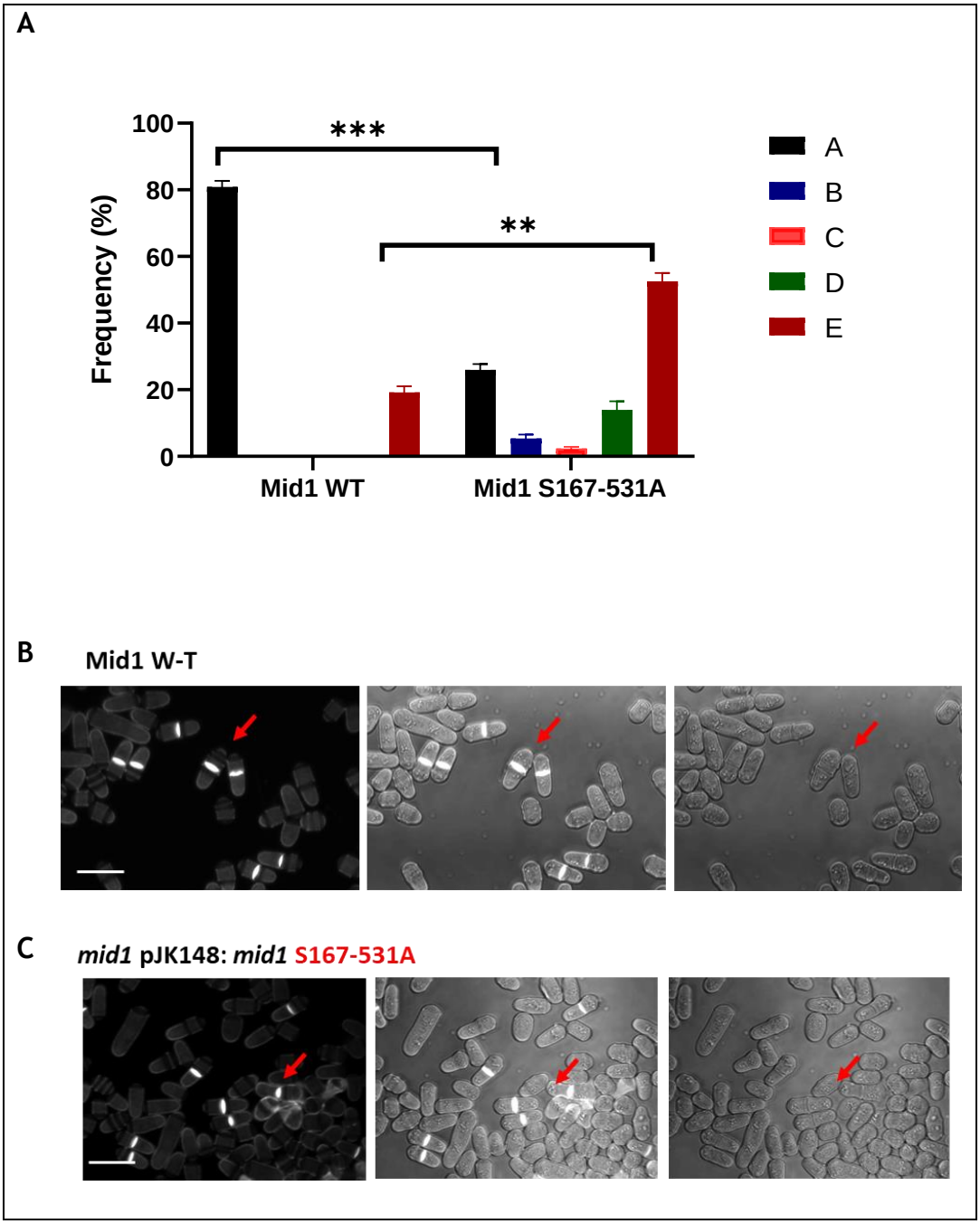

Figure 5-9 Classification and quantification of synthetic septation defects in Mid1p wild-type and *mid1* phospho-mutant S167-531A cells. Division septa were visualized using calcofluor-white, examined by the fluorescence confocal microscope, and each phenotype's frequency was recorded. 400 cells in total were counted over three technical replicates, performed on three independent occasions for each genotype. Wild-type (GG1276) and *mid1* phospho-mutant S167-531A (GG 3307) strains were cultured in liquid YE media at 28ºC for 18 hours. (A) 2-way ANOVA statistical analysis for the quantification of frequencies of the localization phenotypes in Mid1p W-T and *mid1* phospho-mutant S167A- S531A cells, the frequencies were compared. Asterisks (***) denote a p-value <0.0001, (**) denote a p-value =0.0005, and Error bars represent SEM. representative images of calcofluor-white stained cells. The scale bar represents 30 µm. (B and C) Characterized representative images of septation phenotypes.

To identify the importance of Mid1p septation in cell division, calcofluor-white staining was utilized to investigate the function and frequency of septation in *mid1* phospho-mutant synthetic strains. Septation studies were conducted by imaging *S. pombe* cells with a calcofluor-white stain and confocal microscope. *S. pombe* cells were cultured for 18 hours in 50 ml of liquid YE medium at 28^{0}C shaking. Using the bright field and DAPI filters of an LSM 880 confocal microscope equipped with a Zeiss 63X Plan -APOCHROMAT oil-immersion objective lens, cell septa were visualized. Using ZEN 3.4, cell images were collected and processed (blue edition). Utilizing a Graph pad prism, the cells were statistically quantified. Three independent experiments involving the counting of 400 cells resulted in numerical analysis.

We focused on the role of *mid1* phospho-mutant septation frequencies distribution and characterized as shown in (Figure 5-7, Figure 5-8, and Figure 5-9). The frequencies of the various septation distribution classes (Class A-normal septum, Class B-misaligned septum, Class C-multiple septa, Class D-delayed separation after septation, and Class E-absent of septa).

Comparing most of the serine to alanine or aspartic acid *mid1* phospho-mutant cells to that of the wild-type revealed no statistically significant differences in the percentage of septation. However, the septation percentages of S332A (Figure 5-8) and S167-531A (Figure 5-9) cells were significantly different from those of wild-type cells. Comparing the septation percentage of *mid1* cells to those of S332A and S167-531A reveals notable similarities in terms of Class A and Class E septation phenotypes. In addition, the Class E (absent septa) phenotype was significantly increased in S332A and S167-531A *mid1* phospho-mutant cells when compared to the wild-type cells, and a significant decrease in Class A (normal septum) phenotype was observed in S332A, and S167-531A *mid1* phospho-mutant cells when compared the wild-type cells.

The result suggests that mutation of serine position S332A and S167-531A affects normal septation frequencies and distribution of Mid1p during cell division. Interestingly phosphorylation of Mid1p potentially promotes the function of Mid1p and we have identified S332A and S167-531A as potential sites for regulating cytokinesis in *S. pombe*, this was detected by observing a significant decrease in the frequencies of septa when septation studies were conducted. The result indicates that these amino acid residues are important for Mid1p function.

5.4 Investigating the localization of GFP-Mid1p in *S. pombe*

5.4.1 Generation of GFP-*mid1* phospho-mutants

To further investigate *mid1* phospho-mutants, we characterized the localization of previously identified *mid1* phospho-mutants of Mid1p and examined the distribution of cellular components in *mid1* phospho-mutants. We adopted the strategy of Paoletti and Chang (2000), who determined the cellular localization of Mid1p during the *S. pombe* cell cycle by constructing a strain with four copies of GFP-tagged to the chromosomal locus of the *mid1* gene using a PCR-based recombination method. They classified Mid1p localization into three distinct stages based on the timing of the cell cycle (Paoletti and Chang, 2000).

Attaching four GFP copies to Mid1p is intended to amplify the GFP signal so that Mid1p can be visualized in cells. Notably, this method did not affect the function of Mid1p, as cells containing Mid1p coupled to multiple copies of GFP displayed a growth phenotype similar to that of wild-type cells and retained their rod shape. To replicate Paoletti and Chang's approach, we designed wild-type Mid1p, Mid1p phospho-resistant, and Mid1p phospho-mimetic mutants combined with four copies of GFP. In this section, we selected some *mid1* phospho-mutant strains, this selection based on our previous results that show striking genetic interaction between the *mid1* phospho-mutant and other cytokinesis-associated proteins such as *vps4Δ*, *plo1-ts35*, and *ark1-ts* as shown in Chapter 3. Serine to alanine S328A, S332A, S531A, 523-531A, and S167-531A and serine to aspartic acid S328D, S332D, S531D, 523-531D, and S167-531D were used for the GFP-localization investigation.

Therefore, we examined the effects of GFP-*mid1* phospho-mutants on the growth defects and morphology of *S. pombe* cells to determine their significance. *mid1* genes with phospho-site mutations were generated and integrated into the chromosomal DNA of *S. pombe mid1Δ* cells in a single copy again using pJK148. The plasmid was first linearized, then transformed into an *S. pombe* strain with a point mutation in the *leu*$^{+}$ gene and finally, prototrophy selection was carried out (Siam *et al.*, 2004). To generate a panel of mutant *S. pombe* strains, each variant of the *mid1* gene had either photo-mimetic or

phospho-resistant residues S328, S332, S531, S523-531, and S167-531. The mutations were introduced both singly and in multiple. As a positive control, we integrated the wild-type *mid1* gene into *mid1Δ* cells to generate Mid1p-4GFP pJK148.

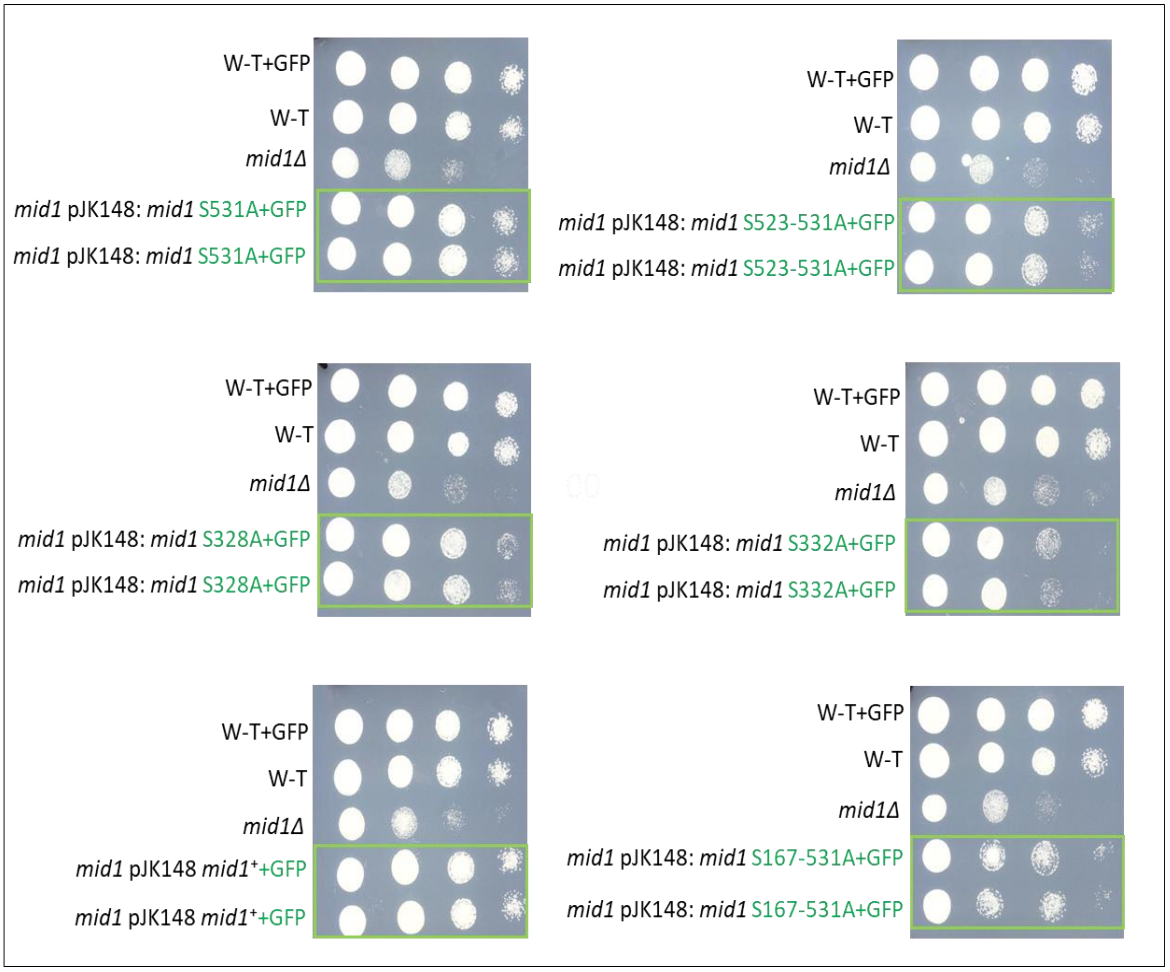

Figure 5-10 GFP-*mid1* phospho-resistant mutant cells (S>A) reveal growth defects: Analysis of the viable growth defects phenotypes of GFP-wild-type (W-T) GFP-*mid1*ΔpJK148: *mid1*$^{+}$ (GG 1347), *mid1*Δ (GG 1129), GFP-*mid1*ΔpJK148: *mid1*S328A (GG 3536), GFP-*mid1*ΔpJK148: *mid1*S332A (GG 3546), GFP-*mid1*ΔpJK148: *mid1*S531A (GG 3556), *mid1*ΔpJK148: GFP-*mid1*S523-531A (GG 3514), and GFP-*mid1*ΔpJK148: *mid1*S167-531A (GG 3530). Strains grown at 28ºC on solid YE medium and suspended at a concentration of 1.5x10^{6} cells/ml, cells were subjected to a 10-fold serial dilution. Pipetted cells were placed on solid YE media and incubated. After two days of cell growth on a solid YE medium, the *mid1* phospho-mutants were examined and interpreted.

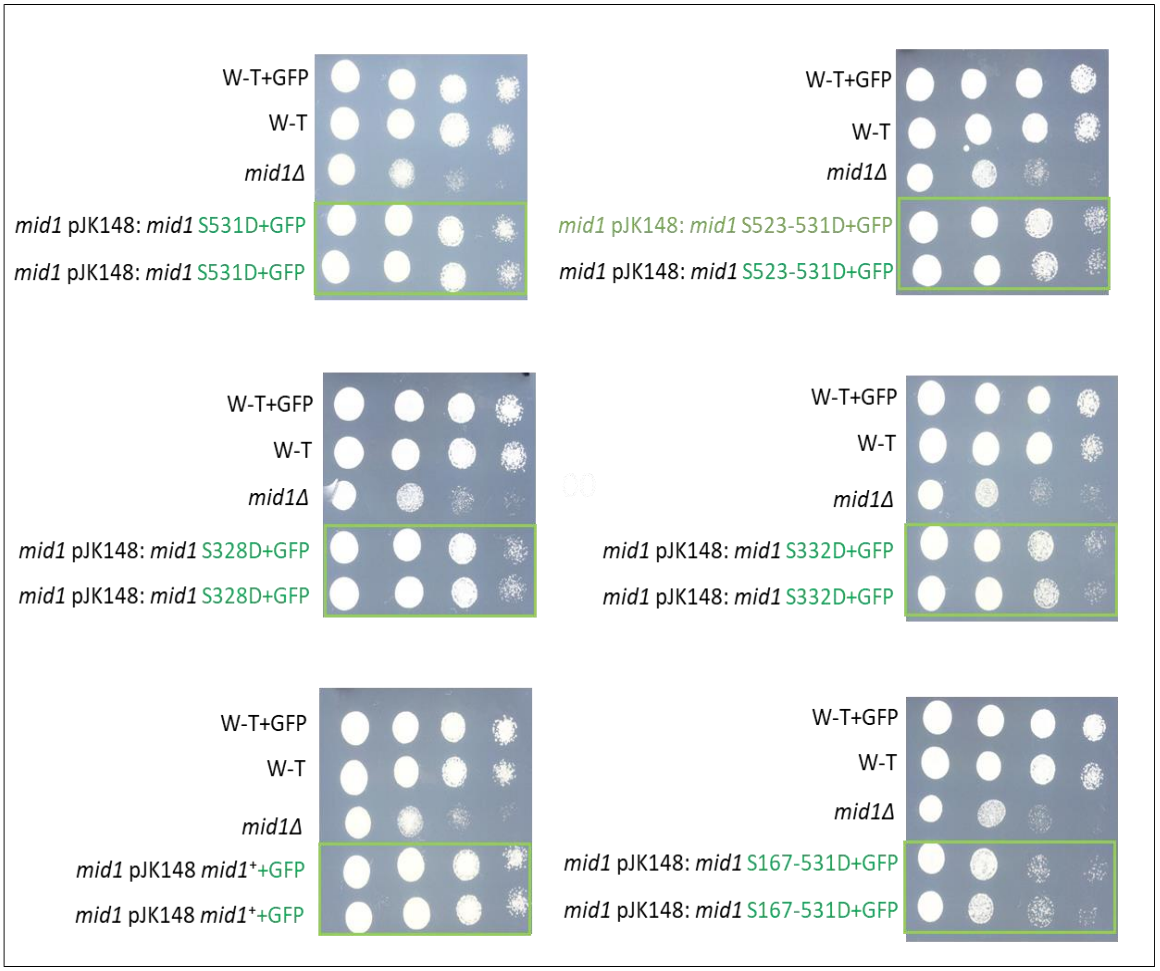

Figure 5-11 GFP-*mid1* phospho-mimetic mutant cells (S>D) reveal growth defects: Analysis of the viable growth defects phenotypes of GFP-wild-type (W-T) GFP-*mid1*ΔpJK148: *mid1*$^{+}$ (GG 1347), *mid1*Δ (GG 1129), GFP-*mid1*ΔpJK148: *mid1*S328D (GG 3541), GFP-*mid1*ΔpJK148: *mid1*S332D (GG 3562), GFP-*mid1*ΔpJK148: *mid1*S531D (3524), *mid1*ΔpJK148: GFP-*mid1*S523-531D (GG 3520), and GFP-*mid1*ΔpJK148: *mid1*S167-531D (GG 3552). Strains grown at 28ºC on solid YE medium and suspended at a concentration of 1.5x10^{6} cells/ml, cells were subjected to a 10-fold serial dilution. Pipetted cells were placed on solid YE media and incubated. After two days of cell growth on a solid YE medium, the *mid1* phospho-mutants were examined and interpreted.

In the preliminary experiments, the viable growth defect phenotypes of GFP-Mid1p phospho-resistant and phospho-mimetic mutations were investigated. In each instance where strains were grown on a solid YE medium, colonies were observed, and in the majority of serine-to-alanine or serine-to-aspartic acid mutant strains, cell growth appeared comparable to wild-type (Figure 5-10 and Figure 5-11). However, GFP-S332A, GFP-S167-531A (Figure 5-10) and GFP-S167-531D (Figure 5-11) cells grew slower than Mid1p cells, which was an intriguing finding. Compared to the wild-type cells, the GFP-S332A and GFP-S167-531A cells displayed a significant decrease. In contrast to the wild-type, GFP-S332D exhibited a normal and stable growth phenotype and exhibited no significant growth defects. This information indicates that GFP-S328A, GFP-S531A, and GFP-S523-531A (Figure 5-10) as well as GFP-S328D, GFP-S332D, GFP-S531D, and GFP-S523-531D (Figure 5-11), grew comparably to the wild-type, further suggesting that mutating these amino acids don't have an impact on growth rate of Mid1p during the process of division in *S. pombe*.

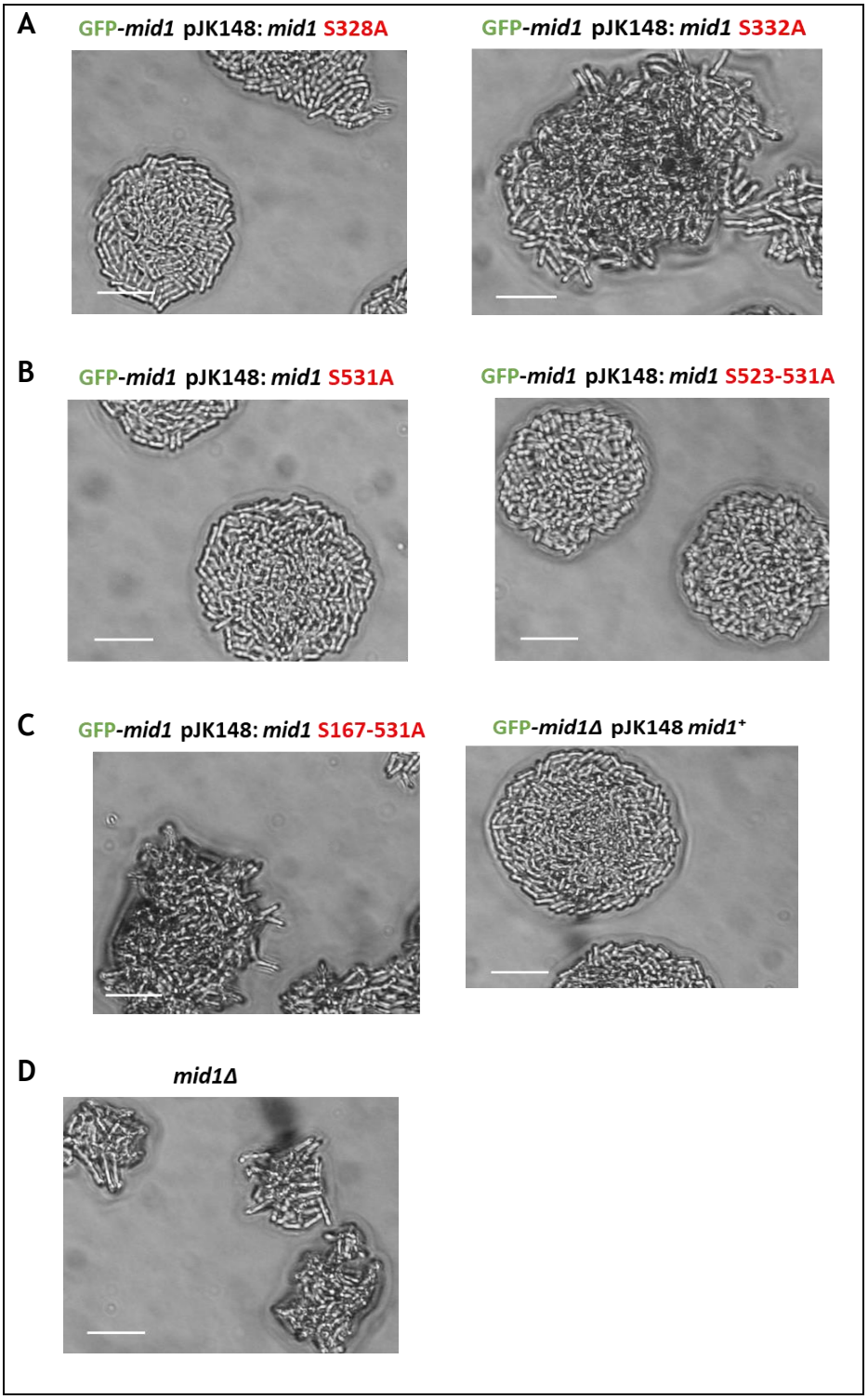

Figure 5-12 GFP-*mid1* phospho-resistant mutants reveal the morphological defect. Analysis of the morphological defect of GFP-wild-type (W-T) GFP-*mid1*ΔpJK148: *mid1*$^{+}$ (GG 1347), *mid1*Δ (GG 1129), GFP-*mid1*ΔpJK148: *mid1*S328A (GG 3536), GFP-*mid1*ΔpJK148: *mid1*S332A (GG 3546), GFP-*mid1*ΔpJK148: *mid1*S531A (GG 3556), *mid1*ΔpJK148: GFP-*mid1*S523-531A (GG 3514), and GFP-*mid1*ΔpJK148: *mid1*S167-531A (GG 3530). Strains grown at 28ºC on solid YE medium and suspended at a concentration of 1.5x10^{6} cells/ml, cells were subjected to a 10-fold serial dilution. Pipetted cells were placed on solid YE media and incubated. After two days of cell growth on a solid YE medium, the *mid1* phospho-mutants were examined and interpreted. The scale bar represents 50 µm.

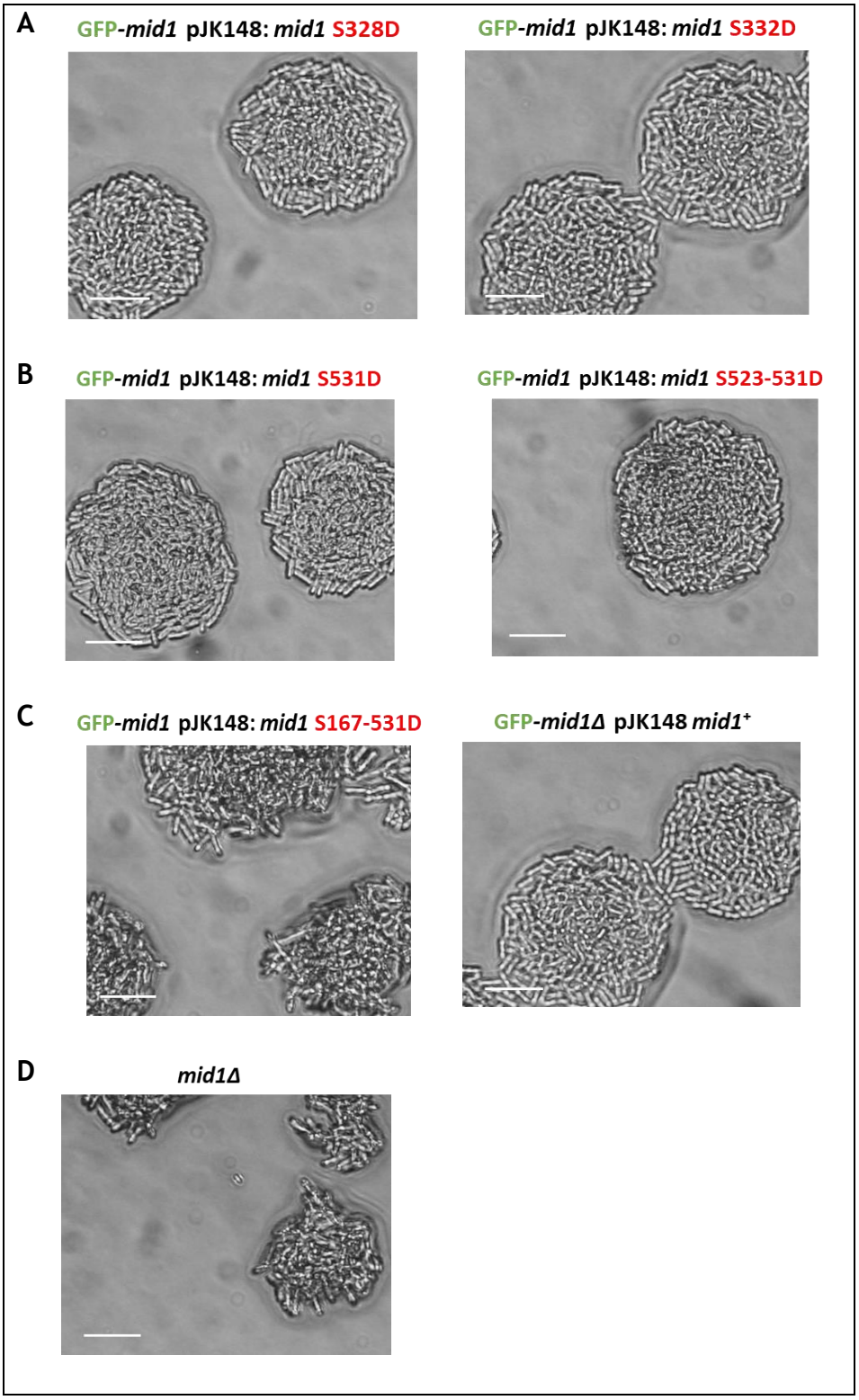

Figure 5-13 GFP-*mid1* phospho-mimetic mutants reveal the morphological defect. Analysis of the morphological defect of GFP-wild-type (W-T) GFP-*mid1*ΔpJK148: *mid1*$^{+}$ (GG 1347), *mid1*Δ (GG 1129), GFP-*mid1*ΔpJK148: *mid1*S328D (GG 3541), GFP-*mid1*ΔpJK148: *mid1*S332D (GG 3562), GFP-*mid1*ΔpJK148: *mid1*S531D (3524), *mid1*ΔpJK148: GFP-*mid1*S523-531D (GG 3520), and GFP-*mid1*ΔpJK148: *mid1*S167-531D (GG 3552). Strains grown at 28ºC on solid YE medium and suspended at a concentration of 1.5x10^{6} cells/ml, cells were subjected to a 10-fold serial dilution. Pipetted cells were placed on solid YE media and incubated. After two days of cell growth on a solid YE medium, the *mid1* phospho-mutants were examined and interpreted. The scale bar represents 50 µm.

All GFP-*mid1* phospho-mutants were observed microscopically and we investigated the phenotype of synthetic colony defects caused by *mid1* phospho-resistant (S>A) and phospho-mimetic (S>D) mutations. In each instance where strains were grown on a solid YE medium, colonies were observed. In most of the serine to alanine and serine to aspartic acid mutated strains, rod-shaped cells with colonies resembling wild-type were observed. However, it was observed that GFP-*mid1* S332A, GFP-*mid1* S167-531A (Figure 5-12), and GFP-*mid* S167-531D (Figure) cells had slow, defective colonies and similar morphology to *mid1Δ* cells. Compared to wild-type cells, the GFP-*mid1* S332A and GFP-*mid1* S167-531A mutants exhibited significant defects with disoriented colonies. Whereas GFP-*mid1* S332D exhibited no significant difference in terms of colonies and morphological defect, the cells showed normal rod-shaped sizes and an organized colony phenotype significantly similar to that of the wild-type, it did not exhibit any significant differences in terms of colony size or morphological defect. This information demonstrates that GFP-S328A, GFP-S531A, and GFP-S523-531A (Figure 5-12) and GFP-S328D, GFP-S332D, GFP-S531D, and GFP-S523-531D (Figure) have normal rod-shaped sizes and an organized colony phenotype comparable to the wild-type, suggesting that these sites are not directly involve in growth and colony formation during division in *S. pombe*.

5.4.2 Localization of GFP-Mid1p during cytokinesis

After the characterization of the growth and colony defect of the GFP-*mid1* phospho-resistant and phospho-mimetic strains. In this section, GFP-*mid1* phospho-mutant localization distribution in cells was characterized to examine how phosphorylation may influence *S. pombe* during cytokinesis, and the frequency of localization patterns in each GFP-*mid1* phospho-mutants was quantified. *S. pombe* strains grown in liquid YE media at 28^{0}C were visualized using an LSM 880 confocal microscope. The localization phenotypes of GFP-Mid1p in wild-type and GFP-*mid1* phospho-mutant cells were characterized, and statist]ically quantified the localization frequency of the different phenotypes for each strain was determined. The phenotype frequencies of GFP-Mid1p wild-type and GFP-*mid1* phospho-mutant strains were compared in Figure 5-15, Figure 5-16 and Figure 5-17. The classification of localization phenotypes and the comparative frequency distribution pattern was determined as previously described by (Paoletti and Chang 2000; Rezig *et al.*, 2021):

- Class A - cytoplasm
- Class B - broad band
- Class C - tight band
- Class D - binucleated
- Class E - nuclear
- Class F - nuclear ring

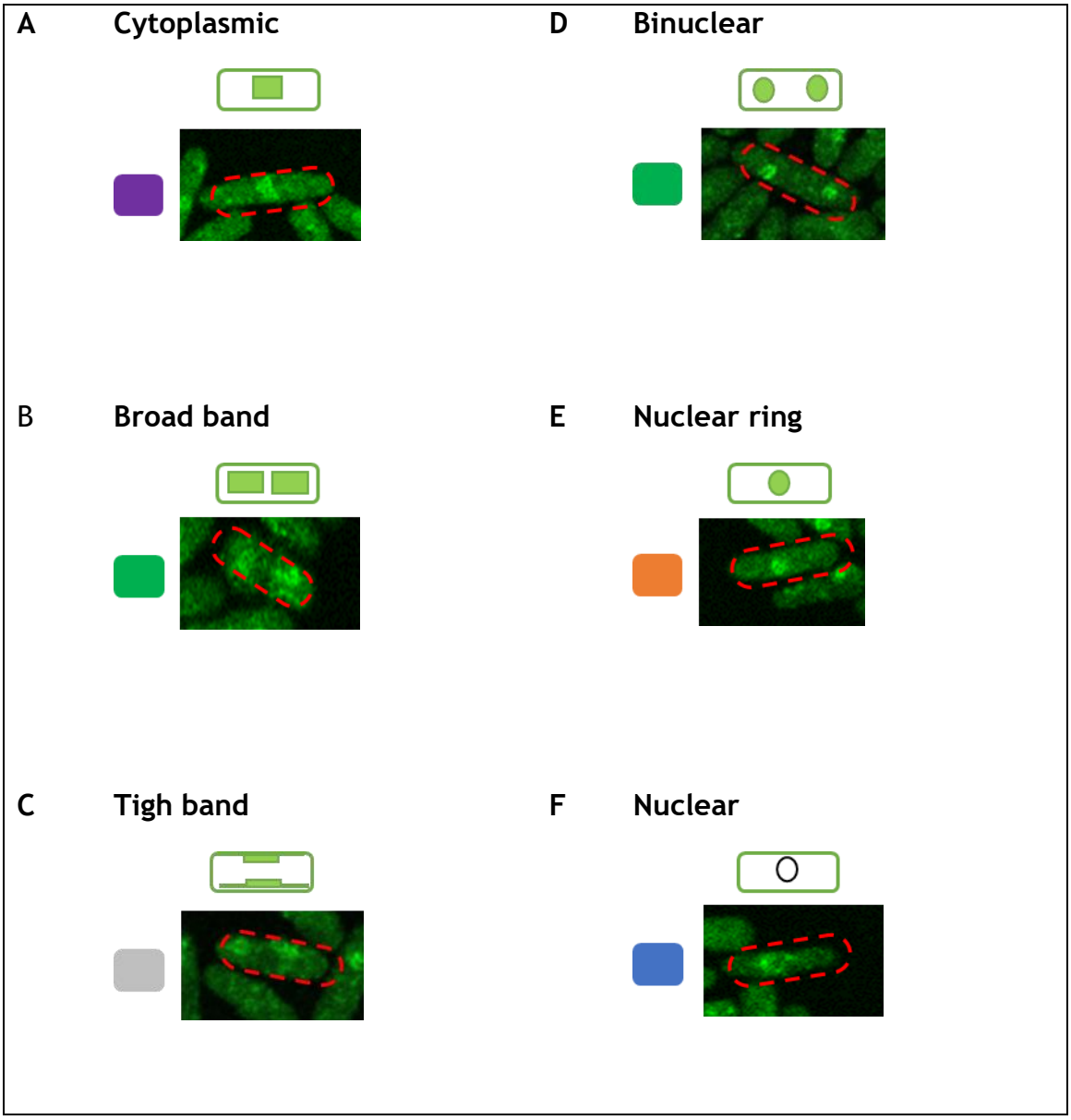

Figure 5-14 Classification of GFP-Mid1p localization phenotypes in *mid1* phospho-mutants. Localization patterns were visualized and examined by the fluorescence confocal microscope, and each phenotype's frequency was recorded. 200 cells in total were counted over three technical replicates, performed on three independent occasions biological replicates for each genotype. Wild-type and phospho-mutant strains were cultured in liquid YE media at 28ºC for 18 hours and visualized using LSM 880 confocal microscope. Panel A-F show representative cells illustrating observed localization pattern of *mid1* phospho-mutant. Schematic diagram above panels represents each phenotype: (A) cytoplasmic, (B) broad band, (C) tight band, (D) binucleated, (E) nuclear, and (F) Nuclear ring.

The distribution of cells between GFP-Mid1p in wild-type and S332A GFP-*mid1* phospho-mutant cells is shown in Figure 5-15, and the localization patterns of GFP-Mid1p in wild-type cells revealed significant variations in the sample population when compared. Class A phenotype showed ~25% of cells GFP-Mid1p wild-type cytoplasmic localization pattern while ~40 % of cells were observed in GFP-*mid1* phospho-mutant cytoplasmic localization pattern. Similarly, Class B phenotype revealed ~18% of cells GFP-Mid1p wild-type broad band localization pattern but ~ 12% of cells of GFP-*mid1* phospho-mutant was observed in broadband localization pattern. The Class C phenotype revealed that ~8% of cells of GFP-Mid1p wild-type has a tight band localization pattern whereas ~0.2% of cells showed GFP-*mid1* phospho-mutant tight band localization pattern, Class D phenotype showed ~ 20% of cells of GFP-Mid1p wild-type two nucleus localization pattern while ~0.4% of cells showed GFP-*mid1* phospho-mutant two nucleus localization pattern, Class E phenotype showed ~22% of cells of GFP-Mid1p wild-type with a single nucleus localization pattern while ~0.63% of cells showed GPF-*mid1* phospho-mutant with a single nucleus localization pattern and Class F phenotype showed ~12% of cells of GFP-Mid1p wild-type with nuclear ring localization pattern, and ~2% of cells of GFP-*mid1* phospho-mutant was observed with nuclear ring localization pattern.

The distribution of cells between GFP-Mid1p in wild-type *mid1* and S167-531A GFP-*mid1* phospho-mutant cells is shown in Figure 5-16. When compared, the localization patterns of GFP-Mid1p wild-type cells revealed significant differences in the sample population. Similarly, Class A phenotype revealed ~23% of cells GFP-Mid1p wild-type cytoplasmic localization pattern while ~ 31 % of cells were observed in GFP-*mid1* phospho-mutant cytoplasmic localization pattern. Whereas Class D phenotype displayed ~21% of cells of GFP-Mid1p wild-type two nucleus localization pattern but ~ 8% of cells showed GFP-mid1 phospho-mutant two nucleus localization pattern, and Class E phenotype displayed ~22% of cells of GFP-Mid1p wild-type with a single nucleus localization pattern and ~ 9% of cells displayed GPF-*mid1* phospho-mutant with a single nucleus localization pattern.

The cells population sample shown in (Figure 5-11) represented localization frequencies and distribution of cells between GFP-Mid1p wild-type and S523-531A GFP-*mid1* phospho-mutant; the localization patterns of GFP-Mid1p wild-type cells revealed significant variations in the sample population when compared. Similarly, Class C phenotype displayed ~ 7% of cells of GFP-Mid1p wild-type with tight band localization pattern, while ~ 0.15% of cells showed GFP-*mid1* phospho-mutant tight band localization pattern. The Class D phenotype showed ~21% of cells of GFP-Mid1p wild-type two nucleus localization pattern while ~ 1% of cells showed GFP-*mid1* phospho-mutant two nucleus localization pattern, whereas the Class E phenotype showed ~ 22% of cells of GFP-Mid1p wild-type with a single nucleus localization pattern and ~ 2% of cells showed GPF-*mid1* phospho-mutant with a single nucleus localization pattern.

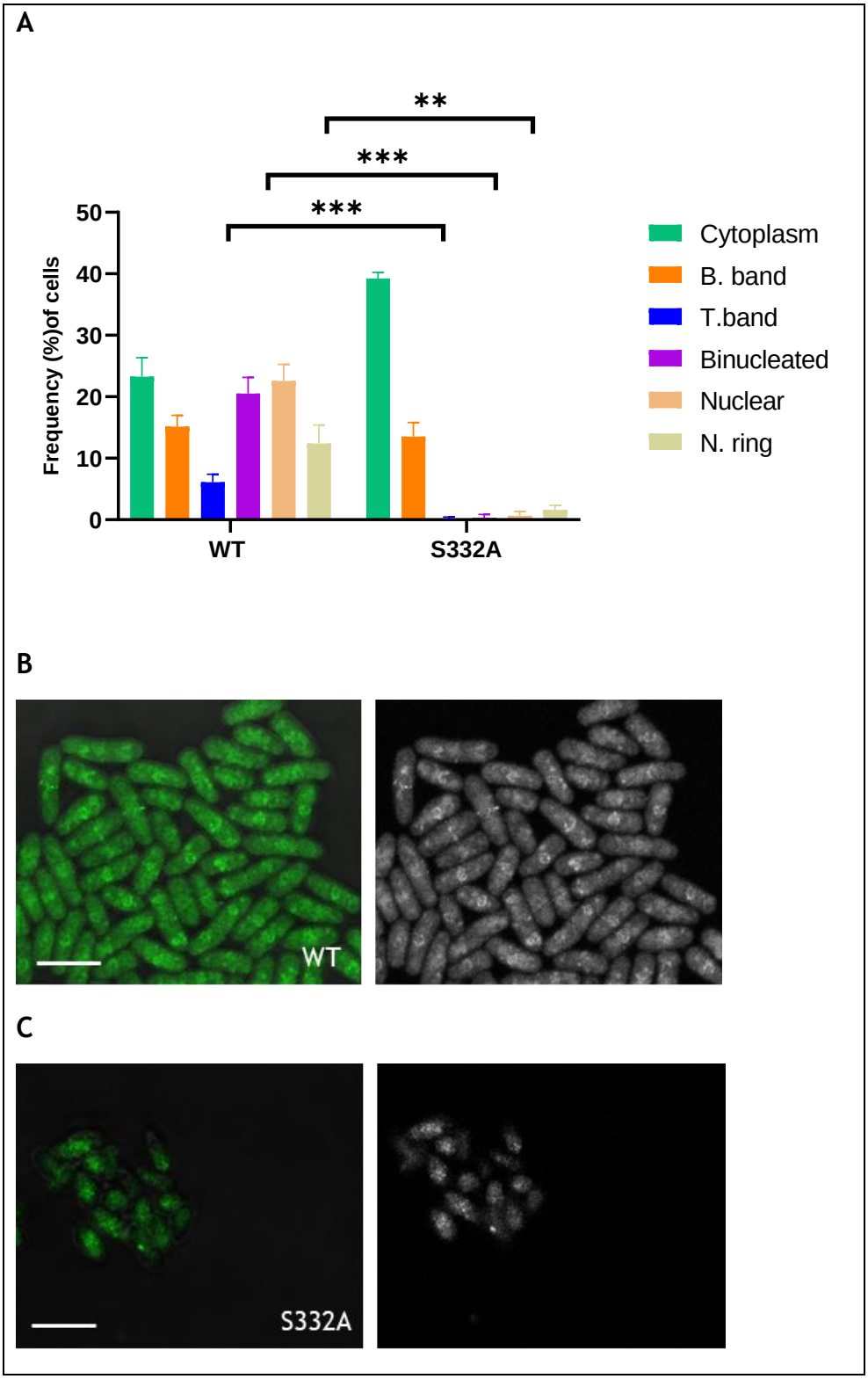

Figure 5-15 Classification and quantification of GFP-Mid1p localization phenotypes in wild-type and *mid1* phospho-mutant S332A cells. Localization patterns were visualized and examined by the fluorescence confocal microscope, and each phenotype's frequency was recorded. 200 cells in total were counted over three technical replicates, performed on three independent occasions for each genotype (biological replicates). Wild-type and phosphor-mutant strains were cultured in liquid YE media at 28ºC for 18 hours. (A) 2-way ANOVA statistical analysis for the quantification of frequencies of the localization phenotypes in Mid1p W-T and *mid1* phospho-mutant cells, the frequencies were compared. Asterisks (***) denote a p-value =0.0003, (***) denote a p-value =0.0007, (**) denote a p-value =0.0065 and Error bars represent SEM. representative images of Calcofluor-White stained cells. The scale bar represents 10 µm. (B and C) Characterized representative images of GFP-Mid1p localization phenotypes.

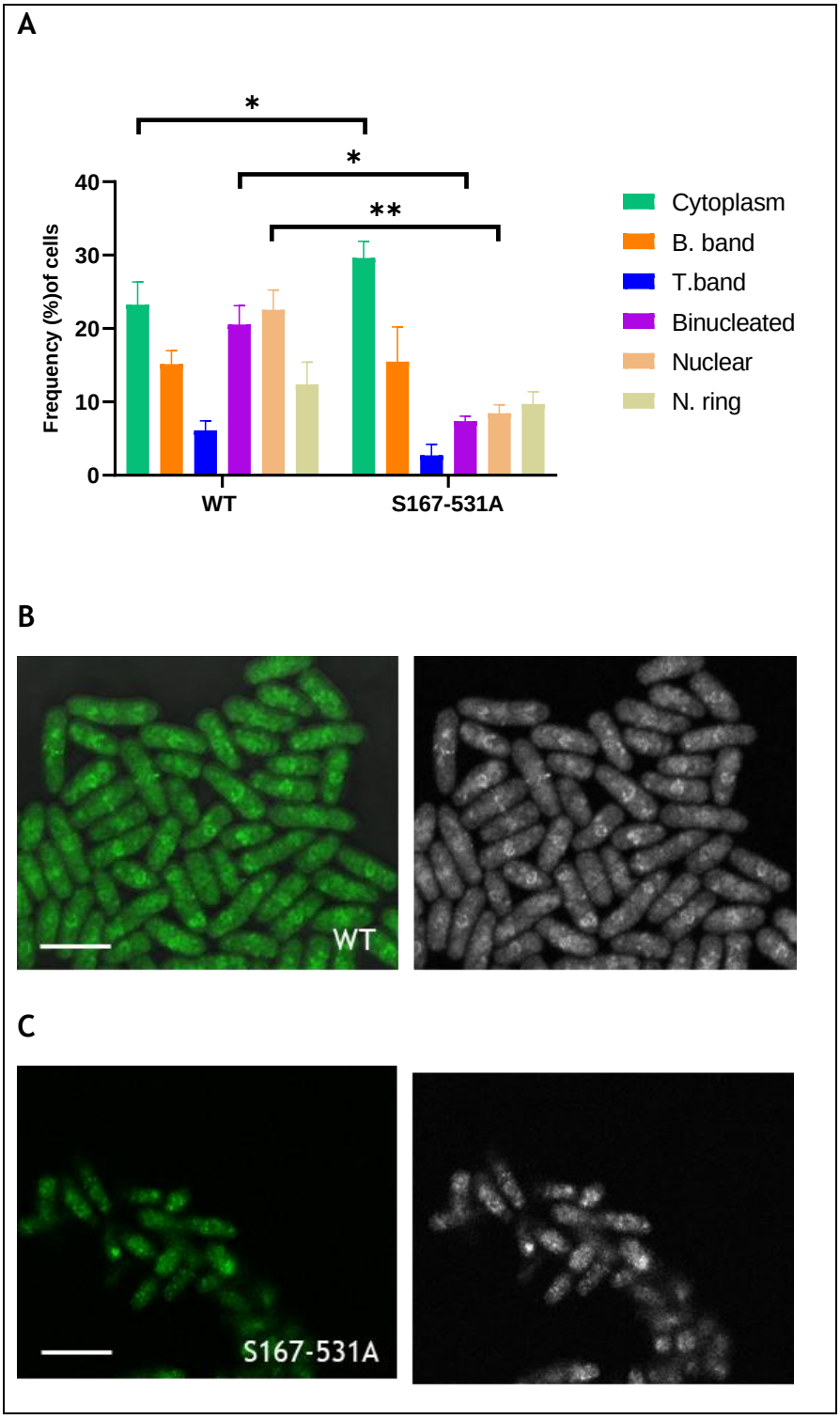

Figure 5-16 Classification and quantification of GFP-Mid1p localization phenotypes in wild-type and *mid1* phospho-mutant cells. Localization patterns were visualized and examined by the fluorescence confocal microscope, and each phenotype's frequency was recorded. 200 cells in total were counted over three technical replicates, performed on three independent occasions for each genotype (biological replicates). Wild-type and phospho-mutant strains were cultured in liquid YE media at 28ºC for 18 hours. (A) 2-way ANOVA statistical analysis for the quantification of frequencies of the localization phenotypes in Mid1p W-T and *mid1* phospho-mutant cells, the frequencies were compared. Asterisks (**) denote a p-value =0.0045, (**) denote a p-value =0.0207, (*) denote a p-value =0.0221 and Error bars represent SEM. representative images of Calcofluor-White stained cells. The scale bar represents 10 µm. (B and C) Characterized representative images of GFP-Mid1p localization phenotypes.

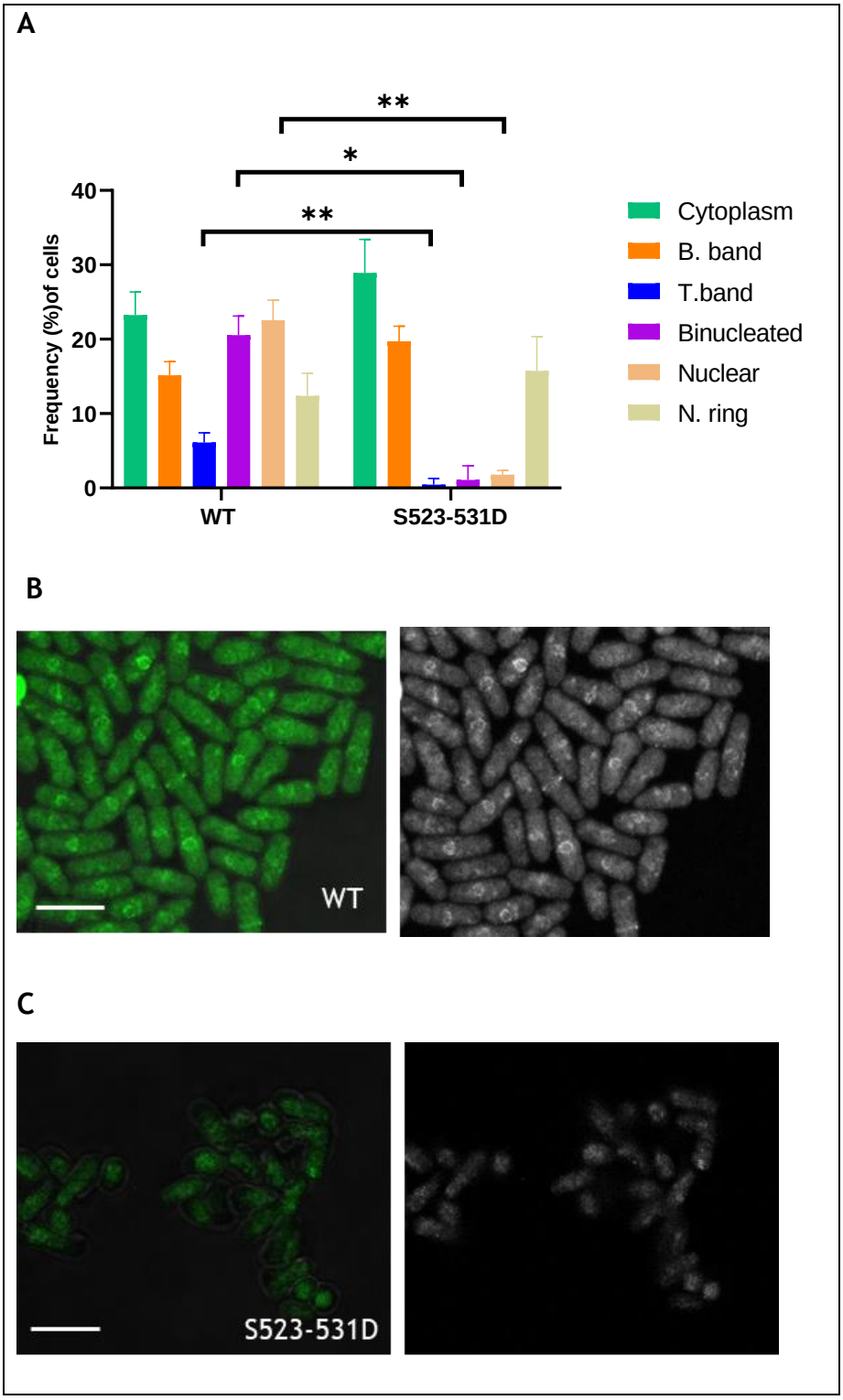

Figure 5-17 Classification and quantification of GFP-Mid1p localization phenotypes in wild-type and *mid1* phospho-mutant cells. Localization patterns were visualized and examined by the fluorescence confocal microscope, and each phenotype's frequency was recorded. 200 cells in total were counted over three technical replicates, performed on three independent occasions for each genotype (biological replicates). Wild-type and phosphor-mutant strains were cultured in liquid YE media at 28ºC for 18 hours. (A) 2-way ANOVA statistical analysis for the quantification of frequencies of the localization phenotypes in Mid1p W-T and *mid1* phospho-mutant cells, the frequencies were compared. Asterisks (**) denote a p-value =0.0039, (*) denote a p-value =0.0114, (**) denote a p-value =0.0099 and Error bars represent SEM. representative images of Calcofluor-White stained cells. The scale bar represents 10 µm. (B and C) Characterized representative images of GFP-Mid1p localization phenotypes.

5.5 Summary

The result presented in this Chapter 5 demonstrated that Mid1p phosphorylation is important in cell division and specifically during cytokinesis in *S. pombe*. Phosphorylation of Mid1p caused defective growth, defective morphology, a decrease in septation number, and a decrease in localization pattern in dividing *S. pombe* cells. Significant slow, defective growth was observed in serine to alanine S332A and S167-531A *mid1* phospho-resistant mutant strains when compared with the wild-type. However, there were no significant differences in serine to aspartic acid S332D and S167-531D phospho-mimetic mutant strains, as we observed no differences in terms of growth defect with normal and steady growth phenotype compared to the wild-type.

Defective cytokinesis can modify cell replication, reduce size, slow growth and lead to defective morphology. Cellular organization and orientation within a tissue/system determine how the tissue/system separates successfully or not. Disturbed cellular organization within a tissue/system prevents accurate and successful replication and transmission of genetic materials. In fission yeast, the accuracy of the location of the division site is due to the presence of two primary molecular pathways that regulate the assembly of the cytokinetic apparatus in the centre of the cell. To facilitate the appropriate segregation of the genetic material in newly formed daughter cells of the required size and shape, these pathways generate primary information related to the cell division site (Rincon and Paoletti, 2012).

Septation frequencies in Mid1p serine to alanine S332A and S167-531A phospho-resistant mutant strains revealed significant differences in percentages compared to the wild-type. Class E phenotypes (absent of septa) were increased compared to wild-type. Such an increased in frequencies of Class E phenotype could indicate delayed cytokinesis, mis-timed cytokinesis, or defective septum degradation. Previously, the septation phenotype frequency distribution of wild-type strain was described (Bhutta *et al.*, 2014: Rezig *et al.*, 2019). Wild-type cells in this study were defined as being ~80% Class A and ~20% Class F. The overrepresentation of Class F in this study may be due to various yeast strains' differing cultivating techniques. Because phenotypic classification is a subjective process, people may record either Class A or Class F differently. Importantly, in

this work, yeast strains were grown for 18 hours at 28°C with shaking in liquid YE medium before being stained with calcofluor-white. We also observe significant slow, defective growth and scattered colony morphology in serine to alanine GFP-S332A and GFP-S167-531A GFP-phospho-resistant mutant strains.

Localization frequencies of cellular components in serine to alanine GFP -S167-531A GFP-S332A GFP-phospho-resistant mutant strains and phospho-mimetic mutant GFP -S523-531D revealed significant differences in percentages compared to the wild-type. However, localization frequencies and distribution of cellular components of serine to GFP-aspartic acid mutants GFP-S332D and other mutants strains revealed no significant similarities to the wild-type.

We continued to investigate the localization and frequency distribution patterns of GFP-Mid1p in wild-type cells and *mid1* GFP-phospho-mutant strains. We observed a significant reduction in the distribution of the Class A-Cytoplasm, Class B-broad band, Class C-tight band, Class D-binucleated, Class E-single nuclear, and Class F-nuclear ring in GFP-S332A, GFP-S167-531A GFP-phospho-resistant mutant strains and GFP -S523-531D GFP-phospho-mimetic mutant strain. However, the localization and distribution frequencies of the cellular components of serine to GFP-aspartic acid mutants GFP-S332D and other mutants strains revealed no significant similarities to the wild-type.

The search for the role, relevance, and function of Mid1p phosphorylation revealed slow, defective, and morphologic growth patterns in *mid1* phospho-mutants. This is in tandem with defects in growth and morphology also observed by Magliozzi *et al*. (2020) when *pak1* was mutated leading to defective contractile actomyosin ring (CAR) assembly and genetic interactions during cytokinesis mutants noted. Defects in Mid1p signalling lead to misplaced and defective cell division, however, the mechanism driving defective synthetic phenotypes and incorrect placement of the contractile assembly is unclear. We demonstrated that Mid1p phosphorylation is important in the control of cytokinesis in *S. pombe* which is in tandem with the studies of Almonacid *et al*. (2011) and Willet *et al*. (2019).

This study also revealed that Mid1p regulation could act in conjunction with protein kinases such as Plo1p and Ark1p kinase which is consistent with the studies of Magliozzi *et al*. (2020). In addition, new morphologies were observed in GFP-*mid1* phospho-mutants localization pattern. The *mid1* phospho-mutants showing *S. pombe* elongation of the cell and not being able to divide; this could be due to inaccurate signalling from the synthetic tethering of Mid1p cortical nodes because of phosphorylation of the specific phospho-sites. However, we also speculate the reason why other *mid1* phospho-mutants were able to grow, form normal colonies, and have no defective phenotype is that the phospho-mutants were able to rescue and recruit synthetic tethering of Mid1p to cortical nodes.

5.6 Conclusions

Our search for the relevance and function of Mid1p phosphorylation revealed slow, defective, and morphologic growth patterns in *mid1* phospho-mutants. The result implies that mutation of serine position S332A and S167-531A affect common growth and division of *S. pombe* cells. Interestingly, phosphorylation of Mid1p potentially promotes the normal function of Mid1p and we have identified S332A and S167-531A as potential sites for regulating cytokinesis in *S. pombe*. This was detected by observing a significant defective growth, defective morphology, and decreased frequencies of septa compared to the Mid1p wild-type. We also identified a significant decrease in the number of cytoplasm, nuclear, nodes, and other cellular components during GFP-Mid1p localization distribution studies. The result indicates that these amino acid residues are important for Mid1p function.

Chapter 6 Discussion

6.1 Anillin/Mid1p interacts with ESCRT-associated Vps4p proteins to regulate the cell cycle in *S. pombe*

6.1.1 Background

In eukaryotes anillin/Mid1p proteins perform a conserved role in distributing components during cytokinesis, and the mechanisms of anillin/Mid1p accumulation at the membrane and ring both depend on phosphorylation (Kim *et al.*, 2017). Serine phosphorylation is one sort of post-translational modification (PTMs) that regulates the activity of proteins and is important for many cellular activities as PTMs are involved in practically all biological process (Tasmia *et al.*, 2022). Protein phosphorylation is a reversible PTM in which an amino acid residue is phosphorylated these being serine (S), tyrosine (Y), and threonine (T) in eukaryotic organisms (Vlastaridis *et al.*, 2017).

Understanding the reversible or irreversible nature of phosphorylation in fission yeast is vital to understand how Mid1p regulates cellular activity through kinases. Despite the fact that phosphorylation has been shown to impair function and cause the complex to dissociate, the balance between phosphorylation and dephosphorylation may be significant (Vlastaridis *et al.*, 2017). Anillin homologues serve similar activities in higher eukaryotic organisms, and anillin/Mid1p proteins play important roles during cytokinesis in the cell cycle. These responsibilities are centred on its structural ability to predict and regulate cell division sites in the equatorial region of the cell (Rezig *et al.*, 2022).

In this study, we primarily focussed on *mid1* phospho-mutants to understand the genetic and physical interactions between the *mid1* and ESCRT-associates *vps4* genes and proteins, and the mechanisms by which they work together and regulate one another during cytokinesis. To learn more about how ESCRT proteins are controlled in fission yeast during cytokinesis, we also investigated other proteins that interact with anillin/Mid1p. Here, we outline a physical interaction between Vps4p and the anillin Mid1p that is essential for both Mid1p's correct placement and cell viability during cell division.

6.2 Identification of genetic interaction between Mid1p and Vps4p

The findings in this thesis expand on the previously identified and recognised role of ESCRT protein in fission yeast cytokinesis. These studies also showed that polo-like kinase Plo1p, aurora kinase Ark1p, and CDC14 phosphatase Clp1p are three cell cycle regulators with which ESCRT proteins interact. These findings provide the framework for the regulation of ESCRT proteins to control cytokinesis (Bhutta *et al.*, 2014; Rezig *et al.*, 2021). We looked into the ESCRT proteins interactions with the anillin/Mid1p protein to learn more about how they might work along other cell cycle regulators to control cytokinesis. Mid1p is essential for cytokinesis because it forms equatorial nodes which results in an annular structure that dictates where the division plane is located (Rincon and Paoletti 2012; Sun *et al.*, 2015).

To begin this investigation, we looked for genetic interactions between *mid1* genes and genes that encodes ESCRTs and ESCRT-associated proteins. In order to look for synthetic phenotypes, double mutant fission yeast strains were created that had chromosomal deletion of *mid1* (*mid1Δ*) and individual chromosomal deletion of ESCRT genes from E-0 to E-II and *vps4* and search for synthetic phenotypes. Therefore, *mid1Δ* was combine with *sst4Δ* (E-0), *sst6Δ* and *vps28Δ* (E-I), *vps36Δ* and *vps25Δ* (E-II), *vps20Δ*, *vps32Δ* and *vps2Δ* (E-III), and *vps4Δ* (Iwaki *et al.*, 2007; Bhutta *et al.*, 2014). With the exception of *mid1Δ vps4Δ,* which failed to establish a viable colony and had a synthetically lethal phenotype, double mutants were created in each case that were viable. The ESCRT machinery is assembled to catalyse membrane remodelling events that lead to the final separation of the daughter cells. This process is facilitated by many cytokinesis proteins as well as ESCRT-I and III classes of proteins in addition to the ATPase Vps4p (Elia *et al.*, 2011; Goliand *et al.*, 2018).

6.2.1 Mid1p and Vps4p

To study the effect of phosphorylation of Mid1p protein by aurora and polo kinases, and phosphorylated residues identified using mass spectrophotometry (*section 3.3.2*). Striking genetic interaction between *mid1* and ESCRT-associated protein *vps4* was discovered using a yeast genetic approach. We also discovered that double mutants of *mid1* phospho-mutant *vps4Δ,* and single *mid1* phospho-mutant, results in defective growth phenotypes and impaired morphology.

Defective cytokinesis can affect how cells replicate, slow growth, can result in abnormal defective morphology. Magliozzi *et al*. (2020) also noted defects in growth and morphology when *pak1* was modified resulting in defective contractile actomyosin ring (CAR) assembly and genetic interactions during cytokinesis mutants. The removal of Mid1p from the membrane is phosphorylation-dependent because altering the levels of Mid1p at the membrane can compromised cytokinesis progression. In eukaryotes, the appropriate positioning of the division site may be dependent on the Mid1p protein at the membrane phospho-regulation (Willet *et al*., 2019). Cell division and the mislocalization of cellular components are both caused by poor or incomplete cytokinesis; however, it is unknown what causes the incorrect synthetic phenotypes and improper positioning of the contractile assembly. In the presence of change of Mid1p or the absences of Mid1p function, the *mid1* phospho-mutant displayed impaired growth and morphological abnormalities (Rezig *et al*., 2021).

A cell organization and orientation inside an organism affect how well the cell separates successfully, but an unsettling cellular structure can obstruct accurate transfer of genetic material during replication. In fission yeast, the presence of the two main molecular pathways that control the matching formation of the cytokinesis apparatus in the cell centre accounts for the accuracy of the division site localization. For the proper segregation of the genetic material in the newly created daughter cells of the required size and shape, these pathways produce crucial information relating to the cell division site (Rincon and Paoletti, 2012).

Here, we suggest that the genetic interaction between Mid1p and Vps4p potentially regulates Mid1p-dependent node recruitment, initiation, and attachment to the plasma membrane to determine the division plane in *S. pombe*. It is noteworthy to mention that the Mid1p interacts with Vps4p *in vitro* contains the PH domain, suggesting the binding of Vps4p to this region may regulate interaction with the cell cortex (Figure 6-1).

6.2.2 Mid1p and protein kinase Ark1-TS and Plo1-TS

Following the identification of the genetic interaction between *mid1* and *vps4* genes, we looked to further establish the significance of protein kinases during the process of the cell cycle in *S. pombe*. We investigated the relevance of the genetic interaction between *mid1* phospho-mutants, temperature sensitive *ark1-ts* and *plo1-ts* mutants. We crossed the strains comprising *mid1* phospho-mutant, *plo1-ts35,* and *ark1-ts11* genes and identified synthetic double mutants. Viable colonies were observed in all cases with no synthetic phenotype lethality in the mutants created (Figure 3-9 and Figure 3-10), with a summary of all the double mutants generated in this study (Table 3-1). The double mutant between *mid1* phospho-mutant, *ark1-ts* and *plo1-ts* caused defects in growth and morphology. The results revealed strong genetic interactions between *mid1* and both *plo1* and *ark1* genes suggesting that they are all implicated in regulating cell cycle events in *S. pombe*.

The results suggest that the Mid1p-dependent node localization pathway, which is regulated by Aurora and Plo1 kinases is crucial for controlling cellular function. Therefore, we hypothesise that the function and interaction to control cell cycle events depend on the phosphorylation of Mid1p by Aurora and Plo1p kinases. In this regard, it is tempting to hypothesise that the activity of *ark1* and *plo1* controls how *mid1* and *vps4* interact. However, it is important to highlight that the regions of Mid1p phosphorylated by these kinases do not include the binding region for *vps4*. Interestingly, N-terminal region of Mid1p is reported to phospho-regulate protein kinases, phosphorylation of N-terminal region of Mid1p by Plo1p triggers Mid1p release from the nucleus and promotes the association of Mid1p with node at interphase leading to mitotic entry (Almonacid *et al.*, 2011; Rezig *et al.*, 2021).

Similarly, the process of CR formation in *S. pombe* has been well explored, several minutes after the G2/M transitions, Mid1p in nodes localises myosin II to the cell center through interaction with Rng2 and induces actin polymerization from the nodes by recruiting a formin Cdc12 (Laporte *et al.*, 2011; Saha and Pollard 2012a; Takaine *et al.*, 2014). Both Myosin II and F-actin then interact, and CR formation rapidly progresses in metaphase (Wu *et al.*, 2003). Although, Mid1p sequentially organises cortical nodes containing RIc1 before mitosis, but they remained in the equatorial region without F-actin appearance until late anaphase. This is highlighted specifically as interesting point that may perhaps explain the difference in timing of CR formation (Yasuda *et al.*, 2016). During G2 phase in *S. pombe*, Mid1p is released from the nucleus which is in the middle of the cell and moves to the proximal cell cortex where it interacts with Cdr2 and other proteins with similar functions to form nodes (Akamatsu *et al.,* 2014; Rincon *et al.,* 2014; Yasuda *et al.*, 2016).

Mid1p anchored nodes are essential for CR placement in the middle of the cell. In *S. pombe*, a number of mechanisms function jointly to guarantee that Mid1p localised to the middle cortex. The tip complex consisting of Tea1 with its allied proteins and Pom1 occludes Mid1p nodes from the cell tips (Celton-Morizur *et al.*, 2006). However, Mid1p independent mechanisms that place CR in the cell middle or occlude CR formation at the cell tip may exist in *S. pombe* (Rincon *et al.*, 2014). Recently it was discovered that Pom1 homologue in *Saccharomyces. japonicus* (*S. japonicus*) plays a key role for determining the division site through controlling the CR anchoring protein Cdc15. It is possible that *S. japonicus* may largely depend on Mid1p dependent mechanisms for CR placement. (Gu *et al.*, 2015). In their study, they demonstrated that a gene deletion of *mid1*$^{+}$ did not intensify the defect in CR placement of *Δpom1*-null cells, suggesting that Mid1p possibly plays a minor role in placing the cell division site as compared to pom1 in *S. japonicus*. However, Pom1 is not important for cell proliferation and growth in *S. japonicus*, possibly that another pathway may also function to control the cell division site in *S. japonicus* (Gu *et al.*, 2015).

6.3 Direct physical interaction between Mid1p and Vps4p

We explored the biochemical interaction between the N-terminal, Middle terminal, and C-terminal domains of Mid1p protein to analyse the direct physical interaction with Vps4p in order to further investigate the relevance of ESCRT-associated Vps4p during cell cycle in fission yeast. Here, we describe a physical interaction between Vps4p and Mid1p that is crucial for proper cell division and growth. The physical interaction between the N-terminal domain, Middle and C-terminal domain of Mid1p and Vps4p protein was examined in a pull-down experiment. Notably, we found positive direct physical interaction between the C-terminal domain of Mid1p and Vps4p, indicating that C-terminal domain of Mid1p and Vps4p interact biochemically, but we saw no physical interactions between the N-terminal and Middle of Mid1p with Vps4p (Figure 4-12). We suggest that the localization of the division site in fission yeast is determined by a physical interaction between the Vps4p and Mid1p-control dependent node linking to the plasma membrane. It is important to note that the PH domain is present in the Mid1p domain that interact with Vps4p *in vitro*, suggesting that binding of Vps4p to the region may regulate how cell division in *S. pombe* occur.

The fission yeast initiates cytokinesis by assembly nodes on the plasma membrane during interphase (Figure 6-1), Mid1p cortical anchorage recruitment of cytokinesis proteins lead to interactions with myosin filaments results in the condensation of nodes into the actomyosin ring (Celton-Morizur *et al.*, 2006). Mid1p cortical anchorage depends on the PH domains and its potential interaction with Vps4p might stabilize this interaction. Since Vps4p physically interacts with proteins and residues within the C-terminal domain of Mid1p which contains membrane binding motifs, we speculate that Vps4p may facilitate Mid1p cortical anchorage to promote *S. pombe* cell separation (Sun *et al.*, 2015). Recent research has identified phosphorylation and methylation within C-terminal of Cse4 (K131) and (R143) impacts the stability of centromeric nucleosomes in the context of defects in outer kinetochore proteins (Nguyen *et al.*, 2023). Even though both C- and N-terminus methylation of Cse4 exhibit negative genetic interactions with kinetochore mutants and defects in centromere integrity, there is a difference in which they affect the kinetochore structure and function. The phenotypes for the C-terminus methylation were

observed when combined with mutations in the outer kinetochore component, whereas the phenotypes for N-terminal methylation were detected when combined with mutations in the inner kinetochore components (Anedchenko *et al.*, 2019; Nguyen *et al.*, 2023). It is possible that the C-terminal, the N-terminal methylation of Cse4 could be regulated by the cell cycle in a manner that coordinate the assembly of kinetochore components and faithful chromosome segregation (Anedchenko *et al.*, 2019; Mishra *et al.*, 2019; Mishra *et al.*, 2021).

Methylated Cse4-R37 is flanked by two of the phosphorylation residues S33 and S40 (Boechmann *et al.*, 2013; Mishra and Basrai, 2019). The interactions between these two PTMs of Cse4 and their physiological significance for chromosome segregation remain to be investigated. Research from yeast and other eukaryotes systems have highlighted the importance of the crosstalk between PTMs in determining their activity and function (Liu *et al.*, 2020; Smith *et al.*, 2020). For instant phosphorylation, and methylation of kinetochore protein Dam1 by Set1 methyltransferase inhibits its phosphorylation by Ip11 kinase, which is critical for faithful chromosome segregation and cell viability (Zhang *et al.*, 2005). It is of great interest to explore for possible crosstalk between phosphorylation and methylation in cellular processes in yeast.

6.3.1 Schematics of interaction between Mid1p and Vps4p during cell cycle

We established a genetic and physical interaction between *mid1* and *vps4* through series of catalysed activities by genes, proteins, and protein kinesis such as *plo1* and *ark1* (Figure 6-1). This potential interaction was identified by yeast genetic approach and pull-down biochemical analysis between Mid1p N-terminal, Middle and C-terminal against Vps4p. We identified that C-terminal of Mid1p interact with Vps4p.

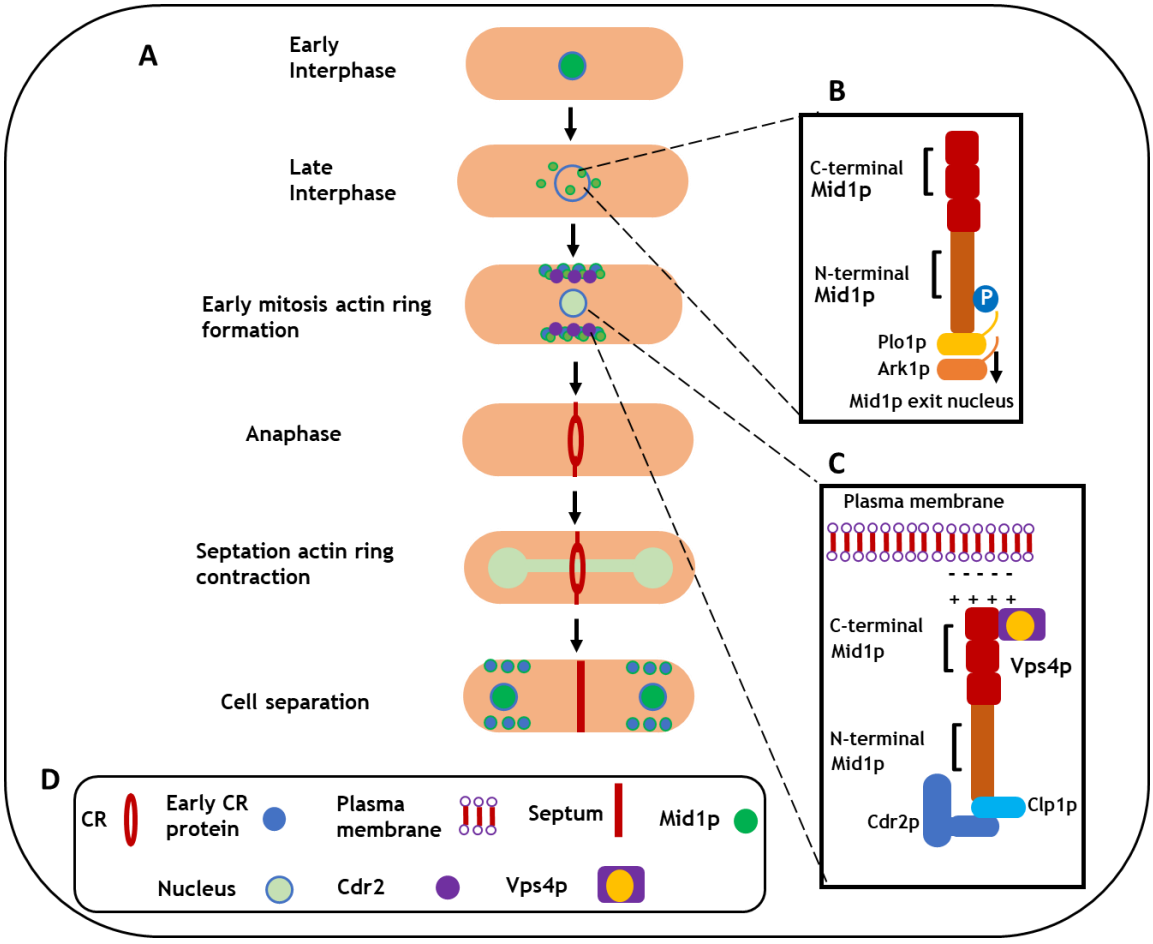

Figure 6-1 Schematic representation of Mid1p and ESCRT-associated Vps4p dependent regulation in *S. pombe*. The identification of genetic and physical interactions between *mid1* and *vps4* genes and proteins. **(A)** Anillin-like Mid1p interact with protein kinesis to localize during cell cycle in *S. pombe*. **(B)** Phosphorylation of Mid1p by Plo1p and Ark1p kinases triggers the release off nodes from the nucleus and interact with the N-terminal domain of Mid1p. **(C)** Mid1p interact with type-I and type II nodes, these nodes are attached to the plasma membrane through the C-terminal domain by sequential assembly of Mid1p substrates Cdr1p, and Cdr2p to interact with the cell membrane through the PH and C2 domains of Mid1p. Vps4 catalyse the interaction between Mid1p C-terminal domain and the plasma membrane. **(D)** Structural definition of key cellular components used in this schematic; CR represent contractile ring.

To further understand the effect of phosphorylation between phospho-mutant and Vps4p, we examined pull-down interactions between wild-type Mid1p, *mid1* phospho-mutant, and Vps4p in detail. We investigated the effects of phosphorylation of Mid1p concerning its physical interaction with Vps4p, and a large C-terminal fragment of Mid1p. The large segment contains the two phospho-sites that were mutated from serine 523, 531 (S) to aspartic (D) acid and incorporated into the "C-term" domain which interacts with Vps4p in addition to the two phospho-sites that we believe are essential for cytokinesis in fission yeast.

The result showed a direct physical interaction between wild-type Mid1p and Vps4p, but no physical interactions between *mid1* phospho-mutant and Vps4p (Figure 4-18). The lack of physical interaction between *mid1* phospho-mutant and Vps4p which is phosphorylated on 523 and 531, could be as explained by the timing of the cell cycle activities. Since the stages of cytokinesis in *S. pombe* can be slowed down or speed up by modifying the sequence Mid1p by phosphorylation. We speculate that the correct coordination of Mid1p during cell division may have been hindered by the timing of Mid1p node, function and activity during cytokinesis. Mid1p phosphorylation during different stages of the cell cycle regulates several aspects of Mid1p function, Cdk1p product of *cdc2* gene, phosphorylation of Mid1p during the G2 kinases. Plo1p phosphorylates about six sites among the first 100 residues of Mid1p during G2 which drive the export of Mid1p from nucleus to the equatorial type 1 nodes and is required for the recruitment of Myo2p to nodes. Localization of Plo1p to the contractile ring depends also on Mid1p (Bhäler *et al.*, 1998; Almonacid *et al.*, 2011).

Therefore, we draw conclusions that the function of Mid1p and its interaction with these proteins to regulate cell cycle events depends on the phosphorylation of these amino acid residues. We hypothesise that the interaction of Mid1p and Vps4p is regulated by the activity of Ark1p and Plo1p, phosphorylation at region of Mid1p containing phospho-acceptor sites have shown to regulate the interaction of Mid1p with cell cycle related protein such as Plo1p, Ark1p and Sid1p. Plo1p phosphorylates residues of Mid1p and trigger Myosin II recruitment to the contractile ring while Sid1p phosphorylate Mid1p to facilitate export from the cortex (Willet *et al.*, 2019).

6.4 Mid1p localization in cytokinesis

Fission yeast is particularly useful for understanding cytokinesis because it separates by medial fission, which implies a contractile actomyosin ring (CAR) affecting the process of cell separation. CAR triggers the constriction force to separate a single cell into two daughters during cytokinesis (Willet *et al.*, 2015; Kim *et al.*, 2017). Staining of the septa with the calcofluor white allows for the obvious identification of yeast septation phenotype to determine how Mid1p influence septation in fission yeast (Rezig *et al.*, 2019).

Phosphorylation of Mid1p at serine position 332 to alanine is important during fission yeast division because a significant increase in the frequency of Class D and E septation phenotypes representing delayed septation and absence of septa was noted in this study (Figure 5-8). This finding suggests that Mid1p play a role in regulating and coordinating fission yeast division site placement, with this serine residue important for this function. A similar result was noted when multiple serine sites were phosphorylated to alanine, S167-531A (Figure 5-9), which may imply a link between Mid1p regulation and ESCRT machinery during fission yeast cytokinesis. However, the precise systematic molecular mechanism by which Mid1p phosphorylation impeded separation during cytokinesis is uncertain, as the progress of cell division in *S. pombe* requires numerous families of proteins that carry out coordinated functions. In this study, we showed that Mid1p phosphorylation is required for facilitating correct septation during cell division; we also note that modifying Mid1p through phosphorylation results in improper division or a delay in process of division leading us to speculate that regulation of function Mid1p could act in conjunction with protein kinases to enable proper division.

Next, we looked into the anillin/Mid1p localization frequency, as CAR node precursors are required to position the CAR in the middle of the cell, and Mid1p shuttles between the nucleus and the cortical nodes established by SAD kinase Cdr2p, during interphase which concentrate at nodes in late interphase (Almonacid *et al.*, 2011). In GFP *mid1* phospho-mutant cells, we found obvious growth and morphological defects at serine GFP-S332A and GFPS167-531D. The phosphorylation of the specific phospho-sites may have resulted in incorrect interaction from the tethering complex of Mid1p cortical nodes, which could interpret as resulting in the observed reduction in *S. pombe* growth rate. The distribution of class A cytoplasmic, class B broad band, class C tight band, class D binuclear, and class E single nuclear localization frequencies was significantly reduced in GFP *mid1* phospho-mutant serine sites S332A, GPF-S523-531, and GFP-S167-531A phospho-resistant strain (Figure 5-16, Figure 5-17 and Figure 5-18). We hypothesise that the defective growth rate might involve mislocalization of nodes, improper positioning of the nodes, and incomplete cytokinesis. Suggests the importance of Mid1p node localization pathway in regulating cellular function. This interaction led us to speculate that the function of Mid1p

is regulated by proper and timely nodes attached to the plasma membrane (Figure 6-1).

Magliozzi *et al*. (2020) determined that Pak1p regulates the localization of the substrates Mid1p and Cdc15p to the CAR and indicated Pak1p systematically phosphorylates the N-terminal of Mid1p which promotes its association with cortical nodes that act as CAR precursors. This mislocalization correlates with exceptional cytokinesis with defects and misplaced distribution of cellular components, Mid1p recruits cytokinetic node proteins, including myosin II Myo2p, myosin light chain Cdc15p and forming Cdc12p, and Mid1p is fused into the contractile ring (CR) along with type 2 node components. When constriction begins, Mid1p leaves the CR and re-accumulates in the nucleus, while the node remains in the CR (Wu *et al*., 2006; Akamatsu *et al*., 2014).

In eukaryotes, cytokinesis is facilitated by the constriction of an actomyosin contractile ring (Glotzer, 2017). In *S. pombe*, the CR forms mid-cell during mitosis from clusters of proteins at the medial cell cortex called nodes. Mid1p localizes to nodes and is required for CR assembly at the mid-cell. When CR constriction begins, Mid1p leaves the division site (Rincon and Paoletti, 2012; Rincon and Paoletti, 2016). Here, however, we speculate that other *mid1* phospho-mutants were able to grow, form normal colonies, and have no defective phenotype because the phospho-mutants were able to rescue and recruit synthetic tethering of Mid1p to cortical nodes.

The knowledge of cytokinesis mechanisms is most advanced in fission yeast (Laplante *et al*., 2016). In fission yeast we do know the estimated concentrations of the key cytokinesis proteins and the sequence of events leading to cellular division (Wu and Pollard, 2005; Laplante *et al*., 2016). Molecularly explicit computer models can account for both the time course of contractile ring formation and the constriction rate and pressure produced by the contractile ring; however, these models call for a number of unproven assumptions about the organisation of the nodes and other proteins (Laplante *et al*., 2016). Similarly, quantification of fluorescence microscopy has documented the precise times at which cytokinesis proteins are recruited to the equator of fission yeast cells (Laplante *et al*., 2016).

6.5 Proposed model for phosphorylation of Mid1p

During interphase, there is continuous accumulation of structures known as nodes (type I and type II nodes) within the surface of the plasma membrane in preparation for cytokinesis. Type I nodes which is form around the equator during early interphase and have the kinases Cdr1p, Cdr2p and Wee1p. The scaffold protein Blt1p, kinesin Kl8p and Rho-GEF Gef2p make up the type II nodes (Akamatsu *et al.*, 2014). Mid1p leaves the nucleus during G2 phase and connects with type I nodes that are already positioned around the nucleus and plasma membrane. Type II nodes are components of the contractile ring, when the contractile ring dissembles at the end of the constriction, the type II nodes emerge and diffused within of the plasma membrane until they are captured by stationary type I nodes in the of the cell (Akamatsu *et al.*, 2014; Chatterjee and Pollard, 2019).

In this study, we propose a model describing how Mid1p phosphorylation regulates fission yeast cytokinesis and cell division progression. Our findings are proposed with a concept (Figure 6-1) that suggest that Mid1p phosphorylation in *S. pombe* can slow or delay division during cytokinesis. Wild-type Mid1p allow assembly of proteins and substrates for interactions that proceed to efficient cell division. The interaction between nodes, Mid1p and recruitments of Myo2p leads to a harmonious interaction with actin to form contractile ring thereby resulting in the completion of cytokinesis and successful cell division. However, modification through phosphorylation of Mid1p at serine 332, which results in delayed, abnormal growth, abnormal septation and localization. Several *S. pombe* proteins are known to affect growth and localization and we speculate that incorrect signal and insufficient interactions might impact growth and localization during cell division.

In *S. pombe* chromosomal deletion of the *mid1* gene or modification of the coding sequence indicates striking defects in septation and localization phenotypes resulting in delayed, defective, and multiple septa cells. This illustrates the requirement of Mid1p for the correct division.

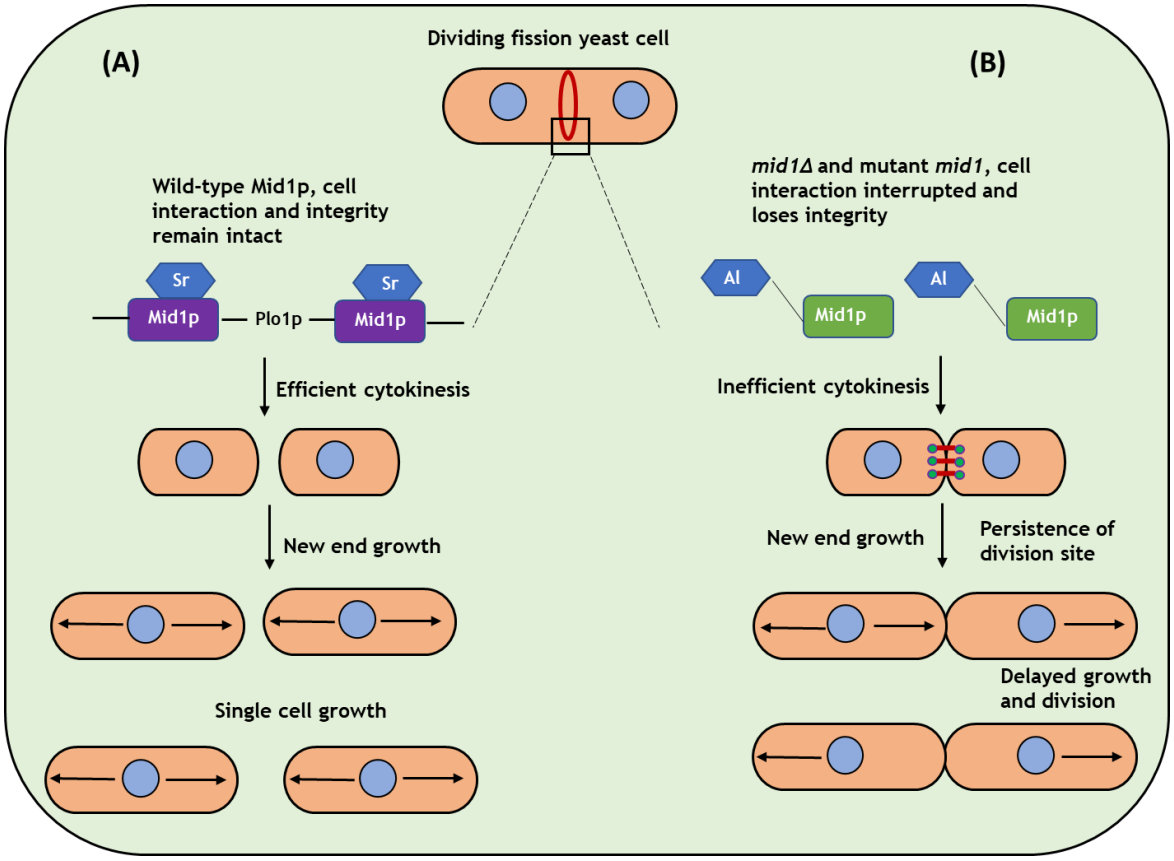

Figure 6-2 Proposed model of phosphorylation of Mid1p growth and localization in *S. pombe*. During interphase, there is an accumulation of nodes within the surface of the plasma membrane that triggers the process of cytokinesis through protein kinesis. During G2, Mid1p serves as a scaffold for multiple proteins during cytokinesis. **(A)** Show wild-type Mid1p with efficient cytokinesis and progression of cell cycle events, it shows a normal separation of cell with integrity **(B)** Show phosphorylation of Mid1p by Plo1p with inefficient cytokinesis and delayed growth, separation, and loss of cell integrity. It shows cells persistently trying to separate but ending up sticking to each other. Sr represent serine, Al represents alanine.

6.6 Conclusions

In this thesis, we identify a unique genetic interaction between *mid1* phospho-mutants, *plo1-ts35*, *ark1-ts11,* and *vps4* genes. Making double mutants revealed striking genetic interactions, defective growth, and abnormal morphological traits implying that these mutants are essential and important during cell cycle in *S. pombe*. We studied the impact of Mid1p phosphorylation by imaging and analyzing the cellular localization pattern of separation of *mid1* phospho-mutant identified in the study. The analysis showed septation defects and mislocalization at S332 *mid1* phospho-mutant indicating the importance of Mid1p in cortical anchorage and nuclear localization during cell division. The mislocalization pattern presents strong evidence that Mid1p is implicated in the recruitment of endosomal vesicle elements to drive cytokinesis processes. Cytokinesis by fission yeast is compromised by the loss of anillin/Mid1p function because cytokinesis organizing centres, called nodes, are misplaced, and fail to acquire myosin-II, so they assemble slowly into abnormal contractile ring (Chatterjee and Pollard, 2019). Defects in cytokinesis affects the survival of single eukaryotic organisms and can lead to tumour formation in higher eukaryotic organism (Pollard and Wu, 2010).

In conclusion, we identified an essential phosphorylation site at S332 to be important in supporting the equatorial zone of Mid1p using a genetic approach and microscopic screening. We demonstrated that the systematic recruitment of nodes, myosin, anillin, and actin to the equatorial zone by phosphorylation of fission yeast Mid1p may regulate septation and localization processes (Garno *et al.*, 2021). Therefore, we conclude that the phosphorylation of these amino acid residues is important for the Mid1p function and its interaction with these proteins to regulate cell cycle events. It is tempting to speculate that the interactions of Mid1p and Vps4p are regulated and coordinated by the activity of Ark1p and Plo1p and it is also important to note that the regions of Mid1p phosphorylated by these kinases do not include the binding region of Vps4p (Rezig *et al.*, 2021).

6.7 Future studies

This current study provides the framework to further investigate the molecular dynamics of Mid1p and the upstream regulation of kinases during cytokinesis.

- To determine whether *mid1* phospho-sites single, double, and multiple points mutations (S332A, S531A, S523-531A and S167-531A) pull-down Vps4p?

The study of genetic and physical interaction between Mid1p different domains and Vps4p, we have performed pull-down experiments with N-terminal, middle and C-terminal, and *mid1* phospho-mutant S523-531D, which C-terminal domain and wild-type Mid1p indicates a physical interaction with Vps4p. It will be interesting to further aim at identifying the specific phospho-sites responsible for poll-down activity with Vps4p. The approach to selectively probe the specific phospho-sites identified to determine how each site may or relate with Vps4p in terms of pull-down. The result will bring to knowledge the function of phosphorylation Mid1p during cell division in *S. pombe*.

- To Investigate phosphorylation regulation using live-cell time imaging of Mid1p localization

Live-cell recording with GFP-tubulin or mCherry-tubulin could be recorded to further understand *mid1* phospho-mutant undergoing cytokinesis at various time intervals using incubated spinning-disk microscope (Intelligent Imaging). This will give a detailed understanding of the stages of separation including further quantification of the sizes of the cell during the process of division. The results from this propose study will further provide detailed understanding of Mid1 localization and the interplay between Mid1p membrane localization, Mid1p nodes localization to the membrane lining the septum during interphase.

- Immunoblotting analysis to detect the presence, size, and abundance of wild-type Mid1p and *mid1* phospho-mutants.

It is important to investigate and detect the presence of wild-type Mid1p and *mid*1 phospho-mutant proteins using western blotting. Post-translational modification affect protein folding and stability. Western blot analysis will be a informative technique to study the phosphorylation mutations used during this study to detect if these mutations affect protein stability. Similarly, GFP-Mid1p and GFP-*mid1* phospho-mutants should be detected and analyzed using western blotting as this will further give insight to the information already obtained through co-localization study.

- To determine the effect of Mid1p phosphorylation using mammalian cells (*in vivo* study)

All designs and experiments presented in this study were created and carried out by *in vitro* assays. The *in vitro* experiments and results represent a simple experimental design to investigate the yeast genetic, pull-down biochemical analysis and co-localization, but the results obtained *in vitro* may not be projected to be certain to be replicated *in vivo*. Therefore, it could be necessary to replicate and substantiate these results with observation *in vivo* experiments and results using mammalian cells.

7 Appendix 1 - Summary of double mutants and growth defects of *mid1* phospho-mutant *vps4*Δ, *plo1,* and *ark1* created in the study

7.1 Double mutant of *mid1* phospho-mutant S167A and *vps4*Δ

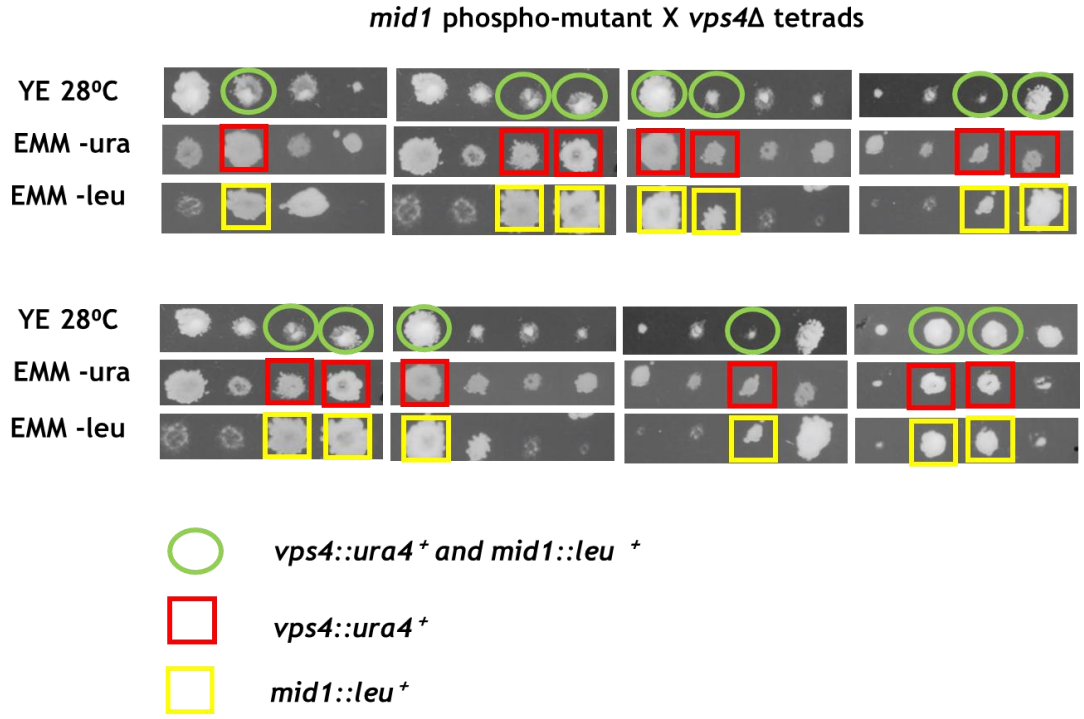

Figure 7-1 Identification of fission yeast double *mid1* phospho-mutant S167A *vps4*Δ generated by ascus dissection. Yeast strains were mated on solid ME medium at 25ºC for two days and then transferred to solid YE medium for ascus dissection using a Singer MSM Ascus Dissector. Spores from each tetrad were placed at sequential horizontal grid positions and allowed to form colonies, then replica plated to two solid media: EMM lacking uracil (EMM -ura) and EMM lacking leucine (EMM -leu). This was incubated at 28ºC until the growth of colonies, the double mutants are boxed in green, red, and yellow. The double mutants were created in three (n=3) independent experiments for each genotype, given a GG number respectively (GG 3450) and stored in 30% glycerol in the Glasgow yeast collection at -80ºC.

7.2 Double mutant of *mid1* phospho-mutant S328A and *vps4*Δ

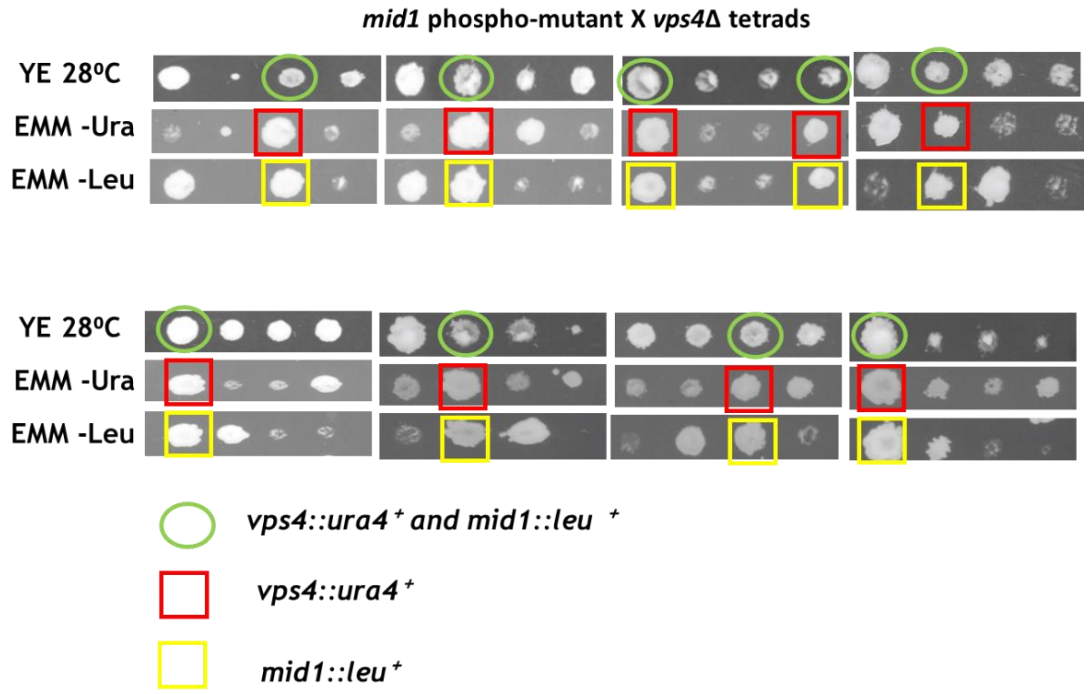

Figure 7-2 Identification of fission yeast double *mid1* phospho-mutant S328A *vps4*Δ generated by ascus dissection. Yeast strains were mated on solid ME medium at 25ºC for two days and then transferred to solid YE medium for ascus dissection using a Singer MSM Ascus Dissector. Spores from each tetrad were placed at sequential horizontal grid positions and allowed to form colonies, then replica plated to two solid media: EMM lacking uracil (EMM -ura) and EMM lacking leucine (EMM -leu). This was incubated at 28ºC until the growth of colonies, the double mutants are boxed in green, red, and yellow. The double mutants were created in three (n=3) independent experiments for each genotype, given a GG number respectively (GG 3456) and stored in 30% glycerol in the Glasgow yeast collection at -80ºC.

7.3 Double mutant of *mid1* phospho-mutant S332A and *vps4*Δ

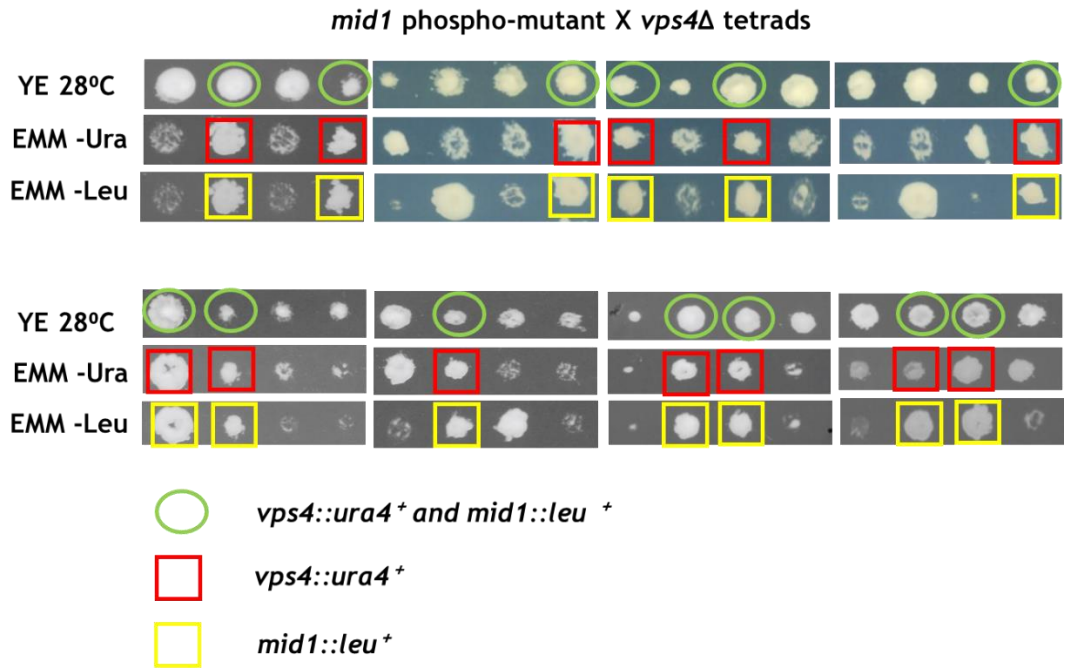

Figure 7-3 Identification of fission yeast double *mid1* phospho-mutant S332A *vps4*Δ generated by ascus dissection. Yeast strains were mated on solid ME medium at 25ºC for two days and then transferred to solid YE medium for ascus dissection using a Singer MSM Ascus Dissector. Spores from each tetrad were placed at sequential horizontal grid positions and allowed to form colonies, then replica plated to two solid media: EMM lacking uracil (EMM -ura) and EMM lacking leucine (EMM -leu). This was incubated at 28ºC until the growth of colonies, the double mutants are boxed in green, red, and yellow. The double mutants were created in three (n=3) independent experiments for each genotype, given a GG number respectively (GG 3485), and stored in 30% glycerol in the Glasgow yeast collection at -80ºC.

7.4 Double mutant of *mid1* phospho-mutant S523D and *vps4*Δ

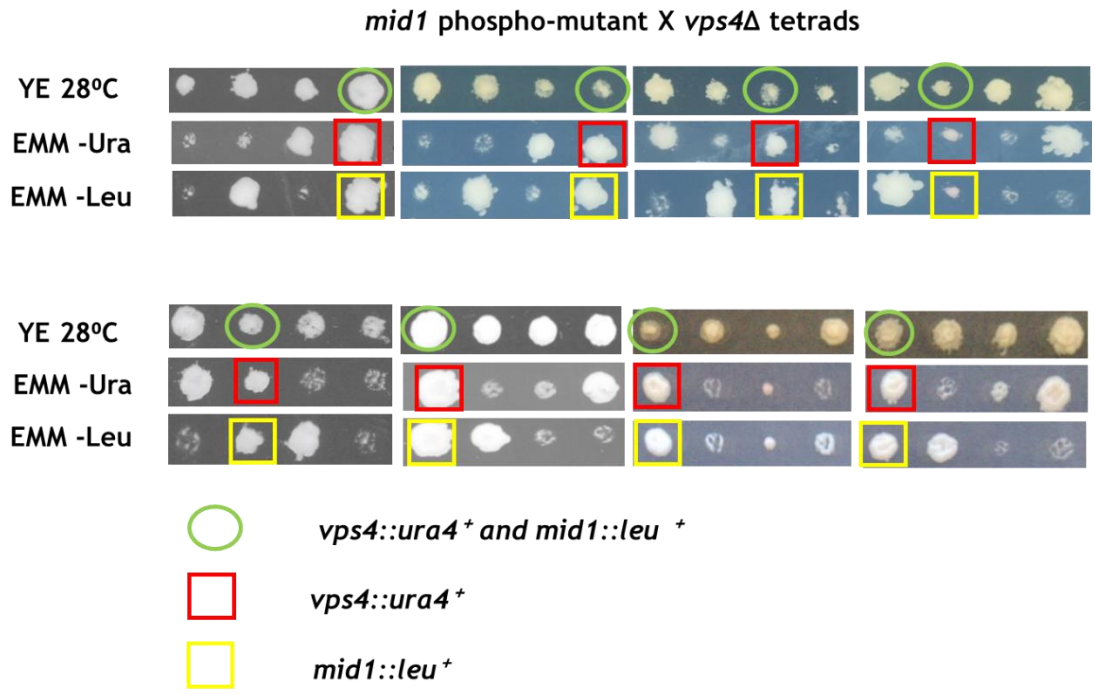

Figure 7-4 Identification of fission yeast double *mid1* phospho-mutant S523D *vps4*Δ generated by ascus dissection. Yeast strains were mated on solid ME medium at 25ºC for two days and then transferred to solid YE medium for ascus dissection using a Singer MSM Ascus Dissector. Spores from each tetrad were placed at sequential horizontal grid positions and allowed to form colonies, then replica plated to two solid media: EMM lacking uracil (EMM -ura) and EMM lacking leucine (EMM -leu). This was incubated at 28ºC until the growth of colonies, the double mutants are boxed in green, red, and yellow. The double mutants were created in three (n=3) independent experiments for each genotype, given a GG number respectively (GG 3318), and stored in 30% glycerol in the Glasgow yeast collection at -80ºC.

7.5 Double mutant of *mid1* phospho-mutant S332A and *plo-ts35*

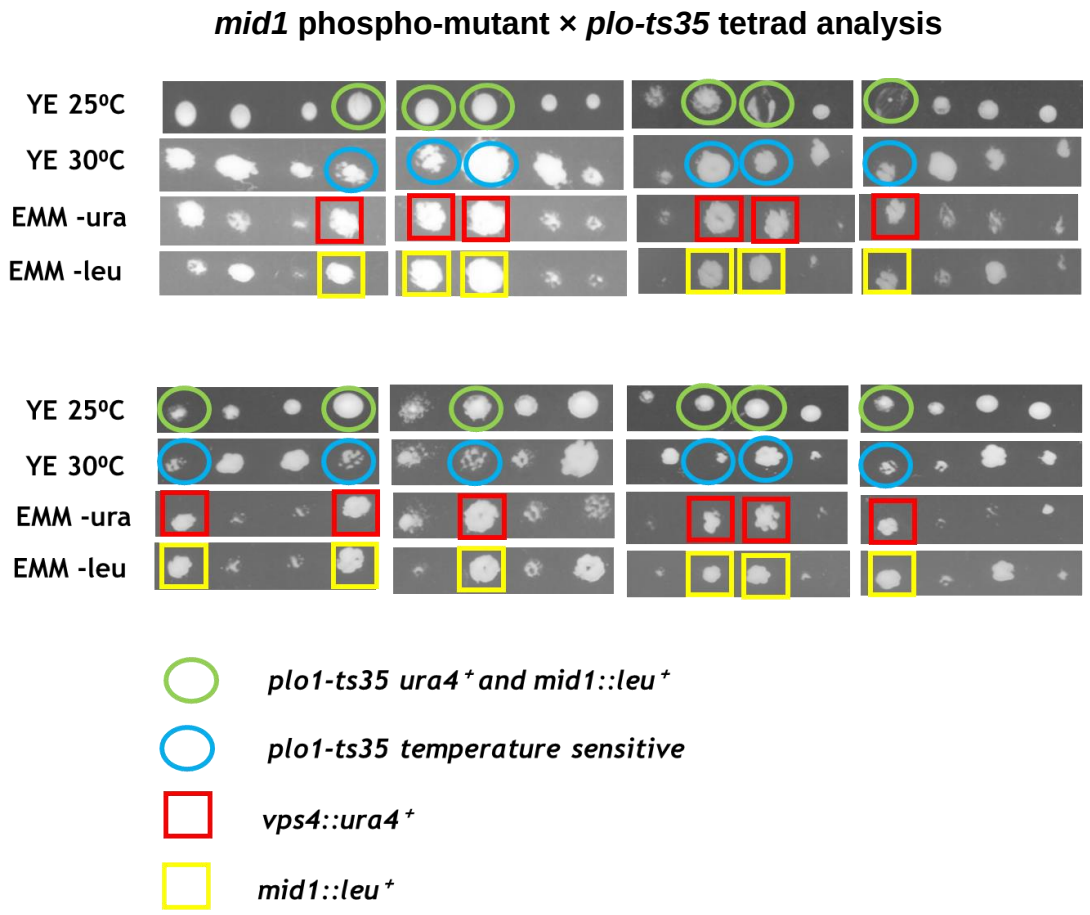

Figure 7-5 Identification of fission yeast double *mid1* phospho- mutants S332A *plo1-ts35* generated by ascus dissection. Yeast strains were mated on solid ME medium at 25ºC for two days and then transferred to solid YE medium for ascus dissection using a Singer MSM Ascus Dissector. Spores from each tetrad were placed at sequential horizontal grid positions and allowed to form colonies, then replica plated to two solid media: EMM lacking uracil (EMM -ura) and EMM lacking leucine (EMM -leu). This was incubated at 28ºC until the growth of colonies, the double mutants are boxed in green, blue, red, and yellow. The double mutants were created in three (n=3) independent experiments for each genotype, given a GG number respectively (GG 3411), and stored in 30% glycerol in the Glasgow yeast collection at -80ºC.

7.6 Double mutant of *mid1* phospho-mutant S523D and *plo-ts35*

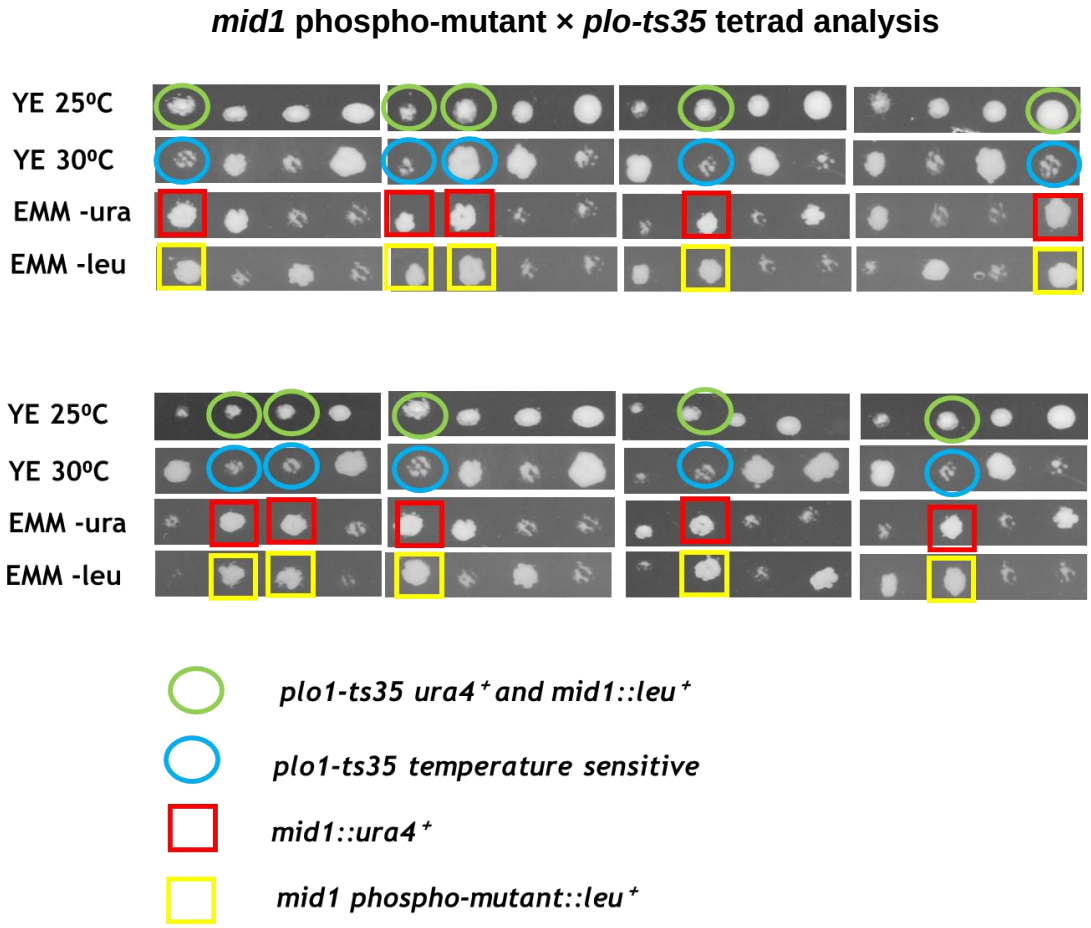

Figure 7-6 Identification of fission yeast double *mid1* phospho- mutants S523D *plo1-ts35* generated by ascus dissection. Yeast strains were mated on solid ME medium at 25ºC for two days and then transferred to solid YE medium for ascus dissection using a Singer MSM Ascus Dissector. Spores from each tetrad were placed at sequential horizontal grid positions and allowed to form colonies, then replica plated to two solid media: EMM lacking uracil (EMM -ura) and EMM lacking leucine (EMM -leu). This was incubated at 28ºC until the growth of colonies, the double mutants are boxed in green, blue, red, and yellow. The double mutants were created in three (n=3) independent experiments for each genotype, given a GG number respectively (GG 3415), and stored in 30% glycerol in the Glasgow yeast collection at -80ºC.

7.7 Double mutant of *mid1* phospho-mutant S523-531D and *plo-ts35*

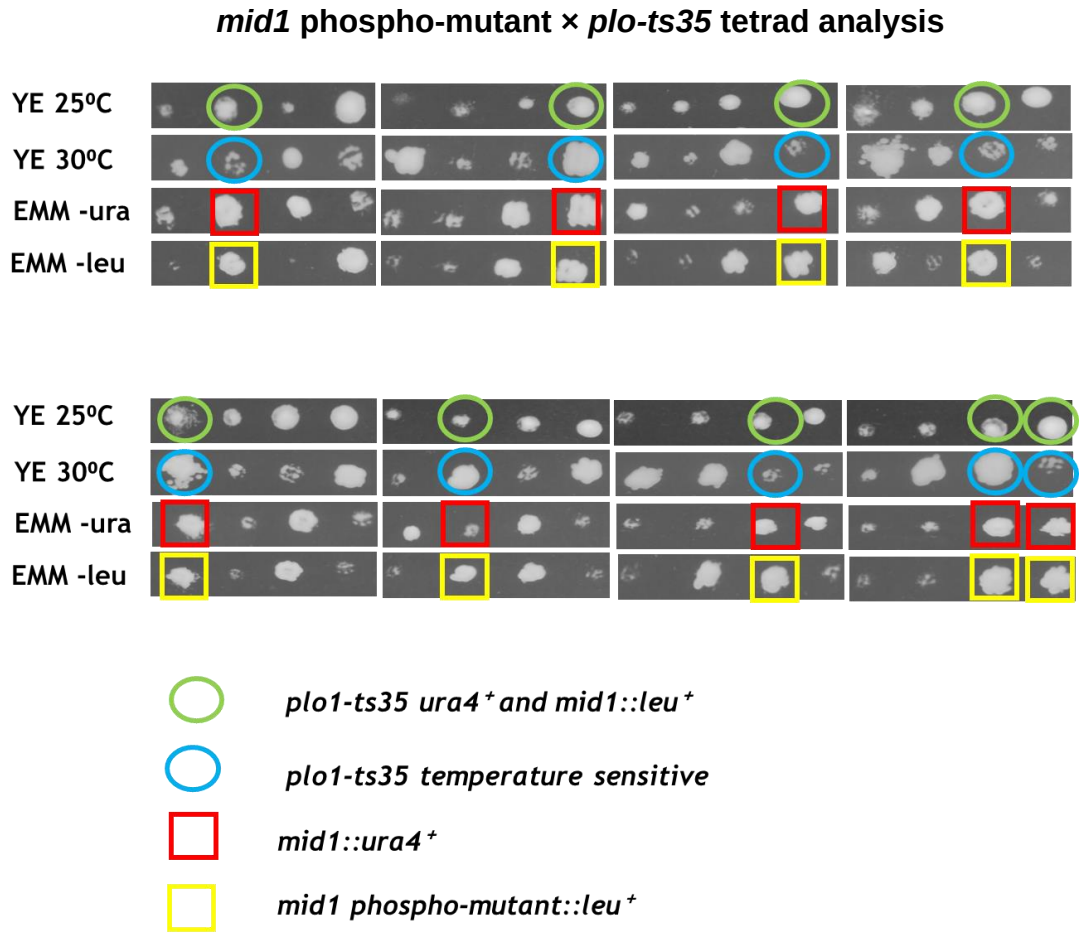

Figure 7-7 Identification of fission yeast double *mid1* phospho- mutants S523-531D *plo1-ts35* generated by ascus dissection. Yeast strains were mated on solid ME medium at 25ºC for two days and then transferred to solid YE medium for ascus dissection using a Singer MSM Ascus Dissector. Spores from each tetrad were placed at sequential horizontal grid positions and allowed to form colonies, then replica plated to two solid media: EMM lacking uracil (EMM -ura) and EMM lacking leucine (EMM -leu). This was incubated at 28ºC until the growth of colonies, the double mutants are boxed in green, blue, red, and yellow. The double mutants were created in three (n=3) independent experiments for each genotype, given a GG number respectively (GG 3447), and stored in 30% glycerol in the Glasgow yeast collection at -80ºC.

7.8 Double mutant of *mid1* phospho-mutant S332A and *ark1-ts11*

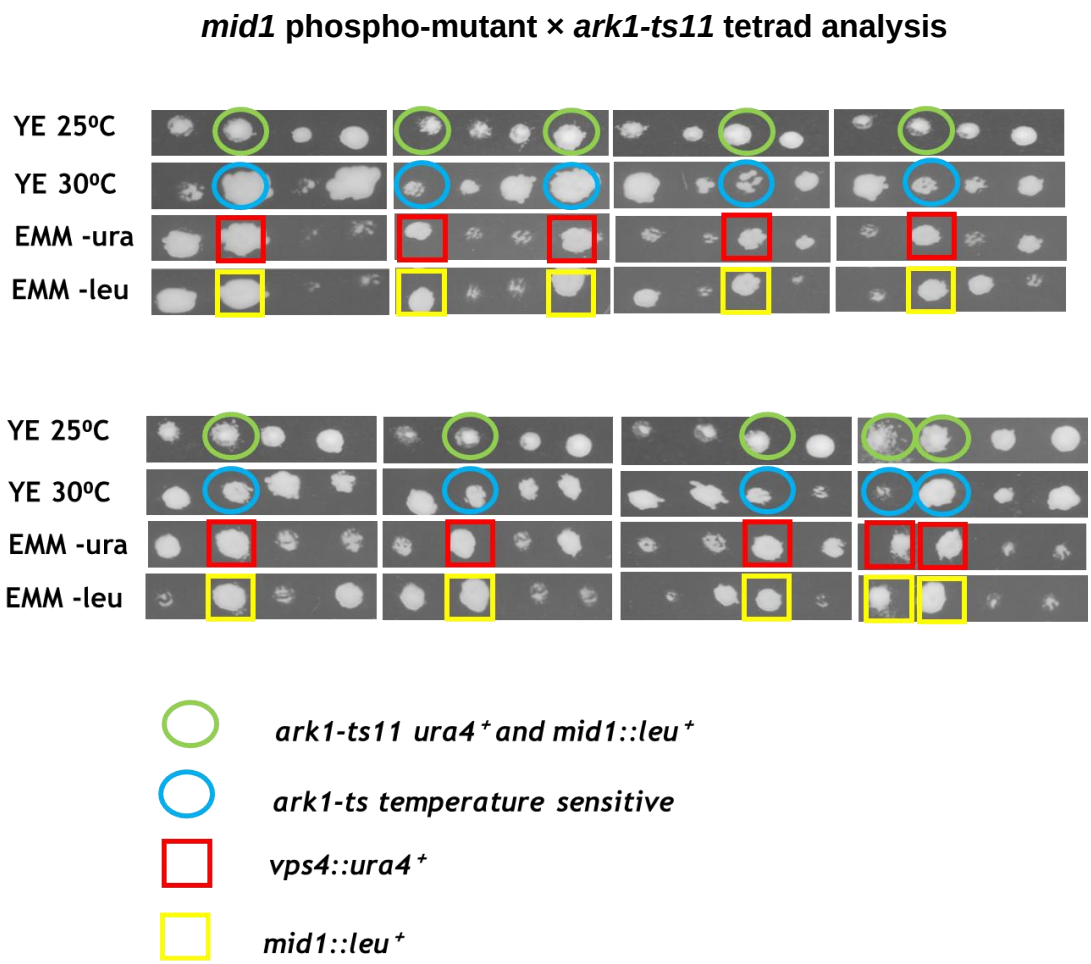

Figure 7-8 Identification of fission yeast double *mid1* phospho- mutants S332A *ark1-ts11* generated by ascus dissection. Yeast strains were mated on solid ME medium at 25ºC for two days and then transferred to solid YE medium for ascus dissection using a Singer MSM Ascus Dissector. Spores from each tetrad were placed at sequential horizontal grid positions and allowed to form colonies, then replica plated to two solid media: EMM lacking uracil (EMM -ura) and EMM lacking leucine (EMM -leu). This was incubated at 28ºC until the growth of colonies, the double mutants are boxed in green, blue, red, and yellow. The double mutants were created in three (n=3) independent experiments for each genotype, given a GG number respectively (GG 3342), and stored in 30% glycerol in the Glasgow yeast collection at -80ºC.

7.9 Double mutant of *mid1* phospho-mutant S523D and *ark1-ts11*

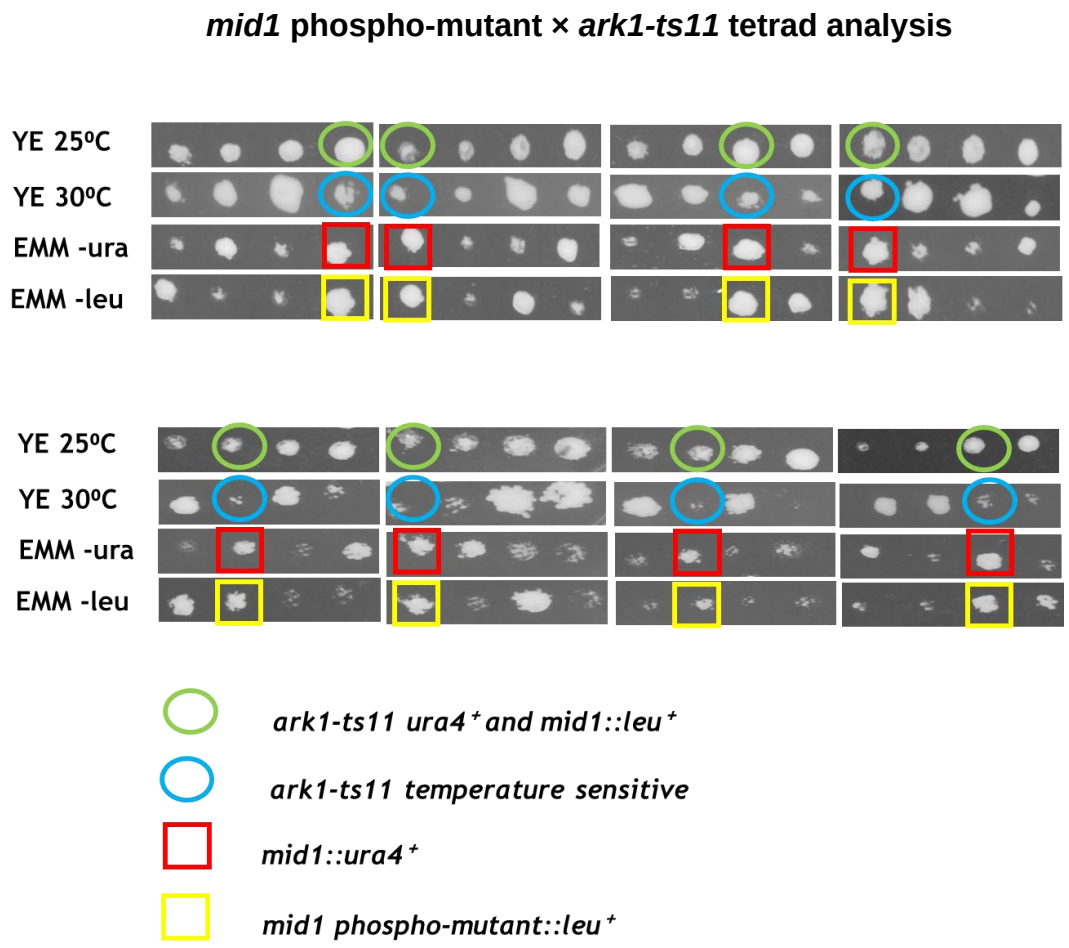

Figure 7-9 Identification of fission yeast double *mid1* phospho- mutants S523D *ark1-ts11* generated by ascus dissection. Yeast strains were mated on solid ME medium at 25ºC for two days and then transferred to solid YE medium for ascus dissection using a Singer MSM Ascus Dissector. Spores from each tetrad were placed at sequential horizontal grid positions and allowed to form colonies, then replica plated to two solid media: EMM lacking uracil (EMM -ura) and EMM lacking leucine (EMM -leu). This was incubated at 28ºC until the growth of colonies, the double mutants are boxed in green, blue, red, and yellow. The double mutants were created in three (n=3) independent experiments for each genotype, given a GG number respectively (GG 3235), and stored in 30% glycerol in the Glasgow yeast collection at -80ºC.

8 Appendix 2 Summary of synthetic viable phenotypes of *mid1* phospho-mutant *vps4*Δ*, plo1,* and *ark1* created in the study

8.1 Synthetic viable phenotypes of *mid1* phospho-mutant and *vps4*Δ (S167D and S167A)

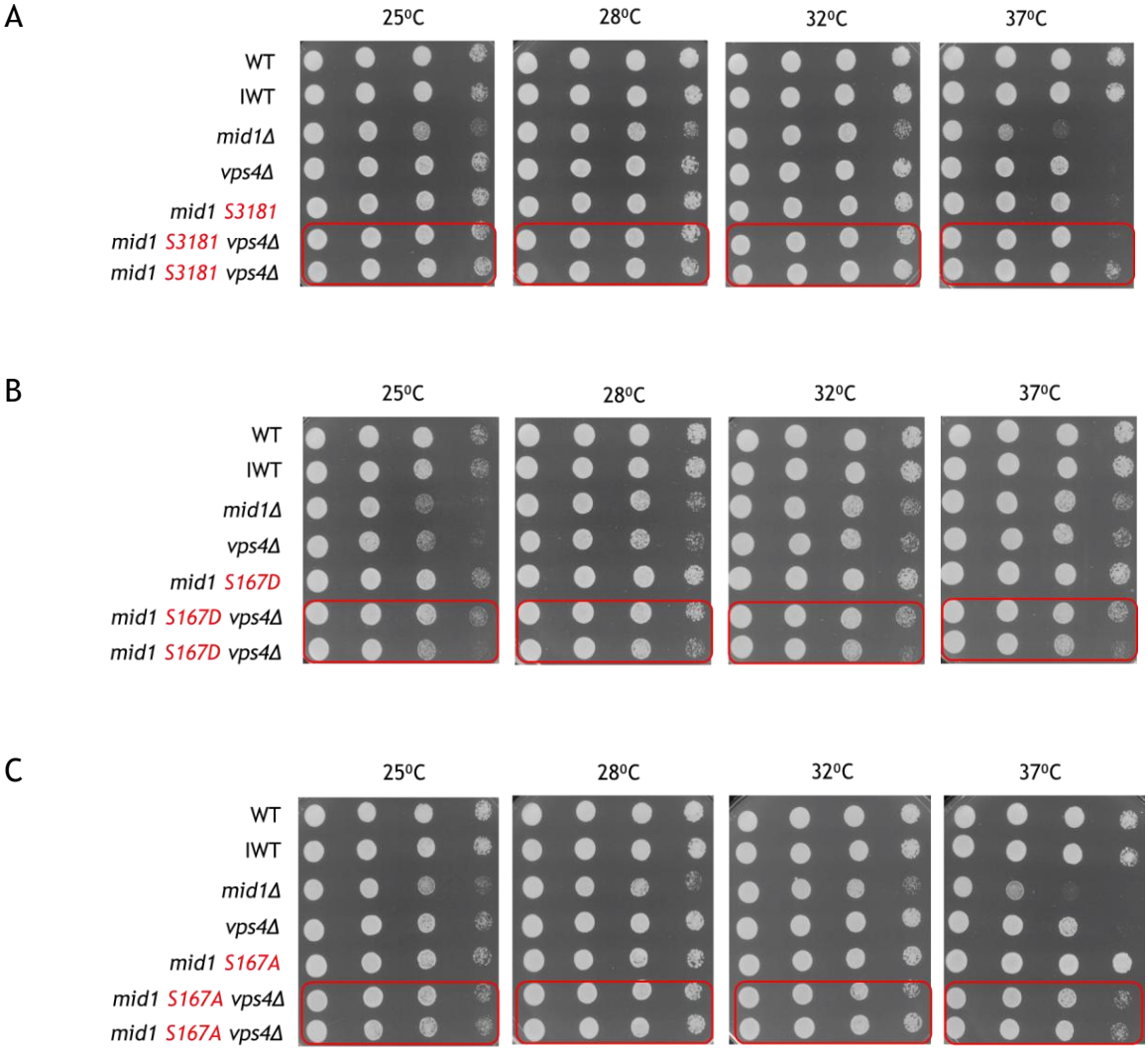

Figure 8-1 *mid1* phospho-mutant (S167D and S167A) shows synthetic viable phenotypes with *vps4*Δ. Synthetic viable phenotypes and colony analysis of wild-type, parent cells, *mid1*Δ, and double mutant isolates. All the cells were suspended at 1.5x10^6 cells/ml and subjected to 10-fold serial dilution. Cells suspended were pipetted onto solid YE media and incubated at four different temperatures (25ºC, 28ºC, 32ºC, and 37ºC). The analysis of growth phenotype was captured and interpreted after two days of cell growth on a solid YE medium. A double mutant wild-type and *vps4*Δ (GG 3487), B double mutant of *mid1* phospho-mutant *S167D* and *vps4*Δ (GG 33283), and C double mutant of *mid1* phospho-mutant *S167A* and *vps4*Δ (GG 3450). WT is wild-type, IWT is integrated wild-type, *mid1*Δ *is* Mid1p deletion, and *vps4*Δ is Vps4p deletion. Double mutants indicating growth rate defects are represented in red circles.

8.2 Synthetic viable phenotypes of *mid1* phospho-mutant and *vps4*Δ (S328D and S328A)

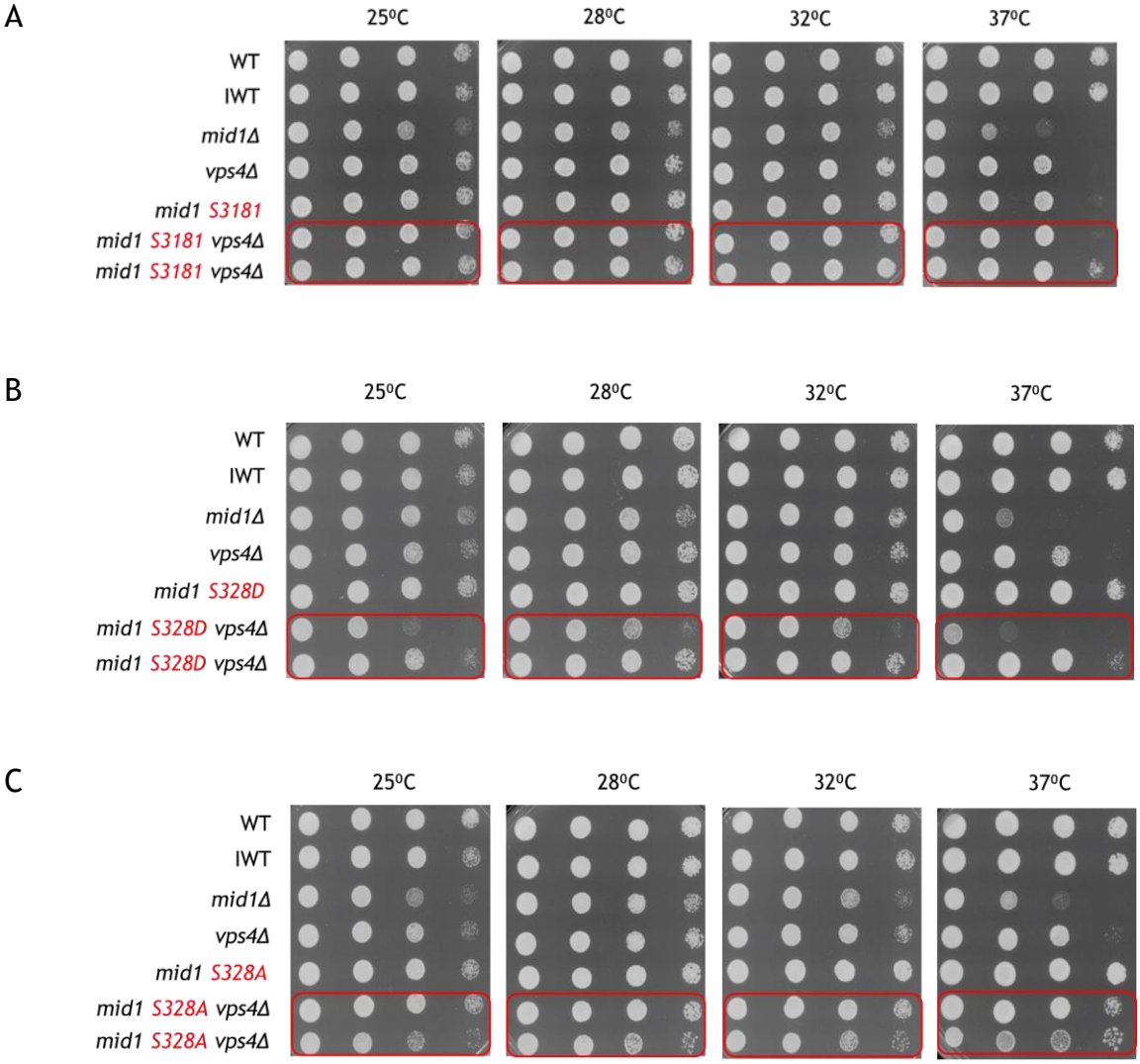

Figure 8-2 *mid1* phospho-mutant (S328D and S328A) shows synthetic viable phenotypes with *vps4*Δ. Synthetic viable phenotypes and colony analysis of wild-type, parent cells, *mid1*Δ, and double mutant isolates. All the cells were suspended at 1.5x10^6 cells/ml and subjected to 10-fold serial dilution. Cells suspended were pipetted onto solid YE media and incubated at four different temperatures (25ºC, 28ºC, 32ºC, and 37ºC). The analysis of growth phenotype was captured and interpreted after two days of cell growth on a solid YE medium. A double mutant wild-type and *vps4*Δ (GG 3487), B double mutant of *mid1* phospho-mutant *S328D* and *vps4*Δ (GG 3481), and C double mutant of *mid1* phospho-mutant *S328A* and *vps4*Δ (GG 3456). WT is wild-type, IWT is integrated wild-type, *mid1*Δ *is* Mid1p deletion, and *vps4*Δ is Vps4p deletion. Double mutants indicating growth rate defects are represented in red circles.

8.3 Synthetic viable phenotypes of *mid1* phospho-mutant and *vps4*Δ (S523D-S523A)

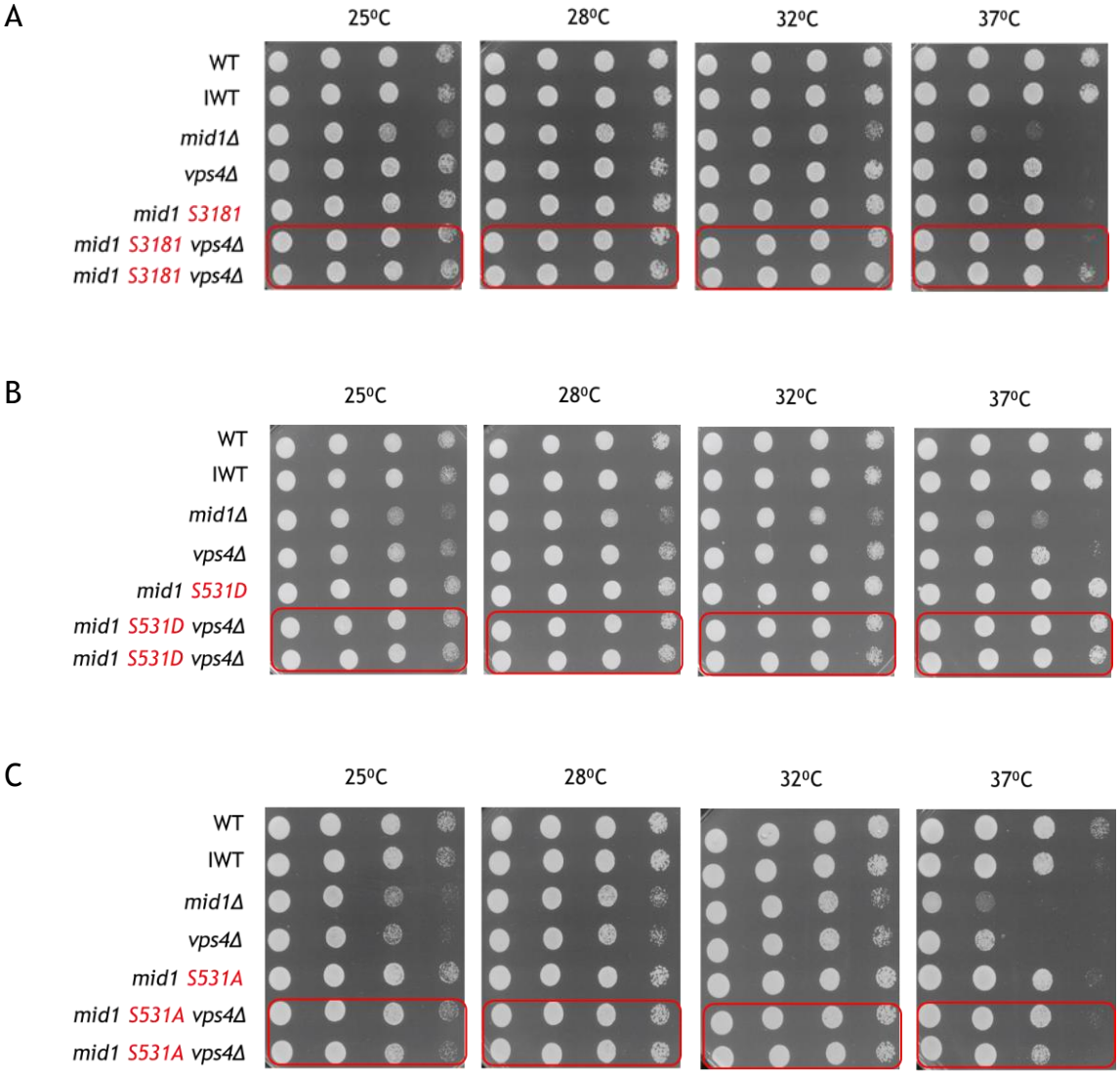

Figure 8-3 *mid1* phospho-mutant (S523D-S523A) shows synthetic viable phenotypes with *vps4*Δ. Synthetic viable phenotypes and colony analysis of wild-type, parent cells, *mid1*Δ, and double mutant isolates. All the cells were suspended at 1.5x10^6 cells/ml and subjected to 10-fold serial dilution. Cells suspended were pipetted onto solid YE media and incubated at four different temperatures (25ºC, 28ºC, 32ºC, and 37ºC). The analysis of growth phenotype was captured and interpreted after two days of cell growth on a solid YE medium. A double mutant wild-type and *vps4*Δ (GG 3487), B double mutant of *mid1* phospho-mutant *S531D* and *vps4*Δ (GG 3318), and C double mutant of *mid1* phospho-mutant *S531A* and *vps4*Δ (GG 3315). WT is wild-type, IWT is integrated wild-type, *mid1*Δ *is* Mid1p deletion, and *vps4*Δ is Vps4p deletion. Double mutants indicating growth rate defects are represented in red circles.

8.4 Synthetic viable phenotypes of *mid1* phospho-mutant and *vps4*Δ (S167-332D and S167-332A)

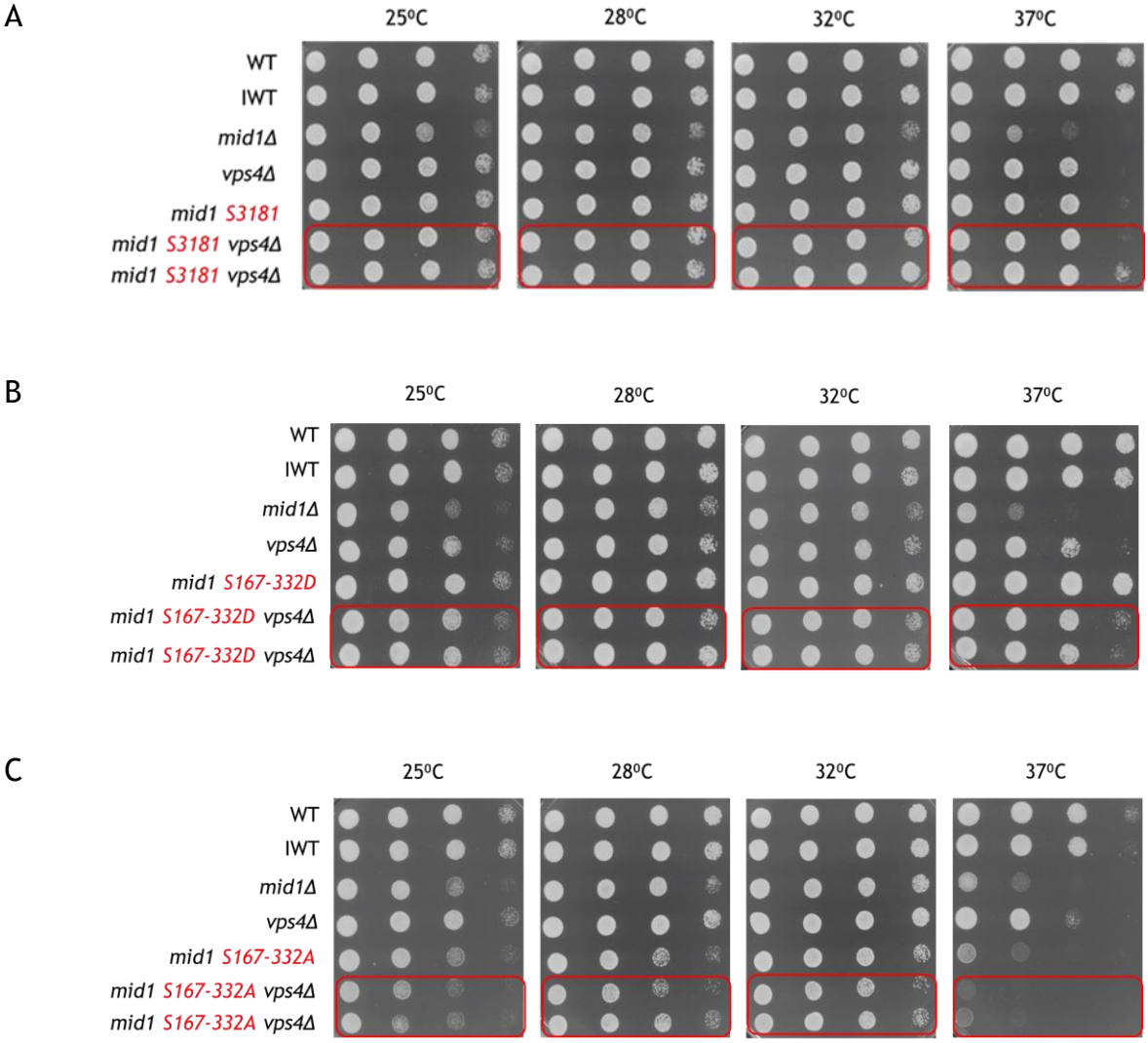

Figure 8-4 *mid1* phospho-mutant (S167-332D and S167-332A) shows synthetic viable phenotypes with *vps4*Δ. Synthetic viable phenotypes and colony analysis of wild-type, parent cells, *mid1*Δ, and double mutant isolates. All the cells were suspended at 1.5x10^6 cells/ml and subjected to 10-fold serial dilution. Cells suspended were pipetted onto solid YE media and incubated at four different temperatures (25ºC, 28ºC, 32ºC, and 37ºC). The analysis of growth phenotype was captured and interpreted after two days of cell growth on a solid YE medium. A double mutant wild-type and *vps4*Δ (GG 3487), B double mutant of *mid1* phospho-mutant *S167-332D* and *vps4*Δ (GG 3421), and C double mutant of *mid1* phospho-mutant *S167-332A* and *vps4*Δ (GG 3419). WT is wild-type, IWT is integrated wild-type, *mid1*Δ *is* Mid1p deletion, and *vps4*Δ is Vps4p deletion. Double mutants indicating growth rate defects are represented in red circles.

8.5 Synthetic viable phenotypes of *mid1* phospho-mutant and *vps4*Δ (S523-531D and S523-531D)

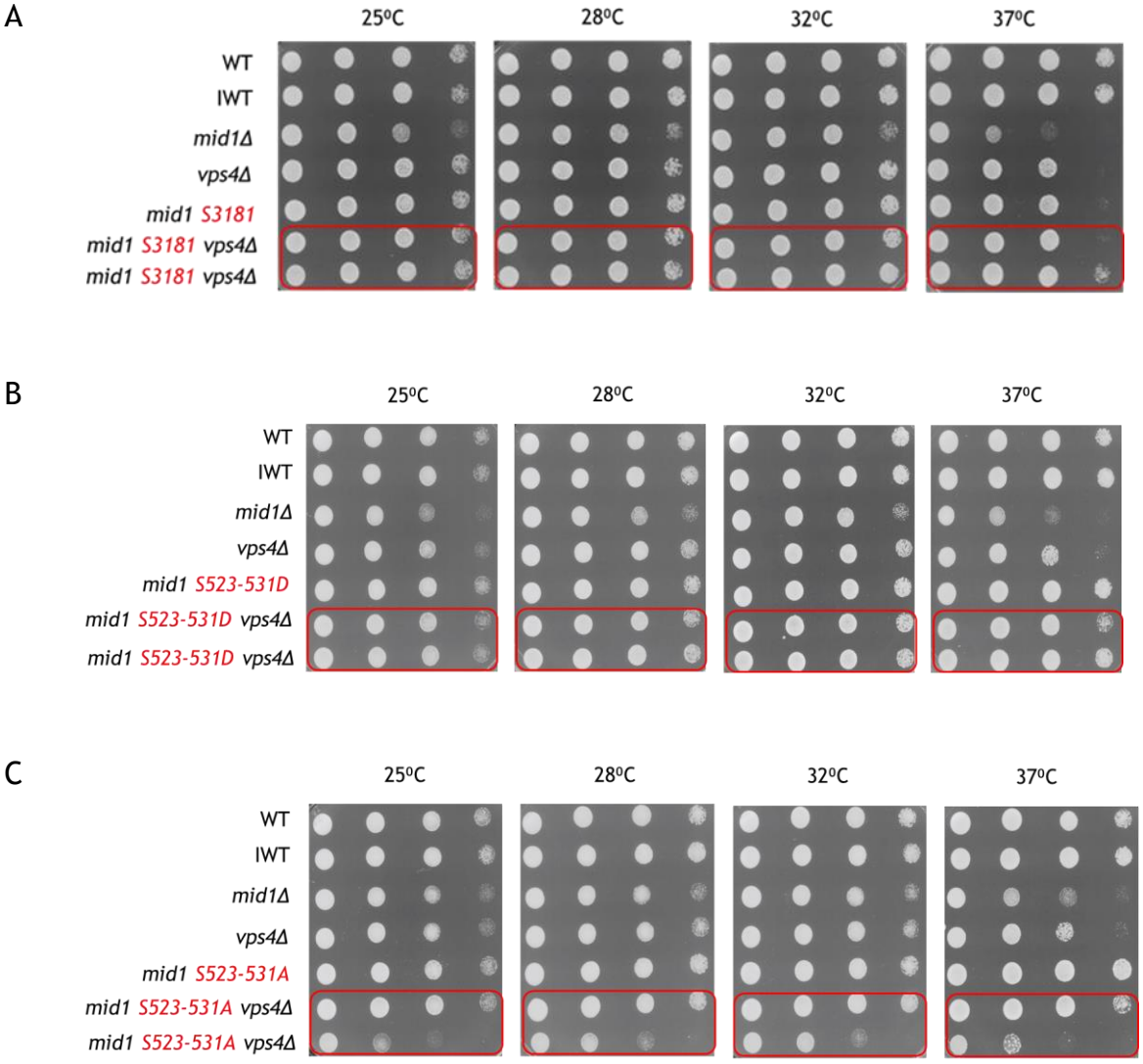

Figure 8-5 *mid1* phospho-mutant (S523-531D and S523-531D) shows synthetic viable phenotypes with *vps4*Δ. Synthetic viable phenotypes and colony analysis of wild-type, parent cells, *mid1*Δ, and double mutant isolates. All the cells were suspended at 1.5x10^6 cells/ml and subjected to 10-fold serial dilution. Cells suspended were pipetted onto solid YE media and incubated at four different temperatures (25ºC, 28ºC, 32ºC, and 37ºC). The analysis of growth phenotype was captured and interpreted after two days of cell growth on a solid YE medium. A double mutant wild-type and *vps4*Δ (GG 3487), B double mutant of *mid1* phospho-mutant *S523-531D* and *vps4*Δ (GG 3257), and C double mutant of *mid1* phospho-mutant *S523-531A* and *vps4*Δ (GG 3260). WT is wild-type, IWT is integrated wild-type, *mid1*Δ *is* Mid1p deletion, and *vps4*Δ is Vps4p deletion. Double mutants indicating growth rate defects are represented in red circles.

8.6 Synthetic viable phenotypes of *mid1* phospho-mutant and *plo1-ts35* (S332D and S332A)

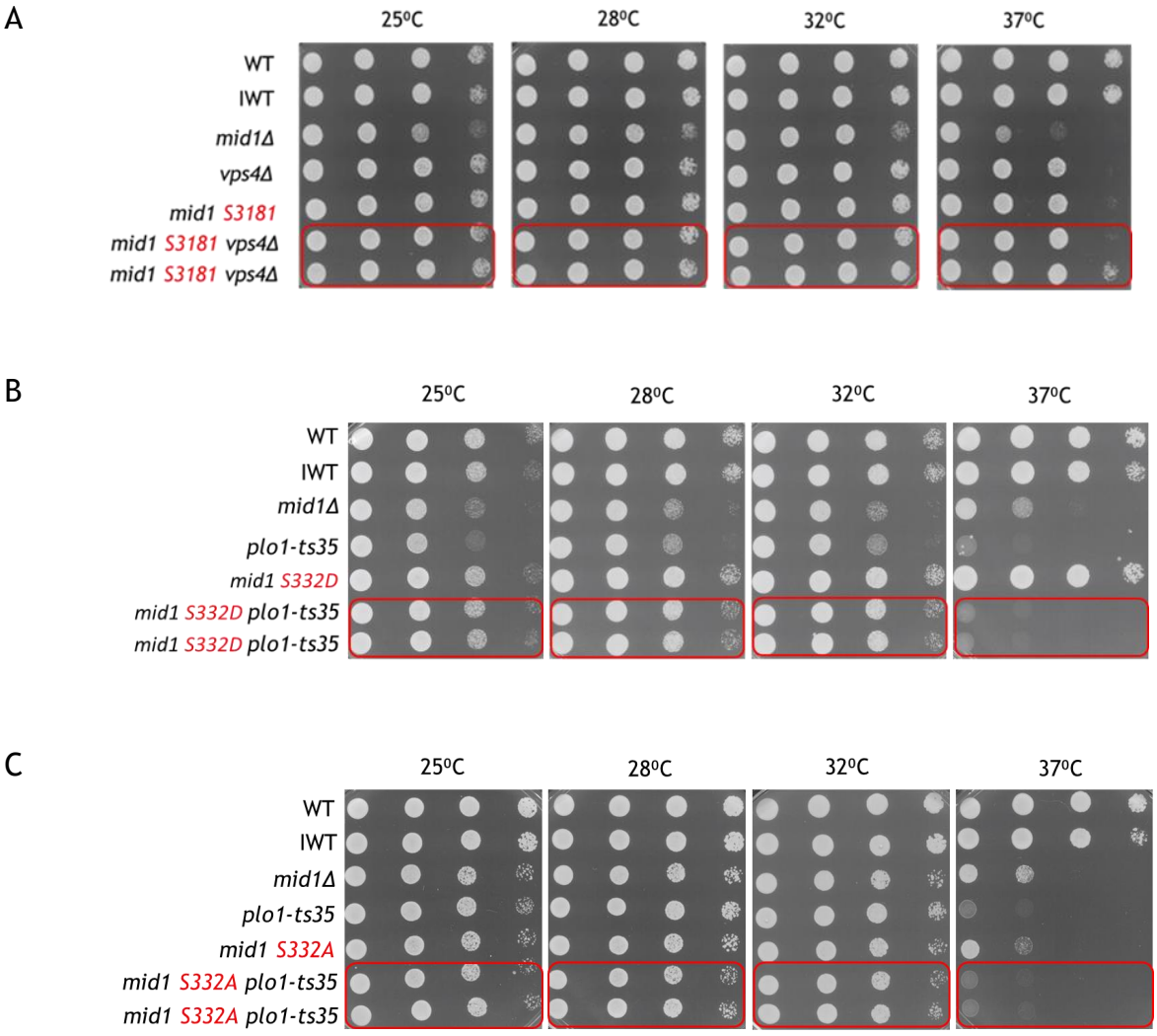

Figure 8-6 *mid1* phospho-mutant (S332D and S332A) shows synthetic viable phenotypes with *plo1-ts35*. Synthetic viable phenotypes and colony analysis of wild-type, parent cells, *mid1*Δ, and double mutant isolates. All the cells were suspended at 1.5x10^6 cells/ml and subjected to 10-fold serial dilution. Cells suspended were pipetted onto solid YE media and incubated at four different temperatures (25ºC, 28ºC, 32ºC, and 37ºC). The analysis of growth phenotype was captured and interpreted after two days of cell growth on a solid YE medium. A double mutant wild-type and *vps4*Δ (GG 3487), B double mutant of *mid1* phospho-mutant *S332D* and *plo1-ts35* (GG 3224), and C double mutant of *mid1* phospho-mutant *S332A* and *plo1-ts35* (GG 3469). WT is wild-type, IWT is integrated wild-type, *mid1*Δ *is* Mid1p deletion, and *vps4*Δ is Vps4p deletion. Double mutants indicating growth rate defects are represented in red circles.

8.7 Synthetic viable phenotypes of *mid1* phospho-mutant and *plo1-ts35* (S531D and S531A)

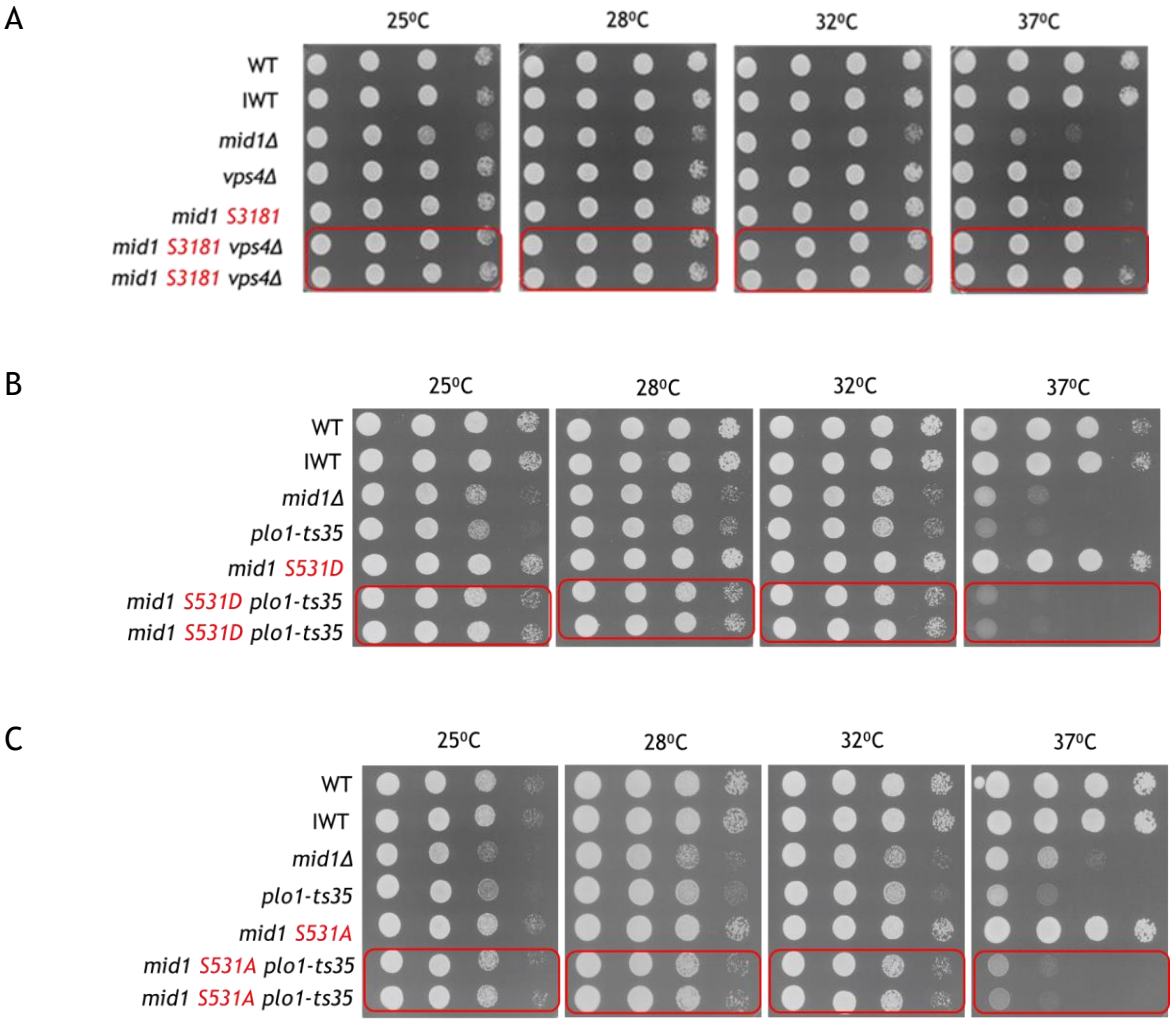

Figure 8-7 *mid1* phospho-mutant (S531D and S531A) shows synthetic viable phenotypes with *plo1-ts35*. Synthetic viable phenotypes and colony analysis of wild-type, parent cells, *mid1*Δ, and double mutant isolates. All the cells were suspended at 1.5x10^6 cells/ml and subjected to 10-fold serial dilution. Cells suspended were pipetted onto solid YE media and incubated at four different temperatures (25ºC, 28ºC, 32ºC, and 37ºC). The analysis of growth phenotype was captured and interpreted after two days of cell growth on a solid YE medium. A double mutant wild-type and *vps4*Δ (GG 3487), B double mutant of *mid1* phospho-mutant *S531D* and *plo1-ts35* (GG 3419), and C double mutant of *mid1* phospho-mutant *S531A* and *plo1-ts35* (GG 3428). WT is wild-type, IWT is integrated wild-type, *mid1*Δ *is* Mid1p deletion, and *vps4*Δ is Vps4p deletion. Double mutants indicating growth rate defects are represented in red circles.

8.8 Synthetic viable phenotypes of *mid1* phospho-mutant and *plo1-ts35* (S167-332D and S167-332A)

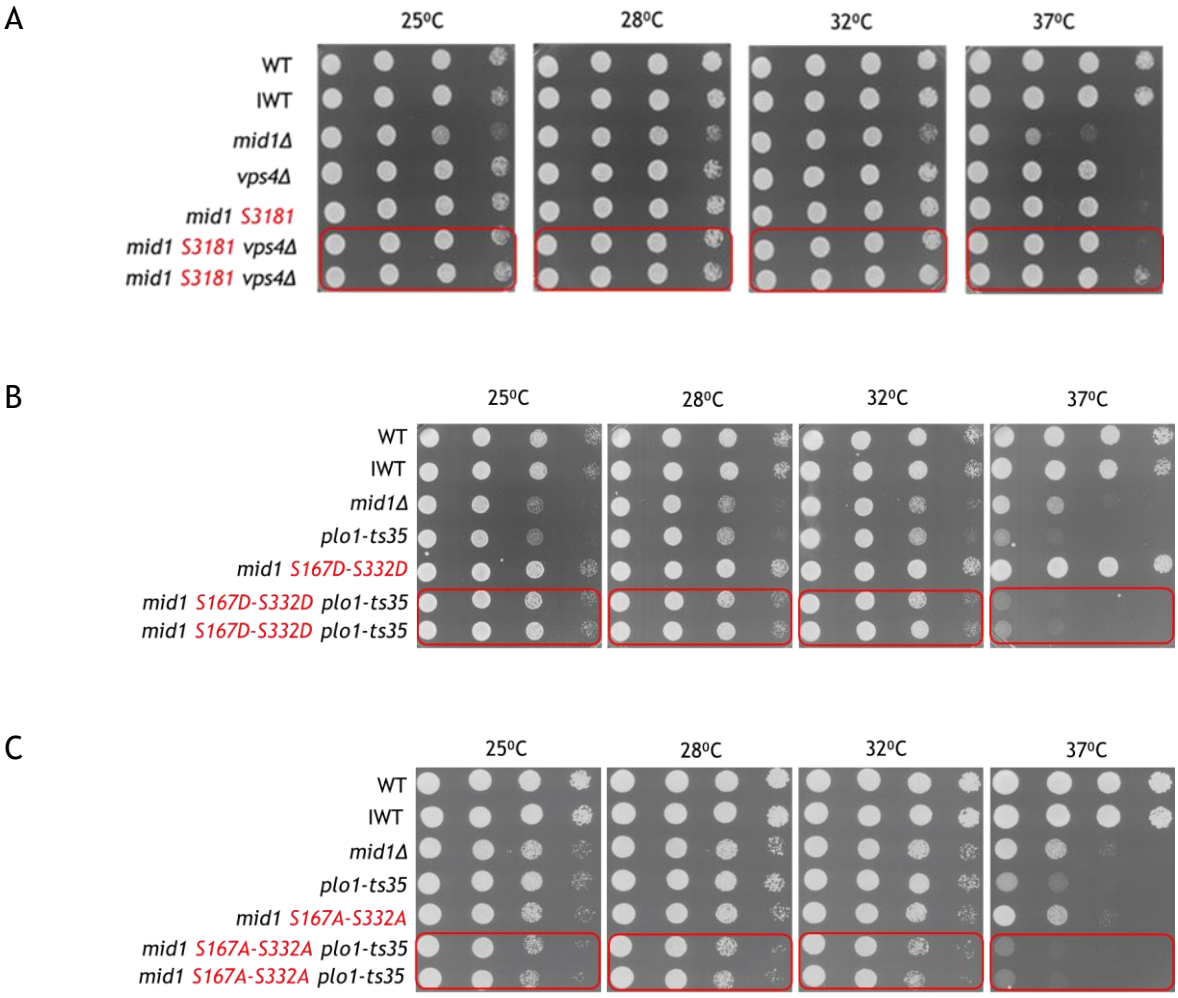

Figure 8-8 *mid1* phospho-mutant (S167-332D and S167-332A) shows synthetic viable phenotypes with *plo1-ts35*. Synthetic viable phenotypes and colony analysis of wild-type, parent cells, *mid1*Δ, and double mutant isolates. All the cells were suspended at 1.5x10^6 cells/ml and subjected to 10-fold serial dilution. Cells suspended were pipetted onto solid YE media and incubated at four different temperatures (25ºC, 28ºC, 32ºC, and 37ºC). The analysis of growth phenotype was captured and interpreted after two days of cell growth on a solid YE medium. A double mutant wild-type and *vps4*Δ (GG 3487), B double mutant of *mid1* phospho-mutant *S167-332D* and *plo1-ts35* (GG 3422), and C double mutant of *mid1* phospho-mutant *S167-531A* and *plo1-ts35* (GG 3467). WT is wild-type, IWT is integrated wild-type, *mid1*Δ *is* Mid1p deletion, and *vps4*Δ is Vps4p deletion. Double mutants indicating growth rate defects are represented in red circles.

8.9 Synthetic viable phenotypes of *mid1* phospho-mutant and *plo1-ts35* (S523-531D and S523-531A)

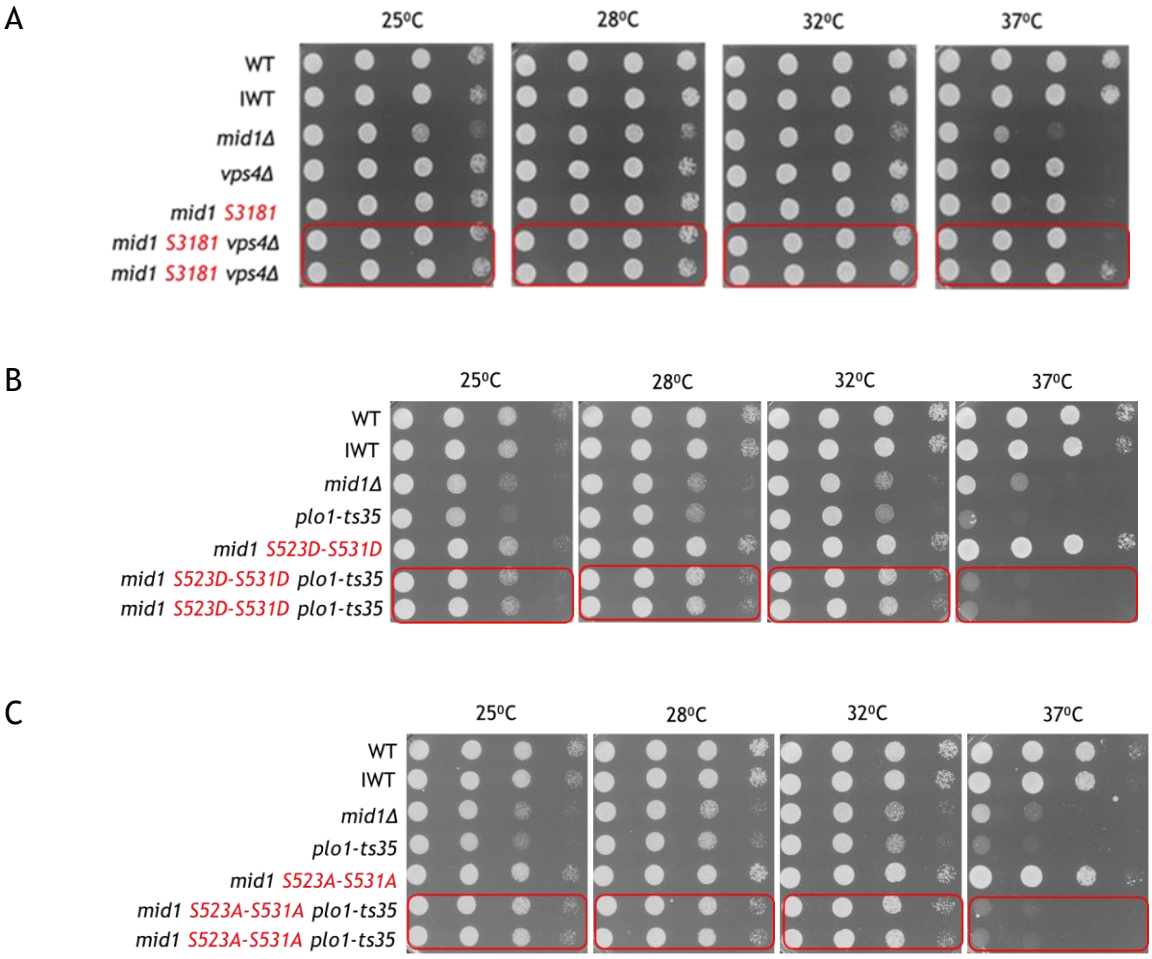

Figure 8-9 *mid1* phospho-mutant (S523-531D and S523-531A) shows synthetic viable phenotypes with *plo1-ts35*. Synthetic viable phenotypes and colony analysis of wild-type, parent cells, *mid1*Δ, and double mutant isolates. All the cells were suspended at 1.5x10^6 cells/ml and subjected to 10-fold serial dilution. Cells suspended were pipetted onto solid YE media and incubated at four different temperatures (25ºC, 28ºC, 32ºC, and 37ºC). The analysis of growth phenotype was captured and interpreted after two days of cell growth on a solid YE medium. A double mutant wild-type and *vps4*Δ (GG 3487), B double mutant of *mid1* phospho-mutant *S523-531D* and *plo1-ts35* (GG 3447), and C double mutant of *mid1* phospho-mutant *S167-531A* and *vps4*Δ (GG 3444). WT is wild-type, IWT is integrated wild-type, *mid1*Δ *is* Mid1p deletion, and *vps4*Δ is Vps4p deletion. Double mutants indicating growth rate defects are represented in red circles.

8.10 Synthetic viable phenotypes of *mid1* phospho-mutant and *ark1-T11* (S167D and S167A)

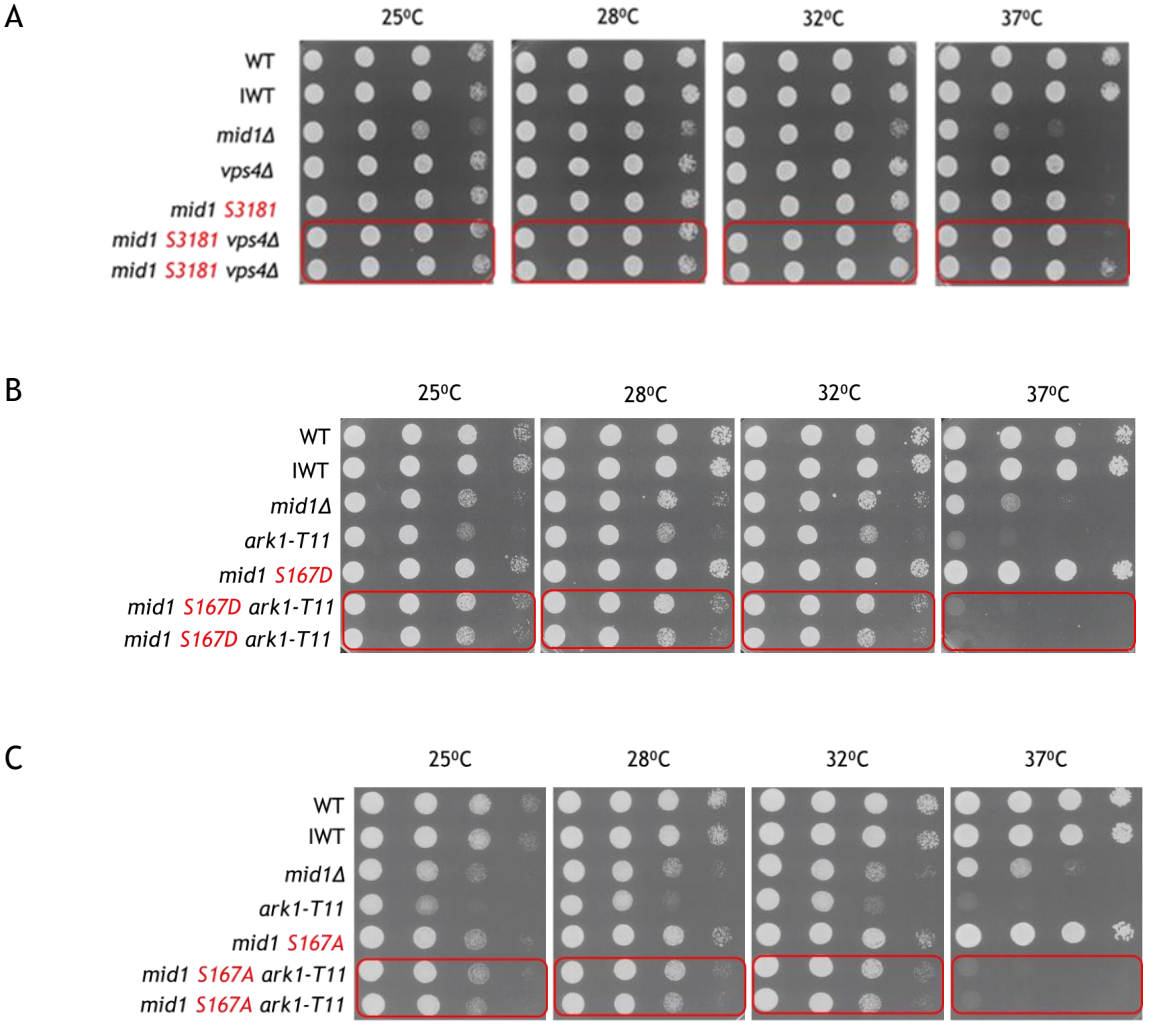

Figure 8-10 *mid1* phospho-mutant (S167D and S167A) shows synthetic viable phenotypes with *ark1-T11*. Synthetic viable phenotypes and colony analysis of wild-type, parent cells, *mid1*Δ, and double mutant isolates. All the cells were suspended at 1.5x10^6 cells/ml and subjected to 10-fold serial dilution. Cells suspended were pipetted onto solid YE media and incubated at four different temperatures (25ºC, 28ºC, 32ºC, and 37ºC). The analysis of growth phenotype was captured and interpreted after two days of cell growth on a solid YE medium. A double mutant wild-type and *vps4*Δ (GG 3487), B double mutant of *mid1* phospho-mutant *S167D* and *ark1-T11* (GG 3324), and C double mutant of *mid1* phospho-mutant *S167A* and *vps4*Δ (GG 3321). WT is wild-type, IWT is integrated wild-type, *mid1*Δ *is* Mid1p deletion, and *vps4*Δ is Vps4p deletion. Double mutants indicating growth rate defects are represented in red circles.

8.11 Synthetic viable phenotypes of *mid1* phospho-mutant and *ark1-T11* (S332D and S332A)

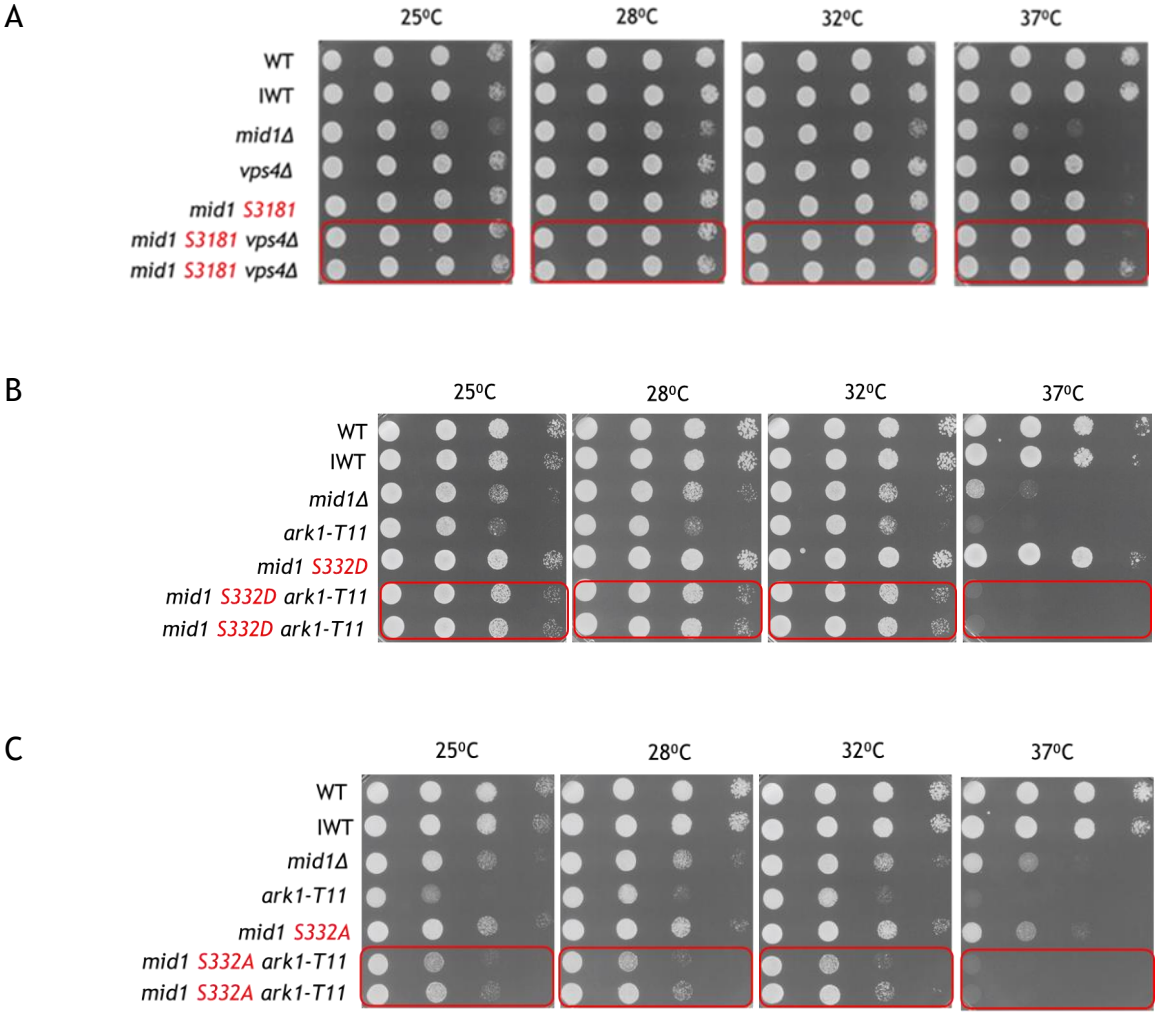

Figure 8-11 *mid1* phospho-mutant (S332D and S332A) shows synthetic viable phenotypes with *ark1-T11*. Synthetic viable phenotypes and colony analysis of wild-type, parent cells, *mid1*Δ, and double mutant isolates. All the cells were suspended at 1.5x10^6 cells/ml and subjected to 10-fold serial dilution. Cells suspended were pipetted onto solid YE media and incubated at four different temperatures (25ºC, 28ºC, 32ºC, and 37ºC). The analysis of growth phenotype was captured and interpreted after two days of cell growth on a solid YE medium. A double mutant wild-type and *vps4*Δ (GG 3487), B double mutant of *mid1* phospho-mutant *S332D* and *ark1-T11* (GG 3339), and C double mutant of *mid1* phospho-mutant *S332A* and *vps4*Δ (GG 3333). WT is wild-type, IWT is integrated wild-type, *mid1*Δ *is* Mid1p deletion, and *vps4*Δ is Vps4p deletion. Double mutants indicating growth rate defects are represented in red circles.

8.12 Synthetic viable phenotypes of *mid1* phospho-mutant and *ark1-T11* (S531D and S531A)

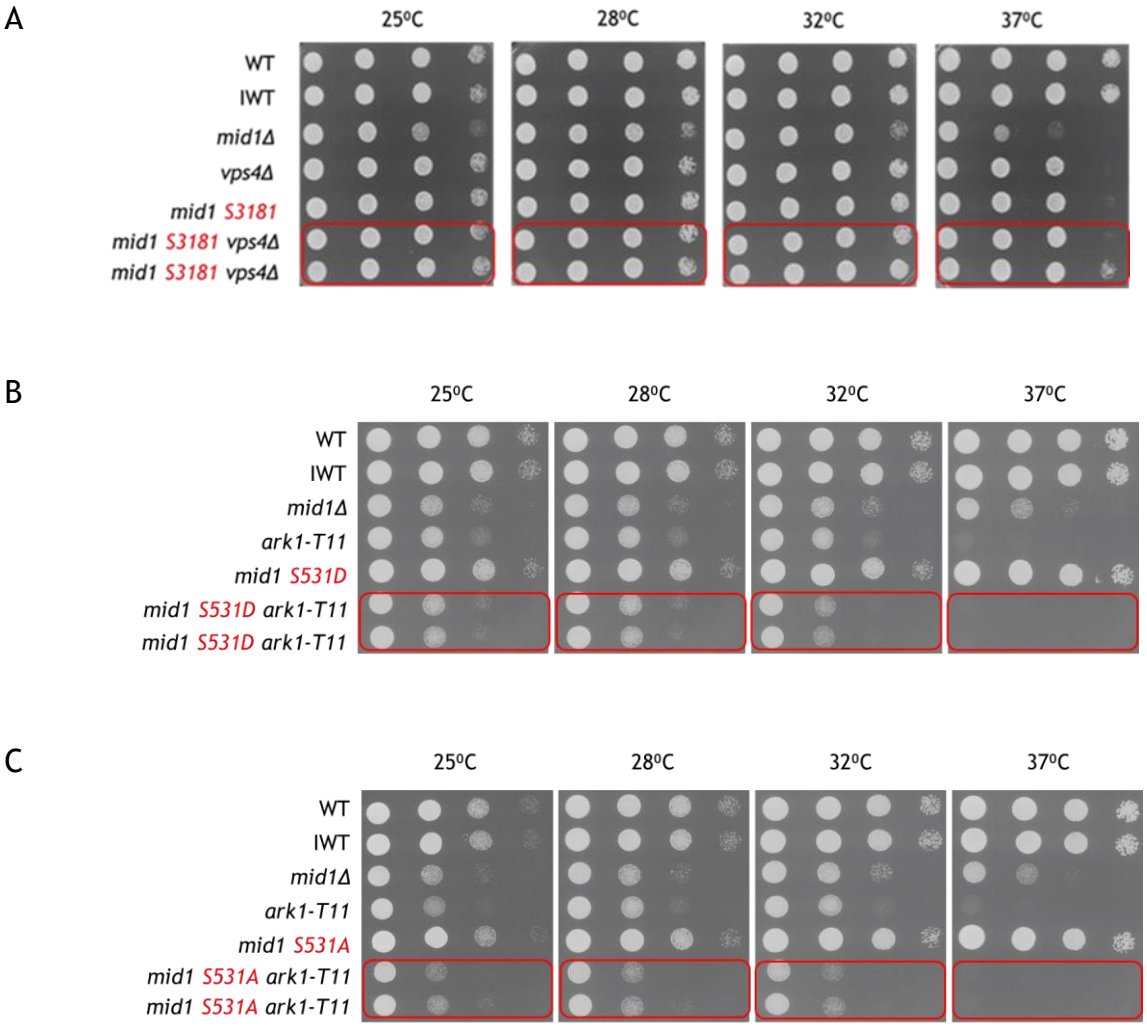

Figure 8-12 *mid1* phospho-mutant (S531D and S531A) shows synthetic viable phenotypes with *ark1-T11*. Synthetic viable' phenotypes and colony analysis of wild-type, parent cells, *mid1*Δ, and double mutant isolates. All the cells were suspended at 1.5x10^6 cells/ml and subjected to 10-fold serial dilution. Cells suspended were pipetted onto solid YE media and incubated at four different temperatures (25ºC, 28ºC, 32ºC, and 37ºC). The analysis of growth phenotype was captured and interpreted after two days of cell growth on a solid YE medium. A double mutant wild-type and *vps4*Δ (GG 3487), B double mutant of *mid1* phospho-mutant *S531D* and *ark1-T11* (GG 3345), and C double mutant of *mid1* phospho-mutant *S531A* and *ark1-T11* (GG 3239). WT is wild-type, IWT is integrated wild-type, *mid1*Δ *is* Mid1p deletion, and *vps4*Δ is Vps4p deletion. Double mutants indicating growth rate defects are represented in red circles.

8.13 Synthetic viable phenotypes of *mid1* phospho-mutant and *ark1-T11* (S523-531A and S523-531A)

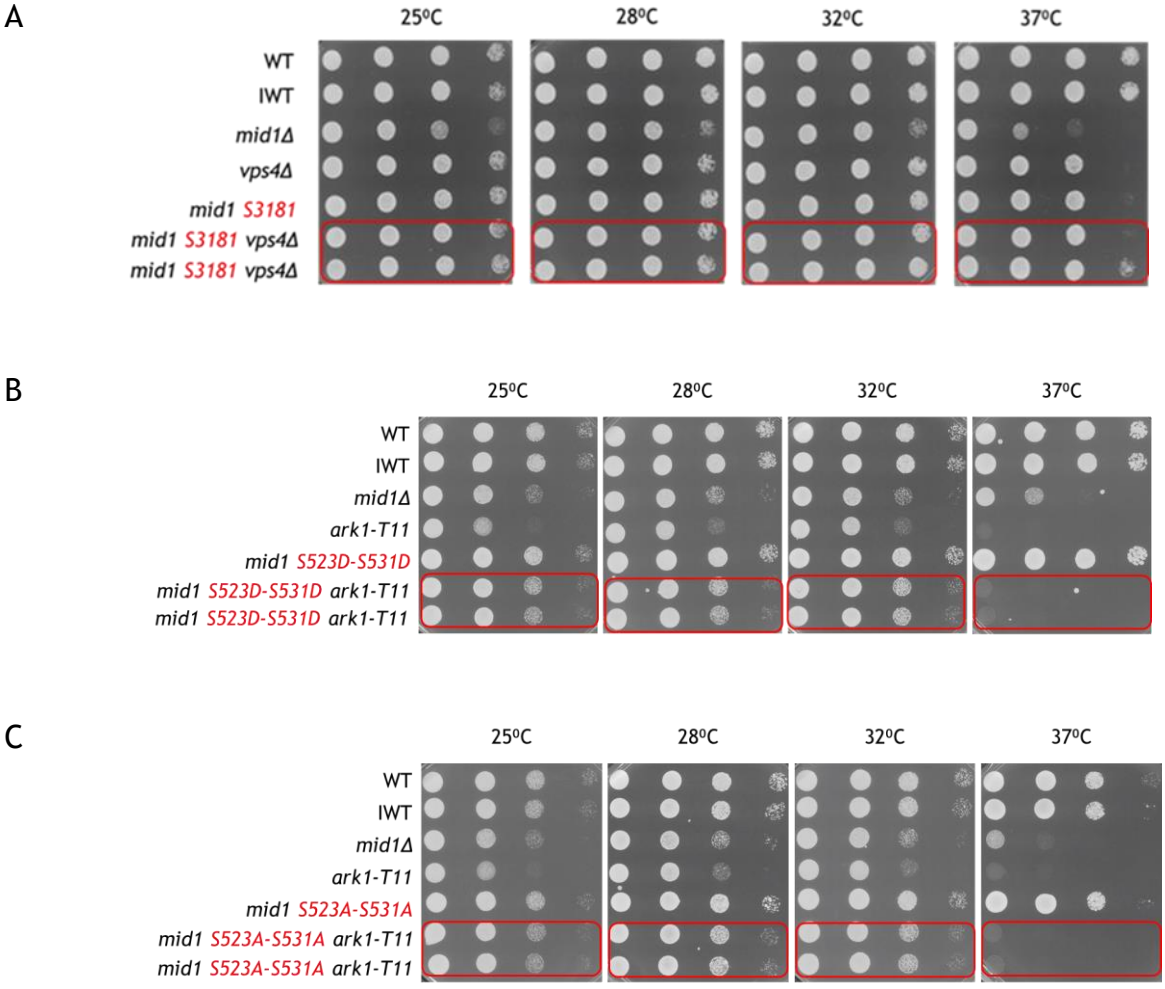

Figure 8-13 *mid1* phospho-mutant (S523-531A and S523-531A) shows synthetic viable phenotypes with *ark1-T11*. Synthetic viable phenotypes and colony analysis of wild-type, parent cells, *mid1*Δ, and double mutant isolates. All the cells were suspended at 1.5x10^6 cells/ml and subjected to 10-fold serial dilution. Cells suspended were pipetted onto solid YE media and incubated at four different temperatures (25ºC, 28ºC, 32ºC, and 37ºC). The analysis of growth phenotype was captured and interpreted after two days of cell growth on a solid YE medium. A double mutant wild-type and *vps4*Δ (GG 3487), B double mutant of *mid1* phospho-mutant *S523-531D* and *vps4*Δ (GG 3246), and C double mutant of *mid1* phospho-mutant *S523-531A* and *ark1-T11* (GG 3242). WT is wild-type, IWT is integrated wild-type, *mid1*Δ *is* Mid1p deletion, and *vps4*Δ is Vps4p deletion. Double mutants indicating growth rate defects are represented in red circles.

8.14 Synthetic viable phenotypes of *mid1* phospho-mutant and *ark1-T11* (S167-332D and S167-332A)

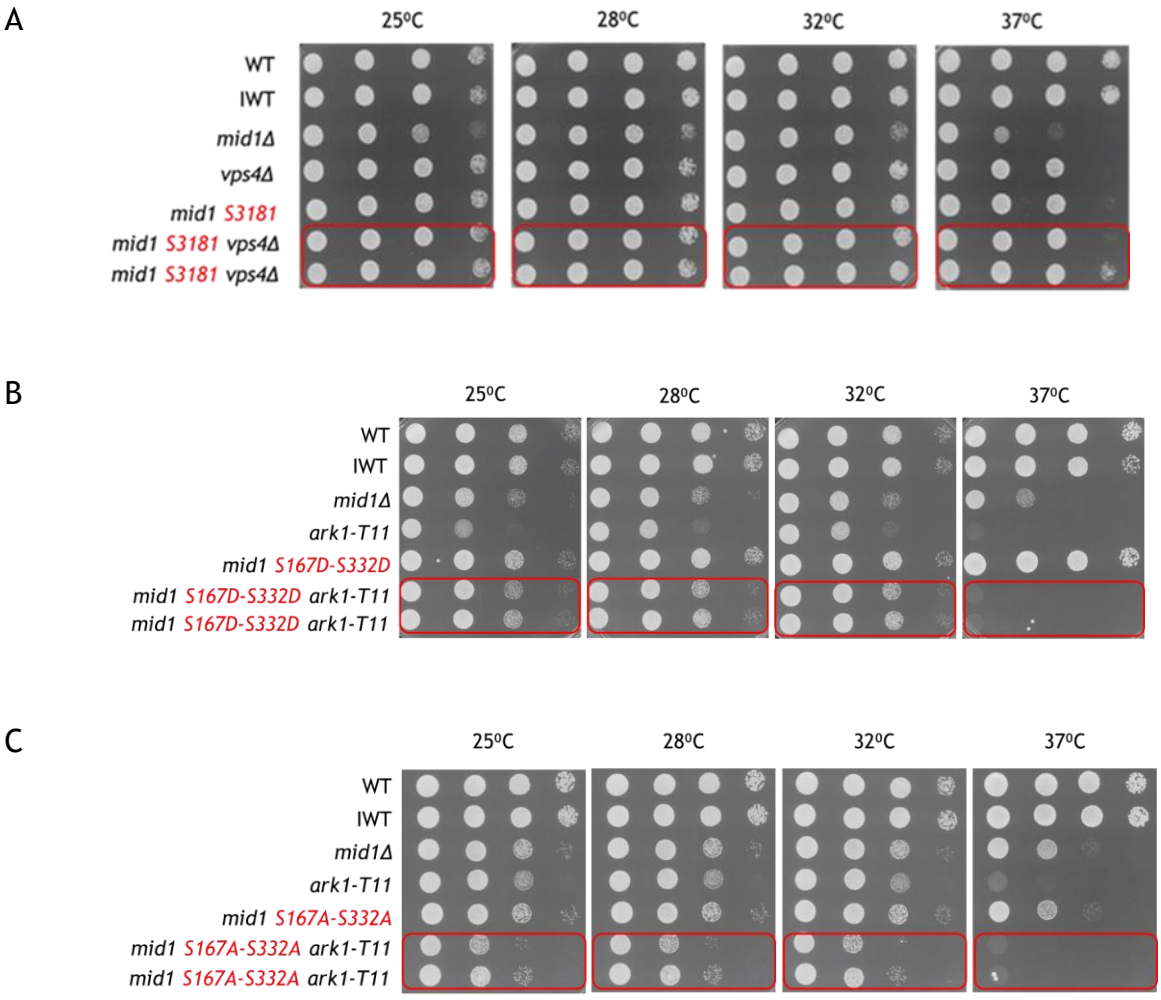

Figure 8-14 *mid1* phospho-mutant (S167-332D and S167-332A) shows synthetic viable phenotypes with *ark1-T11*. Synthetic viable phenotypes and colony analysis of wild-type, parent cells, *mid1*Δ, and double mutant isolates. All the cells were suspended at 1.5x10^6 cells/ml and subjected to 10-fold serial dilution. Cells suspended were pipetted onto solid YE media and incubated at four different temperatures (25ºC, 28ºC, 32ºC, and 37ºC). The analysis of growth phenotype was captured and interpreted after two days of cell growth on a solid YE medium. A double mutant wild-type and *vps4*Δ (GG 3487), B double mutant of *mid1* phospho-mutant *S167-332D* and *vps4*Δ (GG 3349), and C double mutant of *mid1* phospho-mutant *S167-332A* and *ark1-T11* (GG 3352). WT is wild-type, IWT is integrated wild-type, *mid1*Δ *is* Mid1p deletion, and *vps4*Δ is Vps4p deletion. Double mutants indicating growth rate defects are represented in red circles.

9 Appendix 3 Summary of classification of *mid1* phospho-mutant septation and localization phenotype in the study

9.1 Quantification of synthetic septation defective phenotypes in *mid1* phospho-mutant cells

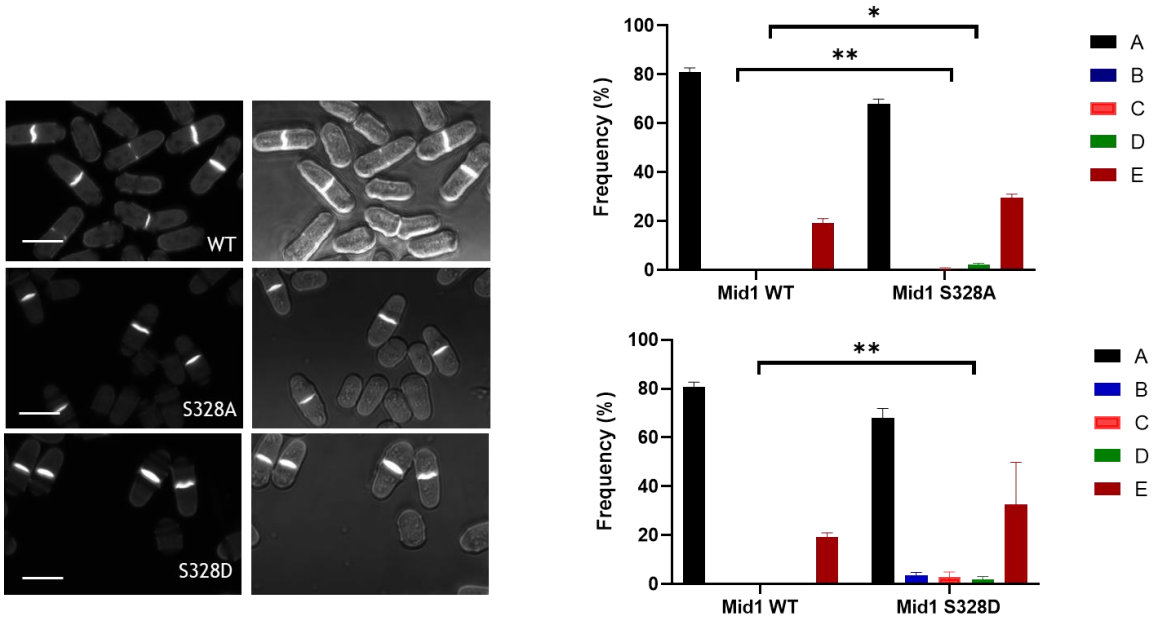

Figure 9-1 Classification and quantification of synthetic septation defects in Mid1p wild-type and *mid1* phospho-mutant cells. Division septa were visualized using calcofluor-white, examined by the fluorescence confocal microscope, and each phenotype's frequency was recorded. 400 cells in total were counted over three technical replicates, performed on three independent occasions for each genotype. Wild-type and *mid1* phospho-mutant strains were cultured in liquid YE media at 28ºC for 18 hours. 2-way ANOVA statistical analysis for the quantification of frequencies of the localization phenotypes in Mid1p W-T and *mid1* phospho-mutant cells, the frequencies were compared. Asterisks (**) denote a p-value =0.002 (*) denote a p-value =0.0119, and Error bars represent SEM. representative images of calcofluor-white stained cells. The scale bar represents 30 µm.

9.2 Quantification of synthetic septation defective phenotypes in *mid1* phospho-mutant cells

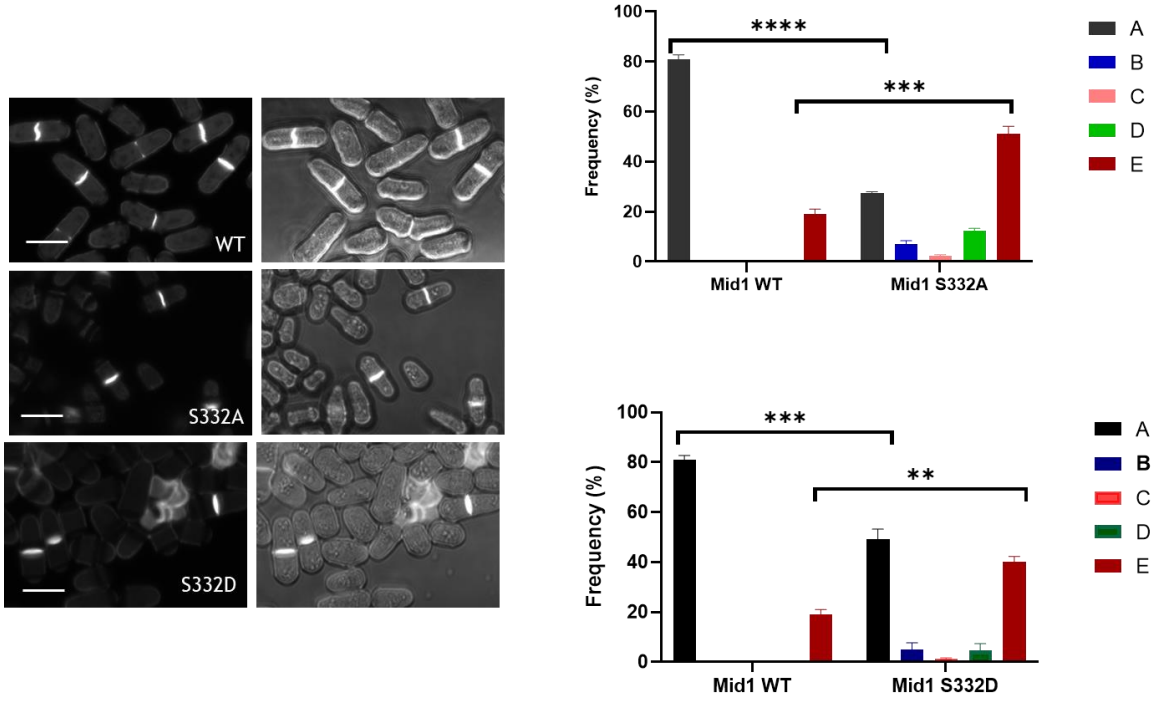

Figure 9-2 Classification and quantification of synthetic septation defects in Mid1p wild-type and *mid1* phospho-mutant cells. Division septa were visualized using calcofluor-white, examined by the fluorescence confocal microscope, and each phenotype's frequency was recorded. 400 cells in total were counted over three technical replicates, performed on three independent occasions for each genotype. Wild-type and *mid1* phospho-mutant strains were cultured in liquid YE media at 28ºC for 18 hours. 2-way ANOVA statistical analysis for the quantification of frequencies of the localization phenotypes in Mid1p W-T and *mid1* phospho-mutant cells, the frequencies were compared. Asterisks (****) denote a p-value <0.0001 (***) denote a p-value =0.0007, and error bars represent SEM. representative images of calcofluor-white stained cells. The scale bar represents 30 µm.

9.3 Quantification of synthetic septation defective phenotypes in *mid1* phospho-mutant cells

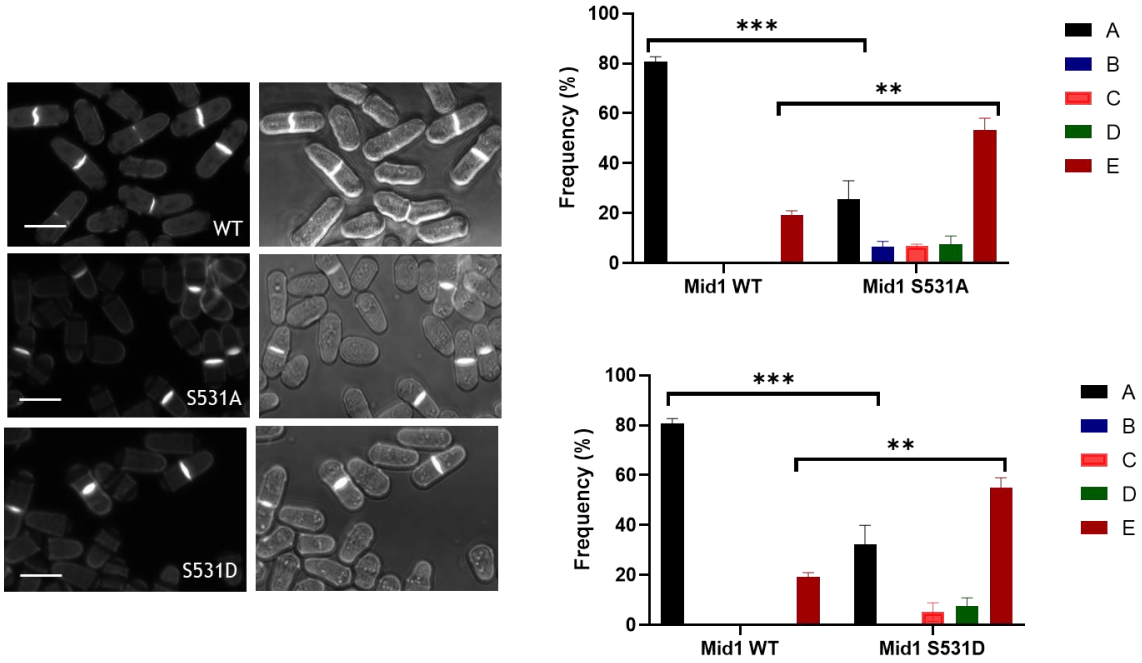

Figure 9-3 Classification and quantification of synthetic septation defects in Mid1p wild-type and *mid1* phospho-mutant cells. Division septa were visualized using calcofluor-white, examined by the fluorescence confocal microscope, and each phenotype's frequency was recorded. 400 cells in total were counted over three technical replicates, performed on three independent occasions for each genotype. Wild-type and *mid1* phospho-mutant strains were cultured in liquid YE media at 28ºC for 18 hours. 2-way ANOVA statistical analysis for the quantification of frequencies of the localization phenotypes in Mid1p W-T and *mid1* phospho-mutant cells, the frequencies were compared. Asterisks (***) denote a p-value =0006 (**) denote a p-value =0.0033, and error bars represent SEM. representative images of calcofluor-white stained cells. The scale bar represents 30 µm.

9.4 Quantification of synthetic septation defective phenotypes in *mid1* phospho-mutant cells

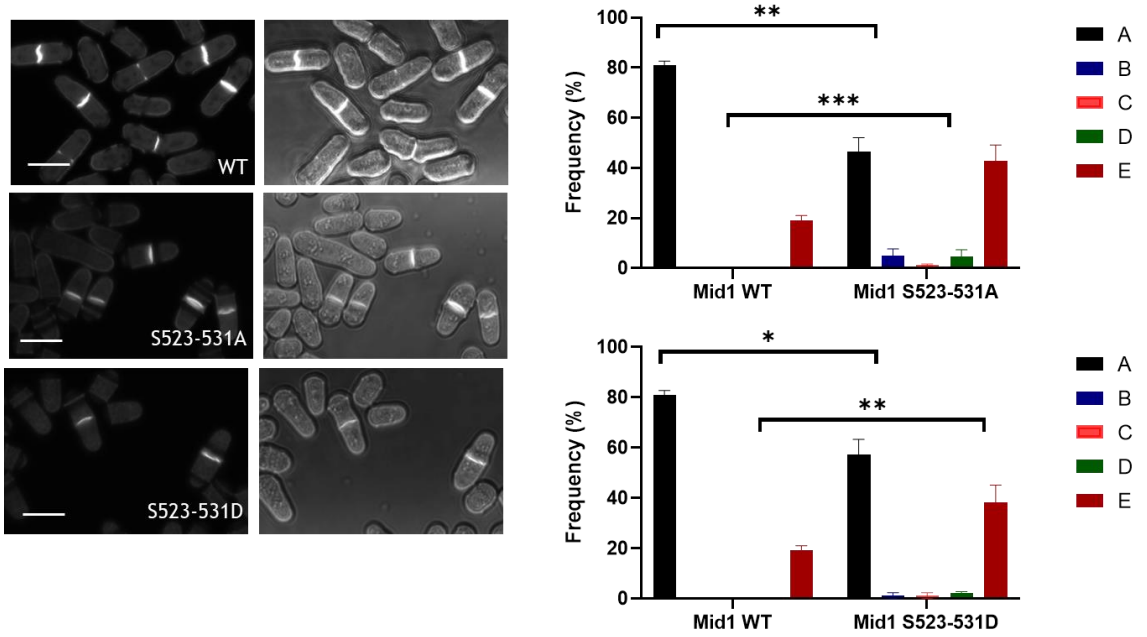

Figure 9-4 Classification and quantification of synthetic septation defects in Mid1p wild-type and *mid1* phospho-mutant cells. Division septa were visualized using calcofluor-white, examined by the fluorescence confocal microscope, and each phenotype's frequency was recorded. 400 cells in total were counted over three technical replicates, performed on three independent occasions for each genotype. Wild-type and *mid1* phospho-mutant strains were cultured in liquid YE media at 28ºC for 18 hours. 2-way ANOVA statistical analysis for the quantification of frequencies of the localization phenotypes in Mid1p W-T and *mid1* phospho-mutant cells, the frequencies were compared. Asterisks (***) denote a p-value =0.0002 (**) denote a p-value =0025, and error bars represent SEM. representative images of calcofluor-white stained cells. The scale bar represents 30 µm.

9.5 Quantification of synthetic septation defective phenotypes in *mid1* phospho-mutant cells

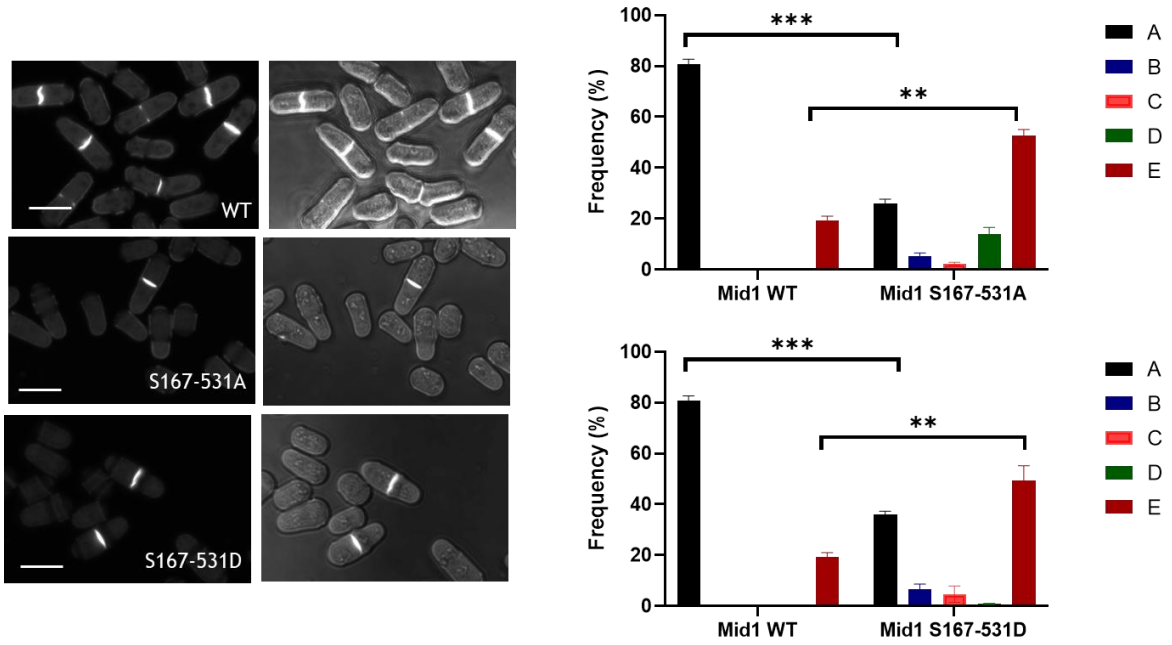

Figure 9-5 Classification and quantification of synthetic septation defects in Mid1p wild-type and *mid1* phospho-mutant cells. Division septa were visualized using calcofluor-white, examined by the fluorescence confocal microscope, and each phenotype's frequency was recorded. 400 cells in total were counted over three technical replicates, performed on three independent occasions for each genotype. Wild-type and *mid1* phospho-mutant strains were cultured in liquid YE media at 28ºC for 18 hours. 2-way ANOVA statistical analysis for the quantification of frequencies of the localization phenotypes in Mid1p W-T and *mid1* phospho-mutant cells, the frequencies were compared. Asterisks (***) denote a p-value <0.0001 (**) denote a p-value =0.0060, and error bars represent SEM. representative images of calcofluor-white stained cells. The scale bar represents 30 µm.

9.6 Quantification of GFP-Mid1p localization phenotypes in wild-type and *mid1* phospho-mutant cells

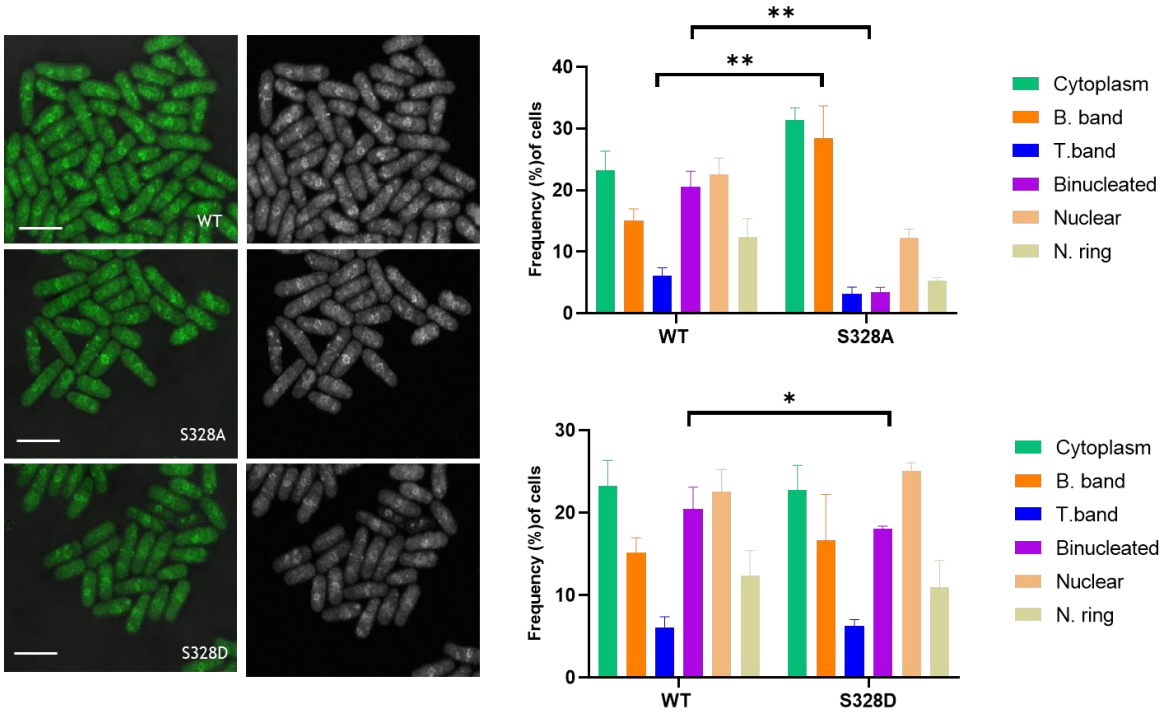

Figure 9-6 Classification and quantification of GFP-Mid1p localization phenotypes in wild-type and *mid1* phospho-mutant cells. Localization patterns were visualized and examined by the fluorescence confocal microscope, and each phenotype's frequency was recorded. 200 cells in total were counted over three technical replicates, performed on three independent occasions for each genotype (biological replicates). Wild-type and phosphor-mutant strains were cultured in liquid YE media at 28ºC for 18 hours. 2-way ANOVA statistical analysis for the quantification of frequencies of the localization phenotypes in Mid1p W-T and *mid1* phospho-mutant cells, the frequencies were compared. Asterisks (**) denote a p-value =0.0013, (**) denote a p-value =0.0036, (*) denote a p-value =0.0065 and error bars represent SEM. representative images of calcofluor-white stained cells. The scale bar represents 10 µm.

9.7 Quantification of GFP-Mid1p localization phenotypes in wild-type and *mid1* phospho-mutant cells

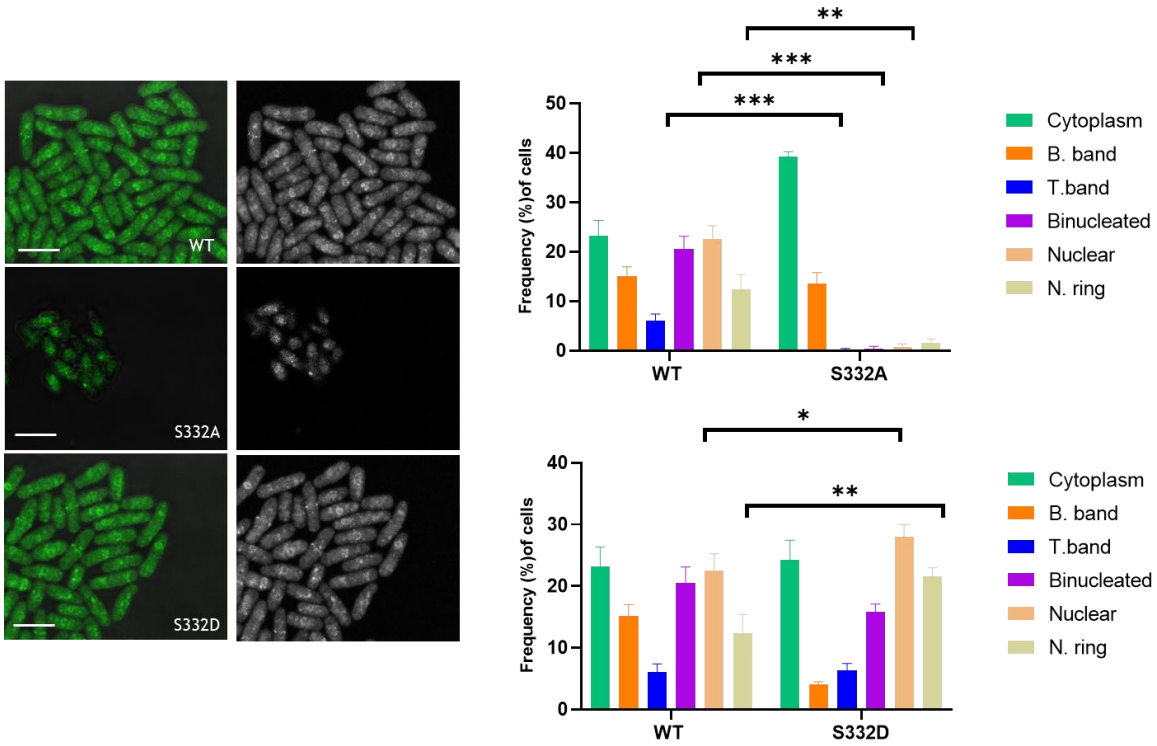

Figure 9-7 Classification and quantification of GFP-Mid1p localization phenotypes in wild-type and *mid1* phospho-mutant cells. Localization patterns were visualized and examined by the fluorescence confocal microscope, and each phenotype's frequency was recorded. 200 cells in total were counted over three technical replicates, performed on three independent occasions for each genotype (biological replicates). Wild-type and phosphor-mutant strains were cultured in liquid YE media at 28ºC for 18 hours. 2-way ANOVA statistical analysis for the quantification of frequencies of the localization phenotypes in Mid1p W-T and *mid1* phospho-mutant cells, the frequencies were compared. Asterisks (***) denote a p-value =0.0003, (***) denote a p-value =0.0007, (**) denote a p-value =0.0065 and error bars represent SEM. representative images of calcofluor-white stained cells. The scale bar represents 10 µm.

9.8 Quantification of GFP-Mid1p localization phenotypes in wild-type and *mid1* phospho-mutant cells

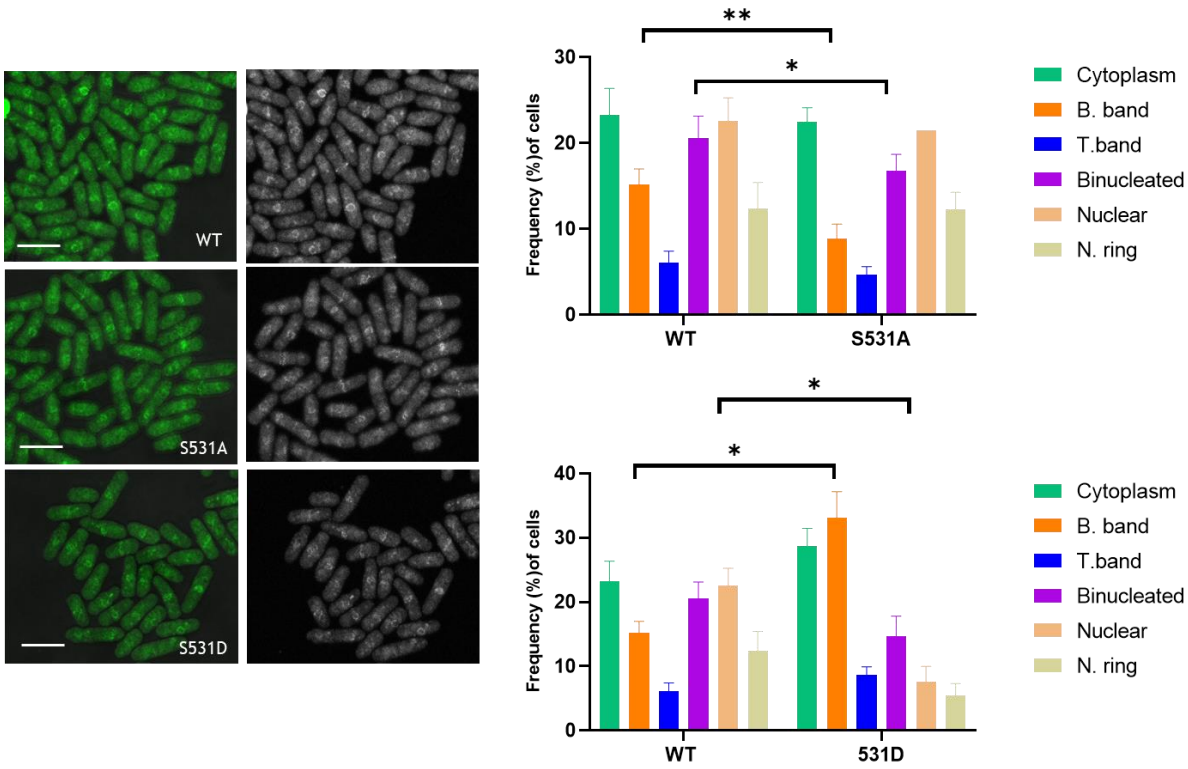

Figure 9-8 Classification and quantification of GFP-Mid1p localization phenotypes in wild-type and *mid1* phospho-mutant cells. Localization patterns were visualized and examined by the fluorescence confocal microscope, and each phenotype's frequency was recorded. 200 cells in total were counted over three technical replicates, performed on three independent occasions for each genotype (biological replicates). Wild-type and phosphor-mutant strains were cultured in liquid YE media at 28ºC for 18 hours. 2-way ANOVA statistical analysis for the quantification of frequencies of the localization phenotypes in Mid1p W-T and *mid1* phospho-mutant cells, the frequencies were compared. Asterisks (**) denote a p-value =0.0020, (*) denote a p-value =0.00270, (**) and error bars represent SEM. representative images of calcofluor-white stained cells. The scale bar represents 10 µm.

9.9 Quantification of GFP-Mid1p localization phenotypes in wild-type and *mid1* phospho-mutant cells

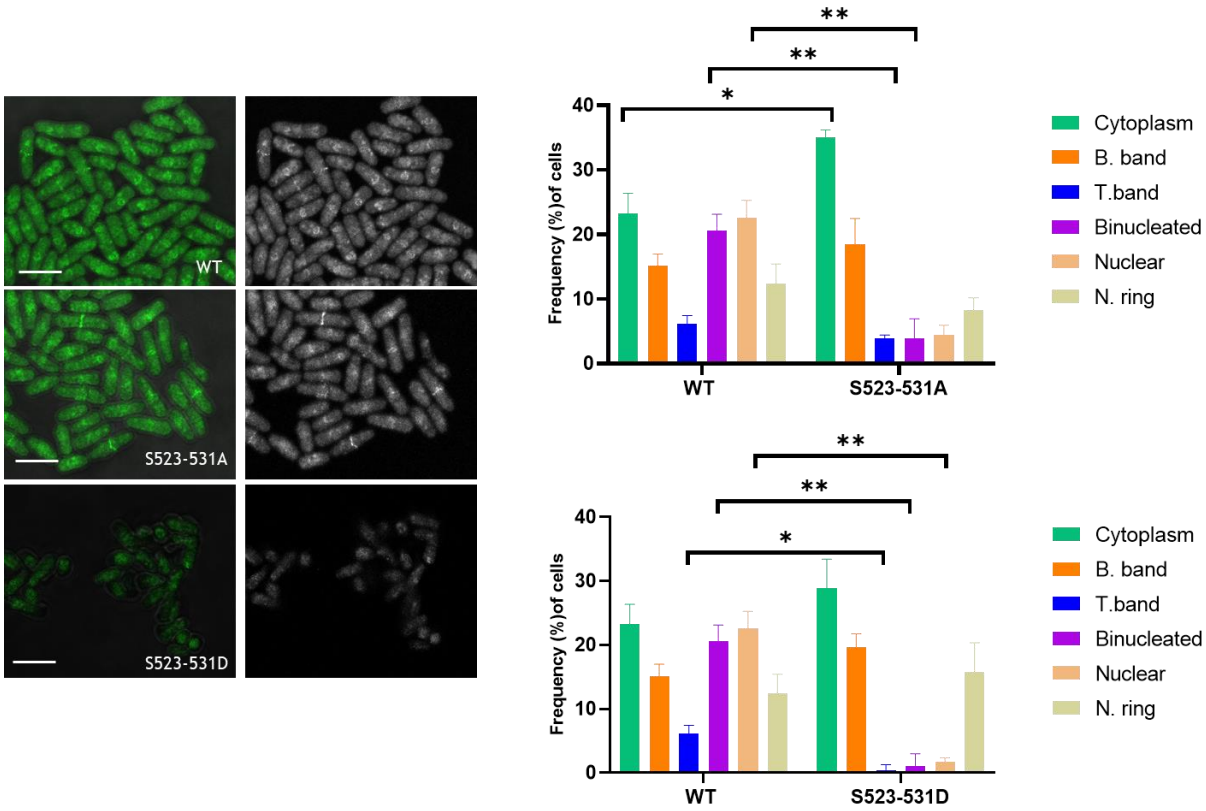

Figure 9-9 Classification and quantification of GFP-Mid1p localization phenotypes in wild-type and *mid1* phospho-mutant cells. Localization patterns were visualized and examined by the fluorescence confocal microscope, and each phenotype's frequency was recorded. 200 cells in total were counted over three technical replicates, performed on three independent occasions for each genotype (biological replicates). Wild-type and phosphor-mutant strains were cultured in liquid YE media at 28ºC for 18 hours. 2-way ANOVA statistical analysis for the quantification of frequencies of the localization phenotypes in Mid1p W-T and *mid1* phospho-mutant cells, the frequencies were compared. Asterisks (**) denote a p-value =0.0080, (**) denote a p-value =0.0022, (*) denote a p-value =0.0171 and error bars represent SEM. representative images of calcofluor-white stained cells. The scale bar represents 10 µm.

9.10 Quantification of GFP-Mid1p localization phenotypes in wild-type and *mid1* phospho-mutant cells

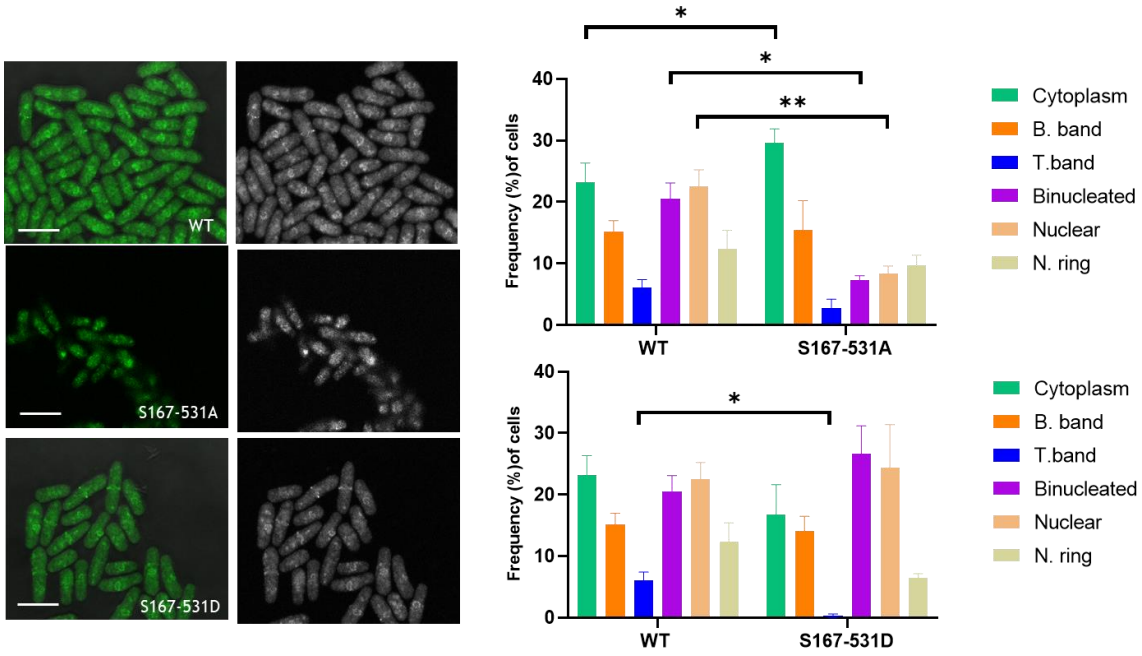

Figure 9-10 Classification and quantification of GFP-Mid1p localization phenotypes in wild-type and *mid1* phospho-mutant cells. Localization patterns were visualized and examined by the fluorescence confocal microscope, and each phenotype's frequency was recorded. 200 cells in total were counted over three technical replicates, performed on three independent occasions for each genotype (biological replicates). Wild-type and phosphor-mutant strains were cultured in liquid YE media at 28ºC for 18 hours. 2-way ANOVA statistical analysis for the quantification of frequencies of the localization phenotypes in Mid1p W-T and *mid1* phospho-mutant cells, the frequencies were compared. Asterisks (**) denote a p-value =0.0045, (*) denote a p-value =0.0221, (*) denote a p-value =0.0207 and error bars represent SEM. representative images of calcofluor-white stained cells. The scale bar represents 10 µm.

Appendix 4

CELL CYCLE
2021, VOL. 20, NO. 18, 1845–1860
https://doi.org/10.1080/15384101.2021.1962637

Taylor & Francis
Taylor & Francis Group

RESEARCH PAPER

OPEN ACCESS Check for updates

Anillin/Mid1p interacts with the ESCRT-associated protein Vps4p and mitotic kinases to regulate cytokinesis in fission yeast

Imane M. Rezig [a], Wandiahyel G. Yaduma [a], Gwyn W. Gould [a,b], and Christopher J. McInerny [c]

[a]Institute of Molecular, Cell and Systems Biology, College of Medical, Veterinary and Life Sciences, University of Glasgow, Glasgow, UK; [b]Strathclyde Institute of Pharmacy and Biomedical Sciences, University of Strathclyde, Glasgow, UK; [c]School of Life Sciences, College of Medical, Veterinary and Life Sciences, University of Glasgow, Glasgow, UK

ABSTRACT

Cytokinesis is the final stage of the cell cycle which separates cellular constituents to produce two daughter cells. Using the fission yeast *Schizosaccharomyces pombe* we have investigated the role of various classes of proteins involved in this process. Central to these is anillin/Mid1p which forms a ring-like structure at the cell equator that predicts the site of cell separation through septation in fission yeast. Here we demonstrate a direct physical interaction between Mid1p and the endosomal sorting complex required for transport (ESCRT)-associated protein Vps4p, a genetic interaction of the *mid1* and *vps4* genes essential for cell viability, and a requirement of Vps4p for the correct cellular localization of Mid1p. Furthermore, we show that Mid1p is phosphorylated by aurora kinase, a genetic interaction of the *mid1* and the aurora kinase *ark1* genes is essential for cell viability, and that Ark1p is also required for the correct cellular localization of Mid1p. We mapped the sites of phosphorylation of Mid1p by human aurora A and the polo kinase Plk1 and assessed their importance in fission yeast by mutational analysis. Such analysis revealed serine residues S332, S523 and S531 to be required for Mid1p function and its interaction with Vps4p, Ark1p and Plo1p. Combined these data suggest a physical interaction between Mid1p and Vps4p important for cytokinesis, and identify phosphorylation of Mid1p by aurora and polo kinases as being significant for this process.

ARTICLE HISTORY
Received 20 May 2021
Revised 1 July 2021
Accepted 10 July 2021

KEYWORDS
Cell cycle; fission yeast; Mid1p; Vps4p; aurora kinase; polo kinase

Introduction

Much is understood about the control and regulation of the cell division cycle, with many critical cell cycle mechanisms identified being evolutionarily conserved, present across the eukaryotic kingdom. One cell cycle stage that has been increasingly studied is cytokinesis where DNA, organelles and cell constituents are partitioned and allocated to two daughter cells during their physical separation. The fission yeast *Schizosaccharomyces pombe* has proven to be an excellent model organism to study the eukaryotic cell cycle [1]. It is especially useful for studying cytokinesis and cell division as, explicit in its name, it divides by medial fission involving a contractile actomyosin ring leading to the process of cell separation, which is similar to these processes in mammalian cells [2].

A number of proteins have been identified that regulate cytokinesis in fission yeast including those in a signal transduction pathway named the Septation Initiation Network (SIN) [3]. The SIN proteins form a pathway that facilitates contractile ring constriction and promotes the formation of a medial cell wall-like structure between the two daughter cells, called the septum. Furthermore, SIN components associate with the spindle pole bodies and link mitotic exit with cytokinesis [4]. Sid2p is one regulator of the SIN-cascade of signaling proteins [5]. It terminates the signaling cascade leading to the transition from the spindle pole bodies to the cell division site promoting the onset of cytokinesis [6]. A recent study identified anillin/Mid1p as a substrate for Sid2p and indicated that the phosphorylation of Mid1p facilitates its removal from the cell cortex during the actomyosin contractile ring constriction [7].

Mid1p forms a ring-like structure at the cell equator that predicts the site of cell separation through the formation of a septum in fission

CONTACT Christopher J. McInerny Chris.McInerny@glasgow.ac.uk
Supplemental data for this article can be accessed here

yeast [8–10]. In cells containing a chromosomal deletion of the *mid1* gene (*mid1Δ*), a misshaped contractile ring is assembled during anaphase when the SIN pathway becomes active; such observations confirm the important role of Mid1p in directing contractile ring assembly to its correct location [11–13].

Many other groups of proteins have a role in septum formation in *S. pombe*. Among these the various classes of ESCRT proteins, including the ESCRT-III regulator Vps4p, were found to be required for septation, suggesting that they have a role in cytokinesis in fission yeast [14,15]. Additional experiments suggested that the ESCRT proteins interacted with established cell cycle regulators including the polo kinase Plo1p, the aurora kinase Ark1p and the CDC14 phosphatase, Clp1p to control these processes [14].

In mammalian cells the absence of the ESCRT proteins leads to inhibition of cytokinesis [15–18]. The ESCRT machinery is assembled to catalyze membrane remodeling events allowing for the final separation of the daughter cells [19]. This process is mediated by many cytokinesis proteins including ESCRT-I and III classes of proteins in addition to the ATPase VPS4 [20].

As a way to further understand the regulation of ESCRT proteins during cytokinesis in fission yeast we sought to identify other proteins that interact with anillin/Mid1p. Here we describe a direct physical interaction between Vps4p and the anillin Mid1p which is required for cell viability and for the correct placement of Mid1p. We further show an interaction between Mid1p and the aurora kinase Ark1p which is required for cell viability and identify phospho-acceptor sites in Mid1p and study their role using mutagenesis. Collectively, our observations reveal novel mechanisms by which cytokinesis is regulated by different classes of proteins acting through Mid1p.

Results and discussion

Genetic and physical interactions between Mid1p and Vps4p in fission yeast

Previously, we identified and characterized the requirement and role of ESCRT proteins for cytokinesis in fission yeast [21]. These experiments also revealed the interaction of ESCRT proteins with three cell cycle regulators, the Polo-like kinase Plo1p, the aurora kinase Ark1p and the CDC14 phosphatase Clp1p. These observations offered a framework by which ESCRT proteins are regulated to control cytokinesis. To further explore ways in which the ESCRT proteins might integrate with other cell cycle regulators to control cytokinesis, we examined their interaction with the anillin Mid1p. Mid1p has a central structural role in cytokinesis forming equatorial nodes to create an annular shaped structure that determines the position of the division plane [13,22].

We initiated this by searching for genetic interactions between the *mid1* gene and genes encoding ESCRTs and ESCRT-associated proteins. Double mutant fission yeast strains were created containing a chromosomal deletion of *mid1* (*mid1Δ*) and individual chromosomal deletions of ESCRT genes from Classes E-0 to E-III and *vps4* and searching for synthetic phenotypes. *mid1Δ* was combined with *sst4Δ* (E-0), *sst6Δ* and *vps28Δ* (E-I), *vps36Δ* and *vps25Δ* (EII), *vps20Δ*, *vps32Δ* and *vps2Δ* (E III), and *vps4Δ* [21,23]. In each case double mutants were created which were viable, with no apparent synthetic phenotypes. The exception was *mid1Δ vps4Δ* which instead failed to form viable colonies, with cells undergoing just a few divisions, and so was synthetically lethal (Figure 1a).

This striking observation demonstrated a genetic interaction between the *mid1* and *vps4* genes, with one explanation that the two encoded proteins interact to control an essential cellular function. Antibodies to yeast Vps4p are not available to test this hypothesis in intact cells, therefore we expressed and purified a full-length His-tagged version of Vps4p protein from bacteria, using the same method to express and purify three different GST-tagged domains of Mid1p. Full length Mid1p was not purified as it is insoluble under such conditions [22,24].

Full length Mid1p is 920 amino acids in length; the three domains used in pull-down experiments described here encompass the amino acids 1–453 (“N-term”), 452–579 (“Middle”) and 798–920 (“C-term”) [24,25]. Of these three domains, only the C-terminal domain comprised amino acids 798–920 was pulled-down by recombinant Vps4p

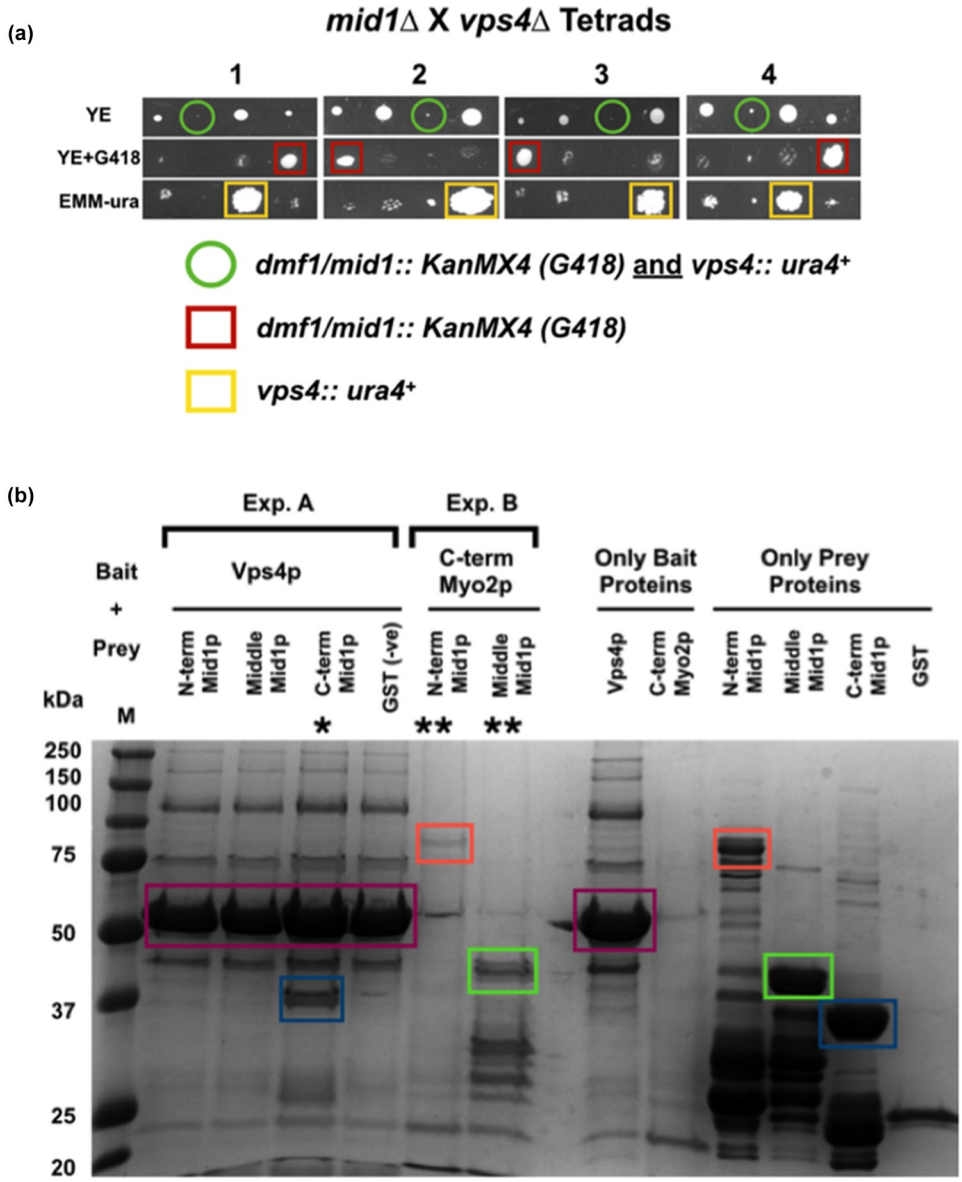

Figure 1. Genetic and physical interactions between *mid1* and *vps4* in fission yeast. (a) Synthetic lethality in *mid1*Δ *vps4*Δ double mutant cells indicates a genetic interaction between the *mid1* and *vps4* genes. Tetrad analysis of h^- *vps4*Δ (*vps4::ura4*$^+$) mated with h^+ *mid1*Δ (*dmf1::KanMX4*) to identify *vps4*Δ *mid1*Δ double mutants that show a synthetic lethal growth phenotype. Tetrads created by mating the two strains on solid ME medium, four spores dissected and allowed to grow on solid YE medium until colonies formed. Colonies replicated to solid YE+G418/KanMX4 and EMM-ura media and incubated to identify growth phenotypes and double mutants. (b) Direct physical interaction between full-length Vps4p and the "C-term" domain of Mid1p. Recombinant GST-tagged (Mid1p domains: "N-term" (aa 1–453), "Middle" (452–579) and "C-term" (793–920)) and 6 His-tagged (Vps4p and "C-term" Myo2p) proteins were expressed in *E. coli* and purified using GST-sepharose beads and Ni-NTA agarose beads, respectively. Exp. A shows eluted prey Mid1p domains captured by bait Vps4p bound to Ni-NTA agarose beads: (*) represents physical interaction of Vps4p and Mid1p "C-term" domain. Exp. B shows eluted prey Mid1p "N-term" and "Middle" domains captured by bait Myo2p bound to Ni-NTA agarose beads as a positive control [38]: (**) represents physical interaction of Mid1p "N-term" and "Middle" domains with "C-term" domain of Myo2p (left panel). The 14.5 kDa "C-term" Myo2p was not detected in this gel. Colored boxes represent predicted proteins: Vps4p purple, Mid1p "N-term" red, Plk1 purple, Mid1p "Middle" green and Mid1p "C-term" dark blue.

(Figure 1b). This indicates a direct physical interaction between Vps4p and the C-terminus of Mid1p, at least *in vitro*, and that this interaction involved residues 798–920 of Mid1p.

Vps4p is required for the correct cellular distribution of Mid1p

To further understand the interaction between Vps4p and Mid1p we examined the requirement

for Vps4p to control the cellular distribution of GFP-tagged Mid1p during the cell cycle. Mid1p distribution has been well characterized and shown to move from the nucleus to the equatorial region to form nodes and a medial ring, that predicts the site of cell cleavage during septation [8].

Wild-type cells showed three patterns of GFP-Mid1p: localization to the nucleus, cytoplasmic, and equatorial nodes, as previously reported (Figure 2a) [5,8]). By contrast, GFP-Mid1p in *vps4*Δ cells showed different patterns. Although cytoplasmic GFP-Mid1p was similar to wild-type, additional plasma membrane localization was observed (Figure 2b). In some cells GFP-Mid1p localized to only one node and the plasma membrane, or localized to three nodes in other cells. The frequencies of these abnormal phenotypes in *vps4*Δ cells were compared with wild-type and showed significant differences (quantified in Figure 2b for wild-type and Figure 2c for *vps4*Δ, and compared in Figure 2d). Overall, GFP-Mid1p localization was considerably altered by the absence of *vps4*$^{+}$ (Figure 2d).

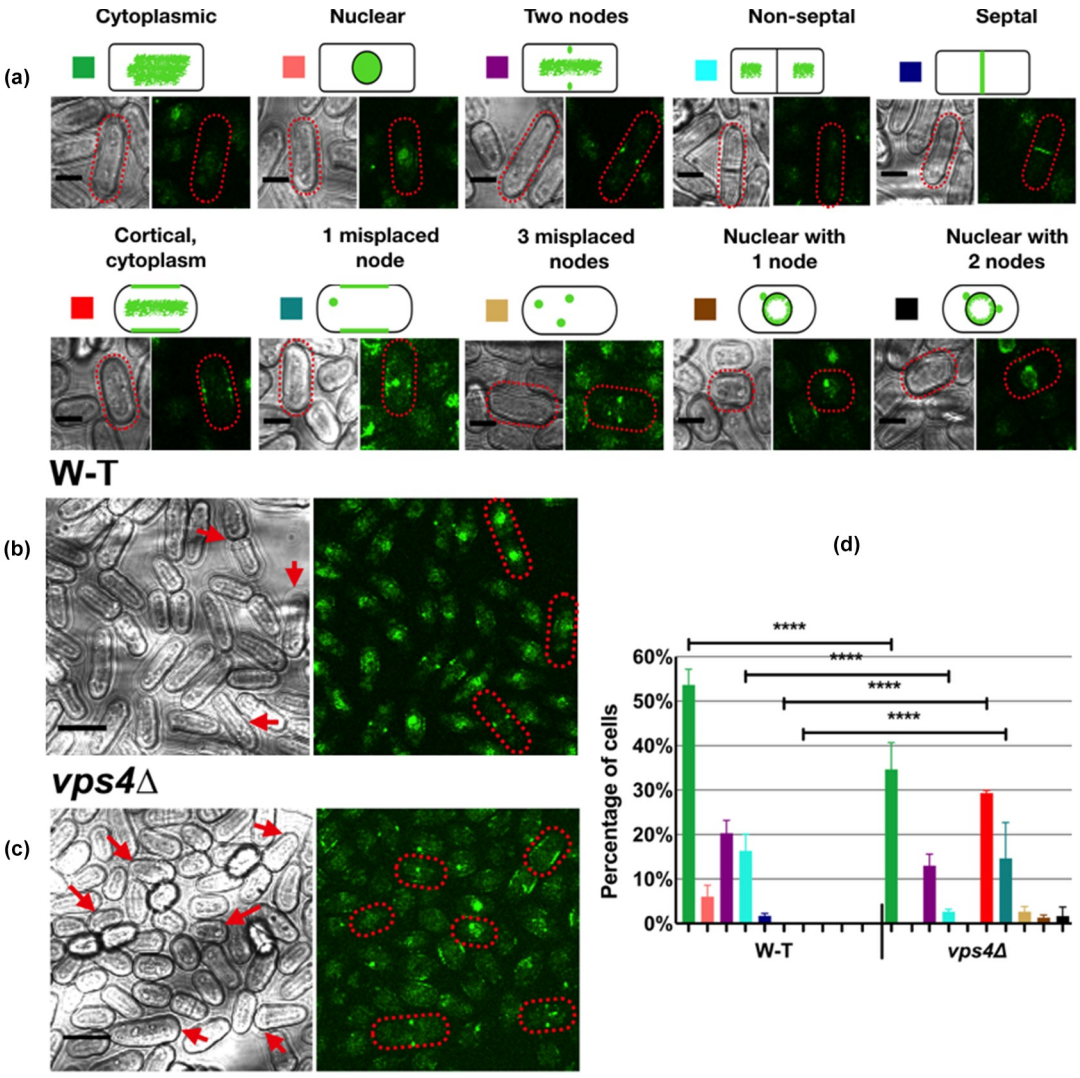

Figure 2. GFP-Mid1p cellular localization is disrupted in *vps4*Δ cells. Wild-type (w-t) and *vps4*Δ (*vps4::ura*$^{+}$) *S. pombe* strains containing GFP-Mid1p grown at 25°C in liquid YE medium to mid-exponential phase and visualized by confocal microscopy. (a) Key to characterized GFP-Mid1p localization phenotypes. Scale bar, 5 µm. Bright-field and fluorescent images of cells of GFP-Mid1p localization phenotypes for wild-type (W-T) (b) and *vps4*Δ (c) cells. Scale bar, 10 µm. The images presented in (A, B and C) are scanned in a single focal plane using a laser scanning confocal microscope. (d) Two-way ANOVA analysis of frequencies of localization phenotypes in *vps4*Δ compared to wild-type (W-T). Asterisks (****) denote *p* values <0.0001 indicating significant differences to wild-type. Error bars, SEM.

These results, in addition to the observation that the *mid1* and *vps4* genes interact genetically and that the Mid1p and Vps4p physically interact *in vitro*, suggest that Mid1p and Vps4p coordinate to regulate the *S. pombe* cell cycle.

Genetic and physical interactions between Mid1p and Ark1p in fission yeast

We hypothesized that *mid1* and *ark1* genes interact to accomplish *S. pombe* cytokinesis as we and others have shown that aurora kinases modulate ESCRT protein function [17,21,26–28]. To test this both genetic and biochemical approaches were taken.

First, a *mid1*Δ strain was crossed with strains containing temperature sensitive *ark1*-T11 mutations to generate double *mid1*Δ *ark1*-T11 mutant strains. The *mid1*Δ *ark1*-TS double mutant failed to form viable colonies (Figure 3a). Such a synthetic lethality indicates a genetic interaction between the *mid1* and *ark1* genes.

As with *mid1* and *vps4* such a genetic interaction might be explained by a physical interaction between Mid1p and Ark1p proteins. Since Ark1p is a protein kinase, and any interactions are likely to be low affinity and transient, we tested whether

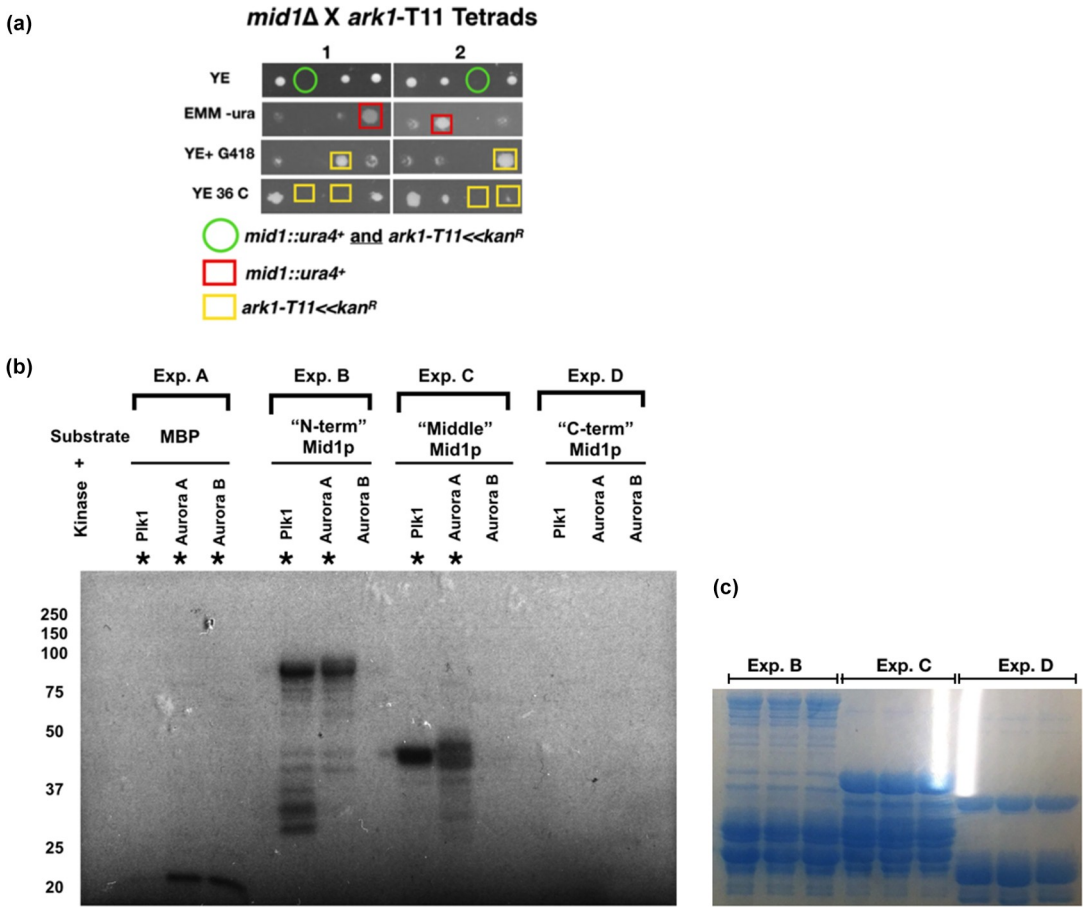

Figure 3. Genetic and physical interactions between *mid1* and *ark1* in fission yeast. (a) Synthetic lethality in *mid1*Δ *ark1*-T11 double mutant cells indicates genetic interaction between *mid1*$^+$ and *ark1*$^+$ genes. Tetrad analysis of h$^+$ *ark1*-T11 (*ark1*-T11 *Kan*^{R}) crossed with h$^-$ *mid1*Δ (*mid1::ura*$^+$) to identify *mid1*Δ *ark1*-T11 double mutants that show a synthetic lethal growth phenotype. Tetrads created by mating the two strains on solid ME medium, four spores dissected and allowed to grow on solid YE medium until colonies formed. Colonies replicated to solid YE+G418/KanMX4 and EMM-ura media and incubated to identify growth phenotypes and double mutants. (b) Plk1 and Aurora A kinases phosphorylate Mid1p "N-term" and "Middle" domains. Recombinant GST-tagged Mid1p domain proteins "N-term" (aa 1–453), "Middle" (452–579) and "C-term" (798–920) were purified and analyzed by *in vitro* phosphorylation assays. In "Exp. A" myelin basic protein (MBP) was a used as a positive control for kinase activity. In "Exp. B", "Exp. C" and "Exp. D" the "N-term", "Middle" and "C-term" domains of Mid1p were substrates with the kinases Plk1, Aurora A or Aurora B, respectively. Asterisks (*) indicate detected *in vitro* phosphorylation signals. (c) Coomassie Blue stained gel of the indicated experiments confirms equal protein loading.

Mid1p can be phosphorylated by aurora kinase, using an *in vitro* phosphorylation approach with recombinant Mid1p domains purified from *E. coli*. These experiments were performed with the human aurora kinases aurora A and aurora B, and the human polo kinase Plk1 (Figure 3b). Phosphorylation of both the "N-term" and "Middle" Mid1p domains by aurora A and Plk1 was detected, but not by aurora B (Figure 3b, Exp. B and Exp. C). In contrast, no phosphorylation was detected of the "C-term" Mid1p domain by any of the three kinases aurora A, aurora B or Plk1 (Figure 3b, Exp. D).

Ark1p is required for the correct cellular distribution of Mid1p

To further analyze the interaction of Ark1p and Mid1p in *S. pombe* we examined the effect of two different temperature sensitive *ark1* mutants, *ark1*-T11 and *ark1*-T8, on Mid1p distribution in cells (Figure 4).

In *ark1*-T11 cells GFP-Mid1p showed wild-type phenotypes (Figure 4a). But in addition, new localization patterns were apparent, where GFP-Mid1p localization showed nuclear exclusion with the appearance of a ring encircling the nucleus. The frequencies of these phenotypes were quantified and compared to wild-type cells revealing significant differences (Figure 4b). In *ark1*-T8 cells GFP-Mid1p showed new additional localization patterns (Figure 4d). Cells were observed to be round and shorter than the rod-shaped wild-type cells and GFP-Mid1p localization presented nuclear exclusion with the appearance of a ring that encircled the nucleus. While some cells had one nucleus others showed two, three, or even four nuclei. The frequencies of these phenotypes were quantified and

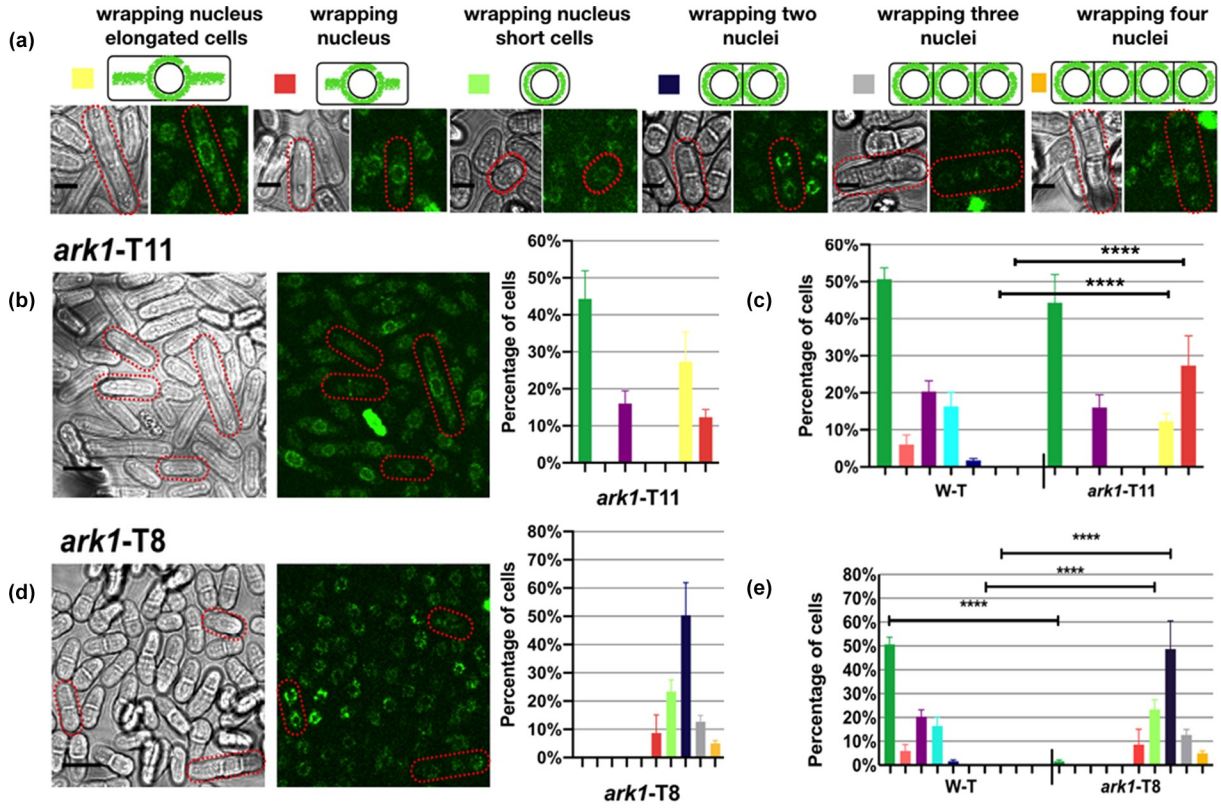

Figure 4. GFP-Mid1p cellular localization is disrupted in *ark1*-T11 and *ark1*-T8 cells. Wild-type (w-t), *ark1*-T11 and *ark1*-T8 *S. pombe* strains containing GFP-Mid1p were grown at 25°C (the permissive temperature for these temperature sensitive mutants) in liquid YE medium to mid-exponential phase and visualized by confocal microscopy. (a) Key to characterized GFP-Mid1p localization phenotypes. Scale bar, 5 µm. Bright and green fluorescent images of cells (left) and quantitative analysis of GFP-Mid1p localization phenotypes (right) for *ark1*-T11 (b) and *ark1*-T8 (d). Scale bar, 10 µm. (c, e) Two-way ANOVA analysis of frequencies of localization phenotypes in *ark1*-T11 and *ark1*-T8 compared to wild-type (W-T). Asterisks (****) denote p values <0.0001 indicating a significant difference to wild-type. Error bars = SEM.

compared to wild-type cells revealing significant differences (Figure 4e). These data support the hypothesis that Mid1p and Ark1p coordinate to regulate the *S. pombe* cell cycle.

The growth temperature of the temperature sensitive *ark1* mutants affects the activity of the Ark1p protein but also causes cell cycle arrest; therefore, any phenotypes observed from growing the strains at a restrictive temperature cannot not be solely attributed to the absence/inactivation of Ark1p protein as they may instead be a secondary consequence of the cell cycle arrest. To avoid this complication, the yeast cells were grown at the permissive temperature when they complete the cell cycle and divide, so that any phenotypes observed are considered the result of a "partial" absence/inactivation of the Ark1p protein. For this reason, we are unable to determine whether the multinucleated cells phenotype in the *ark1*-TS mutants is solely a result of altered GFP-Mid1P localization; however, we note that others have reported the multinucleated cells phenotype in *ark1* mutant strain [29].

Identification of Mid1p amino acid residues phosphorylated by aurora and polo kinases

To further explore phosphorylation of Mid1p by aurora and polo kinases a mass spectrophotometry approach was used to identify phospho-acceptor sites. The "N-term" and "Middle" domains of Mid1p gel fragments from *in vitro* kinase assay reactions identical to those shown Figure 3b, but with non-labeled ATP, were excised and subjected to nano-scale liquid chromatographic tandem mass spectrometry (nLC-MS/MS) to generate a Mid1p phospho-acceptor sites map (Figure 5). This analysis identified 35 potential Mid1p residues phosphorylated by either Plk1 or aurora A kinases (S3 Table). In parallel we examined other published databases on fission yeast phosphoproteomes to refine and confirm the number of Mid1p phospho-acceptor sites. Most of these studies used a stable isotope labeling by amino acid in cell culture approach. We selected four studies which studied the *S. pombe* global proteome and identified several additional Mid1p specific phospho-acceptor sites [30–33].

The Mid1p phosphorylation events identified by mass spectrophotometry are summarized in S3 Table, alongside those described by the four published studies. The red highlighted residues represent overlap with the residues identified reported in this work. The phospho-acceptor sites map shows a total of six potential phospho-acceptor

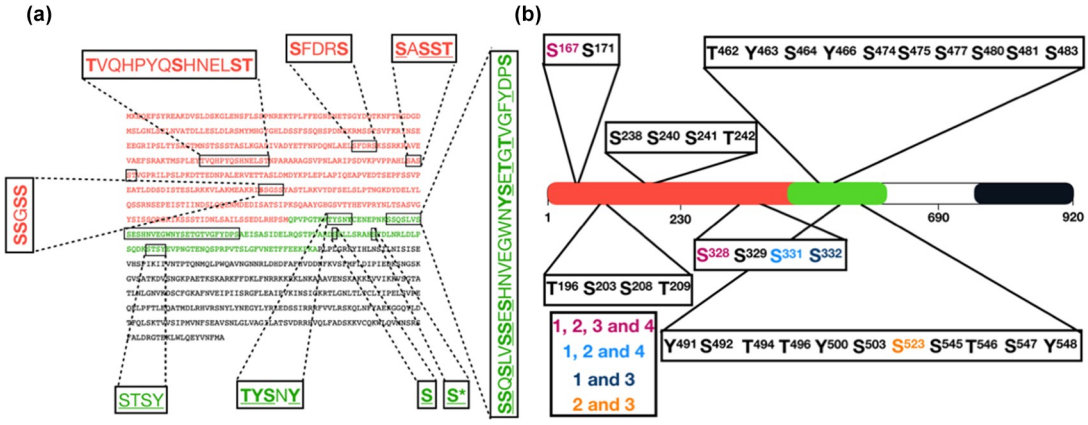

Figure 5. Identification of Mid1p phospho-acceptor sites by mass-spectrometry analysis (MSA) and published studies. (a) Mid1p full-length amino acid sequence with "N-term" and "Middle" domains indicated in red and green. Highlighted peptides show 35 phosphorylated amino acid residues identified by MSA of *in vitro* phosphorylation reactions for the kinases Plk1 (bold), Aurora A (underlined) or both (bold and underlined). (b) Five Mid1p phospho-acceptor sites generated from comparison of the 35 MSA amino acids with Mid1p phosphorylated amino acids identified in four published proteomic studies [30–33]. Amino acids identified by MSA and four independent studies (pink), MSA and three studies (light blue), and MSA and two studies (dark blue and orange). Asterisk (*) indicates a sixth serine phospho-acceptor site at position 531 derived from [31,32] and [33].

sites distributed along the "N-term" and "Middle" Mid1p sequence, five of which were identified here, and the sixth was added from the published studies (Figure 5b). These are the serine residues S167, S328, S331, S332, S523 and S531.

We used the GPS 5.0 online computational prediction tool to predict phosphorylation sites of Mid1p and it found positions S167, S328 as potential phospho-acceptor sites for Plk1, aurora kinase respectively; S523 and S531, as potential phospho-acceptor sites for aurora and/or Plk1 (http://gps.biocuckoo.cn/download.php).

To confirm the new phospho-acceptor sites identified in Mid1p *in vitro* phosphorylation experiments involving bacterially expressed phospho-resistant mutant (serine to alanine) forms of the "N-term" and "Middle" domains of Mid1p with aurora A and Plk1 kinases were completed (Figure 6). These experiments reveled markedly reduced phosphorylation of the Mid1p phospho-resistant mutant S167A by both aurora A and Plk1 kinases, and S523A by aurora A alone. These observations support the suggestion that the S167 and S523 residues are phosphorylated by the aurora A and Plk1 kinases, at least *in vitro*.

Biological relevance of amino acid residues phosphorylated by aurora and polo kinases in Mid1p

As another way to examine the role of the aurora and polo kinase phospho-acceptor sites identified in Mid1p we analyzed the effect of their mutation *in vivo* in fission yeast. Importantly, such an approach allowed confirmation of the relevance in yeast of the phospho-acceptor sites in Mid1p identified using mammalian orthologous protein kinases. *S. pombe* cells exhibit morphology defects in the absence of Mid1p function. Therefore, we tested the effect of mutations of Mid1p phospho-acceptor sites in fission yeast on cell morphology to assay their relevance.

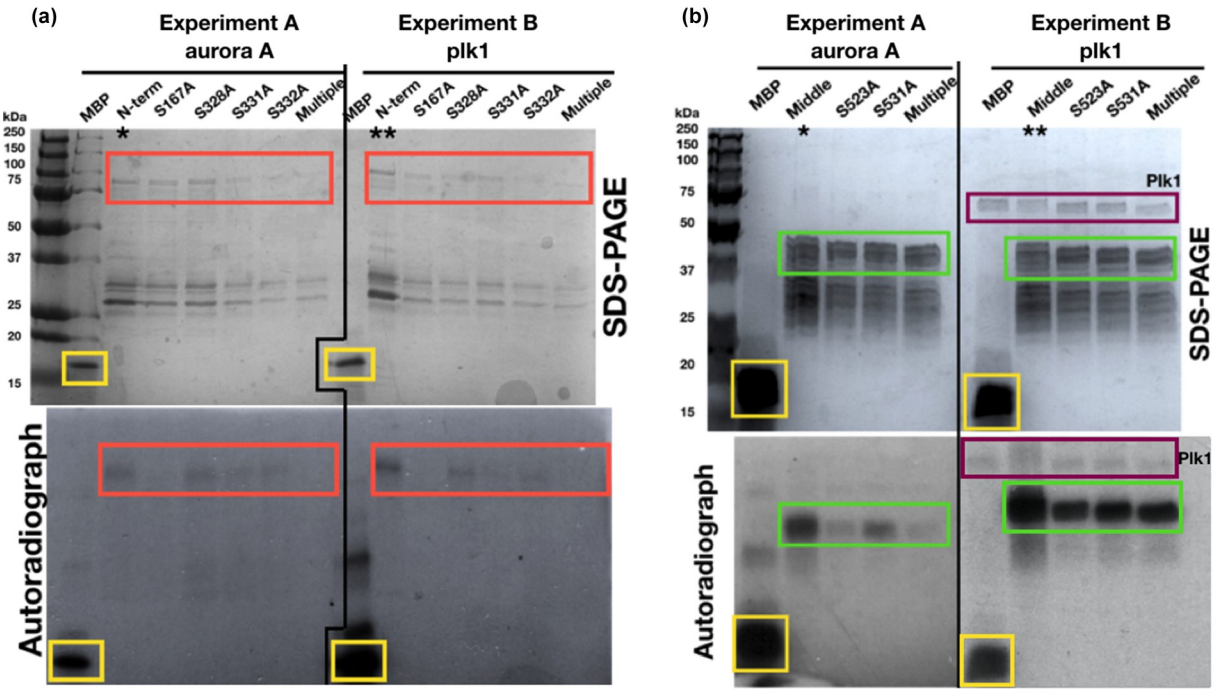

Figure 6. Reduced *in vitro* phosphorylation of Mid1p "N-term and "Middle" phospho-resistant mutants by Plk1 and Aurora A kinases. Recombinant GST-tagged Mid1p "N-term" (a) and "Middle" (b) domains phospho-resistant mutants were expressed and purified in *E. coli*. Proteins subjected to *in vitro* phosphorylation experiments with Aurora A (Exp. A) or Plk1 (Exp. B) kinases. Asterisks (* and **) indicate wild-type Mid1p "N-term" and Mid1p "Middle" recombinant proteins used as positive controls. Colored boxes represent predicted proteins: MBP yellow, Mid1p "N-term" species red, Plk1 purple, and all Mid1p "Middle"-related species green. "Multiple" indicates mutations in all four phospho-acceptor sites. GFP-Mid1p is imaged in *ark1* wild-type cells (Fig 2B).

Versions of the *mid1* gene containing phospho-acceptor site mutations were generated and integrated in single copy into chromosomal DNA of *S. pombe mid1*Δ cells. Each version of the *mid1* gene had either a phospho-mimetic (S > D) or a phospho-resistant (S > A) point mutation(s) of the serine residues S167, S328, S331, S332, S523 or S531 to create a panel of mutant *S. pombe* strains (S1 Fig). Such *mid1* mutations were made both singly and in combination. As a positive control we integrated the wild-type *mid1*$^{+}$ gene into *mid1*Δ cells to create *mid1*Δ pJK148:*mid1*$^{+}$. This resulted in cells that behaved and looked identical to wild-type, both on solid medium and in liquid culture (Figure 7 and S1 Fig), confirming that the integration event had not effected Mid1p activity.

Mid1p phospho-mutants in *mid1Δ* cells

Initial experiments examined the effect of Mid1p phospho-mimetic or phospho-resistant mutations in *mid1Δ* cells. Strains were grown on solid

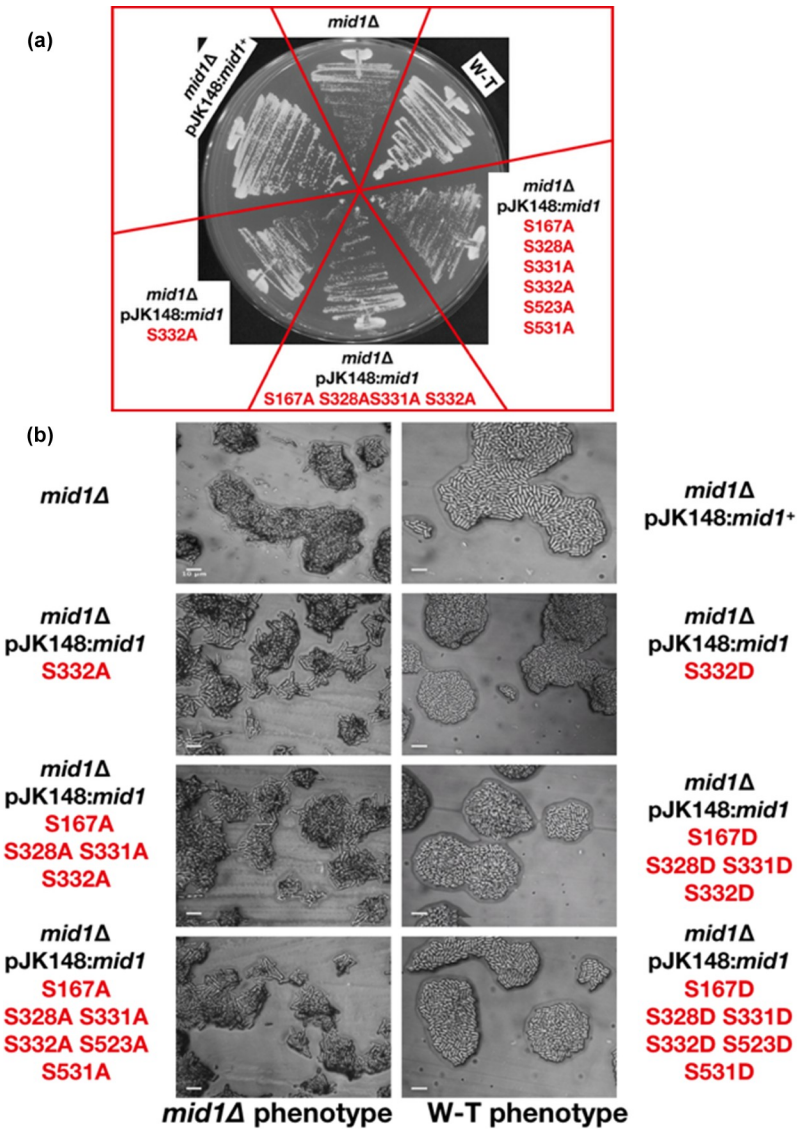

Figure 7. The S332 phospho-acceptor site is required for Mid1p function. Three phospho-resistant *mid1* mutant strains *mid1* S332A, *mid1* S167A S328A S331A S332A, and *mid1* S167A S328A S331A S332A S523A S531A, and the three phospho-mimetic mutants *mid1* mutant strains S332D, *mid1* S167D S328D S331D S332D, and *mid1* S167D S328D S331D S332D S523D S531D streaked to single colonies on solid YE at 25°C to compare growth rates (a) and colony morphology (b). Controls: *mid1*Δ and wild-type (w-t) cells. Scale bar, 10 μm.

medium, with the formation of colonies observed in all cases. In most strains where serine was changed to either alanine or aspartic acid cell morphology appeared similar to wild-type (Figure 7, S4 Fig, S4 Table and S5 Fig). However, interestingly, *mid1* S332A cells (but not *mid1* S332D) had defects in morphology similar to those observed in *mid1*Δ cells, with slower growth at 25°C (Figure 7). These data indicate a requirement of the phospho-acceptor S332 for Mid1p function.

Furthermore, other phenotypes were revealed when certain Mid1p phospho-mutants were cultured in liquid medium. For example, *mid1* S523A and *mid1* S531A mutants displayed morphology defects (S2 Fig). In contrast, the equivalent phospho-mimetic mutants *mid1* S523D or *mid1* S531D did not.

Mid1p phospho-mutants in *ark1*-T11 cells

To examine the role of Mid1p phosphorylation in its interaction with Ark1p we crossed the strains containing phospho-mimetic/resistant versions of *mid1* with *ark1*-T11 mutant cells and searched for synthetic phenotypes in double mutants. Viable colonies were observed in most cases with no synthetic phenotypes detected in many double mutants (S4 Table). However, *mid1* S523A *ark1*-T11 and *mid1* S531A *ark1*-T11 double mutants showed cell morphology defects when cells were grown in liquid culture more severe than the single mutant strains (S3 Fig and S4 Table). These defects were not observed in the equivalent *mid1* S523D *ark1*-T11 or *mid1* S531D *ark1*-T11 double mutants. The cell morphology defects observed in *mid1* S523A *ark1*-T11 and *mid1* S531A *ark1*-T11 double mutants were defined as loss of the rod-like shape of cells. This suggests a role for these two phospho-acceptor sites in Mid1p function during the *S. pombe* cell cycle to ensure medial division plane placement, and consequently equal sized and rod-shaped daughter cells.

Mid1p phospho-mutants in *plo1-ts35* cells

To examine the role of Mid1p phosphorylation in its interaction with Plo1p we crossed strains containing phospho-mimetic/resistant versions of *mid1* with *plo1-ts35* mutant cells and searched for synthetic phenotypes in double mutants. Viable colonies were observed in all cases with no synthetic phenotypes detected for the majority of double mutants (S4 Table). However, colony formation on solid medium was slower for *mid1* S332A *plo1-ts35* double mutants, and more severe cell morphology phenotypes were observed, compared to the single mutant strains (S5 Fig). These defects were not observed in the equivalent *mid1* S332D *plo1-ts35* double mutants. Such genetic interactions suggest a link between the regulation of Mid1p and Plo1p.

Mid1p phospho-mutants in *vps4Δ* cells

To examine the role of Mid1p phosphorylation in its interaction with Vps4p we crossed strains containing phospho-mimetic/resistant versions of *mid1* with *vps4*Δ mutant cells and searched for synthetic phenotypes in double mutants, Viable colonies were observed in all cases with no synthetic phenotypes detected (S4 Fig and S4 Table). However, colony formation on solid medium was slower for *mid1* S523A S531A *vps4*Δ double mutants, and more severe cell morphology phenotypes were observed, compared to the single mutant strains. Strikingly, cells had defects in morphology similar to those observed in *mid1*Δ cells (Figure 8). The same serine residues changed to alanine S523D or S531D had no such effect when combined with *vps4Δ* (S4 Fig and S4 Table). These genetic interactions suggest a link between the regulation of Mid1p by both Vps4p and Ark1p.

Conclusions

In fission yeast the Mid1p protein has important roles during cytokinesis during the cell cycle, with anillin homologues having similar functions in higher eukaryotes. These roles center around its structural function in predicting and controlling the site of cell division in the equatorial region of the cell. Here we have identified new classes of proteins with which Mid1p interacts, and explored the mechanism by which these proteins cooperate and regulate each other and cell growth/morphology.

Mid1p and Vps4p

Genetic and biochemical approaches revealed a direct physical interaction of Mid1p with the ESCRT-associated protein Vps4p. Furthermore,

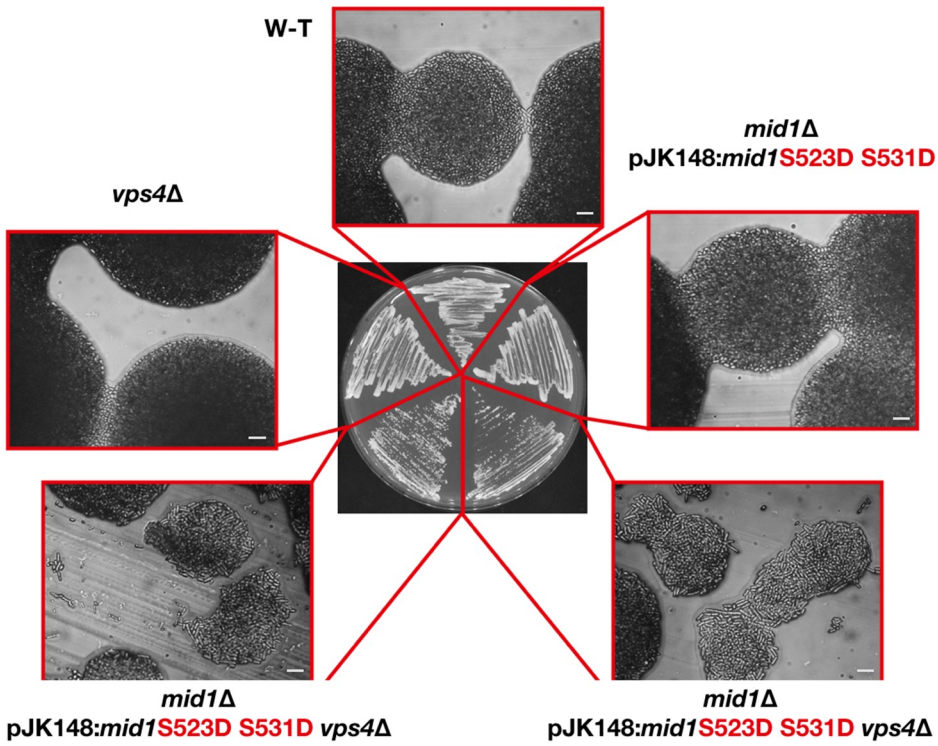

Figure 8. The Mid1p S523 and S531 phospho-acceptor sites regulate its interaction with Vps4p. Strains streaked to single colonies on solid YE medium and grown at 25°C to compare growth rates and colony morphology. Controls: *vps4*Δ and wild-type (w-t) cells. Scale bar, 10 µm.

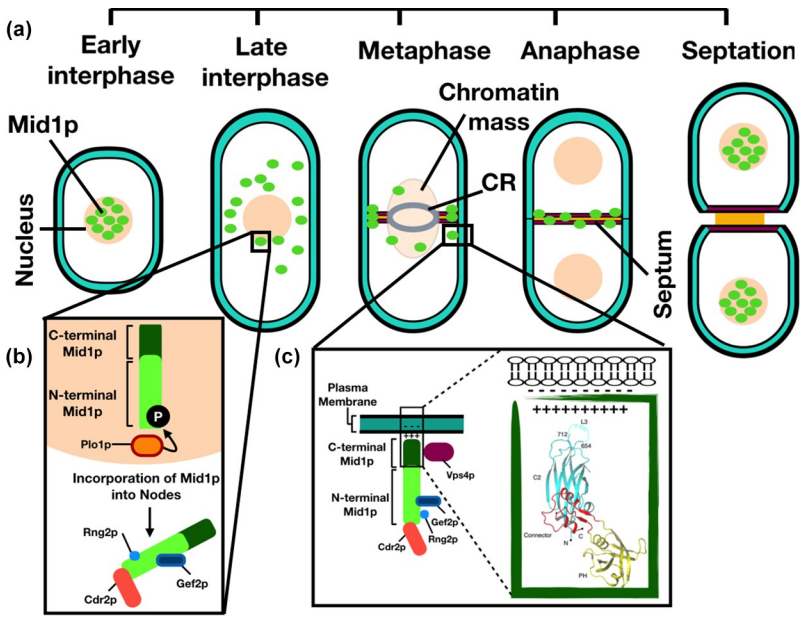

Figure 9. Interaction of Mid1p and Vps4p to regulate *S. pombe* septation. (a) Schematic representation of Mid1p localization during *S. pombe* cell cycle stages. CR = contractile ring. (b) Mid1p is phosphorylated by Plo1p to promote mitotic entry, during which Rng2p and other proteins interact with the N-terminal domain of Mid1p. (c) In mitosis, Mid1p forms nodes which are attached to the plasma membrane via the lipid binding motifs present within the Mid1p C-terminal domain. Green box represent the overall structure of Mid1p C-terminal region (aa 579–920) containing: the C2 domain (cyan), the connector domain (red) and the PH domain (yellow); dotted lines represent the lipid binding loop. Structure adapted from [13]. The Vps4p interaction with the C-terminal domain of Mid1p potentially regulates this process.

we demonstrated that a chromosomal deletion of the *vps4*$^{+}$ gene caused defects in the cellular localization of GFP-Mid1p. These defects included mis-localization of Mid1p-dependent nodes whereby one node is randomly positioned, or three nodes were present. This suggests a role of Vps4p in the Mid1p-dependent node localization pathway, which led us to hypothesize that the function of Mid1p is regulated by Vps4p during nodes attachment to the plasma membrane (Figure 9).

Two types of nodes are involved in *S. pombe* actomyosin ring assembly and contraction (Figure 9, Panel A). Mid1p cortical anchorage first drives the recruitment of cytokinesis proteins, then interactions with myosin filaments causes the condensation of nodes into the actomyosin ring. Mid1p cortical anchorage depends on the PH domain [13] and its potential interaction with Vps4p might stabilize this interaction. Since Vps4p physically interacts with residues within the C-terminal domain of Mid1p, which contains membrane binding motifs, we speculate that Vps4p may facilitate Mid1p cortical anchorage to promote *S. pombe* medial division (Figure 9, Panel C).

We suggest that a physical interaction between Vps4p and Mid1p regulates Mid1p-dependent node attachment to the plasma membrane to determine the division plane in *S. pombe*, and that this interaction directly or indirectly involves Mid1p PH domain cell cortex anchorage (Figure 9, Panel C). It is interesting to note that the domain of Mid1p that interacts with Vps4p *in vitro* (Figure 1) contains the PH domain, suggesting that binding of Vps4p to this region may regulate interaction with the cell cortex (Figure 9).

Phosphorylation of Mid1p

Genetic and biochemical approaches revealed a direct physical interaction of Mid1p with the aurora kinase, Ark1p in fission yeast. Furthermore, human aurora A was shown *in vitro* to phosphorylate the Mid1p the "N-term" and "Middle" domains. Mapping of the amino acids in Mid1p phosphorylated by aurora A and Plk1 revealed 35 potential phospho-acceptor sites with, importantly, some of these sites independently identified in four *S. pombe* global proteomic studies (Figure 5). Such combined analysis suggested six potential serine phospho-acceptor sites in Mid1p: S167, S328, S331, S332, S523 and S531. Subsequent *in vitro* kinase assay experiments confirmed the *in vitro* phosphorylation of the serine S167, S331 and S523 phospho-acceptor sites of Mid1p by aurora A and Plk1 kinases (Figure 6).

As the *in vitro* kinases assay approach used to identify the phospho-acceptor sites in Mid1p utilized human purified aurora kinase and polo kinase it was important to confirm the biological relevance of the sites in fission yeast. This was especially the case for the kinase assay using aurora A, as fission yeast Ark1p more closely resembles aurora B. To do this we examined the effect of mutations of these Mid1p serine phospho-acceptor sites *in vivo* on cell morphology in wild-type, *ark1*-T11, *plo1-ts35* and *vps4*Δ *S. pombe* cells (S4 Table and S5 Fig). In wild-type cells defective cell morphology phenotypes were observed for the Mid1p phospho-resistant mutants S332A, S523A and S531A (Figure 7 and S2 Fig), and the phospho-mimetic S523D and S531D when combined with mutations in *vps4, ark1*, or *plo1* (Figure 8 and S4 Table). Similarly, defective cells morphologies were detected in *mid1* S523A *ark1*-T11 and *mid1* S531A *ark1*-T11 double mutants (S3 Fig). Unexpectedly, defective cell growth phenotypes were observed in S332A, S523A and S531A related mutants, but not in S167A and S331A related mutants which instead showed a decreased level of *in vitro* phosphorylation by both aurora and Plk1 or Plk1 only, respectively (Figure 6) when compared to wild-type Mid1p phosphorylation levels by the two kinases (S5 Table). It could be that the effect produced by this mutation is subtle and not detected using this simple assay; alternatively mutation of one phospho-acceptor site might modulate phosphorylation at a distinct site. It will be important in future studies to determine whether Mid1p cellular localization is affected by these mutations, and what the consequence might be for Mid1p function.

Overall, we conclude that the phosphorylation of these amino acid residues is important for Mid1p function in fission yeast and its interaction with these proteins to regulate cell cycle events. It is tempting to speculate that the interaction of Mid1p and Vps4p is regulated by the activity of Ark1p and/or Plo1p, but it is important to note that the regions of Mid1p phosphorylated by these kinases do not include the binding region for Vps4p. Hence, phosphorylation in adjacent

regions may modulate binding via conformational changes in Mid1p, as regions containing the phospho-acceptor sites have been shown to regulate the interaction of Mid1p with other proteins, including Plo1p and Sid1p. Plo1p phosphorylates residues within the first 100 amino acids of Mid1p to trigger Myosin II recruitment during contractile ring assembly [34]. Later at contractile ring constriction Sid1p phosphorylates Mid1p to facilitate its export from the cell cortex [7]. Future experiments will be aimed at unraveling how the Mid1p interactome is modified both by association with Vps4p and by phosphorylation by mitotic kinases.

Materials and Methods

Yeast media and general techniques

General molecular procedures were performed, with standard methodology and media used for the manipulation of *S. pombe* [35,36]. The yeast strains used in this study are shown in S1 Table. Cells were routinely cultured using liquid or solid complete (YE) or minimal (EMM) medium, at 25°C or 30°C.

DNA constructs

The DNA constructs used in this study are listed in S2 Table. Some were synthesized and cloned by either GenScript or Invitrogen. All constructs were sequenced before use.

Bacterial expression DNA constructs

Four fragments of the *mid1*$^+$ gene encoding the amino acids 1–453 "N-terminus", 452–579 "Middle", 578–799, 798–920 "C-term" [25] were synthesized and cloned into *Bam* HI/*Xho* I of pGEX-4 T-1. Full-length *vps4*$^+$ was synthesized and cloned into *Nde* I/*Bam* HI of pET-14b. The C-terminal domain of *myo2*$^+$ was synthesized and cloned into *Nde* I/*Bam* HI of pET-14b.

Mid1 phospho-mimetic/resistant mutants

Eighteen versions of the *mid1* gene with different phospho-mimetic/resistant mutations were synthesized, along with a wild-type *mid1*$^+$ control. All had the wild-type *mid1*$^+$ promoter in ~1 kbp of DNA upstream of *mid1*$^+$ open reading frame, and were each cloned into *Kpn* I/*Sac* I of pJK148. Integration of the pJK148:*mid1* genes (1–19) into *S. pombe mid1Δ* cells was through homologous recombination after linearization of pJK148:*mid1* with *Nde* I in the *leu1*$^+$ gene. The resulting panel of phospho-mimetic/resistant mutant strains is listed in S1 Table and S1 Fig.

Recombinant protein purification

GST-Mid1p, 6His-Vps4p or 6His-C-term Myo2p plasmids were grown in BL21 *E. coli* until an OD of 0.6–0.8, with protein production induced by adding 1 mM IPTG. Mid1p 578–799 was not found to be expressed under these conditions, and so was not used for further experiments.

Bacterial pellets were produced by centrifugation with cells re-suspended in 20 ml re-suspension buffer with EDTA-free protease inhibitors; for GST-Mid1p fusion proteins PBS buffer (137 mM NaCl, 2.7 mM KCl, 10 mM Na_2HPO4 and 1.8 mM KH_2PO4, pH 7.4) was used, whereas for 6His-Vps4p, HEPES buffer (25 mM HEPES, 400 mM KCl and 10% (v/v) glycerol, pH 7.4) was used. Cells were then lysed by sonication, where a final concentration of 1 mg ml^{-1} lysozyme was added for cell wall digestion followed by sonication, with 0.1% (v/v) Triton X-100 added prior to lysis. A clear lysate was produced by centrifugation. GST-tagged fusion proteins were purified using 1 ml l^{-1} glutathione beads in PBS buffer, while 6His-tagged Vps4p or C-term Myo2p were purified using 500 µl l^{-1} Ni-NTA beads in HEPES buffer, either for 2 h or overnight at 4°C. Mid1p was eluted from glutathione beads using Reduced glutathione buffer. Vps4p or C-term Myo2p were washed and eluted from Ni-NTA beads using HEPES buffers. Elution was carried out for 2 h at 4°C. Samples of proteins from each step were subjected to SDS-PAGE to determine elution efficiency.

Pull-down experiments

Pull-down experiments utilized Ni-NTA beads-immobilized bait proteins (6His-Vps4p or 6His-C-term Myo2p) and prey-eluted proteins (GST-Mid1p: "N-terminus," "Middle", or "C-terminus") to investigate protein–protein interactions. Bait

proteins were loaded onto Ni-NTA beads by incubation in PBS containing 0.01% (v/v) Triton X-100 for 1 h (4°C). After loading, the mixture was washed with PBS containing 0.01% (v/v) Triton X-100, and beads were blocked for nonspecific binding by incubation in PBS containing 0.2% fish-skin gelatin. The beads mixture was incubated with prey protein in PBS with 0.01% (v/v) Triton X-100. Subsequently, beads were washed with PBS containing 0.01% (v/v) Triton X-100 three times, 0.5% (v/v) glycerol and 0.2% (w/v) fish skin gelatin three times, and with PBS alone four times. Proteins were eluted from beads by boiling in Laemmli sample buffer (LSB) (75 mM Tris pH 6.8, 12% (w/v) SDS, 60% (v/v) glycerol, 600 mM DTT and 0.6% (w/v) Bromophenol Blue) and samples were subjected to SDS-PAGE.

In vitro kinase assays

Assays combined either human Plk1 (0.023 µg/µl), aurora A (0.01 µg/µl), aurora B (0.01 µg/µl) and myelin basic protein (MBP; 2.5 µg) (Sigma–Aldrich and Biaffin GmbH) or one of the three Mid1p domains ("N-term", "Middle" or "C-term" 2.5 µg). Kinase, substrate proteins, 1 µCi [γ-^{32}P] ATP, 10 mM ATP and kinase assay buffer (25 mM MOPS, 25 mM $MgCl_2$, 1 mM EDTA and 0.25 mM DTT, pH 7.2) were mixed in a total volume of 20 µl; the reaction was initiated by adding 5 µl ATP cocktail and incubated at 30°C for 1 h and terminated by the addition of LSB; samples were subjected to SDS-PAGE followed by autoradiography or phospho-imaging. Following detection of *in vitro* phosphorylation signals, mass spectrometric analysis was carried out by the Dundee FingerPrints Proteomics service (http://proteomics.lifesci.dundee.ac.uk/).

Confocal microscopy

GFP-tagged *mid1*$^+$ [37] was examined by a He/Ne and Ag laser system of Zeiss LSM microscope using 63X high NA 1.4 objective lens. Cell images were collected using Zeiss Pascal software and processed using ImageJ, Microsoft PowerPoint and Keynote software. Numerical analysis was completed from three independent experiments where 200–250 cells were counted. When GFP-foci were counted, care was taken to scan the entire depth of the cell to ensure that all foci present were quantified. Yeast colonies grown on solid medium were imaged using a Zeiss Axioscope microscope and a Sony DSC-75 camera.

Acknowledgments

We thank Anne Paoletti, Tomoko Iwaki and Silke Hauf for sharing fission yeast strains used in this study. This work was supported by the Tertiary Education Trust Fund (TETFUND) and Adamawa State College of Education, Nigeria studentship [grant number TETF/DASTD/COE/HONG/ASTD/2016/Vol.1] to WGY. We thank Ian Salt for his input to this project, both with experimental and practical advice. We acknowledge the following for contributions to experiments: Rianne Cort, Laura Downie, Bethany Hutton, Christina Jack, Jack Goddard, Susan McGill, Mark McLean, Chiamaka Okoli, Elena Pescuma, Liam Pollock, James Provan, John Riddell, Aizhan Shagadatova, Ellen Shercliff and Haoying Wang.

Disclosure statement

No potential conflict of interest was reported by the author(s).

ORCID

Imane M. Rezig http://orcid.org/0000-0001-6673-8946
Wandiahyel G. Yaduma http://orcid.org/0000-0002-3600-7162
Gwyn W. Gould http://orcid.org/0000-0001-6571-2875
Christopher J. McInerny http://orcid.org/0000-0002-9201-3479

References

[1] Hoffman CS, Wood V, Fantes PA. An Ancient Yeast for Young Geneticists: a Primer on the *Schizosaccharomyces pombe* Model System. Genetics. 2015;201(2):403–423.
[2] Willet AH, McDonald NA, Gould KL. Regulation of contractile ring formation and septation in *Schizosaccharomyces pombe*. Curr Opin Microbiol. 2015;28:46–52.
[3] Simanis V. *Pombe's* thirteen - control of fission yeast cell division by the septation initiation network. J Cell Sci. 2015;128:1465–1474.
[4] Tomlin GC, Morrell JL, Gould KL. The spindle pole body protein Cdc11p links Sid4p to the fission yeast septation initiation network. Mol Biol Cell. 2002;13:1203–1214.
[5] Akamatsu M, Berro J, Pu KM, et al. Cytokinetic nodes in fission yeast arise from two distinct types of nodes

that merge during interphase. J Cell Biol. 2014;204:977–988.
[6] Sparks CA, Morphew M, McCollum D. Sid2p, a spindle pole body kinase that regulates the onset of cytokinesis. J Cell Biol. 1999;146:777–790.
[7] Willet AH, DeWitt AK, Beckley JR, et al. NDR kinase Sid2 drives Anillin-like Mid1 from the membrane to promote cytokinesis and medial division site placement. Curr Biol. 2019;29:1055–1063.
[8] Paoletti A, Chang F. Analysis of mid1p, a protein required for placement of the cell division site, reveals a link between the nucleus and the cell surface in fission yeast. Mol Biol Cell. 2000;11:2757–2773.
[9] Hachet O, Simanis V. Mid1p/anillin and the septation initiation network orchestrate contractile ring assembly for cytokinesis. Genes Dev. 2008;22:3205–3216.
[10] Almonacid M, Moseley JB, Janvore J, et al. Spatial control of cytokinesis by Cdr2 kinase and Mid1/Anillin nuclear export. Curr Biol. 2009;19(11):961–966.
[11] Chang F, Woollard A, Nurse P. Isolation and characterization of fission yeast mutants defective in the assembly and placement of the contractile actin ring. J Cell Sci. 1996;109(1):131–142.
[12] Saha S, Pollard TD. Anillin-related protein Mid1p coordinates the assembly of the cytokinetic contractile ring in fission yeast. Mol Biol Cell. 2012;23(20):3982–3992.
[13] Sun L, Guan R, Lee IJ, et al. Mechanistic insights into the anchorage of the contractile ring by Anillin and Mid1. Dev Cell. 2015;33(4):413–426. .
[14] Bhutta MS, McInerny CJ, Gould GW. ESCRT function in cytokinesis: location, dynamics and regulation by mitotic kinases. Int J Mol Sci. 2014a;15(12):21723–21739.
[15] Morita E, Colf LA, Karren MA, et al. VPS4 proteins are required for centrosome and spindle maintenance. Proc Natl Acad Sci. 2010;107(29):12889–12894.
[16] Carlton JG, Martin-Serrano J. Parallels between cytokinesis and retroviral budding: a role for the ESCRT machinery. Science. 2007;29(5833):1908–1912.
[17] Carlton JG, Caballe A, Agromayor M, et al. ESCRT-III governs the aurora B-mediated abscission checkpoint through CHMP4C. Science. 2012;336(6078):220–225.
[18] Vietri M, Radulovic M, Stenmark H. The many functions of ESCRTs. Nat Rev Mol Cell Biol. 2020;21(1):25–42.
[19] Elia N, Sougrat R, Spurlin TA, et al. Dynamics of endosomal sorting complex required for transport (ESCRT) machinery during cytokinesis and its role in abscission. Proc Natl Acad Sci. 2011;108(12):4846–4851.
[20] Goliand I, Adar-Levor S, Segal I, et al. Resolving ESCRT-III spirals at the intercellular bridge of dividing cells using 3D STORM. Cell Rep. 2018;24(7):1756–1764.
[21] Bhutta MS, Roy B, Gould GW, et al. A complex network of interactions between mitotic kinases, phosphatases and ESCRT proteins regulates septation and membrane trafficking in *S. pombe*. PLoS ONE. 2014b;9(10):e111789.
[22] Rincon SA, Paoletti A. Mid1/anillin and the spatial regulation of cytokinesis in fission yeast. Cytoskeleton. 2012;69(10):764–777.
[23] Iwaki T, Onishi M, Ikeuchi M, et al. Essential roles of class E Vps proteins for sorting into multivesicular bodies in *Schizosaccharomyces pombe*. Microbiology. 2007;153(8):2753–2764. .
[24] Chatterjee M, Pollard TD. The functionally important N-terminal half of fission yeast Mid1p anillin is intrinsically disordered and undergoes phase separation. Biochemistry. 2019;58(27):3031–3041.
[25] Saha S, Pollard TD, Wang Y-L. Characterization of structural and functional domains of the anillin-related protein Mid1p that contribute to cytokinesis in fission yeast. Mol Biol Cell. 2012;23(20):3993–4007.
[26] Capalbo L, Mela I, Abad MA, et al. Coordinated regulation of the ESCRT-III component CHMP4C by the chromosomal passenger complex and centralspindlin during cytokinesis. Open Biol. 2016;6(10):160248.
[27] Nähse V, Christ L, Stenmark H, et al. The Abscission Checkpoint: making It to the Final Cut. Trends Cell Biol. 2017;27(1):1–11.
[28] Caballe A, Wenzel DM, Agromayor M, et al. ULK3 regulates cytokinetic abscission by phosphorylating ESCRT-III proteins. Elife. 2015;26(4):e06547.
[29] Leverson JD, Huang HK, Forsburg SL, et al. *Schizosaccharomyces pombe* aurora-related kinase Ark1 interacts with the inner centromere protein Pic1 and mediates chromosome segregation and cytokinesis. Mol Biol Cell. 2002;13:1132–1143.
[30] Koch A, Krug K, Pengelley S, et al. Mitotic substrates of the kinase Aurora with roles in chromatin regulation identified through quantitative phosphoproteomics of fission yeast. Sci Signal. 2011;4:rs6–rs6.
[31] Carpy A, Krug K, Graf S, et al. Absolute proteome and phosphoproteome dynamics during the cell cycle of *Schizosaccharomyces pombe* (fission yeast). Mol Cell Proteomics. 2014;13:1925–1936.
[32] Kettenbach AN, Deng L, Wu Y, et al. Quantitative phosphoproteomics reveals pathways for coordination of cell growth and division by the conserved fission yeast kinase Pom1. Mol Cell Proteom. 2015;14:1275–1287.
[33] Swaffer MP, Jones AW, Flynn HR, et al. Quantitative phosphoproteomics reveals the signaling dynamics of cell-cycle kinases in the fission yeast *Schizosaccharomyces pombe*. Cell Rep. 2018;24:503–514.
[34] Almonacid M, Celton-Morizur S, Jakubowski JL, et al. Temporal control of contractile ring assembly by Plo1 regulation of Myosin II recruitment by Mid1/Anillin. Curr Biol. 2011;21:473–479.
[35] Moreno S, Klar A, Nurse P. Molecular genetic analysis of fission yeast *Schizosaccharomyces pombe*. Methods Enzymol. 1991;194:795–823.

[36] Rezig IM, Bremner SK, Bhutta MS, et al. Genetic and cytological methods to study ESCRT cell cycle function in fission yeast. Methods Mol Biol. 2019;1998:239–250.
[37] Bähler J, Steever AB, Wheatley S, et al. Role of polo kinase and Mid1p in determining the site of cell division in fission yeast. J Cell Biol. 1998;143:1603–1616.
[38] Motegi F, Mishra M, Balasubramanian MK, et al. Myosin-II reorganization during mitosis is controlled temporally by its dephosphorylation and spatially by Mid1 in fission yeast. J Cell Biol. 2004;165:685–695.

CELL CYCLE
2023, VOL. 22, NO. 6, 633–644
https://doi.org/10.1080/15384101.2022.2147655

Taylor & Francis
Taylor & Francis Group

REVIEW

The role of anillin/Mid1p during medial division and cytokinesis: from fission yeast to cancer cells

Imane M. Rezig[a,*], Wandiahyel G. Yaduma[a,b], Gwyn W. Gould[c], and Christopher J. McInerny[a]

[a]School of Molecular Biosciences, College of Medical, Veterinary and Life Sciences, Davidson Building, University of Glasgow, Glasgow, UK; [b]Department of Chemistry, School of Sciences, Adamawa State College of Education Hong, Nigeria; [c]Strathclyde Institute of Pharmacy and Biomedical Sciences, University of Strathclyde, Glasgow, UK

ABSTRACT

Cytokinesis is the final stage of cell division cycle when cellular constituents are separated to produce two daughter cells. This process is driven by the formation and constriction of a contractile ring. Progression of these events is controlled by mechanisms and proteins that are evolutionary conserved in eukaryotes from fungi to humans. Genetic and molecular studies in different model organisms identified essential cytokinesis genes, with several conserved proteins, including the anillin/Mid1p proteins, constituting the core cytokinetic machinery. The fission yeast *Schizosaccharomyces pombe* represents a well-established model organism to study eukaryotic cell cycle regulation. Cytokinesis in fission yeast and mammalian cells depends on the placement, assembly, maturation, and constriction of a medially located actin-myosin contractile ring (ACR). Here, we review aspects of the ACR assembly and cytokinesis process in fission yeast and consider the regulation of such events in mammalian cells. First, we briefly describe the role of anillin during mammalian ACR assembly and cytokinesis. Second, we describe different aspects of the anillin-like protein Mid1p regulation during the *S. pombe* cell cycle, including its structure, function, and phospho-regulation. Third, we briefly discuss Mid1pindependent ACR assembly in *S. pombe*. Fourth, we highlight emerging studies demonstrating the roles of anillin in human tumourigenesis introducing anillin as a potential drug target for cancer treatment. Collectively, we provide an overview of the current understanding of medial division and cytokinesis in *S. pombe* and suggest the implications of these observations in other eukaryotic organisms, including humans.

ARTICLE HISTORY
Received 7 June 2022
Revised 3 November 2022
Accepted 7 November 2022

KEYWORDS
Mid1p; anillin; fission yeast; cytokinesis

1. Introduction

1.1 Anillin-based contractile ring drives cytokinesis in mammalian cells

Cytokinesis initiation requires establishment of a medial division plane, the assembly of an actin-myosin contractile ring (ACR), and the ingression of a cleavage furrow, (*see* [1]for review). The scaffold protein anillin has a pivotal role in organizing the cytokinetic machinery and linking the ACR to the plasma membrane [2].

Anillin was first identified in the fruit fly *Drosophila melanogaster* in 1989 as an Factin-binding protein [3] (Figure 1); homologues of this protein were then characterized in all eukaryotes including the fission yeast Mid1p (also called Dmf1p) [4] [5] (Figure 1), and the human anillin [6] (Figure 1). These anillin-related proteins share a general structure that is conserved in metazoans [7]. The N-terminal region of human anillin includes binding sites for F-actin and myosin; such interactions with anillin are required for organization of the ACR [8]. The C-terminal region of human anillin contains three main domains: a Rho binding domain (RBD), a cryptic domain (C2), and a pleckstrin homology domain (PH); these domains promote efficient recruitment to the plasma membrane [2].

CONTACT Christopher J. McInerny Chris.Mcinerny@glasgow.ac.uk School of Molecular Biosciences, College of Medical, Veterinary and Life Sciences, Davidson Building, University of Glasgow, Glasgow G12 8QQ, UK

*present address: OMICS Research Core Facility, Faculty of Medicine, Kuwait University, Kuwait

Supplemental data for this article can be accessed online at https://doi.org/10.1080/15384101.2022.2147655.

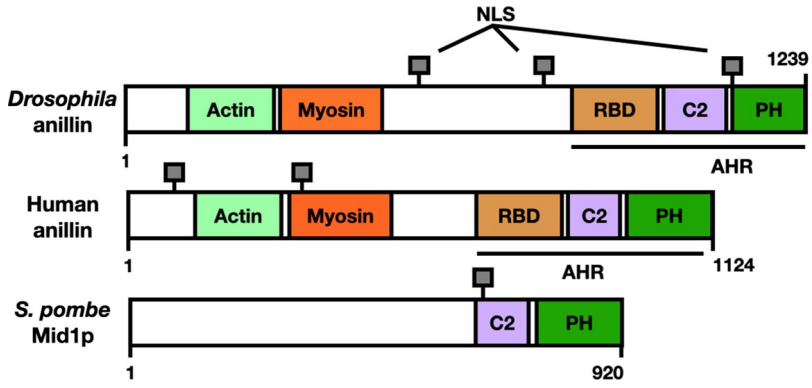

Figure 1. Anillin-related proteins in different systems show structural homology. The different characterized or putative domains are colour coded. RBD: Rho binding domain, C2: cryptic domain, PH: pleckstrin homology domain. Anillin homology region (AHR) and nuclear localization signals (NLS) are indicated. See main text for references.

1.2 Fission yeast as a model organism to study mammalian cytokinesis

The fission yeast *Schizosaccharomyces pombe* is a well-established model organism used for studying the eukaryotic cell cycle due to its short doubling time, simple organization, and tractable genetics [9]. The rod-shaped *S. pombe* cells grow by elongation at cell tips during interphase, then stop growth to divide through the assembly of a medial actin-myosin contractile ring (ACR) composed of actin filaments (F-actin) and type-II myosin (Myo2) [10, 11]. Medial formation of the ACR requires functions of the scaffold protein anillin/Mid1p [12].

Over the past decade, studies with *S. pombe* have led to a comprehensive understanding of Mid1p's function during ACR assembly and cytokinesis [12–16] [17,18] [19].

In this review, we describe aspects of ACR assembly and cytokinesis regulation in fission yeast and the regulation of such events in mammalian cells. First, we briefly describe the role of anillin during mammalian ACR assembly and cytokinesis (Section 2). Second, we focus on the different aspects of Mid1p regulation the *S. pombe* cell cycle, including Mid1p protein structure, biological functions, and phospho-regulation (Section 3). Third, we describe recent findings suggesting a Mid1p-independent ACR assembly mechanism during the *S. pombe* cell cycle (Section 4). Finally, we end with discussion of exciting recent studies that offer new insight into the emerging role of anillin in human tumourigenesis which introduce it as potential drug target for cancer treatments (Section 5).

2. Anillin-dependent assembly of ACR in mammalian cells

2.1 Anillin links the ACR to the plasma membrane during mammalian cell cycle

In mammalian cells, determining the site of division and the formation of a medial ACR involves activation of the small GTPase RhoA pathway [20]. Rho GTPases are regulated through switching their GDP/GTP status, in which activation is triggered by the Rho-specific guanine nucleotide exchange factors (RhoGEFs) through stimulating disassociation of the tightly bound GDP (*see* [21] for review). Exchange factor epithelial cell transforming sequence (ECT2), the direct upstream activator of RhoA, binds and activates GTP-bound RhoA [22]. Activation and recruitment of ECT2 is regulated by the centralspindlin complex during anaphase, with this complex being a heterotetramer composed of two dimers: Male Germ Cell (MgcRacGAP) and the Mitotic Kinesin Like Protein (MKLP1) [23] (Figure 2).

Once RhoA is activated, anillin is recruited to the site of division and integrates the RhoA signaling pathway with ACR formation [24]. Anillin has a direct role in connecting the ACR to the spindle microtubules and the plasma membrane to stabilize the cleavage furrow [8,25]. During abscission the ingressed cleavage furrow, a thin plasma membrane-based intracellular bridge (ICB) composed of bundles

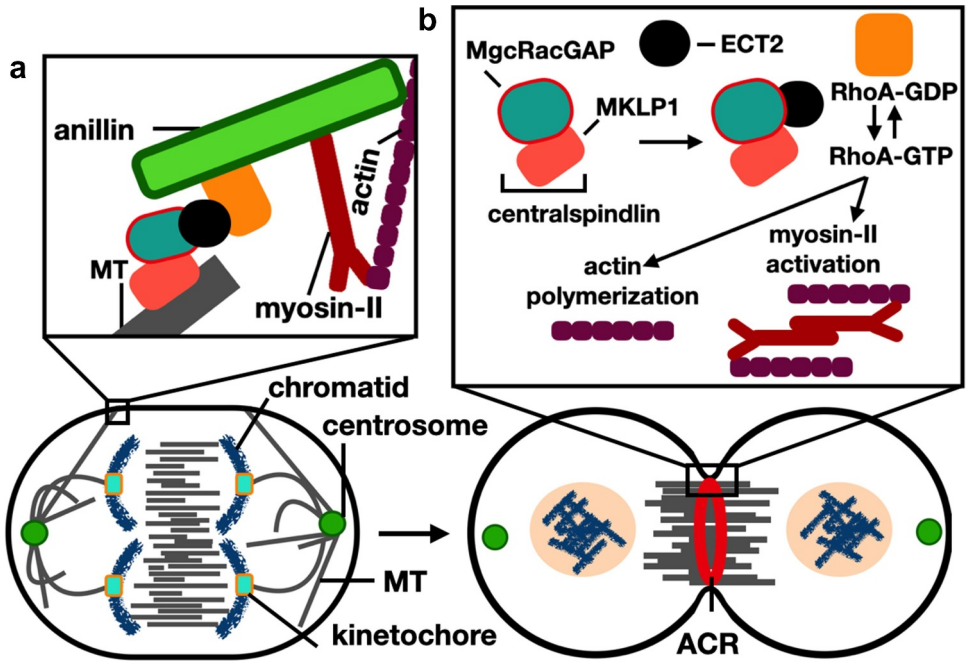

Figure 2. Cleavage furrow formation and ingression during cytokinesis in mammalian cells. Schematic representation of cells in anaphase (left) and telophase (right). (a) Anillin functions in connecting the spindle MT with the ACR through interactions with RhoA (*see* (b) for labels). (b) RhoA GTP-dependent activity is induced by interactions with the MgcRacgap and ECT2, after which leads to polymerization of actin filaments and induction of the phosphorylation-dependent myosin-II activation; these events lead to the formation and ingression of the cleavage furrow through interactions between myosin heads and actin filaments. *See* main text for references.

of microtubules, connects the two daughter cells. Recently, anillin was found to be involved in the biogenesis of the ICB by interacting with septin filaments (SEPT9) and the CIN85 complex to elongate and thin the ICB, whereby CIN85 connects the N-terminal domain of anillin to SEPT9 promoting active elongation of the ICB [25].

Anillin leaves the ICB prior to the last step of abscission [25] and, subsequently, cleavage of the ICB by the Endosomal Sorting Complex Required for Transport (ESCRT) proteins during abscission leads to the final separations of cells [26]. (Figure 2) describes the role of anillin during mammalian cytokinesis, *see* **Table S1** for *S. pombe* homologue proteins.

3. Mid1p-dependent assembly of ACR in *S. pombe* cells

3.1 Medial positioning of the ACR in *S. pombe* is linked to the position of the nucleus and Mid1p localization to assemble cortical nodes

The nucleus in *S. pombe* cells is medially positioned. This is achieved through the microtubules (MTs) organizing center which form the MTs into antiparallel bundles along the long axis of the cell during interphase [27,28]. It was suggested by [29]that medial positioning is preserved in *S. pombe* nuclei due to the opposing pushing forces generated by the interphase MTs located on both cell ends, and that growth of MTs at cell tips pushes the nucleus. Furthermore, computer modeling revealed that these pushing forces are balanced to create a mechanism for medial positioning of the nucleus [29]. Based on a significant body of evidence, it is hypothesized that the position of the nucleus is critical for medial ACR positioning in *S. pombe*.

Daga and Chang [30] tested this hypothesis and demonstrated that moving the nucleus away from the cell center in *S. pombe* influences the position of ACR assembly during early mitosis. Such nuclear displacement experiments resulted in the formation of multiple ACRs.

Mid1p is non-essential for viability in *S. pombe*, however, the absence of Mid1p leads to cytokinesis failure at higher temperatures [4]. Since the identification and characterization of Mid1p, its localization pattern throughout the cell cycle of *S. pombe* has been extensively studied [12–16] [17,18] [19].

Initially, Mid1p localizes to the nucleus and shuttles between the nucleus and cell cortex using nuclear localization (NLS, Figure 3) and nuclear export (NES, Figure 3) sequences during interphase and early mitosis [12]. Mid1p is then phosphorylated by the polo-like kinase Plo1p which targets the export of Mid1p from the nucleus to the cytoplasm [13], where it recruits several other proteins to assemble two types of nodes [33].

Type-I interphase nodes are composed of Mid1p and the Cdr1p and Cdr2p kinases [34]. Type-II interphase nodes form from components of the previous division disassembled ACR, including Gef2p, Blt1p, Klp8p, and Nod1p [33]. Type-I nodes interact with the cell membrane through the pleckstrin homology (PH) domain and the cryptic (C2) domains of Mid1p [2], while Type-II nodes interact through the phospholipid-binding protein Blt1p [35]. Upon the onset of mitosis Myo2p, Rlc1p, Cdc4p, Rng2p, Cdc12p, and Cdc15p are recruited to interphase nodes to form the cytokinesis nodes [36,37]. Cdc12p is responsible for the polymerization of actin filaments and, at this stage, interactions between Myo2p and the polymerized actin filaments lead to cytokinesis nodes condensation assembly of the ACR [38]. Schematic representations of Mid1p domain organization-binding sites of cytokinesis proteins, and Mid1p-dependent ACR assembly mechanism are shown in Figures 3 and 4, respectively.

The number and composition of cytokinesis nodes has been extensively studied in fission yeast [19–33] [34–36] [37,38] [39–41]. However, some studies underestimated the number of cytokinesis nodes due to limitations in imaging techniques and the lack of a 3D reconstitution approach. For example, closely spaced nodes cannot be resolved using conventional confocal microscopy.

Using super-resolution single-molecule localization microscopy [42] showed that cytokinesis nodes are uniform in size and composition. A recent study by Sayyad and Pollard [43] used a 3D reconstitution approach using Airyscan fluorescence imaging in live *S. pombe* cells to count the total number of single cytokinesis nodes. Using Blt1p as a cytokinesis marker in wild-type cells, 190 cytokinesis nodes were detected at the cell equator during early mitosis. Furthermore, 85% of Blt1p-mEGFP in these nodes is incorporated into the ACR during early mitosis [43].

3.2 Medial positioning of the ACR in *S. pombe* is mediated by Pom1p kinase

The dual-specificity tyrosine-regulated kinase (DYRK) Pom1p plays a regulatory role in medial positioning of the ACR in *S. pombe* through a "tip occlusion" inhibitory mechanism [44], whereby a Pom1p-based gradient emanating from the cell tips act as a negative signal to regulate division plane placement. Additionally, reversible binding of Pom1p to the plasma membrane is affected by its phosphorylation status [45].

The polarity determinant Tea4p phosphatase is deposited at the cell tips through interactions with microtubules [46]. Tea4p recruits Pom1p to the cell cortex through de-phosphorylation, and this triggers lateral movement of Pom1p at the plasma membrane through Pom1's lipid-binding region. Pom1p is then released into the cytoplasm through auto-phosphorylating its lipid-binding region [44]. [47] confirmed *in vitro* and *in vivo* intermolecular auto-phosphorylation of Pom1p; furthermore, Pom1p gradient decay length showed a strong negative correlation with Pom1p amplitude,

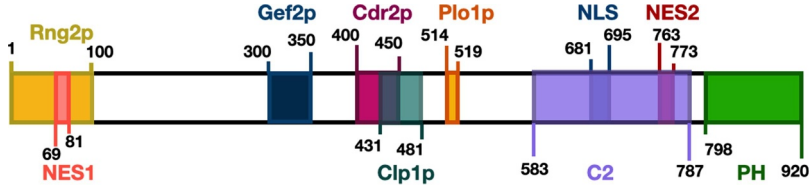

Figure 3. Schematic of *S. pombe* Mid1p domain organization and the binding sites of proteins involved in cytokinesis. (A) Rng2p [13], Gef2p [31], Cdr2p [14], Clp1p [32] and Plo1p [13] binding sites in addition to the nuclear export sequence NES, C2 domain, nuclear localization sequence NLS, and pleckstrin homology domain PH [12], are shown in different colours.

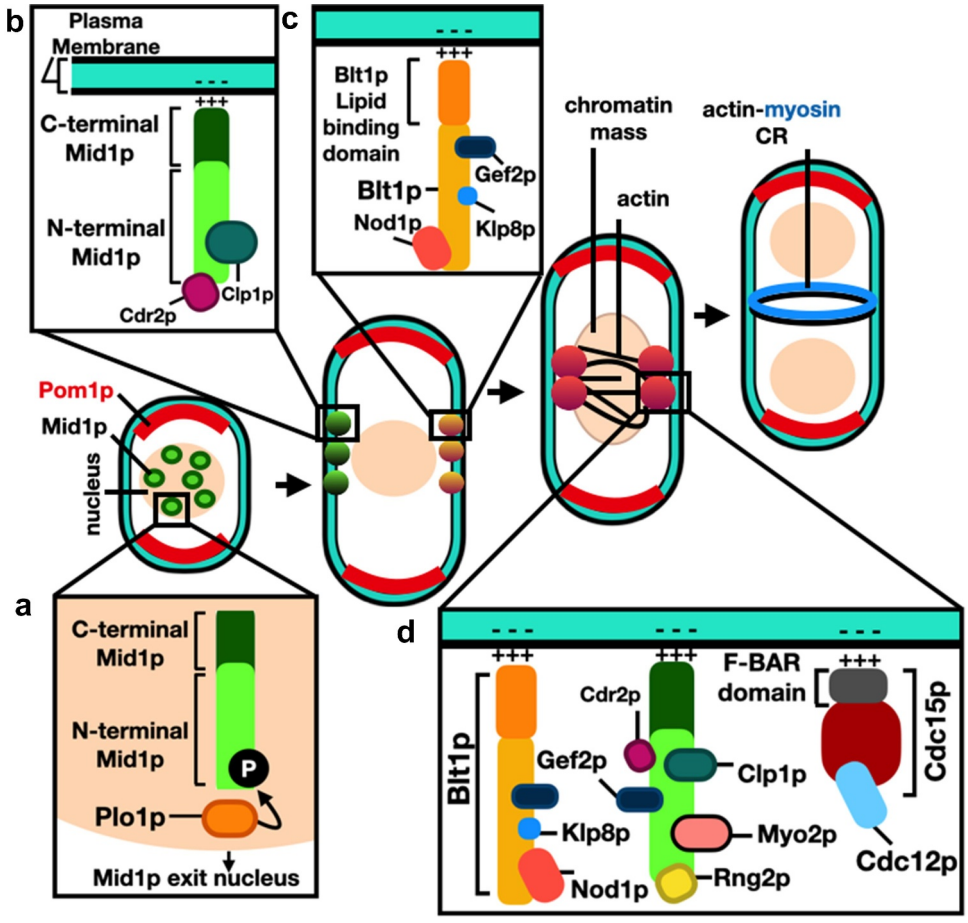

Figure 4. Mid1p-dependent actin-myosin contractile ring (ACR) assembly in *S. pombe*. (a) Phosphorylation of Mid1p by Plo1p kinase triggers its release from the nucleus. (b) Type-I interphase nodes form by sequential recruitment of Mid1p, Cdr1p and Cdr2p, they interact with the cell membrane through the PH and C2 domains of Mid1p. (c) Type-II interphase nodes form by sequential recruitment of Gef2p, Blt1p, Klp8p and Nod1p, they interact through the membrane binding domain of Blt1p. (d) Cytokinesis nodes form when Type-II interphase nodes are captured by Type-I nodes after they migrate to the medial cortex, and upon the onset of mitosis, Myo2p, Rng2p, Cdc12p and Cdc15p are recruited to interphase nodes, cytokinesis nodes then condense into the actin-myosin contractile ring. *See* main text and Table S1 for references and mammalian homologue proteins. .

suggesting that this correlation results from a buffering mechanism on the decay length.

[48] utilized super resolution microscopy to track individual Pom1p molecules inside *S. pombe* cells. They found that Pom1p travels between clusters in a "hopping" manner to move from the cell tip toward the medial region of the cell, with these clusters creating the gradient. Additionally, they confirmed Pom1p distribution at the plasma membrane through the cycle of Pom1p gradient phosphorylation and de-phosphorylation events [49]. revealed that the PP2C phosphatase Ptc1p dephosphorylates Pom1p *in vitro*, and both proteins are able to form complexes *in vivo*. They propose a scenario where Ptc1p influences Pom1p distribution through reversing its phosphorylation status. Another recent study by [50] looked at the status of Pom1p in the absence of Mid1p. They found that Pom1p prevents division at cell tips even in the absence or mislocalization of Mid1p. Their results also revealed that the phosphorylation of the mitotic inducer Cdc15p by Pom1p kinase disrupts its membrane-binding ability; this disruption inhibits Cdc15p's scaffolding function during cytokinesis. Such studies emphasize a need to understand the control of phosphorylation dynamics in Mid1p, as discussed in (Section 3.4).

3.3 The structure and molecular function of Mid1p

Saha and Pollard [18] investigated the biological functions of Mid1p domains during the *S. pombe* cell cycle and found that residues (1–149) of Mid1p are essential for the correct orientation and positioning of septa. Furthermore, the same residues (1–149) are required but not sufficient for the localization of full-length Mid1p to cortical nodes. However, residues (1–452) facilitate Mid1p functions including localization and concentration in cortical nodes during mitosis, while residues (1–578) are required for the assembly of several node components including Myo2p and Cdc15, and residues (579–797) resemble the insoluble domain of Mid1p and facilitate condensation of nodes into the ACR.

Residues (798–920) of Mid1p contain the C-terminal PH domain [5,18]. The structure of Mid1p has two membraneanchoring elements, the C2 lipid-binding domain and the PH domain [2]. The Mid1p-N452 domain, composed of the Mid1p N-terminal residues (1452), is intrinsically disordered, and this flexible nature may facilitate the export of Mid1p from the nucleus during early mitosis [15]. Interestingly, this domain of Mid1p contains multiple residues that are phosphorylated when expressed in insect cells. This appears to regulate self-association of Mid1p-N452. Present models suggest that phosphorylation (e.g. by Plo1p - *see* Section 3.4) could control Mid1p export from the nucleus by "solubilizing" the protein, as non-phosphorylated Mid1p-N452 has increased tendency to aggregate [15]. Of note, this domain does not interact with Myo2 [15]. A schematic representation of the Mid1p structural domains is shown in (Figure 5).

It is worth noting that both mammalian anillin and *S. pombe* Mid1p share functional similarities, hence both are multi-domain scaffolding proteins and bridge the cell cortex with the ACR during mammalian [51] and *S. pombe* [33] cytokinesis, respectively. Furthermore, functional analysis of mammalian anillin and *S. pombe* Mid1p showed that both proteins have cryptic membrane associating elements and bind to membrane lipids through a C2 cryptic domain [2]. The following section describes Mid1p molecular structure and phospho-regulation during *S. pombe* cell cycle.

3.4 Phospho-regulation of Mid1p

[15]investigated the phosphorylation of Mid1p N-terminal region including residues (1–452): Mid1p-N452. They used two methods: the disorder-enhanced phosphorylation predictor (DISPHOS) tool to predict phosphorylation sites, and matrix-assisted laser desorption/ionization (MALDI) mass spectrometry to identify phosphorylated residues. Such analyses confirmed Mid1pN452 phosphorylation by six of the nine consensus Sid2p phosphorylation sites [52], three of four minimal consensus Cdk1p phosphorylation sites [53], and one of the eight consensus Plo1p phosphorylation sites [54]. Phospho-regulation of Mid1p by various kinases is discussed below.

Early studies by [55]described a physical interaction between the *S. pombe* polo-like kinase Plo1p and Mid1p proteins, and that this interaction was required for the correct localization of

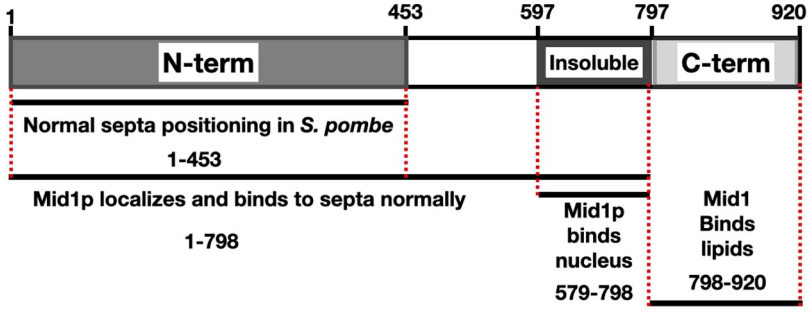

Figure 5. A schematic of Mid1p domains and their role during mitosis and cytokinesis in S. pombe. (a) Mid1p residues 1-453 resemble the N-terminal domain. (b) Mid1p residues 579-797 resemble the Insoluble domain. (c) Mid1p residues 798-920 resemble the C-terminal PH domain. Red broken lines represent Mid1p domain boundaries. Black lines represent fragments of Mid1p sufficient for the role denoted below each line. Figure adapted from Saha and Pollard (2012).

Mid1p to the ACR. It was later confirmed by [13] that phosphorylation of residues within the first 100 amino acids of the N-terminal region of Mid1p by Plo1p triggers Mid1p release from the nucleus and promotes the association of Mid1p with interphase nodes leading to mitotic entry. Such phosphorylation also facilitates Myo2p recruitment to medial cortical nodes.

While Mid1p has a regulatory role of ACR medial assembly, the NDR-family kinase Sid2p has a controlling role during the later stages of cytokinesis to promote ring constriction and septation leading to completion of cell division. However, Mid1p departs from the site of division at ACR constriction onset [5]; this event is concurrent with the translocation of Sid2p from spindle pole bodies (SPBs) to the ACR [56]. Sid2p consensus phosphorylation motifs are found in the Mid1p amino acid sequence [52].

[19]found that a Mid1p phospho-deficient mutant that cannot be phosphorylated by Sid2p kinase remains attached to the plasma membrane throughout cytokinesis. Furthermore, after completion of cell division this mutant over-accumulates in interphase nodes and leads to early recruitment of ACR proteins to interphase nodes. This study also confirmed the phosphorylation of Mid1p by Sid2p on residues within the N-terminal domain (1–578); additionally, it provided evidence that removal of Mid1p from the cell cortex is driven by this phosphorylation event.

[16]revealed that Cdc42-activated polarity kinase (Pak1p) is localized to the assembling ACR and maintains this localization during septation. In this study, a large-scale phosphoproteomic screen identified Mid1p and Cdc15p as Pak1p substrates. Disturbing the Pak1p/Mid1p signaling pathway produced defective and misplaced ACRs; however, such defective phenotypes are rescued by synthetic tethering of Mid1p to cortical nodes. Therefore, it is suggested that Pak1p phosphorylation of the N-terminal region of Mid1p promotes its association with interphase nodes.

Interestingly, the N-terminal region of Mid1p is phospho-regulated by three kinases. Phosphorylation by Plo1p promotes Mid1p nuclear export and the onset of mitosis [13], phosphorylation by Pak1p promotes Mid1p association with interphase nodes [16]; and phosphorylation by Sid2p promotes Mid1p removal from the cell cortex [19]. Phospho-regulation of Mid1p is schematically represented in Figure 6.

Recent work tested the genetic interactions *in S. pombe* between three classes of genes: *mid1*, the ESCRT *vps4*, and the aurora kinase *ark1*. Genetic interactions were detected between the *mid1* gene and both *vps4* and *ark1* genes; such interactions suggest a link between the regulation of Mid1p's function by both Vps4p and Ark1p [17,57]. Furthermore, it was found that Vps4p physically interacts with the C-terminal region of Mid1p, with this interaction important for the localization of Mid1p in cells. It appears that the function of Mid1p is regulated by associating with Vps4p, with this association directly or indirectly involving the Mid1p PH domain cell cortex anchorage to regulate Mid1p-dependent node cortical attachment to promote medial division [17].

Mid1p phospho-regulation was examined by combining three approaches: *in vitro* phosphorylation studies, tandem mass spectrometry (nLC-MS

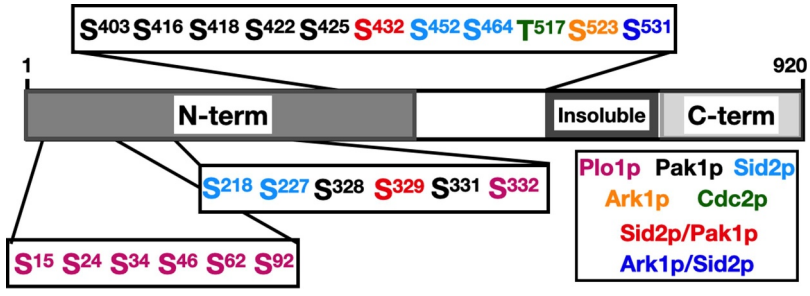

Figure 6. Schematic of *S. pombe* Mid1p phospho-regulation. Phosphorylation sites of Mid1p - *see* Figure 5 legend for Mid1p domain structure - by Plo1p [13, 17], Cdc2p [13], Pak1p [16], Ark1p [17], and Sid2p [19]. Please *see* Table S2 for description of each phosphorylation event.

/MS) analysis and interrogating published *S. pombe* global proteomic data. Such approaches identified several amino acid residues as potential phospho-acceptor sites in Mid1p by aurora and polo-like kinases (Figure 6), with S332, S523, and S531 required for the function of Mid1p in *S. pombe* [17].

Despite the major role of Mid1p is cytokinesis, recent studies suggest that Mid1p is dispensable for the organization of cytokinesis proteins into nodes [58]. The next section therefore discusses Mid1p-independent ACR assembly mechanisms.

4. Mid1p-independent assembly of ACR during the *S. pombe* cell cycle

4.1 Mid1p-independent molecular organization of nodes during the *S. pombe* cell cycle

In *S. pombe*, a chromosomal deletion of the *mid1* gene (*mid1*Δ) causes dramatic defects in septation phenotypes resulting in branched and multi-septated cells; furthermore, ACR assembly is delayed in *mid1*Δ cells [5,14,59]. This confirms the requirement of Mid1p function for correct division plane positioning. It is known that Mid1p recruits Rng2p to the division site, which results in the accumulation of ACR components [60]. However, is Mid1p solely responsible for regulating the ACR position?

To address this question [61], performed a "rewiring" experiment and examined the localization of several proteins in reconstituted cells, which are *S. pombe* cells artificially made to divide medially in the absence of Mid1p. Medial division in these *mid1* mutants was restored by artificial targeting of Rng2p, Cdc12p, and Myo2p to the division site. However, in these cells the ACR assembles late during anaphase suggesting that an interaction of Mid1p with one or more ACR proteins is required for ACR assembly during early mitosis. Assembly of the ACR is a complex process. Fortunately, there is a growing understanding of ACR protein composition, mechanism of assembly, and its function; but what is molecular structure of the ACR?

To answer this question [62]used super-resolution microscopy and fluorescence resonance energy transfer (FRET) to examine 29 ACR protein components and determined their spatial organization relative to the plasma membrane. This allowed the classification of ACR protein components into three layers: a proximal layer (0–0.8 nm) composed of scaffold proteins such as Mid1p and Cdc15p; an intermediate layer (80–160 nm) composed of a network of cytokinesis accessory proteins such as Rng2p; and a distal layer (160–350 nm) composed of Factin, the motor domain of myosin. Although prior knowledge indicates when proteins are recruited to the ACR, with the three layers of proteins corresponding to the order of assembly of ACR components, additional studies are required to reveal the spatial organization of signaling components of the ACR [33, 36] [37,42].

A recent study by [58]investigated the molecular organization of four cytokinesis proteins, Rng2p, Myo2p, Cdc12p, and Cdc15p, in the absence of Mid1p. They found that ACRs with the ability to constrict assemble from loops of strands composed of actin filaments and cytokinesis proteins in *mid1*Δ cells. Additionally, nodes were observed in the strands of these cells confirming that Mid1p is unnecessary for the organization of cytokinesis nodes components. Two types of strands were identified in *mid1*Δ cells, nascent strands with nodes organized into short-linked strings, and enduring strands with nodes aligning onto long strands across the cell length. These data suggest that Mid1p is dispensable for ACR positioning and organization of cytokinesis into nodes.

5. Cytokinesis, anillin, and cancer

5.1 The function of anillin in the eukaryotic cell cycle and its role in tumourigenesis

In mammalian cells, positive signals generated by the central spindle with anillin connecting the ACR to the cell cortex ensure medial placement of the ACR [51]. The scaffolding protein anillin is essential for cytokinesis regulation, and its inhibition results in cytokinesis failure and cell multi-nucleation [6]. Anillin is composed of two functional parts: the N-terminal region, triggering actin polymerization and myosin-II activation leading to the assembly of a stable ACR [63]; and the C- terminal region, associating with RhoA, septins, and $PI(2,4)P_2$ connecting the ACR to the cell cortex [2,64].

Anillin is a substrate for mitotic kinases and its recruitment to the equatorial membrane is regulated by phosphorylation. Kim and colleagues identified phosphorylation of a single residue, S635, as a key determinant mediating cytokinesis regulating anillin's recruitment to the equatorial cortex and mediating stabilization of the cleavage furrow [65].

Following its discovery, anillin was studied mainly by cell and developmental biologists to discover the mechanisms of cell division, without being associated with human diseases. However, numerous recent studies suggest that anillin is involved in tumorigenesis in various types of cells. For example [66], demonstrated that anillin is overexpressed in human gastric cancer (GC) tissues and that depletion of anillin in these tissues inhibits the proliferation of GC cells. Additionally, a recent study by Xiao and colleagues (2020) investigated the regulation mechanism of anillin in human hepatocellular carcinoma (HCC). They found that anillin had a significant facilitating effect on cell proliferation *in vitro* and induced remarkable HCC tumor growth *in vivo*. The transcription factor SRY-Box transcription factor 4 (SOX4) had an increase in expression profile which correlates with anillin; it also interacts with specific DNA sequences in the anillin gene promoter region. The microRNA miR-138 was identified as an upstream regulator of SOX4, and overexpression of anillin was induced by a potential axis of both transcription elements: SOX4 and miR-138 [67]. Overall, similar results from studies in HCC suggest a molecular mechanism with which anillin might induce tumourigenesis [68,69]. Therefore, targeting anillin and/or its upstream regulators is a potential innovative strategy for HCC treatment.

Broadly, similar results were observed in breast cancer cell lines, where knocking down anillin significantly reduces the migration of breast cancer cells [70]. Similarly, transiently knocking down anillin protein in breast cancer cells increased the number of senescent cells, with cells accumulating in the G2/M phase of the cell cycle with effects on cell morphology including poly-nucleated cells [71]; such effects are consistent with the role of anillin during cytokinesis. Additionally, anillin is markedly overexpressed in breast cancer cells [72; 73]. A mechanism for anillin function to induce tumor activity was proposed by [73]. They suggested that such tumor-promoting activity involves transcriptional re-programming of breast cancer cells affecting their self-renewal and differentiation properties. Whatever the explanation, it is clear that the mis-regulation of anillin in human cells is associated with multiple forms of tumorigenesis and cancer.

6. Concluding remarks

How eukaryotic cells establish medial division to complete duplication and division remains a fascinating and complex question. Studies with fission yeast have revealed important aspects of medial division including proteins participating during cytokinesis, mechanisms of division site specification, and medial ACR assembly. The scaffold proteins anillin and Mid1p play important roles during mammalian and fission yeast cell cycle, respectively. In this review, we address important questions on how the current understanding of fission yeast cytokinesis can be applied to understand the regulation of cytokinesis in mammalian cells.

Phospho-regulation of Mid1p is required to regulate *S. pombe* cell cycle events starting with Mid1p release from the nucleus to promote the association of Mid1p with interphase nodes leading to mitotic entry [13], then Mid1p association with interphase nodes [16], and finally the removal of Mid1p from the cell cortex during the later stages of cytokinesis [19]. Mid1p is a major component of cytokinesis nodes serving as precursors of the ACR during cytokinesis. Recent advances in microscopic methods allowed the dissection of the structural organization of such assemblies revealing the relationship of cytokinesis nodes and cell size [43].

Cytokinesis failure can occur due to multiple mechanisms, including altered expression of proteins that regulate cytokinesis initiation or progression [74]. Attention is being drawn toward the use of cell cycle regulators of cytokinesis as biomarkers of several cancer types, and recent reviews describe the roles of anillin [75], aurora kinases [76], and polo-like kinases [77] in tumourigenesis. Furthermore, anillin and these mitotic

kinases have further cell cycle roles beyond controlling cytokinesis, which may be also related to tumorigenesis, and so could be important potential drug targets in future cancer treatments.

Disclosure statement

No potential conflict of interest was reported by the author(s).

Funding

This work was supported by the Tertiary Education Trust Fund (TETFUND) and Adamawa State College of Education, Nigeria studentship [grant number TETF/DASTD/COE/HONG/ASTD/2016/Vol.1] to WGY

Data availability statement

The authors confirm that the data used in this review paper are available within the cited references.

ORCID

Christopher J. McInerny http://orcid.org/0000-0002-9201-3479

References

[1] Glotzer M. The molecular requirements for cytokinesis. Science. 2005;307(5716):1735–1739.
[2] Sun L, Guan R, Lee IJ, et al. Mechanistic Insights into the anchorage of the contractile ring by anillin and Mid1. Dev Cell. 2015;33(4):413–426.
[3] Miller KG, Field CM, Alberts BM. Actin-binding proteins from *Drosophila* embryos: a complex network of interacting proteins detected by F- actin affinity chromatography. J Cell Biol. 1989;109(6 Pt 1):2963–2975.
[4] Chang F, Woollard A, Nurse P. Isolation and characterization of fission yeast mutants defective in the assembly and placement of the contractile actin ring. J Cell Sci. 1996;109(1):131–142.
[5] Sohrmann M, Fankhauser C, Brodbeck C, et al. The *dmf1/mid1* gene is essential for correct positioning of the division septum in fission yeast. Genes Dev. 1996;10(21):2707–2719.
[6] Oegema K, Savoian MS, Mitchison TJ, et al. Functional analysis of a human homologue of the *Drosophila* actin binding protein Anillin suggests a role in cytokinesis. J Cell Biol. 2000;150(3):539–552.
[7] D'Avino PP. How to scaffold the contractile ring for a safe cytokinesis - lessons from anillin-related proteins. J Cell Sci. 2009;122(8):1071–1079.
[8] Straight AF, Field CM, Mitchison TJ. Anillin binds nonmuscle Myosin II and regulates the contractile ring. Mol Biol Cell. 2005;16(1):193–201.
[9] Fantes PA, Hoffman CS. A brief history *of Schizosaccharomyces pombe* research: a perspective over the past 70 years. Genetics. 2016;203(2):621–629.
[10] Kitayama C, Sugimoto A, Yamamoto M. Type II myosin heavy chain encoded by the *myo2* gene composes the contractile ring during cytokinesis in *Schizosaccharomyces pombe*. J Cell Biol. 1997;137(6):1309–1319.
[11] Rincon SA, Paoletti A. Mid1/Anillin and the spatial regulation of cytokinesis in fission yeast. Cytoskeleton. 2012;69(10):764–777.
[12] Paoletti A, Chang F, Stearns T. Analysis of Mid1p, a protein required for placement of the cell division site, reveals a link between the nucleus and the cell surface in fission yeast. Mol Biol Cell. 2000;11(8):2757–2773.
[13] Almonacid M, Celton-Morizur S, Jakubowski JL, et al. Temporal control of contractile ring assembly by Plo1 regulation of Myosin II recruitment by Mid1/anillin. Curr Biol. 2011;21(6):473–479.
[14] Almonacid M, Moseley JB, Janvore J, et al. Spatial control of cytokinesis by Cdr2 kinase and Mid1/anillin nuclear export. Curr Biol. 2009;19(11):961–966.
[15] Chatterjee M, Pollard TD. The functionally important N-terminal half of fission yeast Mid1p anillin is intrinsically disordered and undergoes phase separation. Biochemistry. 2019;58(27):3031–3041.
[16] Magliozzi JO, Sears J, Cressey L, et al. Fission yeast Pak1 phosphorylates anillin-like Mid1 for spatial control of cytokinesis. J Cell Biol. 2020;219(8):e201908017.
[17] Rezig IM, Yaduma WG, Gould GW, et al. Anillin/Mid1p interacts with the ESCRT-associated protein Vps4p and mitotic kinases to regulate cytokinesis in fission yeast. Cell Cycle. 2021;20(18):1845–1860.
[18] Saha S, Pollard TD, Wang Y-L. Characterization of structural and functional domains of the anillin-related protein Mid1p that contribute to cytokinesis in fission yeast. Mol Biol Cell. 2012;23(20):3993–4007.
[19] Willet AH, DeWitt AK, Beckley JR, et al. NDR kinase Sid2 drives anillin-like Mid1 from the membrane to promote cytokinesis and medial division site placement. Curr Biol. 2019;29(6):1055–1063.e2.
[20] Basant A, Glotzer M. Spatiotemporal Regulation of RhoA during Cytokinesis. Curr Biol. 2018;28(9):R570–580.
[21] Petronczki M, Tedeschi A. Cell division: switching on ECT2 in a non-canonical fashion. Curr Biol. 2020;30(16):R947–949.
[22] Kim J-E, Billadeau DD, Chen J. The tandem BRCT domains of Ect2 are required for both negative and

positive regulation of Ect2 in cytokinesis. J Biol Chem. 2005;280(7):5733–5739.
[23] Yüce O, Piekny A, Glotzer M. An ECT2-centralspindlin complex regulates the localization and function of RhoA. J Cell Biol. 2005;170(4):571–582.
[24] Chen A, Arora PD, McCulloch CA, et al. Cytokinesis requires localized β-actin filament production by an actin isoform specific nucleator. Nat Commun. 2017;8 (1):1530.
[25] Panagiotou TC, Chen A, Wilde A. An anillin-CIN85-SEPT9 complex promotes intercellular bridge maturation required for successful cytokinesis. Cell Rep. 2022;40(9):111274.
[26] Nähse V, Christ L, Stenmark H, et al. The abscission checkpoint: making it to the final cut. Trends Cell Biol. 2017;27(1):1–11.
[27] Ashraf S, Tay YD, Kelly DA, et al. Microtubuleindependent movement of the fission yeast nucleus. J Cell Sci. 2021;134 (6):jcs253021.
[28] Chang F, Nurse P. How fission yeast fission in the middle. Cell. 1996;84(2):191–194.
[29] Tran PT, Marsh L, Doye V, et al. A mechanism for nuclear positioning in fission yeast based on microtubule pushing. J Cell Biol. 2001;153(2):397–411.
[30] Daga RR, Chang F. Dynamic positioning of the fission yeast cell division plane. PNAS USA. 2005;102 (23):8228–8232.
[31] Ye Y, Lee IJ, Runge KW, et al. Roles of putative RhoGEF Gef2 in division-site positioning and contractile-ring function in fission yeast cytokinesis. Mol Biol Cell. 2012;23(7):1181–1195.
[32] Clifford DM, Wolfe BA, Roberts Galbraith RH, et al. The Clp1/Cdc14 phosphatase contributes to the robustness of cytokinesis by association with anillin-related Mid1. J Cell Biol. 2008;181(1):79–88.
[33] Akamatsu M, Berro J, Pu KM, et al. Cytokinetic nodes in fission yeast arise from two distinct types of nodes that merge during interphase. J Cell Biol. 2014;204 (6):977–988.
[34] Moseley JB, Mayeux A, Paoletti A, et al. A spatial gradient coordinates cell size and mitotic entry in fission yeast. Nature. 2009;459(7248):857–860.
[35] Guzman-Vendrell M, Baldissard S, Almonacid M, et al. Blt1 and Mid1 provide overlapping membrane anchors to position the division plane in fission yeast. Mol Cell Biol. 2013;33(2):418–428.
[36] Laporte D, Coffman VC, Lee IJ, et al. Assembly and architecture of precursor nodes during fission yeast cytokinesis. J Cell Biol. 2011;192(6):1005–1021.
[37] Wu JQ, Kuhn JR, Kovar DR, et al. Spatial and temporal pathway for assembly and constriction of the contractile ring in fission yeast cytokinesis. Dev Cell. 2003;5 (5):723–734.
[38] Vavylonis D, Wu JQ, Hao S, et al. Assembly mechanism of the contractile ring for cytokinesis by fission yeast. Science. 2008;319(5859):97–100.
[39] Akamatsu M, Lin Y, Bewersdorf J, et al. Analysis of interphase node proteins in fission yeast by quantitative and superresolution fluorescence microscopy. Mol Biol Cell. 2017;28(23):3203–3214.
[40] Deng L, Moseley JB, Lew DJ. Compartmentalized nodes control mitotic entry signaling in fission yeast. Mol Biol Cell. 2013;24(12):1872–1881.
[41] Pan KZ, Saunders TE, Flor-Parra I, et al. Cortical regulation of cell size by a sizer cdr2p. Elife. 2014;3: e02040.
[42] Laplante C, Huang F, Tebbs IR, et al. Molecular organization of cytokinesis nodes and contractile rings by superresolution fluorescence microscopy of live fission yeast. PNAS USA. 2016;113(40):E5876–5885.
[43] Sayyad WA, Pollard TD. The number of cytokinesis nodes in mitotic fission yeast scales with cell size. Elife. 2022;11:e76249.
[44] Huang Y, Chew TG, Ge W, et al. Polarity determinants Tea1p, Tea4p, and Pom1p inhibit division-septum assembly at cell ends in fission yeast. Dev Cell. 2007;12(6):987–996.
[45] Hachet O, Berthelot-Grosjean M, Kokkoris K, et al. A phosphorylation cycle shapes gradients of the DYRK family kinase Pom1 at the plasma membrane. Cell. 2011;145(7):1116–1128.
[46] Chiou JG, Balasubramanian MK, Lew DJ. Cell Polarity in Yeast. Annu Rev Cell Dev Biol. 2017;33(1):77–101.
[47] Hersch M, Hachet O, Dalessi S, et al. Pom1 gradient buffering through intermolecular autophosphorylation. Mol Syst Biol. 2015;11(7):818.
[48] Gerganova V, Floderer C, Archetti A, et al. Multiphosphorylation reaction and clustering tune Pom1 gradient mid-cell levels according to cell size. Elife. 2019;8:e45983.
[49] Gerganova V, Bhatia P, Vincenzetti V, et al. Direct and indirect regulation of Pom1 cell size pathway by the protein phosphatase 2C Ptc1. Mol Biol Cell. 2021;32 (8):703–711.
[50] Bhattacharjee R, Mangione MC, Wos M, et al. DYRK kinase Pom1 drives F-BAR protein Cdc15 from the membrane to promote medial division. Mol Biol Cell. 2020;31(9):917–929.
[51] Piekny AJ, Glotzer M. Anillin is a scaffold protein that links RhoA, actin, and myosin during cytokinesis. Curr Biol. 2008;18(1):30–36.
[52] Chen CT, Feoktistova A, Chen JS, et al. The SIN kinase Sid2 regulates cyto-plasmic retention of the *S. pombe* Cdc14-like phosphatase Clp1. Curr Biol. 2008;18 (20):1594–1599.
[53] Swaffer MP, Jones AW, Flynn HR, et al. CDK substrate phosphorylation and ordering the cell cycle. Cell. 2016;167(7):1750–1761.e16.
[54] Suzuki K, Sako K, Akiyama K, et al. Identification of non-Ser/Thr-Pro consensus motifs for Cdk1 and their roles in mitotic regulation of C2H2 zinc finger proteins and Ect2. Sci Rep. 2015;5(1):7929.

[55] Bähler J, Pringle JR. Pom1p, a fission yeast protein kinase that provides positional information for both polarized growth and cytokinesis. Genes Dev. 1998;12 (9):1356–1370.
[56] Sparks CA, Morphew M, McCollum D. Sid2p, a spindle pole body kinase that regulates the onset of cytokinesis. J Cell Biol. 1999;146(4):777–790.
[57] Bhutta MS, Roy B, Gould GW, et al. A complex network of interactions between mitotic kinases, phosphatases and ESCRT proteins regulates septation and membrane trafficking in *S. pombe*. PLoS One. 2014;9 (10):e111789.
[58] Bellingham-Johnstun K, Anders EC, Ravi J, et al. Molecular organization of cytokinesis node predicts the constriction rate of the contractile ring. J Cell Biol. 2021;220(3):e202008032.
[59] Celton-Morizur S, Bordes N, Fraisier V, et al. C-terminal anchoring of Mid1p to membranes stabilizes cytokinetic ring position in early mitosis in fission yeast. Mol Cell Biol. 2004;24(24):10621–10635.
[60] Padmanabhan A, Bakka K, Sevugan M, et al. IQGAP-related Rng2p organizes cortical nodes and ensures position of cell division in fission yeast. Curr Biol. 2011;21(6):467–472.
[61] Tao EY, Calvert M, Balasubramanian MK. Rewiring Mid1pindependent medial division in fission yeast. Curr Biol. 2014;24(18):21812188.
[62] McDonald NA, Lind AL, Smith SE, et al. Nanoscale architecture of the *Schizosaccharomyces pombe* contractile ring. Elife. 2017;6:e28865.
[63] Piekny AJ, Maddox AS. The myriad roles of anillin during cytokinesis. Semin Cell Dev Biol. 2010;21(9):881–891.
[64] Field SJ, Madson N, Kerr ML, et al. PtdIns(4,5)p2 functions at the cleavage furrow during cytokinesis. Curr Biol. 2005;15(15):1407–1412.
[65] Kim H, Johnson JM, Lera RF, et al. Anillin phosphorylation controls timely membrane association and successful cytokinesis. PLoS Genet. 2017;13(1):e1006511.
[66] Jia H, Gao Z, Yu F, et al. Actin-binding protein anillin promotes the progression of hepatocellular carcinoma *in vitro* and in mice. Exp Ther Med. 2021;21(5):454.
[67] Xiao JX, Xu W, Fei X, et al. Anillin facilitates cell proliferation and induces tumor growth of hepatocellular carcinoma via miR-138/SOX4 axis regulation. Transl Oncol. 2020;13(10):100815.
[68] Chen J, Li Z, Jia X, et al. Targeting anillin inhibits tumorigenesis and tumor growth in hepatocellular carcinoma via impairing cytokinesis fidelity. Oncogene. 2022;41(22):3118–3130.
[69] Lian YF, Huang YL, Wang JL, et al. Anillin is required for tumor growth and regulated by miR-15a/mir-16-1 in HBV-related hepatocellular carcinoma. Aging (Albany NY). 2018;10(8):1884–1901.
[70] Zhou W, Wang Z, Shen N, et al. Knockdown of ANLN by lentivirus inhibits cell growth and migration in human breast cancer. Mol Cell Biochem. 2015;398(1–2):11–19.
[71] Magnusson K, Gremel G, Rydén L, et al. ANLN is a prognostic biomarker independent of Ki-67 and essential for cell cycle progression in primary breast cancer. BMC Cancer. 2016;16(1):904.
[72] Dai X, Chen X, Hakizimana O, et al. Genetic interactions between ANLN and KDR are prognostic for breast cancer survival. Oncol Rep. 2019;42(6):2255–2266.
[73] Wang D, Naydenov NG, Dozmorov MG, et al. Anillin regulates breast cancer cell migration, growth, and metastasis by non-canonical mechanisms involving control of cell stemness and differentiation. Breast Cancer Res. 2020;22(1):3.
[74] Lens SMA, Medema RH. Cytokinesis defects and cancer. National Reviews Cancer. 2019;19(1):32–45.
[75] Tuan NM, Lee CH. Role of anillin in tumour: from a prognostic biomarker to a novel target. Cancers (Basel). 2020;12(6):1600.
[76] Lin X, Xiang X, Hao L, et al. The role of Aurora-A in human cancers and future therapeutics. Am J Cancer Res. 2020 10(9):2705–2729.
[77] Zhang X, Wei C, Liang H, et al. Polo-like kinase 4's critical role in cancer development and strategies for Plk4-targeted therapy. Front Oncol. 2021;11:587554.
[78] Bähler J, Steever AB, Wheatley S, et al. Role of polo kinase and Mid1p in determining the site of cell division in fission yeast. J cell Biol. 1998;14(6):16031616.
[79] Chang F, Drubin D, Nurse P. Cdc12p, a protein required for cytokinesis in fission yeast, is a component of the cell division ring and interacts with profilin. J Cell Biol. 1997;137(1):169–182.
[80] Fankhauser C, Reymond A, Cerutti L, et al. The S. pombe cdc15 gene is a key element in the reorganization of F-actin at mitosis. Cell. 1995;82(3):435–444.
[81] Jourdain I, Brzezińska EA, Toda T. Fission yeast Nod1 is a component of cortical nodes involved in cell size control and division site placement. PLoS One. 2013;8 (1):e54142.
[82] Le Goff X, Motegi F, Salimova E, et al. The *S. pombe rlc1* gene encodes a putative myosin regulatory light chain that binds the type II myosins myo3p and myo2p. Journal of Cell Sciences. 2000;113 (23):4157–4163.
[83] McCollum D, Balasubramanian MK, Pelcher LE, et al. (1995). Schizosaccharomyces pombe cdc4+ gene encodes a novel EF-hand protein essential for cytokinesis. *Journal of Cell Biology*, 130(3):651–660.
[84] Motegi F, Mishra M, Balasubramanian MK, et al. Myosin-II reorganization during mitosis is controlled temporally by its dephosphorylation and spatially by Mid1 in fission yeast. J cell Biol. 2004;165 (5):685–695.
[85] Petersen J, Paris J, Willer M, et al. The *S. pombe* aurora-related kinase Ark1 associates with mitotic structures in a stage dependent manner and is required for chromosome segregation. J Cell Sci. 2001;114 (24):4371–4384.

List of References

Addi, C., Presle, A., Fremont, S., Cuvelier, F., Rocancourt, M., Milin, F., Schmutz, S., Chamot-Rooke, j., Douche, T., Duchateau, M., Giai Gianetto, Q., Salles, A., Menager, H., Matondo, M., Zimmermann, P., Gupta-Rossi, N., and Echard, A. (2020). The flemmingsome reveals an ESCRT to membrane coupling via ALIX/syntenin/syndecan-4 required for the completion of cytokinesis. *Nature Communications, 11*(1), 1941. https://doi.org/10.1038/s41467-020-15205-z.

Akamatsu, M., Berro, J., Pu, K.M., Tebbs, I.R., and Pollard, T.D. (2014). Cytokinetic nodes in fission yeast arise from two distinct types of nodes that merge during interphase. *Journal of Cell Biology*, 204, 977–988. https://doi.org/10.1083/jcb.201307174.

Alam, S. L., Sun, J., Payne, M., Welch, B. D., Blake, B, K., Davis, D. R., Meyer, H. H., Emr, S. D., and Sundquist, W. I. (2004). Ubiquitin interactions of NZF zinc fingers. *The EMBO journal,* 23(7), 1411-1421. https://doi.org/10.1038/sj.emboj.7600114.

Albererts, B., Johnson, A., Lewis, J., Raff, M., Roberts, K., and Walter, P. (2007). *Molecular Biology of the Cell,* 3: 401. https://doi.org/10.1093/aob/mcg023.

Almonacid, M., Celton-Morizur, S., Jakubowski, J.L., Dingli, F., Loew, D., Mayeux, A., Chen, J.S., Gould, K.L., Clifford, D.M., and Paoletti, A. (2011). Temporal control of contractile ring assembly by Plo1 regulation of myosin II recruitment by Mid1/anillin. *Current Biology*, 21, 473–479. https://doi.org/10.1016/j.cub.2011.02.003.

Alonso Y Adell, M., Migliano, S. M., and Teis, D. (2016). ESCRT-III and Vps4: a dynamic multipurpose tool for membrane budding and scission. *The FEBS journal,* 283(118), 3288-3302. https://doi.org/10.1111/febs.13688.

Anedchenko, E. A., Samel-Pommerencke, A., Tran Nguyen, T. M., Shahnejat-Bushehri, S., Popsel, J., Lauster, D., Hermann, A., Rappsilber, J., Cuomo, A., Bonaldi, T., and Ehrenhofer-Murray, A. E. (2019). The kinetochore module Okp1^{CENP-Q}/Ame1^{CENP-U} is a reader for N-terminal modifications on the centromeric histone Cse4 $^{CENP-A}$. *The EMBO Journal,* 38(1), e98991. https://doi.org/10.15252/embj.201898991.

Azad, K., Guilligay, D., Boscheron, C., Maity, S., De Franceschi, N., Sulbaran, G., Effantin, G., Wang, H., Kleman, J. P., Bassereau, P., Schoehn, G., Roos, W. H., Desfosses, A., and Weissenhorn, W. (2023). Structural basis of CHMP2A-CHMP3 ESCRT-III polymer assembly and membrane cleavage. *Nature Structural and Molecular Biology,* 30(1), 81-90. https://doi.org/10.1038/s41594-022-00867-8.

Babst, M., Katzmann, D. J., Snyder, W. B., Wendland, B., and Emr, S. D. (2002). Endosome-associated complex, ESCRT-II, recruits transport machinery for protein sorting at the multivesicular body. *Developmental cell,* 3(2), 283-289. https://10.1016/s1534-5807(02)00219-8.

Bähler J., Steever A. B., Wheatley S., Wang Y., Pringle J. R., Gould K. L., and McCollum D. (1998). Role of polo kinase and Mid1p in determining the site of cell division in fission yeast. *Journal of Cell Biology*, 143, 1603–1616. https://doi.org/10.1083/jcb.143.6.1603.

Baird, N. A., Etter, P. D., Atwood, T. S., Currey, M. C., Shiver, A. L., Lewis, Z. A., Selker, E. U., Cresko, W. A., and Johnson, E. A (2008). Rapid SNP Discovery and genetic mapping using sequenced RAD markers. *PLOSONE,* 3(10), e3376. https://doi.org/10.1371/journal.pone.0003376.

Bauer, I., Brune, T., Preiss, R., and Kolling, R. (2015). Evidence for a nonendosomal function of the Saccharomyces cerevisiae ESCRT-III-like protein Chm7. *Genetics*, 201(4), 1439-1452. https://doi.org/10.1534/genetics.115.178939.

Beach, D. H. (1983). Cell type switching by DNA transposition in fission yeast. *Nature,* 305, 682-688. https://doi.org/10.1038/305682a0.

Beach, D. H., and Klar, A. J. (1984). Rearrangements of the transposable mating-type cassettes of fission yeast. *EMBO Journal,* 3(3), 603-610. https://doi.org/10.1002/j.1460-2075.1984.tb01855.x.

Bellingham-Johnstun, K., Anders, E. C., Ravi, J., Bruinsma, C., Laplante, C. (2021). Molecular organization of cytokinesis node predicts the constriction rate of the contractile ring. *Journal of Cell Biology*, 220. https://doi.org/10.1083/jcb.202008032.

Bellingham-Johnstun, K., Commer, B., Levesque, B., Tyree, Z. L., Laplante, C. (2022). Imp2p forms actin-dependent clusters and imparts stiffness to the contractile ring. *Molecular Biology of the Cell*, 33, ar145. https://doi.org/10.1091/mbc.E22-06-0221.

Bellingham-Johnstun, K., Tyree, Z. L., Martinez-Baird, J., Thorn, A., Laplante, C. (2023). Actin-Microtubule Crosstalk Imparts Stiffness to the Contractile Ring in Fission Yeast. *Cells*, (6):917. https://doi.org/10.3390/cells12060917. PMID: 36980258; PMCID: PMC10047812.

Berlin, A., Paoletti, A., and Chang, F. (2003). Mid2p stabilizes septin rings during cytokinesis in fission yeast. *The Journal of Cell Biology*, 160(2), 1083-1092. https://doi.org/10.1083/jcb.200212016.

Bhutta, M. S., Roy, B., Gould, G. W. and McInerny, C.J. (2014). A complex network of interactions between mitotic kinases, phosphatases, and ESCRT proteins regulates septation and membrane trafficking in *S. pombe*. *PLoS ONE,* 9(10): e111789. https://doi.org/10.1371/journal.pone.0111789.

Boeckmann, L., Takahashi, Y., Au, W. C., Mishra, P. K., Choy, J. S., Dawson, A. R., Szeto, M. Y., Waybright, T. J., Hegerc, C., McAndrew, C., Goldsmith, P. K., Veenstra, T. D., Baker, R. E., and Basrai, M. A. (2013). Phosphorylation of centromeric histone H3 variant regulates chromosome segregation in *Saccharomyces cerevisiae*. *Molecular Biology of the Cell,* 24(12), 2034-2044. https://doi.org/10.1091/mbc.E12-12-0893.

Bringmann, H., Hyman, A. A. (2005). A cytokinesis furrow is positioned by two consecutive signals. *Nature*, 436, 731-734. https://doi.org/10.1038/nature03823.

Brunner, D., and Nurse, P. (2000). CLIP170-like tip1p spatially organizes microtubular dynamics in fission yeast. *Cell*, 102: 695-704. https://doi.org/10.1016/s0092-8674(00)000091-x.

Cam, H. P., and Whitehall. S. (2016). Analysis of heterochromatin in *Schizosaccharomyces pombe*. *Cold Spring Harbor Protocols*. https://doi.org/10.1101/pdb.top079889.

Carlton, J. (2010). The ESCRT machinery: a cellular apparatus for sorting and scission. *Biochemical Society Transaction*, 38 (6): 1397-1412. https://doi.org/10.1042/BST0381397.

Carlson L. A., Shen, Q. T., Pavlin, M. R., and Hurley, J. H. (2015). ESCRT filaments as spiral springs. *Developmental Cell,* 35. 397-398. https://doi.org/10.1016/j.devcel.2015.11.007.

Carpy, A., Krug, K., Graf, S., Andre, K., Sasa, P., Silke H., and Boris, M. (2014). Absolute proteome and phosphoproteome dynamics during the cell cycle of *Schizosaccharomyces pombe* (fission yeast). *Molecular Cell Proteomics*, 13:1925–1936. https://doi.org/10.1074/mcp.M113.035824.

Celton-Morizur, S., Bordes, N., Fraisier, V., Tran, P.T., and Paoletti, A. (2004). C-terminal anchoring of mid1p to membranes stabilizes cytokinetic ring position in early mitosis in fission yeast. *Molecular and Cellular Biology,* 24, 10621–10635. https://doi.org/10.1128/MCB.24.24.10621-10635.2004.

Celton-Morizur, S., Racine, V., Sibarita, J. B and Paoletti, A. (2006). Pom1 kinase links division plane position to cell polarity by regulating Mid1p cortical distribution. *Journal of Cell Science*, 119(22): 4710-4718. https://doi.org/10.1242/jcs.03261.

Chatterjee, M., and Pollard, T. D. (2019). The functionally important N-terminal half of fission yeast Mid1p anillin is intrinsically disordered and undergoes phase separation. *Biochemistry,* 58, 3031-3041. https://doi.org/10.1021/acs.biochem.9b00217.

Chen, C. T., Feoktisova, A., Chen, J. S., Shim, Y. S., Clifford, D. M., Gould, K. L., and McCollum, D. (2008). The SIN kinase Sid2 regulates cytoplasmic retention of the *S. pombe* Cdc14-like phosphatase Clp1. *Current Biology*, 18(20), 1594-1599. https://doi.org/10.1016/j.cub.2008.08.067.

Cheffings T. H., Burroughs, N. J., and Balasubramanian M. K. (2016). Actomyosin ring formation and tension generation in eukaryotic cytokinesis. *Current Biology,* R719-R737. https://doi.org./10.1016/j.cub.2016.06.071.

Chiaruttini, N., Redondo-Morata, L., Colom, A., Humbert, F., Lenz, M., Scheuring, S., and Roux, A. (2015). Relaxation of Loaded ESCRT-III Spiral Springs Drives Membrane Deformation. *Cell,* 163(4), 866-879. https://doi.org/10.1016/j.cell.2015.10.017.

Christ, L., Wenzel, E. M., Liestol, K., Raiborg, C., Campsteijn, C., and Stentmark, H. (2016). ESCRT-I/II function as parallel ESCRT-III recruiters in cytokinetic abscission. *The Journal of Cell Biology,* 212(5), 499-513. https://doi.org/10.1083/jcb.201507009.

Chuang, C. L., Lu, Y. N., Wang, H. C., and Chang, H. Y. (2014). Genetic dissection reveals that Akts is the critical kinase downstream of LRRK2 to phosphorylate and inhibit FOXO1 and promotes neuron survival. *Human Molecular Genetics,* 23(21), 5649-5658. https://doi.org/10.1093/hmg/ddu281.

Daigaku, Y., Keszthelyi, A., Muller, C. A., Miyabe, I., Brooks, T., Retkute, R., Hubank, M., Nieduszynski, C. A., and Carr, A. M. (2015). A global profile of replicative polymerase usage. *Nature Structural & Molecular Biology,* 22(3), 192-198. https://doi.org/10.1038/nsmb.2962.

Dogterom, M., Koenderink, G. H. (2019). Actin-microtubule crosstalk in cell biology. *Nature Review Molecular Cell Biology*, 20, 38-54. https://doi.org/10.1038/s41580-018-0067-1.

Egel, R. (1971). Physiological aspects of conjugation in fission yeast. *Planta, 98* (1), 89–96. https://doi.org/10.1007/BF00387025.

Egel, R., Beach, D. H., and Klar, A. J. (1984). Genes required for initiation and resolution steps of mating-type switching in fission yeast. *Proceedings of the National Academy of Sciences U.SA,* 81: 3481-3485. https://doi.org/10.1073/pnas.81.11.3481.

Ekwall, K., and Thon, G. (2016). Genetics of *Schizosaccharomyces pombe*. *Cold Spring Harbor Protocol*. https://doi.org/10.1101/pdb.top07772.

Elia, A. E., Cantley, L. C., and Yaffe, M. B. (2003). Proteomic screen finds pSer/pThrbinding domain localizing Plk1 to mitotic substrates. *Science*, 299. 1228-1231. https://doi.org/10.1126/science.1079079.

Elia, N., Sougrat, R., Spurlin, T. A., Hurley, J. H., and Lippincott-Schwartz, J. (2011). Dynamics of endosomal sorting complex required for transport (ESCRT) machinery during cytokinesis and its role in abscission. *Proceedings of the National Academy of Sciences USA,* (108) 4846-4851. https://doi.org/10.1073/pnas.1102714108.

Fabrikant, G., Lata, S., Riches, J. D., Briggs, J. A., Weissenhorn, W., and Kozlov, M. M. (2009). Computational model of membrane fission catalyzed by ESCRT-III. *PLoS Computational Biology*, 5(11), e1000575. https://doi.org/10.1371/journal.pcbi.1000575.

Fantes. P., Nurse, P. (1977). Control of cell size at division in fission yeast by a growth m-modulated size control over nuclear division. *Experimental Cell Research*, 107 (2): 377-86. https://doi.org/10.1016/0014-4827(77)90359-7.

Feoktistova, A., Magnelli, P., Abeijon, C., Perez, P., Lester, R. L., and Gould, K. L. (2001). Coordination between fission yeast glucan formation and growth requires a sphingolipase activity. *Genetics,* 158(4), 1397-1411. https://doi.org/10.1093/genetics/158.4.1397.

Field, C. M., Coughlin, M., Doberstein, S., Marty, T., and Sullivan, W. (2005). Characterization of *anillin mutants* reveals essential roles of septin localization and plasma membrane integrity. *Development for Advances in Developmental Biology and Stem Cells,* 132(12), 2849-2860. https://doi.org//10.1242/de.0843.

Foethke, D., Makushok, T., Brunner, D., and Nedelec, F. (2009). Force and length-dependent catastrophe activities explain interphase microtubule organisation in fission yeast. *Molecular System Biology,* 5: 241. https://doi.org/10.1038/msb.2008.76.

Forsburg, S. L. (2003). Overview of *Schizosaccharomyces pombe*. *Current Protocols in Molecular Biology*, *64*, 13.4.1 13.4.3. https://doi.org/10.1002/0471142727.

French, B. T., and Straight, A. F. (2013). Swapping CENP-A at centromere. *Nature Cell Biology,* 15(9), 1028-1030. https://doi.org/10.1038/ncb2833.

Garno, C., Irons, Z. H., Gamache, C. M., McKim, Q., Reyes, G., Wu X., Shuster C. C., and Henson J. H. (2021) Building the cytokinetic contractile ring in an early embryo: Initiation as clusters of myosin II, anillin and septin, and visualization of a septin filament network. *PLoS ONE,* 16(12). https://doi.org/10.1371/ journal.pone.0252845.

Glotzer, M. (2001). Animal cell cytokinesis, *Annual Review of Cell and Developmental Biology*, 17: 351–386. https://doi.org/10.1146/annual.cell bio.17.1.351.

Glotzer, M. (2017). Cytokinesis in metazoa and fungi. *Cold Spring Harbor Perspectives in Biology,* 9:a022343. https://doi.org/10.1101/cshperspect.a022343.

Goliand, I., Nachmias, D., Gershony, O., and Elia, N. (2014). Inhibition of ESCRT-II-CHMP6 interactions impedes cytokinesis abscission and leads to cell death. *Molecular Biology of the Cell*, 25(23), 3740-3748. https://doi.org/10.1091/mbc.E14-08-1317.

Goliand, I., Adar-Levor, S., Segal, I., Nachmias, D., Dadosh, T., Kozlov, M. M., and Elia, N. (2018). Resolving ESCRT-III spirals at the intercellular bridge of dividing cells using 3D STORM. *Cell Reports,* 24, 1756-1764. https://doi.org/10.1016/j.celrep.2018.07.051.

Gomes, F. C., Pataro, C., Guerra, J. B., Neves, M. J., Correa, S. R., Moreira, E. S., and Rosa, C. A. (2002). Physiological diversity and trehalose accumulation in *Schizosaccharomyces pombe* strains isolated from spontaneous fermentations during the production of the artisanal Brazilian cachaca. *Canadian Journal of Microbiology*, *48*(5), 399-406. https://doi.org/10.1139/w02-032.

Gnad, F. Gunawardena, J., and Mann, M. PHOSIDA. (2011). The posttranslational modification database. *Nucleic Acids Research*, 39(Database issue): D253-60. https://doi.org/10.1093/nar/gkq1159.

Green, R. A., Paluch, E. and Oegema, K. (2012). Cytokinesis in animal cells. *Annual Review of Cell Developmental Biology*, 28(1), 29-58. https://doi.org/10.1146.

Green, M. R, and Sambrook, J. (2012). Molecular cloning: A laboratory manual. Cold Spring Harbor, N.Y: *Cold Spring Laboratory Press*. https://nla.gov.au/nla.cat-vn6039452.

Gromley, A., Yeaman, C., Rosa, J., Redick, S., Chen, C.-T., Mirabelle, S., Guha, M., Sillibourne, J. and Doxsey, S. J. (2005). Centriolin anchoring of Exocyst and SNARE complexes at the midbody is required for secretory-vesicle-mediated abscission. *Cell,* 123, 75-87. https://doi.org/10.1016/j.cell.2005.07.027.

Gu, Y., Yam, C. and Oliferenko, S. (2015). Rewriring of cellular division site selection in evolution of fission yeast. *Current Biology,* 25, 1187-1194 https://doi.org/10.1016/j.cub.2015.02.056.

Guizetti, J., Schermelleh, L., Mäntler, J., Maar, S., Poster, I., Leonhardt, H., Muller-Reichert, T., Gerlich, D. W. (2011). Cortical constriction during abscission involves helices of ESCRT-III-dependent filaments. *Science,* 331(6024), pp.1616–20. https://doi.org/10.1126/science.1201847.

Guizetti, J., and Gerlich, D. W. (2010). Cytokinetic abscission in animal cells. *Seminars in Cell Developmental Biology,* 21, 909-916. https://doi.org/10.1016/j.semcdb.2010.08.001.

Hagan, I. M., and Bagley, S. (2016). Fixed cell imaging of *Schizosaccharomyces pombe*. *Cold Spring Harbour Protocol*. https://doi.org/10.1101/pdb.top079830.

Hagan, I., Carr, A. M., Grallert, A., and Nurse, P. (2016). Fission yeast: A laboratory manual. Cold Spring Harbor, NY: *Cold Spring Harbor Laboratory Press*.

Hatano, T., Palani, S., Papatziamou, D. *et al.* (2022). Asgard archaea shed light on the evolutionary origins of the eukaryotic ubiquitin-ESCRT machinery. *Nature Communication,* 13, 33-98. https://doi.org/10.1038/s41467-022-30656-2.

Hayles, J., and Nurse, P. (2016). Introduction of fission yeast as a model system. In A. M. Carr, I. M. Hagan, A. Grallert, and P. Nurse (Eds.), *Fission yeast: A laboratory manual* pp. 1–11. *Cold Spring Harbor Laboratory Press*. https://doi.org/10.1101/pdb.top079749.

Henne, W. M., Buchkovich, N. J., Zhao, Y., and Emr, S. D. (2012). The endosomal sorting complex ESCRT-II mediates the assembly and architecture of ESCRT-III helices. *Cell,* 151(2), 356-371. https://doi.org/10.1016/j.cell.2012.08.039.

Hercyk, B. S., Onwubiko, U. N., and Das, M. E. (2019). Coordinating septum formation and the actomyosin ring during cytokinesis in Schizosaccharomyces pombe. *Molecular Microbiology*, *112*(6), 1645–1657. https://doi.org/10.1111/mmi.14387.

Hoffman, C. S., Wood, V., and Fantes, P. A. (2015). An ancient yeast for young geneticists: A primer on the *Schizosaccharomyces pombe* model system. *Genetics*, *201*(2), 403–423. https://doi.org/10.1534/genetics.115.181503.

Horväth, P., and Müller-Reichert, T. (2020). A structural view on ESCRT-mediated abscission. *Frontiers in Cell and Developmental Biology*, 8, 586880. https://doi.org/10.3389/fcell.202.586880.

Huang, Y., Chew, T. G., Ge, W., and Balasubramanian, M. K. (2007). Polarity determinants Tea1p, Tea4p, and Pom1p inhibit division-septum assembly at cells in fission yeast. *Developmental Cell*, 12(6), 987-996. https://doi.org/10.1016/j.devcel.2007.03.015.

Huang, Y., Yan, H., and Balasubramanian, M. K. (2008). Assembly of normal actomyosin rings in the absence of Mid1p and cortical nodes in fission yeast. *The Journal of Cell Biology*, 183(6), 979-988. https://doi.org/10.1083/jcb.200806151.

Hurley J. H. (2010). The ESCRT complex. *Critical Review in Biochemistry and Molecular Biology*, 45, 463-487. https://dx.doi.org/10.3109/10409238.2010.502516.

Katmann, D. J., Babst, M. and Emr, S. D. (2001). Ubiquitin-dependent sorting into the multivesicular body pathway requires the function of a conserved endosomal protein sorting complex, ESCRT-1. *Cell*, 106(2), 145-155. https://doi.org/101016/s0092-8674(01)00434-2.

Kaykov, A., and Nurse. P. (2015). The spatial and temporal organisation of origin firing during the S-phase of fission yeast. *Genome Research*, 25(3): 391-401. https://doi.org/10.1101/gr.180372.114

Kettenbach, A, N., Deng, L., Wu, Y., Baldissard, S., Adamo, M, E., Gerber, S, A., and Moseley, J, B. (2015). Quantitative phosphoproteomics reveals pathways for coordination of cell growth and division by the conserved fission yeast kinase Pom1. *Molecular Cell Proteomics*, 14:1275–1287. https://doi.org/10.1074/mcp.M114.045245.

Kim, D. U., Hayles, J., Kim, D., Wood, V., Park, H. O., Won, M., … Hoe, K. L. (2010). Analysis of a genome-wide set of gene deletions in the fission yeast *Schizosaccharomyces pombe*. *Nature Biotechnology*, *28*(6), 617–623. https://doi.org/10.1038/nbt.1628.

Kim, H., Johnson, J. M., Lera, R. F., Brahma, S. and Burkard, M. E. (2017). Anillin Phosphorylation Controls Timely Membrane Association and Successful Cytokinesis. *PLoS Genetics*, 13.1: e1006511. https://doi.org/10.1371.

Koch, A., Krug, K., Pengelley, S., Macek, B., and Hauf, S. (2011). Mitotic substrates of the kinase Aurora with roles in chromatin regulation identified through quantitative phosphoproteomics of fission yeast. *Science Signal*, 4:rs6–rs6. https://doi.org/10.1126/scisignal.2001588.

Kostelansky, M. S., Schluter, C., Tam, Y. Y., Lee, S., Ghir7lando, R., Beach, B., Conibear, E., and Hurley, J. H. (2007). Molecular architecture and functional model of the complete yeast ESCRT-I heterotetramer. *Cell,* 129(3), 485-498. https://doi.org/10.1016/j.cell.2007.03.016.

Laan, L., Pavin, N., Husson, J., Romet-Lemonne, G., Van Duijn, M., López, M.P., Vale, R. D., Jülicher, F., Reck-Peterson, S. L., Dogterom, M. (2012). Cortical dynein controls microtubule dynamics to generate pulling forces that position microtubule asters. *Cell*, 148, 502-514, https://doi.org/10.1016/j.cell.2012.01.007.

Laplante, C., Huang, F., Bewesdorf, J., and Pollard, T. D. (2016). High- speed super -resolution imaging of live fission yeast cells. *Methods in Molecular Biology (Clifton, N.J),* 1367, 45-57. https://doi.org/10.1007/978-1-4939-3145-3_4.

Laporte, D., Coffman, V. C., Lee, I. J, and Wu, J. Q. (2011). Assembly and architecture of precursor nodes during fission yeast cytokinesis. *Journal of Cell Biology*, 192(6): 1005-1021. https://doi.org/10.1083/jcb.201008171.

Leupold, U. (1950). Die Verebung von Hmomothallie and Heterothallie bei *Schizosaccharomyces pombe*. *CR Laboratory Carlsberg Ser. Physiology*, 24, 381-480.

Little, J. N., and Dwyer, N. D. (2021). Cep55: abscission boss or assistant? *Trends Cell Biology*, 31(10): 789-791. https://doi.org/101016/j.tcb.2021.07.006.

Liu, N., Yang, R., Shi, Y., Chen, L., Liu, Y., Wang, Z., Liu, S., Ouyang, L., Wang, H., Lai, W., Mao, C., Wang, M., Cheng, Y., Liu, S., Wang, X., Zhou, H., Cao, Y., Xiao, D., and Tao, Y. (2020). The crosstalk between methylation and phosphorylation in lymphoid-specific helicase drives cancer stem-like properties. *Signal Transduction and Targeted Therapy,* 5(1), 197. https://doi.org/10.1038/s41392-020-00249-w.

Maddox, A. S., Azoury, J., and Dumont, J. (2012). Polar body cytokinesis, *Cytoskeleton,* 69:855-868. https://doi.org/10.1002/cm.21064.

Mageswaran, S. K., Johnson, N. K., Odorizzi, G., and Babst, M. (2014). Constitutively active ESCRT-II suppresses the MVB-sorting phenotype of ESCRT-0 and ESCRT-I mutants. *Molecular Biology of the Cell,* 26(3), 554-568 https://doi.org/10.1091/mbc.E14-10-1469.

Magliozzi J, O., Sears J., Cressey L., Brady M., Opalko H, E., Kettenbach A, N. and Moseley J, B. (2020). Fission yeast Pak1 phosphorylates anillin-like Mid1 for spatial control of cytokinesis. *Journal of Cell Biology*, 3, 219 (8). https://doi.org/10.1083/jcb.201908017.

Mana-Capelli, S., McLean, J. R., Chen, C. T., Gould, K. L., McCollum, D. (2012). The kinesin-14 Klp2 is negatively regulated by the SIN for proper spindle elongation and telophase nuclear positioning. *Molecular Biology of the Cell*, 23, 4592-4600. https://doi.org/10.1091/mbc.E12-07-0532.

Martin-Cuadrado, A. B., Morrell, J. L., Konomi, M., An, H., Petit, C., Osumi, M., Balasubramanian, M., Gould, K. L., Del Rey, F., and de Aldana, C. R. (2005). Role of septins and the exocyts complex in the function of hydrolytic enzymes responsible for fission yeast cell separation. *Molecular Biology of the Cell*, 16(10), 4867-4881. https://doi.org/10.1091/mbc.e04-12-114.

Martin, S. G., and Berthelot-Grosjean, M. (2009). Polar gradients of the DYRK-family kinase Pom1 couple cell length with the cell cycle. *Nature*, 459: 852-856. https://doi.org/10.1038/nature08054.

Matsuo, K., Glahn, D. C., Peluso, M. A., Hatch, J. P., Monkul, E. S., Najt, P., Sanches, M., Zamarripa, F., Li, J., Lancaster, J. L., Fox, P. T., Gao, J. H., and Soares, J. C. (2007). *Prefrontal hyperactivation during working memory task in untreated individuals with major depressive disorder*. Molecular Psychiatry, 12(2) 158-166. https://doi.org/10.1038/sj.mp.4001894.

McDargh, Z., Wang, S., Chin, H. F., Thiyagarajan, S., Karatekin, E., Pollard, T. D., O'Shaughnessy, B. (2021). Myosins generate contractile force and maintain organization in the cytokinetic contractile ring. *Cold Spring Harbor Laboratory*, 2021. 2005. 2002.442363. https://doi.org/10.1101/2021.05.02.442363.

McCullough, J., Frost, A., and Sundquist, W. I. (2018). Structures, functions and dynamics of ESCRT-III/Vps4 Membrane remodelling and fission complexes. *Annual Review of Cell and Developmental Biology*, 34, 85-109. https://doi.org/10.1146/annurev-cellbio-100616-060600.

Mclntosh, J. R., Morphew, M. K., and Giddings, T. H. Jr. (2016). Electron microscopy of fission yeast. *Cold Spring Harbour Protocol*. https://doi.org/10.1101/pdb.top079822.

McNeely, K. C., and Dwyer, N. D. (2020). Cytokinesis and post-abscission midbody remnants are regulated during mammalian brain development. *Academy of Sciences of the United States of America,* 117(17), 9584-9593. https://doi.org/10.1073/pnas.1919658117.

Merigliano, C., Burla, R., La Torre, M., Del Giudice, S., Teo, H., Liew, C, W. et al. (2021). AKTIP interacts with ESCRT I and is needed for the recruitment of ESCRT III subunits to the midbody. *PLoS Genet,* 17 (8): e1009757 https://doi.org/10.1371/journal.pgen.10009757.

Mierzwa, B. E., Chiaruttini, N., Redondo-Morata, L., von Filseck, J. M., Konig, J., Larios, J., Poser, I., Muller-reichert, T., Scheuring, S., Roux, A., and Gerlich, D. W. (2017). Dynamic subunit turnover in ESCRT-III assemblies is regulated by Vps4 to mediate membrane remodelling during cytokinesis. *Nature Cell Biology,* 19(7), 787-798. https://doi.org/10.1038/ncb3559.

Mishra, M., Huang, J., and Balasubramanian, M. K. (2014). The yeast actin cytoskeleton. *FEMS Microbiology Review*. 38: 213-227. https://doi.org/10.1111/1574-6976.12064.

Mishra, P. K., and Basrai, M. A. (2019). Protein kinases in mitotic phosphorylation of budding yeast CENP-A. *Current Genetics,* 65(6), 1325-1332. https://doi.org/10.1007/s00294-019-00997-5.

Mishra, P. K., Olafsson, G., Boechmann, L., Westlake, T. J., Jowhar, Z. M., Dittman, L. E., Baker, R. E., D'Amours, D., Thorpe, P. H., and Basrai, M. A. (2019). Cell cycle-dependent association of polo kinase Cdc5 with CENP-A contributes to faithful chromosome segregation in budding yeast. *Molecular Biology of the Cell,* 30(8), 1020-1036. https://doi.org/10.1091/mbc.E18-09-0584.

Mishra, P. K., Wood, H., Stanton, J., Au, W. C., Eisenstatt, J. R., Boeckmann, L., Sclafani, R. A., Weinreich, M., Bloom, K. S. Thorpe, P. H., and Basrai, M. A. (2021). Cdc7-mediated phosphorylation of Cse4 regulates high-fidelity chromosome segregation in budding yeast. *Molecular Biology of the Cell,* 32(21), ar15. https://doi.org/10.1091/mbc.E21-06-0323.

Mitchison, J. M., and Nurse, P. (1985). Growth in cell length in the fission yeast *Schizosaccharomyces pombe*. *Journal of Cell Sciences,* 75:357-76. https://doi.org/10.1242/jcs.75t.1357.

Moreno, S., Klar, A., and Nurse, P. (1991). Molecular genetic analysis of fission yeast *Schizosaccharomyces pombe*. *Methods in Enzymology,* 194, 795-823. https://doi.org/10.1016/0076-6879(91)94059-I.

Morita, E., Sandrin, V., Chung, H. Y., Morham, S. G., Gygi, S. P., Rodesch, C. K., and Sundquist, W. I. (2007). Human ESCRT and ALIX proteins interact with proteins of the midbody and function in cytokinesis. *The EMBO Journal,* 26(19), 4215-4227. https://doi.org/10.1038/sj.emboj.7601850.

Moseley, J.B., Mayeux, A., Paoletti, A., and Nurse, P. (2009). A spatial gradient coordinates cell size and mitotic entry in fission yeast. *Nature,* 459, 857–860. https://doi.org/10.1038/nature08074.

Moshtohry, M., Bellingham-Johnstun, K., Elting, M. W., Laplante, C. (2022). Laser ablation reveals the impact of Cdc15p on the stiffness of the contractile ring. *Molecular Biology of the Cell*, 33, br9, https://doi.org/10.1091/mbc.E21-10-0515.

Motegi, F., Mishra, M., Balasubramanian, M. K. and Mabuchi, I. (2004). Myosin-II reorganization during mitosis is controlled temporally by its dephosphorylation and spatially by Mid1 in fission yeast. *The Journal of Cell Biology*, 165(5), pp.685-695. https://doi.org/10.1083/jcb.200402097.

Mulvihill, D. P. (2016). Live cell imaging in fission yeast. *Cold Spring Harbour Protocol*. https://doi.org/10.1101/pdb.top090621.

Murray, J. M., Watson, A. T., and Carr, A. M. (2016). Molecular genetic tools and techniques in fission yeast. *Cold Spring Harbor Protocols.* https://doi.org/10.1101/pdb.top087601.

Nandakumar, J., and Cech, T. R. (2013). Finding the end: recruitment of telomerase to telomeres. *Nature reviews. Molecular Cell Biology,* 14(2), 69-82. https://doi.org/10/1038/nrm3505.

Navarro, F. J., and Nurse, P. A. (2012). System screen reveals new elements acting at the G2/M cell cycle control. *Genome Biology*,13(5):R36. https://doi.org/10.1186/gb-2012-13-5-r36.

Neto, H. and Gould, G.W. (2011). The regulation of abscission by multi-protein complexes. *Journal of Cell Science*, 124(19), pp.3199–207. https://doi.org/101242/jcs.083949.

Nursec, P. (1975). Genetic control of cell size at cell division in yeast. *Nature,* 256, 557-551. https://doi.org/10.1038/256547a0.

Nurse, P., and Thuriaux, P. (1980). Regulatory genes controlling mitosis in the fission yeast *Schizosaccharomyces pombe*. *Genetics,* 96(3): 627-637. https://doi.org/10.1093/genetics/96.3.627.

Obita, T., Saksena, S., Ghazi-Tabatabai, S., Gill, D. J., Perisic, O., Emr, S. D and Williams, R. L. (2007). Structural basis for selective recognition of ESCRT-III by the AAA ATPase Vps4. *Nature,* 449(163), 735-739. https://doi.org/10.1038/nature06171.

Oegema, K., Savoian, M. S., Mitchison, T. J., and Field, C. M. (2000). Functional analysis of a human homologue of the Drosophila actin binding protein anillin suggests a role in cytokinesis. *The journal of Cell Biology,* 150(3), 539-552. https://doi.org/10.1083/jcb.150.3.539.

Olmos, Y., Hodgson, L., Mantell, J., Verkade, P., Carlton, J. G. (2015). ESCRT-III controls nuclear envelope reformation. *Nature,* 522, 236-239. https://doi.org/10.1038/nature14503.

Pardo, M., Nurse, P. (2003). Equatorial retention of the contractile actin ring by microtubules during cytokinesis. *Science*, 300, 1569-1574. https://doi.org/10.1126/science.1084671.

Papadopoulou, K., Chen, J. S., Mead, E. et al., (2010). Regulation of cell cycle-specific gene expression in fission yeast by the Cdc14p-like phosphatase Clp1p. *Journal of Cell Science,* 15;123(Pt 24):4374-81. https://doi.org/10.1242/js.073056.

Paoletti, A. and Chang, F. (2000). Analysis of mid1p, a protein required for placement of the cell division site, reveals a link between the nucleus and the cell surface in fission yeast. *Molecular Biology of the Cell,* 11(8): 2757–2773. https://doi.org/10.1091/mbc.11.8.2757.

Petersen, J., and Russell, P. (2016). Growth and the environment of *Schizosaccharomyces pombe*, *Cold Spring Harbour Protocol,* pdb.top079764. https://doi.org/10.1101/pdb.top079764.

Paez Valencia, J., Goodman, K., and Otegui, M. S. (2016). Endocytosis and endosomal trafficking in plants. *Annual Review of Plant Biology,* 67, 309-335. https://doi.org/10.1146/annurev-arplant-043015-112242.

Perez, P., and Ribas, J. C. (2016). Fission yeast cell wall analysis. *Cold Spring Harbour Protocol*. https://doi.org/10.1101/pdb.top079897.

Petrova, B., Dehler, S., Kruitwagen, T., Heriche, J. K., Miura, K., and Haering, C. (2013). Quantitative analysis of chromosome condensation in fission yeast, *Molecular and Current Biology,* 33: 984-998. https://doi.org/10.1128/MCB.0100-12.

Piekny, A. J. and Glotzer, M. (2008). Anillin Is a scaffold protein that links RhoA, actin, and myosin during cytokinesis'. *Current Biology*, 18(1), pp. 30–36. https://doi.org/10.1016/j.cub.2007.11.068.

Piekny, A. J. and Maddox, A. S. (2010). The myriad roles of anillin during cytokinesis. *Seminars in Cell & Developmental Biology*, 21(9), pp. 881–891. https://doi.org/10.1016/j.semcdb.2010.08.002.

Pollard, T. D., and Wu, J. Q. (2010). Understanding cytokinesis: lessons from fission yeast. *Nature Reviews Molecular Cell Biology*, 111, 149-155. https://doi.org/10.1038/nrm2834.

Pollard, T. D., and O'Shaughnessy, B. (2019). Molecular Mechanism of Cytokinesis. *Annual Review of Biochemistry,* 88, 661–689. https://doi.org/10.1146/annurev-biochem-062917-012530.

Preciado López, M., Huber, F., Grigoriev, I., Steinmetz, M. O., Akhmanova, A., Koenderink, G. H., Dogterom, M. (2014). Actin-microtubule coordination at growing microtubule ends. *Nature Communication*, 5, 4778. https://doi.org/10.1038/ncomms5778.

Prekeris, R. and Gould, G. W. (2008). Breaking up is hard to do: membrane traffic in cytokinesis. *Journal of Cell Science*. 121, 1569-1576. https://doi.org/10.1242/jcs.018770.

Raiborg, C., Bache, H. G., Gillooly, D. J., Madshus, I. H., Stang, E., and Stenmark, H. (2009). The ESCRT machinery in endosomal sorting of ubiquitylated membrane proteins. *Nature,* 458, 445-452. https://doi.org/10.1038/ncb791.

Raiborg, C., and Stenmark, H. (2009). The ESCRT machinery in endosomal sorting of ubiquitylated membrane proteins. *Nature,* 458, 445-452. https://doi.org/10.1038.nature07961.

Remy, S., Laporte, M. H., Chassefeyre, R., Chi, K. I. L., Goldberg, Y. and Chatellard, C. (2018). The role of ESCRT during the development and functioning of the nervous system, *Seminars in Cell and Developmental Biology*, 74: 40-49 https://doi.org/10.1016/j.semcdb.2017.08.013.

Ren, X., Kloer, D. P., Kim, Y. C., Ghirlando, R., Saidi, L. F., Hummer, G., and Hurley, J, J. H. (2009). Hybrid structural model of the complete human ESCRT-0 complex. *Structure (London, England: 1993),* 17(3), 406-416. https://doi.org/10.1016/j.str.2009.01.012.

Rezig, I. M., Yaduma, W. G., Gould, G. W. and McInerny, C. J. (2022). The role of Anillin/Mid1p during medial division and cytokinesis: From fission yeast to cancer cells. *Cell Cycle*, https://doi.org/10.1080/15384101.2022.2147655.

Rezig, I. M., Yaduma, W. G., Gwyn, G. W. and McInerny, C. J. (2021). Anillin/Mid1p interacts with the ESCRT-associated protein Vps4p and mitotic kinases to regulate cytokinesis in fission yeast. *Cell Cycle*, 20:18, 1845-1860. https://doi.org/10.1080/15384101.2021.1962637.

Rezig, I. M., Bremner, S. K., Bhutta, M. S., Salt, I. P. , Gould, G. W., and McInerny, C. J. (2019). Genetic and cytological methods to study ESCRT cell cycle function in fission yeast. https://doi.org/10.1101/2019. 12.13.875211.

Rincon S, and Paoletti, A. (2012) Mid1/anillin and the spatial regulation of cytokinesis in fission yeast. *Cytoskeleton (Hoboken)*, 69(10): 764-777. https://doi.org/10.1002/cm.21056.

Rincon, S. A., Bhatia, P., Bicho, C., Guzman-Vendrell, M., Fraisier, V., Borek, W, E., Alves, F., Dingli, F., Loew, D., Rappsilber, J., Sawin, K. E., Martin, S. G., and Paoletti, A. (2014). Pom1 regulates the assembly of cdr2-mid1 cortical nodes for robust spatial control of cytokinesis. *Journal of Cell Biology,* 206: 61-77. https://doi.org./10.1083/jcb.201311097.

Rincon, S. A., and Paoletti, A. (2016). Molecular control of fission yeast cytokinesis. *Seminar in Cell Developmental Biology*, 53, 28–38. https://doi.org/10.1016/j.semcdb.2016.01.007.

Rincon, S. A., Estravis, M., Dingli, F., Loew, D., Tran, T, P., and Paoletti, A. (2017) SIN-dependent dissociation of the SAD kinase Cdr2 from the cell cortex resets the division plane. *Current Biology,* 27(4) 534-542. http://dx.doi.org/10.1016/j.cub.2016.12.050.

Robert-Paganin, J., Pylypenko, O., Kikuti, C., Sweeney, H. L., and Houdusse, A. (2020). Force Generation by Myosin Motors: A Structural Perspective. *Chemical Reviews*, *120*(1), 5–35. https://doi.org/10.1021/acs.chemrev.9b00264.

Roguev, A., Ryan, C. J., Hartsuiker, E., and Krogan, N. (2016). High-throughput quantitative genetic interaction mapping in the fission yeast *Schizosaccharomyces pombe*. *Cold Spring Harbor Protocols*. https://doi.org/10.1101/pdb.top079905.

Sadoul, R., Laporte, M. h., Chassefeyre, R., Il Chi, K., Goldberg, Y., and Chatellard, C. (2018). The role of ESCRT during development and functioning of the nervous system, *Seminars in the Cells and Developmental Biology*, 74. 40-49. https://doi.org/10.1016/j.semcdb.2017.08.013.

Saha, S. and Pollard, T. D. (2012a). Anillin-related protein Mid1p coordinates the assembly of the cytokinetic contractile ring in fission yeast. *Molecular Biology of the Cell*, 23(20), pp.3982-3992. https://doi.org/10.1091/mbc.E12.07.0535.

Saha, S. and Pollard, T. D. (2012b). Characterization of structural and functional domains of the anillin-related protein Mid1p that contribute to cytokinesis in fission yeast. *Molecular Biology of the Cell,* 23(20), pp.3993–4007. https://doi.org/10.1091/mbc.E12-07-0536.

Sajiki, K., Hatanaka, M., Nakamura, T., Takeda, K., Shimanuki, M., Yoshida, T., Hanyu, Y., Hayashi, T., Nakaseko, Y., and Yanagida, M. (2009). Genetic control of cellular quiescene in *S. pombe*. *Journal of Cell Science,* 122: 1418-1429. https://doi.org/10.1242/jcs.046466.

Saksena, S., Wahlman, J., Teis, D., Johnson, A. E., and Emr, S. D. (2009). Functional reconstitution of ESCRT-III assembly and disassembly. *Cell*, 136, 97-109. https://dx.doi.org/10.1016/j.cell.2008.11.013.

Samejima, I., Miller, V. J., Rincon, S. A., Sawin, K. E. (2010). Fission yeast Mto1 regulates diversity of cytoplasmic microtubule organizing centers. *Current Biology*, 20, 1959-1965. https://doi.org/10.1016/j.cub.2010.10.006.

Sayyad, W. A., and Pollard, T. D. (2022). The number of cytokinesis nodes in mitotic fission yeast scale with size. *eLife,* 11, e76249. https://doi.org/10.7554/eLife.76249.

Schiel, J. A., and Prekeris, R. (2013). Membrane dynamics during cytokinesis. *Current Opinion in Cell Biology,* 25(1), 92–98. https://doi.org/10.1016/j.ceb.2012.10.012.

Schiel, J. A., Park, K., Morphew, M. K., Reid, E., Hoenger, A., and Prekeris, R. (2011). Endocytic membrane fusion and buckling-induced microtubule severing mediate cell abscission. *Journal of Cell Science,* 124(Pt 9), 1411–1424. https://doi.org/10.1242/jcs.081448.

Schoneberg, J., Lee, I. H., Iwasa, J. H., Hurley, J. H. (2017). Reverse-topology membrane scission by ESCRT proteins. *Nature Review Molecular Cell biology*, 18(1), 5-17. https://doi.org/10.1038/nrm.2016.121.

Scott, A., Gaspar, J., Stuchell-Brereton, M. D., Alam, S. L., Skalicky, J. J. and Sundquist, W. I. (2005). Structure and ESCRT-III protein interactions of the MIT domain of human VPS4A. *Proceeding of the National Academy of Sciences of the United States of America,* 102(39), 13813-13818. https://doi.org/10.1073/pnas.0502165102.

Shen, Q. T., Schuh, A. L., Zheng, Y., Quinney, K., Wang, L., Hanna, M., Mitchell, J. C., Otegui, M. S., Ahlquist, P., Cui, Q., and Audhya, A. (2014). Structural analysis and modelling reveals new mechanisms governing ESCRT-III spiral filament assembly. *The Journal of Cell Biology*, 206(6), 763-777. https://doi.org/10.1083/jcb.201403108.

Shestakova, A., Hanono, A., Drosner, S., Curtiss, M., Davies, B. A., Katzmann, D. J., and Babst, M. (2010). Assembly of AAA ATPase Vps4 on ESCRT-III. *Molecular Biology of the Cell,* 21, 1059-1071. https://doi.org/10.1091/mbc.re09-07-0572.

Shields, S. B., and Piper, R. C. (2011). How ubiquitin functions with ESCRTs, *Traffic*, 12, 1306-1317. https://doi.org/10.1111/j.1600-0854.1011.01241.x.
Shiflett, S. L., Ward, D. M., Huynh, D., Vaughn, M. B., Simmons, J. C., and Kaplan, J. (2004). Characterization of Vta1p, a class E Vps protein in *Saccharomyces cerevisiae*. *The Journal of Biological Chemistry,* 279(12), 10982-10990. https://doi.org/10.1074/jbc.M312669200.

Si, H., Rittenour, W. R., Xu, K., Nicksarlian, M., Calvo, A. M., and Harris, S. D. (2012). Morphogenetic and developmental functions of the Aspergillus nidulans homologues of the yeast bud site selection proteins Bud4 and AxI2. *Molecular Microbiology,* 85(2), 252-270. https://doi.org/10.1111/j.1365-2958.2012.08108.x.

Siam, R., Dolan, W. P. and Forsburg, S. L. (2004). Choosing and using *Schizosaccharomyces pombe* plasmids. *Methods*, 33(3), pp.189-198. https://doi.org/10.1016/j.ymeth.2003.11.013.

Sipiczki, M. (2000). Where does fission yeast sit on the tree of life? *Genome Biology*, *1*(2), REVIEWS1011. Spirek, M., Benko, Z., Carnecka, M., Rumpf, C., Cipak, L., Batova, M., … Gregan, J. (2010). *S. pombe* genome deletion project: An update. *Cell Cycle*, *9*(12), 2399–2402. https://doi.org/10.4161/cc.9.12.11914.

Slagsvold, T., Aasland, R., Hirano, S., Bache, K. G., Raiborg, C., Trambaiolo, D., Wakatsuki, S., and Stenmark, H. (2005). Eap45 in mammalian ESCRT-II binds ubiquitin via a phosphoinositide-interacting GLUE domain. *The Journal of Biological Chemistry,* 280(20), 19600-19606. https://doi.org/10.1074/jbc.M501510200.

Smith, D. L., Erce, M. A., Lai, Y. W., Tomasetig, F., Hart-Smith, G., Hamey, J. J., and Wilkins, M. (2020). Crosstalk of phosphorylation and arhinine methylation in disordered SRGG repeats of *Saccharomyces cerevisiae* fibrillarin and its association with nucleolar localization. *Journal of Molecular Biology,* 432(2), 448-466. https://doi.org/10.1016/j.jmb.2019.11.006.

Snider, K. H., Sullivan, K. A., and Obrietan, K. (2018). Circadian regulation of hippocampal-dependent memory: Circuits, synapses and molecular mechanisms. *Neural Plasticity,* 7292540. https://doi.org/10.1155/2018/7292540.

Sohrmann, M., Fankhauser, C., Brodbeck, C., and Simanis, V. (1996). The dmf1/mid1 gene is essential for the correct positioning of the division septum in fission yeast. *Genes and Development*, 10, 2707–2719. https://doi.org/10.1101/gad.10.21.2707.

Sparks, C.A., Morphew, M., and McCollum, D. (1999). Sid2p is a spindle pole body kinase that regulates the onset of cytokinesis. *Journal of Cell Biology*, 146, 777–790. https://doi.org/10.1083/jcb.146.4.777.

Stauffer, D. R., Howard, T. I., Nyun, T., and Hollenberg, S. M. (2001). CHMP1 is a novel nuclear matrix protein affecting chromatin structure and cell-cycle progression. *Journal of Cell Science*, 114, 2395-2404. https://doi.org/10.1242/jcs.114.13.2395.

Stoten, C. L., and Carlton, J. G. (2018). ESCRT-dependent control of membrane remodelling during cell division. *Seminars in Cell and Developmental Biology,* 74, 50-65. https://doi.org/10.1016/j.semcdb.2017.08.035.

Stuchell-Brereton, M. D., Skalicky, J. J., Kieffer, C., Karren, M. A., Ghaffarian, S., and Sundquist, W. I. (2007). ESCRT-III recognition by VPS4 ATPases. *Nature,* 449(7163), 740-744. https://doi.org/10.1038/nature06172.

Su, S. S., Tanaka, Y., Samejima, I., Tanaka, K., and Yanagida, M. (1996). A nitrogen starvation induced dormant G_0 state in fission yeast: The establishment from uncommitted G_1 state and its delay for return to proliferation. *Journal of Cell Science,* 109: 1347-1357. https://doi.org/10.1242/jcs.109.6.1347.

Sun, L., Guan, R., Lee, I. J., Liu, Y., Chen, M., Wang, J., Wu, J. Q., and Chen, Z. (2015). Mechanistic insights into the anchorage of the contractile ring by anillin and Mid1. *Developmental Cell,* 33, 413-426. https://doi.org/10.1016/j.devcel.2015.03.003.

Suzuki, K., Sako, K., Akiyama, K., Isoda, M., Senoo, C., Nakajo, N., and Sagata, N. (2015). Identification of non-Ser/Thr-Pro consensus motifs for Cdk1 and their roles in mitotic regulation of C2H2 zinc finger proteins and Ect2. https://doi.org/10.1038/srep07929.

Swaffer, M. P., Jones, A. W., Flynn, H. R., Snijder, A. P., and Nurse, P. (2016). CDK substrate phosphorylation and ordering the cell cycle. *Cell,* 167 (7): 1750-1761. https://doi.org/10.1016/j.cell.2016.11.034.

Swaffer, M, P., Jones, A, W., Flynn, H, R., Snijder, A, P., and Paul, N. (2018). Quantitative phosphoproteomics reveals the signaling dynamics of cell-cycle kinases in the fission yeast *Schizosaccharomyces pombe*. *Cell Reports*, 24:503–514. https://doi.org/10.1016/j.celrep.2018.06.036.

Takaine, M., Numata, O., and Nakano, K. (2011). Fission yeast IQGAP maintains F-actin-independent localization of myosin-II in the contractile ring. *Genes to Cells,* 19(2): 161-176. https://doi.org/10.1111/gtc.12120.

Tang, Z. (2016). Model organisms for studying the cell cycle. *Methods in Molecular Biology,* 1342: 21-57. https://doi.org/10.1007/978-1-4939-2957-3_2.

Tasmia, S. A., Kibria, M. K., Tuly, K. F., Islam, M. A., Khatun, M. S., Hasan, M. M., and Mollah, M. N. H. (2022). Prediction of serine phosphorylation site mapping on *Schizosaccharomyces pombe* by fusing three encoding schemes with the random forest classifier. *Science Report,* 12, 2632. https://doi.org/10.1038/s41598-022-06529-0.

Tasto, J. J., Morrell, J. L., and Gould, K. L. (2003). An anillin homologue, Mid2p, acts during fission yeast cytokinesis to organize the septin ring and promote cell separation. *The Journal of Cell Biology,* 160(7), 1093-1103. https://doi.org/10.1083/jcb.200211126.

Tran Nguyen, T. M., Munhoven, A., Samel-Pommerencke, A., Kshirsagar, R., Cuomo, A., Bonaldi, T. and Ehrenhofer-Murray, A. E. (2023). Methylation of CENP-A/Cse4 on arginine 143 and lysine 131 regulates kinetochore stability in yeast. *Genetics,* 223(4), iyado28. https://doi.org/10.1093/genetics/iyado28.

Tuan, N. M., and Lee, C. H. (2020). Role of anillin in tumour: From a prognostic biomarker to a novel target. *Cancers*, *12*(6), 1600. https://doi.org/10.3390/cancers12061600.

Vlastaridis, P., Kyriakidou, P., Chaliotis, A., Van de Peer, Y., Oliver, S. G and Amoutzias, G. D. (2017). Estimating the total number of phosphoproteins and phosphorylation sites in eukaryotic proteomes. *Gigascience*, 6: (2), giw015 https://doi.org/10.1093/gigascience/giw015.

Vyas, A., Freitas, A. V., Ralston, Z. A., and Tang, Z. (2021). Fission yeast *Schizosaccharomyces pombe*: A unicellular "micromammal" model organism. *Current Protocols*, *1*, e151. https://doi.org/10.1002/cpz1.151.

Wegner, C.S., Rodahl, L.M.W. and Stenmark, H. (2011). ESCRT proteins and cell signalling. *Traffic*, 12(10), pp. 1291–1297. https://doi.org/10.1111/j.1600-0854.2011.01210.

Wenzel D. M., Mackay D. R., Skalicky J. J., Paine, E. L., Miller, M. S., Ullman, K. S., and Sundquist, W. I. (2022). Comprehensive analysis of the human ESRT-III-MIT domain interactome reveals new cofactors for cytokinesis abscission. *eLife*, 11:e77779. https://doi.org/10.7554/eLife.77779.

Willet, A. H., DeWitt, A. K., Beckley, J. R., Clifford, D. M., and Gould, K. L. (2019). NDR kinase Sid2 drives anillin-like Mid1 from the membrane to promote cytokinesis and medial division site placement. *Current Biology*, 29, 1055-1063. https://doi.org/10.1016/j.cub.2019.01.075.

Wollert, T., and Hurley, J. H. (2010). Molecular mechanism of multivesicular body biogenesis by ESCRT complex. *Nature*, 464(7290), 864-869. https://doi.org/10.1038/nature08849.

Wood, V. (2006). How to get the most from fission yeast genome data: A report from the 2006 European Fission Yeast Meeting computing workshop. *Yeast*, *23*(13), 905–912. https://doi.org/10.1002/yea.1419.

Wood, V., Gwilliam, R., Rajandream, M. A., Lyne, M., Lyne, R., Stewart, A., … Nurse, P. (2002). The genome sequence of *Schizosaccharomyces pombe*. *Nature*, *415*(6874), 871–880. https://doi.org/10.1038/nature724.

Wu, J. Q., Sirotkin V., Kovar D. R., Lord M., Beltzner C. C., Kuhn J. R., and Pollard T. D. (2006). Assembly of the cytokinetic contractile ring from a broad band of nodes in fission yeast. *Jour*nal *of Cell Biology*, 174, 391–402. https://doi.org/10.1083/jcb.200602032.

Wu, J. Q., and Pollard, T. D. (2005). Counting cytokinesis proteins globally and locally in fission yeast. *Science (New York, N.Y)*, 310(5746): 310-314. https://doi.org/10.1126/science.1113230

Wu, J. Q., Kuhn, J. R., Kovar, D. R., and Pollard, T. D. (2003). Spatial and temporal pathway for assembly and constriction of the contractile ring in fission yeast cytokinesis. *Development Cell*, 5(5): 723-734. https://doi.org/10.1016/S1534-5807(03)00324-1.

Yasuda, T., Takaine, M., Numata, O., and Nakano, K. (2016). Anillin-related protein Mid1 regulates timely formation for the contractile ring in the yeast *Schizosaccharomyces japonicus*. *Genes to Cells*, 6: 594-607. https://doi.org/10.1111/gtc.12368.

Yeo S. C. L., Xu, L., Ren, J., Boulton, V. J., Wagle, M. D., Liu, C., Ren, G., Wong, P., Zahn, R., Sasajala, P., Yang, H., Piper, R. C., and Munn, A. L. (2003). Vps20p and Vta1p interact with Vps4p and function in multivesicular body sorting and endosomal transport in *Saccharomyces cerevisiae*, 116 (19): 3957-3970. https://doi.org/10.1242/jcs.00751.

Yang, B., Stjepanovic, G., Shen, O., Martin, A. and Hurley, J., H. (2015). Vps4 disassembles an ESCRT-III filament by global unfolding and processive translocation. *Nature Structural and Molecular Biology*, 22(6), pp. 492–498. https://doi.org/10.1038/nsmb.3015.

Zhang, K., Lin, W., Latham, J. A., Riefler, G. M., Schumacher, J. M., Chang, C., Tatchell, K., Hawke, D. H., Kobayashi, R., and Dent, S. Y. (2005). The Set1 methyltransferase opposes 1pI1 aurora kinase functions in chromosome segregation. *Cell,* 122(5), 723-734. https://doi.org/10.1016/j.cell.2005.06.021.

Zhivotovsky, B., and Orrenius, S. (2010). Cell death mechanism: crosstalk and role in disease. *Experimental Cell Research,* 316(8), 1374-1383. https://doi.org/10.1016/j.yexcr.2010.02.037.

Zofall, M., and Grewal, S. I. (2006). RNAi-mediated heterochromatin assembly in fission yeast. *Cold Spring Harbor Symposia on Quantitative Biology*, 71, 487-496. https://doi.org/10.1101/sqb.2006.71.059.